Optimizing Power Allocation in Sensor Networks with Application in Target Classification

Von der Fakultät für Elektrotechnik und Informationstechnik
der Rheinisch-Westfälischen Technischen Hochschule Aachen
zur Erlangung des akademischen Grades eines Doktors
der Ingenieurwissenschaften genehmigte Dissertation

vorgelegt von

Diplom-Ingenieur
Gholamreza Alirezaei

aus Esfahan, Iran

Berichter: Universitätsprofessor Dr. rer. nat. Rudolf Mathar
Universitätsprofessor em. Dr. sc. techn. Heinrich Meyr

Tag der mündlichen Prüfung: 08. Mai 2014

Diese Dissertation ist auf den Internetseiten
der Hochschulbibliothek online verfügbar.

Berichte aus der Kommunikationstechnik

Gholamreza Alirezaei

Optimizing Power Allocation in Sensor Networks with Application in Target Classification

Shaker Verlag
Aachen 2014

Bibliographic information published by the Deutsche Nationalbibliothek
The Deutsche Nationalbibliothek lists this publication in the Deutsche Nationalbibliografie; detailed bibliographic data are available in the Internet at http://dnb.d-nb.de.

Zugl.: D 82 (Diss. RWTH Aachen University, 2014)

Copyright Shaker Verlag 2014
All rights reserved. No part of this publication may be reproduced, stored in a retrieval system, or transmitted, in any form or by any means, electronic, mechanical, photocopying, recording or otherwise, without the prior permission of the publishers.

Printed in Germany.

ISBN 978-3-8440-3115-7
ISSN 0945-0823

Shaker Verlag GmbH • P.O. BOX 101818 • D-52018 Aachen
Phone: 0049/2407/9596-0 • Telefax: 0049/2407/9596-9
Internet: www.shaker.de • e-mail: info@shaker.de

Contents

Acknowledgements **ix**

1 Introduction **1**
1.1 Outline . . . 2

2 Mathematical Preliminaries **3**
2.1 Special Functions . . . 3
2.2 Convexity, Majorization and Inequalities . . . 5
2.3 Convex and Signomial Programming . . . 6
2.4 Power Series Expansion of Functions . . . 8
2.5 Ratio of Two Gamma Functions . . . 9

3 Optimum Power Allocation for Passive Sensor Networks **15**
3.1 Overview and Technical System Description . . . 16
3.1.1 Target signal . . . 17
3.1.2 Sensing channel . . . 18
3.1.3 Sensor nodes . . . 18
3.1.4 Communication channel . . . 19
3.1.5 Fusion center . . . 19
3.1.6 Remarks to the system model . . . 20
3.2 Power Optimization . . . 21
3.2.1 Optimization problem . . . 21
3.2.2 Power allocation subject to individual power constraints . . . 22
3.2.3 Interpretation of the solution . . . 25
3.2.4 Power allocation subject to the sum-power constraint . . . 26
3.2.5 Comparison of the solutions . . . 29
3.2.6 Power allocation subject to both types of power constraints . . . 29
3.2.7 Discussion of the solutions . . . 34
3.2.8 Another access for identifying reliable sensor nodes . . . 34
3.3 Technical Interpretation and Visualization of Results . . . 36
3.3.1 Measurable parameters and technical interpretation of results . . . 36
3.3.2 Visualization of results . . . 38
3.4 Summary . . . 40

4 Optimum Power Allocation for Active Sensor Networks **45**
4.1 Overview and Technical System Description . . . 46
4.1.1 Target object . . . 47

4.1.2 Sensing channel . . . 48
4.1.3 Sensor nodes . . . 49
4.1.4 Communication channel . . . 50
4.1.5 Fusion center . . . 50
4.1.6 Remarks to the system model . . . 51
4.2 Power Optimization . . . 52
4.2.1 Optimization problem . . . 52
4.2.2 Power allocation subject to the sum-power constraint . . . 54
4.2.3 Power allocation subject to individual power constraints . . . 58
4.2.4 Comparison of the solutions . . . 60
4.2.5 Power allocation subject to both types of power constraints . . . 61
4.2.6 A numerical access . . . 65
4.2.7 Discussion of the solutions . . . 67
4.3 Geometric Position of Most Reliable Sensor Nodes . . . 68
4.3.1 Identifying the best sensor nodes . . . 68
4.3.2 Visualization and numerical evaluation . . . 73
4.4 Technical Interpretation and Visualization of Results . . . 73
4.4.1 Measurable parameters and technical interpretation of results . . . 74
4.4.2 Visualization of results . . . 76
4.5 Summary . . . 79

5 Classification 85
5.1 Distribution of the Estimates . . . 85
5.2 Classification Rule and Probability . . . 86
5.3 Instantaneous Classification Probability for Particular Cases . . . 87
5.4 Average Classification Probability . . . 89

6 Error Probability for Nakagami-Distributed Fading 93
6.1 Problem Description and Associated Identities . . . 94
6.2 Functional Properties of the BeNaI . . . 99
6.3 Choosing the Proper Class of Bounds . . . 101
6.4 Bounds and Approximations . . . 101
6.5 Functional Properties of the Bounds . . . 107
6.6 Proof of the Bounds . . . 113
6.7 Analysis of the Bounds . . . 117
6.8 Proof of Relative Errors . . . 121
6.9 Discussion of Results . . . 124
6.10 Open Problems . . . 125
6.11 Summary . . . 125

7 Conclusion 127
7.1 Summary and Contributions . . . 127
7.2 Future Research . . . 128

Glossary **131**

Bibliography **135**

Curriculum Vitae **143**

Acknowledgements

This thesis was written during my time as a research assistant at the *Chair of Theoretical Information Technology* of *RWTH-Aachen*.

First and foremost, I would like to thank my supervisor, Univ.-Prof. Dr. rer. nat. Rudolf Mathar, for giving me a very unique opportunity in pursuing my Ph.D degree. I also would like to thank him for his continuous support and for being an excellent example of fair and practical leadership.

Many thanks to Univ.-Prof. em. Dr. sc. techn. Heinrich Meyr for taking the effort to assess this thesis. He inspired me with new ideas and enhanced this thesis with his advice and experience in various ways.

During my time as a research assistant I was supported by a Ph.D-student-grant. I feel much obliged to thank Univ.-Prof. em. Dr.-Ing. Bernhard Walke for this support.

Although, I have been a hardware designer for a long time, I became familiar with theorization as I was a student. The fact that I am a theorist now is based on endeavors of my deceased tutor Univ.-Prof. em. Dr.-Ing. Dr. E. h. Hans Dieter Lüke. May he rest in peace.

I also would like to say thankyou to both Univ.-Prof. Dr.-Ing. Tobias G. Noll and Univ.-Prof. Dr.-Ing. Dirk Heberling for preparing and encouraging me for the final Ph.D exam.

A special thankyou goes to M.Sc. Omid Taghizadeh and Dipl.-Ing. Johannes Schmitz for their very helpful discussions, suggestions, and for proof-reading parts of this thesis.

I would like to express my deepest gratitude to all my colleagues at the Chair of Theoretical Information Technology. You have helped to create a comfortable and inspiring working environment, every day. Thank you for a good time, I will miss your company.

To this day, I have enjoyed many years of friendship with my former colleagues from the *Institute of High Frequency Technology* of RWTH-Aachen. It is my esteemed honor to thank you for the good time and all adventures.

Ein besonderer Dank gilt meinen Eltern, Frau Soghra Motaghedi und Herrn Azizollah Alirezaei, und der übrigen Familie, die mich über alle Jahre hinweg mit viel Geduld und Zuversicht unersetzlich unterstützt haben.

Aachen, September 2014 Gholamreza Alirezaei

1 Introduction

Recent technological discoveries in distributed systems, clustering and networking protocols, and new smart sensors, enable more intelligent sensor solutions for which we expect a growing global demand and a new range of superior applications. To open new ways of sensing for monitoring and surveilling the real world, intelligent proactive devices are produced at low cost and deployed on a large scale as so-called wireless sensor networks. Competing applications of wireless sensor networks encompass environmental and infrastructural monitoring, industrial and medical sensing and diagnostics, multi-target tracking, detecting as well as classifying. Although all leading applications are differently used, their common ground is based on the '*capability of sensing*'. Individual sensor nodes are in general mostly cheap and thus have limited abilities. In contrast, the collaboration of a large number of distributed sensor nodes allows to perform complex and novel sensing tasks. Since one of the most crucial constraints on sensor nodes is the low power consumption requirement, the aim for energy-aware design and operation results naturally. Wireless sensors are often powered by irreplaceable batteries or even batteryless and thus have to operate on limited energy budgets. Consequently, power consumption and overall system performance are general trade-off objectives. It is a major challenge to balance the resource consumption within the system and to achieve a good system performance at the same time. For this purpose, it is essential to find a suitable mathematical description of objectives and related constraints. In the scope of energy-efficient system design, most of the relevant optimization problems are solved by numerical methods. Since the underlying mathematical structure is often very complicated and thus does not allow an analytical or algebraic solution, the application of heuristics is a common approach. Generally, the complexity of finding energy minimal solutions increases drastically with the number of sensors in the network. Even sophisticated numerical methods fail to compute optimal solutions in real-time. Hence, closed-form analytical and algebraic solutions are the key to achieve maximum overall performance of wireless sensor networks. The last conclusion is the main motivation for this dissertation.

In the present work, we derive mathematical methods and algorithms for optimizing the power allocation in distributed wireless sensor networks that perform both target detection and classification. Our goal is to find analytical solutions in closed-form instead of numerical results. Since closed-form solutions are very difficult to obtain and only achievable in particular cases, this work presents first novel results for dealing with power allocation in distributed radar systems. Passive and active radar systems are investigated under sum-power and individual power constraints per sensor node. In addition, we determine the corresponding classification performance exemplarily for the active radar system. This leads to an investigation of certain classes of integrals

concerning the evaluation of the average classification probability in communication over fading channels. Since the evaluation of average classification probability and average symbol-error probability over fading channels are closely related, we scrutinize corresponding mathematical integrals thoroughly. As main results, we present equivalent equations and mathematical expressions as well as accurate analytical bounds in closed-form for which all corresponding relative errors are explicitly specified and analytically determined.

1.1 Outline

First, mathematical preliminaries and important fundamentals are outlined in Chapter 2. Furthermore, Gautschi's double inequality, which is very important for the statements in Chapter 6, is considered and improved.

In Chapter 3, power allocation in passive radar systems is motivated and optimized. Beginning with an overview of the underlying system model, the corresponding optimization problem is developed. Under sum-power and individual power constraints the optimization problem is solved and discussed. In the case that both types of constraints shall be satisfied simultaneously, an efficient algorithm is given to select the most reliable sensor nodes.

Analogously, the optimization of power allocation in active radar systems is investigated in Chapter 4. First, the system model and the corresponding optimization problem are introduced. Then, the optimization problem subject to sum-power and individual power constraints is solved. In between, selected results are compared and interpreted.

In order to point out an extensive problem, which emerges in evaluating the average classification probability, we first derive the instantaneous classification probability for some particular cases in Chapter 5. Subsequently, the average classification probability is shortly discussed and its relationship to the average symbol-error probability is established.

Finally, the average symbol-error probability is treated in Chapter 6. In particular, we consider the average symbol-error probability in communication over Nakagami fading channels and start with its representation in integral form. In order to gain deep insight, the integral form is converted and in turn described by certain classes of special functions. As main results new representations of the average symbol-error probability are found, which help to deduce accurate approximations and bounds. Hence, two new accurate bounds are derived in closed-form with an explicit specification of corresponding relative errors. In between, selected results are visualized by corresponding curves.

In the conclusions, the content of this thesis is summarized and main contributions are highlighted. Furthermore, an outline for future works is presented.

Parts of this thesis and related topics have been published in [1–13]. Other parts are submitted to journals and proceedings, but are still under revision, e.g., [14].

2 Mathematical Preliminaries

Throughout this work we denote the sets of positive integers (natural numbers), integers, real numbers and complex numbers by $\mathbb{N}$, $\mathbb{Z}$, $\mathbb{R}$ and $\mathbb{C}$, respectively. The imaginary unit is denoted by j. Furthermore, the sets of non-negative integers and non-negative real numbers are denoted by $\mathbb{N}_0$ and $\mathbb{R}_+$, respectively. Moreover, we use the subset $\mathbb{F}_N \subseteq \mathbb{N}$ which is defined as $\mathbb{F}_N \coloneqq \{1, \ldots, N\}$ for any given $N \in \mathbb{N}$.

We use boldface uppercase letters to denote matrices, while boldface lowercase letters denote vectors.

The operations $|z|$, $\|\mathbf{z}\|$ and $|\mathbb{F}_N|$ denote the absolute value of some real or complex number z, the Euclidean norm of some real or complex vector $\mathbf{z}$, and the cardinality (number of elements) of the set $\mathbb{F}_N$, respectively. The notations $\bar{\mathbf{M}}$, $\mathbf{M}'$ and $\bar{\mathbf{M}}'$ represent the complex conjugate, transpose and complex-conjugate transpose of any matrix $\mathbf{M}$, respectively. The expected value of a random variable v and a random vector $\mathbf{v}$ are denoted by $\mathcal{E}[v]$ and $\mathcal{E}[\mathbf{v}]$, respectively. Moreover, the notation $V^\star$ stands for the value of an optimization variable V where the optimum is attained. The logical conjunction is marked as $\wedge$.

A function $\vartheta(x)$ is said to be of order $\mathcal{O}\big(\omega(x)\big)$ as $x \mapsto x_0$ whenever for some $\delta > 0$, $\epsilon > 0$ and all x with $|x - x_0| < \epsilon$ the inequality $|\vartheta(x)| \leq \delta\,|\omega(x)|$ holds.

For convenience of referencing, we briefly introduce some important special functions and summarize their properties, as may be found in the chapters 6, 7, 15 and 26 of [15].

2.1 Special Functions

The Euler's classical gamma function is defined as

$$\Gamma(x) \coloneqq \int_0^\infty t^{x-1}\,\mathrm{e}^{-t}\,\mathrm{d}t\,, \quad x > 0\,. \tag{2.1}$$

It has the well-known properties

$$\Gamma(\tfrac{1}{2}) = \sqrt{\pi}\,,\ \Gamma(1) = \Gamma(2) = 1 \ \text{ and } \ \Gamma(\tfrac{3}{2}) = \tfrac{\sqrt{\pi}}{2}\,. \tag{2.2}$$

Moreover, for all positive real numbers x, the identity

$$\Gamma(x+n) = \Gamma(x) \prod_{i=0}^{n-1} (x+i)\,, \quad n \in \mathbb{N}\,, \tag{2.3}$$

holds, which especially entails $\Gamma(x+1) = x\,\Gamma(x)$. Furthermore, the limit

$$\lim_{n\mapsto\infty} n^{b-a}\,\frac{\Gamma(n+a)}{\Gamma(n+b)} = 1\,, \quad a,b \in \mathbb{R}_+\,, \tag{2.4}$$

is well-known.

We will also use the digamma function

$$\psi(x) \coloneqq \frac{\mathrm{d}}{\mathrm{d}x}\ln\Gamma(x) = \frac{\Gamma'(x)}{\Gamma(x)}\,, \quad x > 0\,, \tag{2.5}$$

where $\Gamma'(x)$ denotes the first derivative of $\Gamma(x)$.

Closely related to the gamma function is the incomplete beta function, which is defined as

$$\mathrm{B}(a,b;x) \coloneqq \int_0^x t^{a-1}(1-t)^{b-1}\mathrm{d}t\,, \tag{2.6}$$

for all positive real numbers a, b and x with $0 < x < 1$. By substitution of $\frac{t}{1+t}$ for t in (2.6), we obtain the identity

$$\mathrm{B}(a,b;x) = \int_0^{\frac{x}{1-x}} \frac{t^{a-1}}{(1+t)^{a+b}}\mathrm{d}t\,. \tag{2.7}$$

For the limit $x \mapsto 1$, the incomplete beta function tends towards the beta function, which is then given by

$$\mathrm{B}(a,b) \coloneqq \frac{\Gamma(a)\,\Gamma(b)}{\Gamma(a+b)} = \mathrm{B}(b,a) = \int_0^\infty \frac{t^{a-1}}{(1+t)^{a+b}}\mathrm{d}t\,. \tag{2.8}$$

The Gauss error function and its complementary version are of central importance in communication theory. However, they are difficult to handle analytically. For all real numbers x, we will hence use the series representation

$$\mathrm{erfc}(x) \coloneqq \frac{2}{\sqrt{\pi}}\int_x^\infty \mathrm{e}^{-t^2}\,\mathrm{d}t = 1 - \frac{2}{\sqrt{\pi}}\sum_{n=0}^\infty \frac{(-1)^n\,x^{2n+1}}{(2n+1)\,n!}\,. \tag{2.9}$$

Another special function of importance for this work is the Gauss hypergeometric function. For all positive real numbers a, b and c, and for all real numbers x, it is defined as

$${}_2\mathrm{F}_1(a,b;c;x) \coloneqq \frac{\Gamma(c)}{\Gamma(a)\,\Gamma(b)}\sum_{n=0}^\infty \frac{\Gamma(a+n)\,\Gamma(b+n)\,x^n}{\Gamma(c+n)\,\Gamma(n+1)}\,. \tag{2.10}$$

If $a > 0$, $b > 0$ and $c > b$, then for all $x > 0$ a corresponding integral representation is known as

$${}_2\mathrm{F}_1(a,b;c;-x) = \frac{\Gamma(c)}{\Gamma(b)\,\Gamma(c-b)}\int_0^1 \frac{t^{b-1}(1-t)^{c-b-1}}{(1+x\,t)^a}\mathrm{d}t\,. \tag{2.11}$$

2.2 Convexity, Majorization and Inequalities

The following geometric properties of functions and sequences are important tools for dealing with optimization problems. Some basic concepts are briefly summarized, see for example [16], [17] and [18].

Definition 2.2.1 (Logarithmically convex functions)**.** Suppose f is a positive real-valued function on $\mathbb{D} \subseteq \mathbb{C}^n$. Then f is called a logarithmically convex function on $\mathbb{D}$, if for all real numbers λ, with $0 < \lambda < 1$, and for all $\mathbf{x}_1, \mathbf{x}_2 \in \mathbb{D}$ the inequality

$$f\big(\lambda \mathbf{x}_1 + (1-\lambda)\mathbf{x}_2\big) \;\leq\; f^{\lambda}(\mathbf{x}_1) f^{1-\lambda}(\mathbf{x}_2) \tag{2.12}$$

holds.

Corollary 2.2.2. *If f is a logarithmically convex function on $\mathbb{D} \subseteq \mathbb{C}^n$, then it is a convex function on $\mathbb{D}$, as well.*

Definition 2.2.3 (Sorting sequences)**.** For a sequence $\mathbf{x} = (x_1, x_2, \ldots, x_N) \in \mathbb{R}^N$, we denote by $\mathbf{x}^{\downarrow} \in \mathbb{R}^N$ a sequence with the same components as in $\mathbf{x}$, but sorted in a descending order. Analogously, we denote by $\mathbf{x}^{\uparrow} \in \mathbb{R}^N$ a sequence with the same components as in $\mathbf{x}$, but sorted in an ascending order.

Definition 2.2.4 (Majorization)**.** Let $\mathbf{x} \in \mathbb{R}^N$ and $\mathbf{y} \in \mathbb{R}^N$ be finite sequences. Then $\mathbf{x}$ is majorized by $\mathbf{y}$, or equivalently $\mathbf{x} \preceq \mathbf{y}$, if the inequalities

$$\sum_{i=1}^{n} x_i^{\downarrow} \;\leq\; \sum_{i=1}^{n} y_i^{\downarrow}, \quad \text{for all } 1 \leq n \leq N, \tag{2.13}$$

and the equality

$$\sum_{i=1}^{N} x_i \;=\; \sum_{i=1}^{N} y_i \tag{2.14}$$

hold.

Corollary 2.2.5. *Let $\mathbf{x} \in \mathbb{R}^N$, $\mathbf{y} \in \mathbb{R}^N$ and $\mathbf{z} \in \mathbb{R}^N$ be finite sequences. If $\mathbf{x}$ is majorized by $\mathbf{y}$, then the inequality*

$$\sum_{i=1}^{N} x_i^{\downarrow} z_i^{\downarrow} \;\leq\; \sum_{i=1}^{N} y_i^{\downarrow} z_i^{\downarrow} \tag{2.15}$$

holds, see [17, p. 133, Proposition H.2.c].

Lemma 2.2.6 (Hölder's inequality)**.** *Suppose both f and g are non-negative real-valued functions on $\mathbb{D} \subseteq \mathbb{C}^n$. Then for all real numbers λ, with $0 \leq \lambda \leq 1$, the inequality*

$$\int_{\mathbb{D}} f^{\lambda}(\mathbf{x}) g^{1-\lambda}(\mathbf{x}) \mathrm{d}\mathbf{x} \;\leq\; \left(\int_{\mathbb{D}} f(\mathbf{x}) \mathrm{d}\mathbf{x} \right)^{\lambda} \left(\int_{\mathbb{D}} g(\mathbf{x}) \mathrm{d}\mathbf{x} \right)^{1-\lambda} \tag{2.16}$$

holds. Equality holds if and only if f^{λ} and $g^{1-\lambda}$ are linearly dependent on $\mathbb{D}$, see [18, p. 140, eq. 6.9.1].

Proof. See for example [18]. □

Lemma 2.2.7 (Weighted power mean inequality)**.** *Suppose that both $x_1, x_2, \ldots, x_N$ and $w_1, w_2, \ldots, w_N$, with $\sum_{n=1}^{N} w_n = 1$, are finite sequences, each consisting of N positive real numbers. Then for all real numbers p and q, with $p < q$, the inequality*

$$\left(\sum_{n=1}^{N} w_n x_n^p \right)^{1/p} \leq \left(\sum_{n=1}^{N} w_n x_n^q \right)^{1/q} \tag{2.17}$$

holds. Equality holds if and only if $x_1 = x_2 = \cdots = x_N$, see [18, p. 13, eq. 2.2.2 and p. 26, eq. 2.9.1].

Proof. See for example [18]. □

Corollary 2.2.8. *By calculating the limits $p \mapsto -\infty$ and $q \mapsto \infty$, we obtain the inequality chain*

$$\min\{x_n \mid 1 \leq n \leq N\} \leq \left(\sum_{n=1}^{N} w_n x_n^r \right)^{1/r} \leq \max\{x_n \mid 1 \leq n \leq N\}, \tag{2.18}$$

for all $r \in \mathbb{R}$, see [18, p. 14, eq. 2.3.1].

Corollary 2.2.9 (Arithmetic and geometric mean inequality)**.** *By calculating the limit $p \mapsto 0$ with $q = 1$, we obtain the inequality chain*

$$\prod_{n=1}^{N} x_n^{w_n} \leq \sum_{n=1}^{N} w_n x_n, \tag{2.19}$$

see [18, p. 17, eq. 2.5.1].

2.3 Convex and Signomial Programming

In the present work, we deal with two special types of optimization problems. The first one is very common and is called a *convex program* for which the *Karush-Kuhn-Tucker conditions* provide both sufficient and necessary conditions for global optimality. The second one, called a *signomial program*, is in general more challenging to solve than *geometric programs*. They need to be defined in the following.

Definition 2.3.1 (Convex program)**.** A *convex optimization problem* is one of the form

$$\begin{aligned} \text{minimize} \quad & f(\mathbf{x}) \\ \text{subject to} \quad & g_i(\mathbf{x}) \leq 0, \quad i = 1, 2, \ldots, m \\ & h_i(\mathbf{x}) = 0, \quad i = 1, 2, \ldots, p \end{aligned} \tag{2.20}$$

where the objective f and all inequality constraints g_i are convex functions, and all equality constraints h_i are affine, see [19, p. 136].

Lemma 2.3.2 (Karush-Kuhn-Tucker conditions)**.** *Let* $(\mathbf{x}^\star, \boldsymbol{\lambda}^\star, \boldsymbol{\nu}^\star) \in \mathbb{R}^n \times \mathbb{R}^m \times \mathbb{R}^p$ *be any globally optimal points of the Lagrangian*

$$L(\mathbf{x}, \boldsymbol{\lambda}, \boldsymbol{\nu}) \coloneqq f(\mathbf{x}) + \sum_{i=1}^{m} \lambda_i g_i(\mathbf{x}) + \sum_{i=1}^{p} \nu_i h_i(\mathbf{x})\,. \tag{2.21}$$

Then the Karush-Kuhn-Tucker conditions

$$g_i(\mathbf{x}^\star) \leq 0\,, \quad i = 1, 2, \ldots, m \tag{2.22a}$$
$$h_i(\mathbf{x}^\star) = 0\,, \quad i = 1, 2, \ldots, p \tag{2.22b}$$
$$\lambda_i^\star \geq 0\,, \quad i = 1, 2, \ldots, m \tag{2.22c}$$
$$\lambda_i^\star g_i(\mathbf{x}^\star) = 0\,, \quad i = 1, 2, \ldots, m \tag{2.22d}$$

and

$$\nabla f(\mathbf{x}^\star) + \sum_{i=1}^{m} \lambda_i^\star \nabla g_i(\mathbf{x}^\star) + \sum_{i=1}^{p} \nu_i^\star \nabla h_i(\mathbf{x}^\star) = 0\,, \tag{2.22e}$$

are sufficient and necessary conditions that $\mathbf{x}^\star$ *is also a globally optimal point of the convex optimization problem* (2.20)*. Here, the notation* ∇f *denotes the gradient of a function* f*.*

Proof. See for example [19]. □

Definition 2.3.3 (Posynomial and signomial)**.** Suppose $\mathbf{x} = (x_1, x_2, \ldots, x_M) \in \mathbb{R}_+^M$, $\mathbf{c} = (c_1, c_2, \ldots, c_N) \in \mathbb{R}^N$ and $\mathbf{y} = (y_{1,1}, y_{1,2}, \ldots, y_{N,M}) \in \mathbb{R}^{NM}$ are finite sequences. A function of the form

$$f(\mathbf{x}) \coloneqq \sum_{n=1}^{N} \left(c_n \prod_{m=1}^{M} x_m^{y_{n,m}} \right) \tag{2.23}$$

is then called a *signomial function*. If we restrict all c_n to be positive, then the function f is called a *posynomial function*, see [20].

Definition 2.3.4 (Signomial program)**.** An optimization problem of the form

$$\begin{aligned} \text{minimize} \quad & f(\mathbf{x}) \\ \text{subject to} \quad & g_i(\mathbf{x}) \leq 0\,, \quad i = 1, 2, \ldots, m \\ & h_i(\mathbf{x}) = 0\,, \quad i = 1, 2, \ldots, p \end{aligned} \tag{2.24}$$

where the objective f, the inequality constraints g_i, and the equality constraints h_i are signomial functions, is called a *signomial program*, see [19, p. 200].

It is important to note that in general signomial programs cannot be transformed into convex optimization problems. Finding sufficient and necessary conditions to ensure global optimality in signomial programs is still an open problem. Hence, we apply the general method of Lagrangian multiplier to solve all optimization problems in the present work, see [21, pp. 321–358] and [22, pp. 275–368].

2.4 Power Series Expansion of Functions

The formal power series expansion is a powerful method for approximation of functions and their asymptotic behavior. By a formal series we mean any infinite series where no assumption is made concerning its convergence. The following two definitions are from [23].

Definition 2.4.1 (Formal series expansion for finite expansion points)**.** Let $f(x)$ be defined and continuous on $\mathbb{D} \subseteq \mathbb{R}$. Let x_0 be a finite point in $\mathbb{D}$. The formal power series

$$\sum_{n=0}^{\infty} a_n (x - x_0)^n \tag{2.25}$$

is said to be an asymptotic power series expansion of $f(x)$, as $x \mapsto x_0$ in $\mathbb{D}$, if the conditions

$$\lim_{x \mapsto x_0} (x - x_0)^{-m} \left(f(x) - \sum_{n=0}^{m} a_n (x - x_0)^n \right) = 0\,, \quad m \in \mathbb{N}_0\,, \tag{2.26}$$

are satisfied. Then we can write

$$f(x) = \sum_{n=0}^{m} a_n (x - x_0)^n + \mathcal{O}\big((x - x_0)^{m+1}\big) \tag{2.27}$$

as x approaches x_0.

Note that the well-known Taylor series expansion is a special case of Definition 2.4.1.

Definition 2.4.2 (Formal series expansion for infinite expansion points)**.** Let $f(x)$ be defined and continuous on a suitable left neighborhood of infinity. The formal power series

$$\sum_{n=0}^{\infty} a_n x^{-n} \tag{2.28}$$

is said to be an asymptotic power series expansion of $f(x)$ as $x \mapsto \infty$ if the conditions

$$\lim_{x \mapsto \infty} x^m \left(f(x) - \sum_{n=0}^{m} a_n x^{-n} \right) = 0\,, \quad m \in \mathbb{N}_0\,, \tag{2.29}$$

are satisfied. Then we can write

$$f(x) = \sum_{n=0}^{m} a_n x^{-n} + \mathcal{O}\big(x^{-m-1}\big) \tag{2.30}$$

as x approaches infinity.

Note that we can also use Definition 2.4.2 for analyzing certain functions on a suitable right neighborhood of minus infinity.

2.5 Ratio of Two Gamma Functions

Definition 2.5.1. For all real numbers $x > -2$, we define the ratio

$$\tau(x) := \frac{\sqrt{\pi}\,\Gamma\left(\frac{x+3}{2}\right)}{\Gamma\left(\frac{x+2}{2}\right)} \ . \tag{2.31}$$

Obviously, $\tau(x)$ is positive. Furthermore, the identities

$$\tau(-1) = 1\,,\ \tau(0) = \frac{\pi}{2} \ \text{ and } \ \tau(1) = 2 \tag{2.32}$$

easily follow from (2.2). According to (2.3) and (2.8), we conclude

$$\tau(x) = \frac{x+1}{2} \int_0^\infty \frac{\mathrm{d}t}{(1+t)^{\frac{x+2}{2}}\,\sqrt{t}} \ . \tag{2.33}$$

The ratio $\tau(x)$ in (2.31) and its properties have been investigated in a series of papers. In [24], W. Gautschi has proposed a lower and an upper bound for this ratio, which are together known as Gautschi's double inequality. This double inequality was later refined and extended by many scientists, primarily by D. Kershaw [25], M. Merkle [26] and F. Qi [27]. For the purpose of the present work, Gautschi's double inequality plays an important role. However, Gautschi's bounds and subsequent improvements are too weak, particularly for the case $-1 \le x < 1$, in order to prove some of the main theorems of the present work. Thus, a new tighter inequality is given in the following theorem.

Theorem 2.5.2. *For all real numbers $x \ge 1$, the inequality*

$$\sqrt{\frac{3x+5}{2}} \ \le \ \tau(x) \tag{2.34}$$

holds. If $-1 \le x \le 1$, then the reverse inequality holds.

In Figure 2.1, both sides of inequality (2.34) are depicted. As can be seen from the graph, lower and upper bound are very close to $\tau(x)$ in their respective range and equality holds for $x = -1$ and $x = 1$.

Note that a converse inequality to (2.34) can simply be obtained by applying the so called *β-transformation*, see [28] and [26].

The proof of Theorem 2.5.2 is not straightforward since the ratio of gamma functions in (2.31) is extremely hard to manipulate. Nevertheless, the proof is simpler viable by a brilliant idea of D. Kershaw, applied in [25]. The main idea behind the proof is to transform the function $\tau(x)$ to obtain two new functions, which do not contain the gamma function and thus are easier to investigate. Subsequently, by analyzing the new functions and their interactions, one is able to conclude necessary conditions in order to prove the assertion in Theorem 2.5.2. Hence, we extend the main idea in the following and consider three different functions simultaneously. Prior to this, we need to introduce some definitions and prerequisites.

Definition 2.5.3. For all positive real numbers $x > \frac{1}{6}$, we define the auxiliary functions

$$w(x) \coloneqq \frac{\tau(2x-2)}{\sqrt{\frac{3(2x-2)+5}{2}}} = \frac{\sqrt{\pi}\,\Gamma\left(x+\frac{1}{2}\right)}{\Gamma(x)} \frac{1}{\sqrt{3x-\frac{1}{2}}}\,, \tag{2.35}$$

$$W(x) \coloneqq \frac{w(x)}{w(x+1)} = \frac{x}{x+\frac{1}{2}} \sqrt{\frac{6x+5}{6x-1}}\,, \tag{2.36}$$

and

$$V(x) \coloneqq w(x)\, w(x+\tfrac{1}{2}) = \frac{\pi x}{\sqrt{3x-\frac{1}{2}}\sqrt{3x+1}}\,. \tag{2.37}$$

The general behavior of above functions is visualized in Figure 2.2. In the following, we discuss analytically their important mathematical properties. In particular, we have to show that the relations $w(x) \leq 1$ and $1 \leq w(x)$ for $\frac{1}{2} \leq x \leq \frac{3}{2}$ and $\frac{3}{2} \leq x$ hold, respectively.

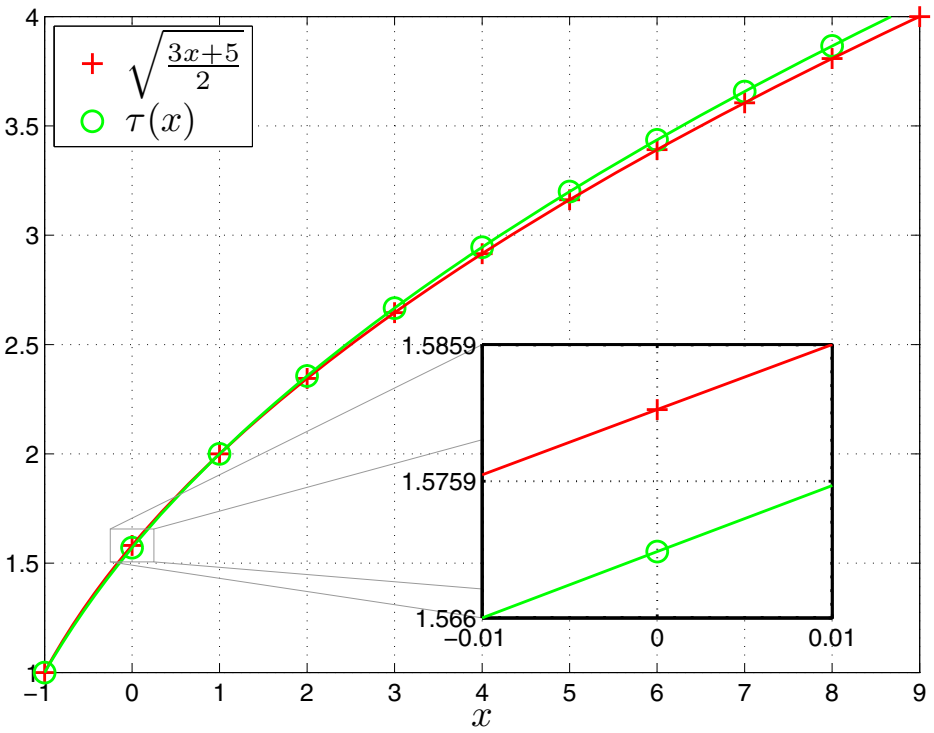

Figure 2.1: The ratio $\tau(x)$ and its associated bounds from Theorem 2.5.2 are visualized for the range of $-1 \leq x \leq 9$. For all $x \geq 1$ the inequality $\sqrt{(3x+5)/2} \leq \tau(x)$ holds while for all $-1 \leq x \leq 1$ the reverse inequality holds. The curves are closely adjacent to one another such that the maximum relative error is less than $\sqrt{\pi/3} - 1$ or equivalently 2.33%. The relative error approaches its maximum as x approaches infinity. The curves intersect one another at $x = -1$ and at $x = 1$.

Lemma 2.5.4. *For all* $x > \frac{1}{6}$,

a) the auxiliary function w *is positive,*

b) it is continuous,

c) it is monotonic for sufficient large x,

d) for $x = \frac{1}{2}$ *and* $x = \frac{3}{2}$, *it holds that*

$$w(\tfrac{1}{2}) = w(\tfrac{3}{2}) = 1 \ , \tag{2.38}$$

e) as $x \mapsto \infty$, *its limit is given by*

$$\lim_{x \mapsto \infty} w(x) = \sqrt{\frac{\pi}{3}} > 1 \ , \tag{2.39}$$

f) and as $x \mapsto \infty$, *the value of its first derivative is determined by*

$$\lim_{x \mapsto \infty} w'(x) \coloneqq \lim_{x \mapsto \infty} \frac{\mathrm{d}w(x)}{\mathrm{d}x} = 0 \ . \tag{2.40}$$

Proof. Positivity and continuity are trivial, because of positivity and continuity of all incorporated functions and operations. Since both gamma functions and the root function are monotonic for sufficient large x, $w(x)$ proceeds monotonically, as well. The identity $w(\frac{1}{2}) = w(\frac{3}{2}) = 1$ simply follows by incorporating (2.2) into (2.35). By using the limit (2.4), we obtain

$$\lim_{x \mapsto \infty} w(x) = \lim_{x \mapsto \infty} \frac{\sqrt{\pi}\,\Gamma(x + \frac{1}{2})}{\Gamma(x)} \frac{1}{\sqrt{3x - \frac{1}{2}}} = \frac{\sqrt{\pi}}{\sqrt{3}} \lim_{x \mapsto \infty} x^{-\frac{1}{2}} \frac{\Gamma(x + \frac{1}{2})}{\Gamma(x)} = \sqrt{\frac{\pi}{3}} \ . \tag{2.41}$$

Since w is continuous, monoton and convergent to a constant as $x \mapsto \infty$, due to (2.39), its slope vanishes as x approaches infinity[1]. □

Lemma 2.5.5. *For all* $x > \frac{1}{6}$,

a) the auxiliary function W *is continuous,*

b) it is strictly decreasing for all $\frac{1}{6} < x < \frac{5}{6}$ *and strictly increasing for all* $x > \frac{5}{6}$, *and*

c) for $x = \frac{1}{2}$ *and* $x \mapsto \infty$, *it holds that*

$$W(\tfrac{1}{2}) = \lim_{x \mapsto \infty} W(x) = 1 \ . \tag{2.42}$$

[1] That the slope is zero as x approaches infinity can also be proved by analyzing the first derivative of $w(x)$ near infinity with the aid of [29, p. 906, eq. 8.371] or by using the bound in [27, Theorem 3].

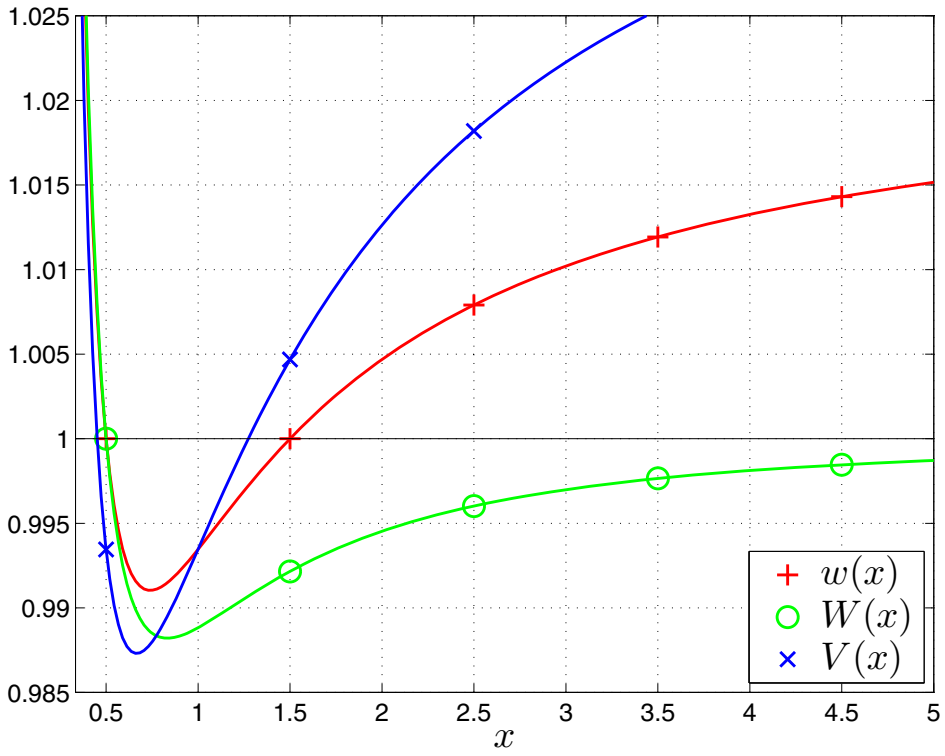

Figure 2.2: The functions $w(x)$, $W(x)$ and $V(x)$ are visualized for $\frac{1}{3} \leq x \leq 5$.

Proof. Continuity is trivial, because all incorporated functions are continuous and all operations preserve continuity. In order to examine monotonicity, we calculate its first derivative which leads to

$$W'(x) := \frac{\mathrm{d}W(x)}{\mathrm{d}x} = \frac{2(6x-5)}{(2x+1)^2(6x-1)^{\frac{3}{2}}\sqrt{6x+5}} \,. \tag{2.43}$$

This derivative is negative for all $\frac{1}{6} < x < \frac{5}{6}$ and positive for all $x > \frac{5}{6}$ which confirm the above assertion. By (2.36), we obtain

$$W(x) = 1 \;\Leftrightarrow\; x\sqrt{6x+5} = (x+\tfrac{1}{2})\sqrt{6x-1} \;\Leftrightarrow\; x = \tfrac{1}{2} \tag{2.44}$$

and

$$\lim_{x\mapsto\infty} W(x) = \lim_{x\mapsto\infty} \frac{x}{x+\frac{1}{2}}\sqrt{\frac{6x+5}{6x-1}} = \lim_{x\mapsto\infty} \frac{x}{x}\sqrt{\frac{6x}{6x}} = 1 \,. \tag{2.45}$$

□

Lemma 2.5.6. *For all $x \geq \frac{1}{2}$, the inequality $W(x) \leq 1$ holds. If $\frac{1}{6} < x < \frac{1}{2}$, then the inequality $W(x) > 1$ holds.*

Proof. Due to Lemma 2.5.5, the auxiliary function W is strictly decreasing for all $\frac{1}{6} < x < \frac{5}{6}$, and due to Lemma 2.5.5 the equality $W(\frac{1}{2}) = 1$ holds. Thus, the inequality

$W(x) > 1$ holds for all $\frac{1}{6} < x < \frac{1}{2}$ while $W(x) \leq 1$ holds for all $\frac{1}{2} \leq x < \frac{5}{6}$. Due to Lemma 2.5.5, the auxiliary function W is strictly increasing for all $x > \frac{5}{6}$, and due to Lemma 2.5.5 the equality $W(x \mapsto \infty) = 1$ holds. Thus, the inequality $W(x) \leq 1$ holds for all $x > \frac{5}{6}$. Due to the continuity in Lemma 2.5.5, the inequality $W(\frac{5}{6}) \leq 1$ holds, as well. □

Lemma 2.5.7. *For all $x \geq \frac{1}{2}$ and for all $n \in \mathbb{N}$, the inequality $w(x) \leq w(x+n)$ holds.*

Proof. The inequality $W(x) = \frac{w(x)}{w(x+1)} \leq 1$ holds for all $x \geq \frac{1}{2}$ due to Lemma 2.5.6. For all $x > \frac{1}{2}$ we can iterate this inequality to derive the inequality chain

$$w(x) \leq w(x+1) \leq w(x+2) \leq \cdots \leq w(x+n) \ , n \in \mathbb{N} \ . \tag{2.46}$$

The above conversion is valid because w is positive based on Lemma 2.5.4. □

Lemma 2.5.8. *For all $x > \frac{5}{6}$, the auxiliary function w is strictly increasing.*

Proof. The function W is strictly increasing for all $x > \frac{5}{6}$ according to Lemma 2.5.5. This leads to a positive slope of W. Thus, we derive from the first derivative of W the inequality

$$W'(x) = \frac{w'(x)w(x+1) - w(x)w'(x+1)}{w^2(x+1)} > 0 \quad \Leftrightarrow \quad w'(x)w(x+1) > w(x)w'(x+1) \ . \tag{2.47}$$

For all $x > \frac{5}{6}$ we can iterate the above relationship to obtain the inequality chain

$$\begin{aligned} w'(x) > \frac{w(x)\,w'(x+1)}{w(x+1)} > \frac{w(x)}{w(x+1)}\,\frac{w(x+1)}{w(x+2)}\,w'(x+2) \\ > \cdots > \frac{w(x)}{w(x+n)}\,w'(x+n) \ , n \in \mathbb{N} \ , \end{aligned} \tag{2.48}$$

which is valid because of Lemma 2.5.4. By considering the limit $n \mapsto \infty$, we obtain

$$w'(x) > \lim_{n \mapsto \infty} \frac{w(x)}{w(x+n)}\,w'(x+n) = 0 \ , \tag{2.49}$$

which is valid due to (2.40) and Lemma 2.5.7. □

By analyzing $w(x)$ and its relation to $W(x)$, we have seen thus far that $w(x)$ is strictly increasing for all $x > \frac{5}{6}$ as well as $w(\frac{3}{2}) = 1$. Hence, it remains to show $w(x) \leq 1$ for all $\frac{1}{2} \leq x \leq \frac{5}{6}$. This is substantiated by the following lemma.

Lemma 2.5.9. *For all $\frac{1}{2} \leq x \leq 1$, the inequality $V(x) \leq w(1)$ holds.*

Proof. By using Definition 2.5.3 and the identity $\Gamma(\frac{3}{2}) = \frac{\sqrt{\pi}}{2}$, we obtain the equation

$$\frac{V(x)}{w(1)} = \frac{\pi x}{\sqrt{3x - \frac{1}{2}}\sqrt{3x+1}}\,\frac{\sqrt{10}}{\pi} = \frac{\sqrt{10}\,x}{\sqrt{3x - \frac{1}{2}}\sqrt{3x+1}} \ . \tag{2.50}$$

Now, we determine for which values of x the right hand ratio is equal to or less than one. This leads to

$$x^2 - \frac{3}{2}x + \frac{1}{2} \leq 0 \quad \Leftrightarrow \quad \frac{1}{2} \leq x \leq 1 \ . \tag{2.51}$$

□

Corollary 2.5.10. *For all $x \geq \frac{3}{2}$, the inequality $w(x) \geq 1$ holds. If $\frac{1}{2} \leq x < \frac{3}{2}$, then $w(x) \leq 1$ holds.*

Proof. The auxiliary function w is strictly increasing for all $x > \frac{5}{6}$ due to Lemma 2.5.8, and it is equal to one at $x = \frac{3}{2}$ due to Lemma 2.5.4. Thus, we obtain $w(x) \geq 1$ for all $x \geq \frac{3}{2}$ as well as $w(x) \leq 1$ for all $\frac{5}{6} < x < \frac{3}{2}$. Furthermore, according to its increasing property, the inequality $w(x + \frac{1}{2}) \geq w(1)$ holds for all $x \geq \frac{1}{2}$. Hence, from Definition 2.5.3 and Lemma 2.5.9 it follows

$$w(x) = \frac{V(x)}{w(x + \frac{1}{2})} \leq \frac{V(x)}{w(1)} \leq 1 \quad \Leftrightarrow \quad \frac{1}{2} \leq x \leq 1 \ . \tag{2.52}$$

In summary, the inequality $w(x) \leq 1$ holds for all $\frac{1}{2} \leq x < \frac{3}{2}$. □

Proof of Theorem 2.5.2. From Corollary 2.5.10, we deduce that $w(x) \geq 1$ for all $x \geq \frac{3}{2}$ and $w(x) \leq 1$ for all $\frac{1}{2} \leq x < \frac{3}{2}$. By replacing x in $w(x)$ with $\frac{x+2}{2}$ we obtain Theorem 2.5.2. □

The function $\tau(x)$ and its bounds from Theorem 2.5.2 are used in Chapter 6 in order to prove and adapt some main theorems concerning the error probability in communication over Nakagami-distributed fading channels.

3 Optimum Power Allocation for Passive Sensor Networks

In the current chapter, we investigate the power allocation problem in distributed sensor networks that are used for passive radar applications. The signal emitted by a target is independently observed by the sensor nodes (SNs). Since these local observations are noisy and thus unreliable, they are fused together as a single reliable observation at a remotely located fusion center to increase the overall system performance. The fusion center uses the best linear unbiased estimator in order to accurately estimate the present target signal. This setup is illustrated in Figure 3.1, whose technical components will be specified in detail later. We demonstrate that the corresponding optimization of the power allocation leads to a signomial program which is in general very difficult to solve, see Definition 2.3.4. Nonetheless, by using the proposed system architecture, fusion rule and objective function we are able to optimize the power allocation analytically and can hence present a closed-form solution to the power allocation problem in amplify-and-forward sensor networks. The key idea is the utilization of the average deviation between the estimated and the actual signal as a metric for defining the objective function. Since the power consumption of the entire network may be limited in various aspects, three different cases of power constraints are discussed and compared with each other. They lead to explicit policies for the optimal power allocation. This briefly describes the main contributions of the current chapter.

A potential application of our approach is passive multiple-radar sensing, where an unknown target signal shall be estimated, detected or classified. Instead of using a complex single-radar system, this task is carried out by a network of cheap and energy-efficient SNs; the so called *distributed passive multiple-radar system* (DPMRS). To achieve comparable system performance, a fusion center combines a multitude of local observations into a single reliable quantity. DPMRSs have worthwhile applications nowadays. Physicists use this type of radar to detect or to determine specific characteristics of particles, for example, in the neutrino telescope '*IceCube Neutrino Observatory*' at the Amundsen-Scott South Pole Station [30] in Antarctica, where a network with over 5000 nodes is implemented. They also use such radars for radio astronomy to study celestial objects, for instance in the '*Karl G. Jansky Very Large Array*' of the National Radio Astronomy Observatory [31] in Socorro County, New Mexico. Many other applications of DPMRSs are military [32] and some few are also for civil uses [33]. Because of the significance of DPMRSs it is important to investigate the power allocation within the sensor network in order to improve the radar accuracy while the overall energy consumption is kept constant [34]. Especially for comparing the performance of different power allocation methods in energy-efficient systems, the

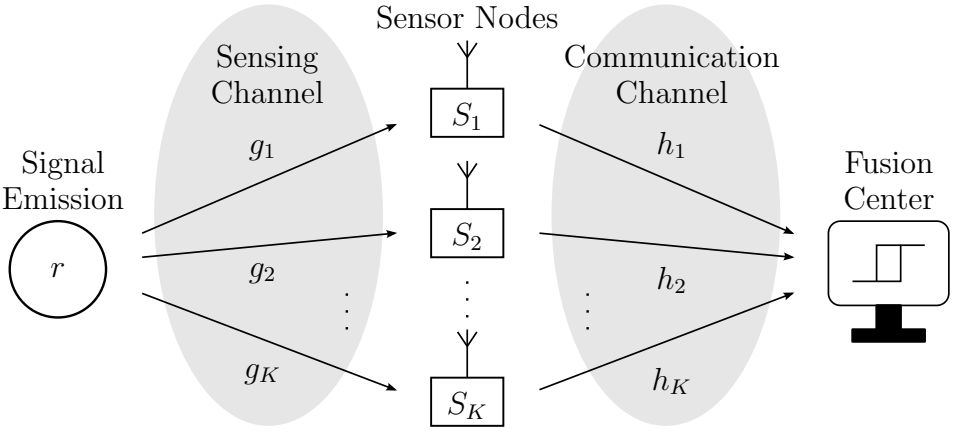

Figure 3.1: Abstract representation of the distributed sensor network.

problem arises how to allocate a given sum-power to the distributed SNs for transmitting the local observations to a fusion center. The problem of finding an optimum power allocation for a distributed radar system and a closed-form of the objective function is extremely hard, and it is even harder to determine optimal points under certain constraints. The main difficulty is associated with finding an explicit representation of the objective function as mentioned in [35]. In the more recent past, some methods have been proposed to solve the power allocation problem. In particular, the authors in [36] investigated some game-theoretic approaches to solve the power allocation problem not focussing on DPMRSs. The investigation of the power allocation only for localization is treated in [37], [38] and [39]. A similar allocation problem is also treated in [40]. The capacity bound and the corresponding power allocation in a single relay system is considered in [41] and [42]. An optimal solution for the power allocation problem is given in [4], where an active radar is considered instead of a passive radar system. Moreover, an optimum power allocation scheme for decode-and-forward parallel relay networks, instead of amplify-and-forward sensor networks, is investigated in [43].

We start with a description of the underlying technical system in the next section. Subsequently, the power allocation problem is specified and analytically solved. The achieved results are then discussed and carefully compared with each other.

3.1 Overview and Technical System Description

At any instance of time, a network of $K \in \mathbb{N}$ independent and spatially distributed SNs receives random observations. If a target signal r is present, then the received power at SN S_k is a part of the emitted power from the jointly observed target source. The type of the source and its signal need not to be specified in detail; only the quadratic mean of the emitted target signal should be known by the observation network. The received signal at each SN is weighted by the corresponding channel coefficient and disturbed by additive noise. It is obvious that the sensing channel is wireless. All SNs continuously take samples from the disturbed received signal and amplify them

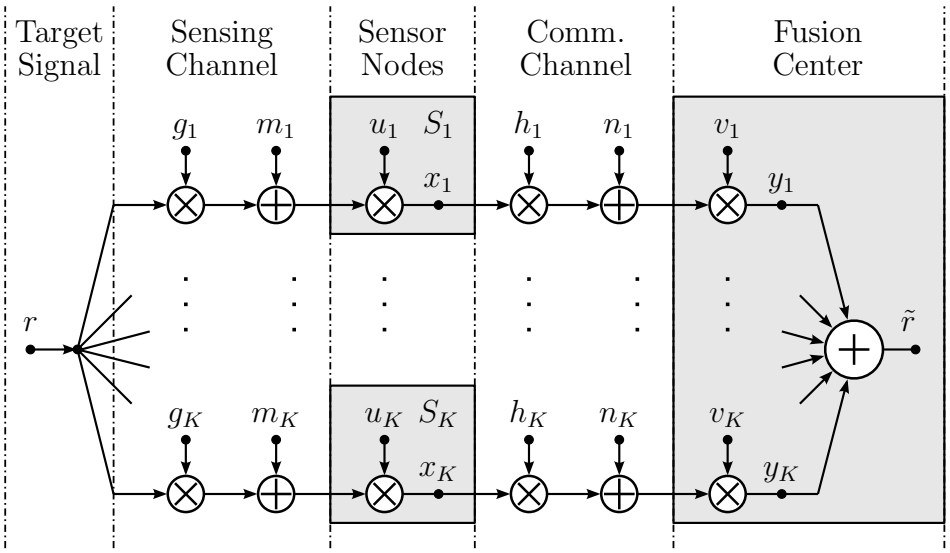

Figure 3.2: System model of the distributed passive sensor network.

without any additional data processing. The local observations of the target signal at each SN are then transmitted to a fusion center which is placed in a remote location. We assume that SNs have only limited sum-power available for communication to the fusion center and that each SN is in addition limited in its transmission power-range. The communication to the fusion center is performed by using distinct waveforms for each SN so as to distinguish the communication of different SNs. Each waveform has to be suitably chosen in order to suppress inter-user (inter-node) interference at the fusion center. Hence, the K received signals at the fusion center are uncorrelated and are assumed to be conditionally independent. Each received signal at the fusion center is influenced by the corresponding channel coefficient and additive noise, as well. The communication channel between the SNs and the fusion center can either be wireless or wired. The disturbed received signals at the fusion center are weighted and combined together in order to obtain a single reliable observation $\tilde{r}$ of the actual target signal r. Note that we disregard time delays within all transmissions and assume synchronized data communication.

In the following subsections, we mathematically describe the underlying system model that is depicted in Figure 3.2. The continuous-time system is modeled by its discrete-time equivalent, where the sampling rate of the corresponding signals is equal to the target observation rate, for the sake of simplicity.

3.1.1 Target signal

In the following, only limited information about the target signal is assumed. We suppose that only the quadratic mean $R \coloneqq \mathcal{E}[|r|^2]$ with $0 < R < \infty$ of the complex-valued target signal r is well known. This knowledge is sufficient for subsequent calculations. Furthermore, the target signal during each observation step is assumed to be static.

3.1.2 Sensing channel

Each propagation path of the sensing channel is described by a corresponding random channel coefficient g_k. For the investigation of the power allocation problem, the concrete realization of the channel coefficients is needed and hence can also be used for postprocessing of the received signals at the SNs. We assume that the channel coefficients are complex-valued and static during each target observation step. Furthermore, the coherence time of sensing channels is assumed to be much longer than the whole length of the classification process. Thus, the expected value and the quadratic mean of each coefficient during each observation step can be assumed to be equal to their instantaneous values, i.e., $\mathcal{E}[g_k] = g_k$ and $\mathcal{E}[|g_k|^2] = |g_k|^2$. In practice, it is often difficult to measure or estimate these coefficients because the network is passive and is hence not able to sound the channel actively. Thus, the results of the present chapter are applicable for scenarios where the channel coefficients can somehow be estimated accurately during each observation process or they are nearly deterministic and thus can be measured before starting the radar task. This is the case, for example for the neutrino telescope where the SNs are installed deep in the icecap.

Furthermore, the channel coefficients are assumed to be jointly independent. Note that the channel coefficients include the radar cross section, the influence of the antenna, the impact of the filters, as well as all additional attenuation of the target signal.

At the input of each SN, the disturbance is modeled by the complex-valued additive white Gaussian noise (AWGN) m_k with zero mean and finite variance $M_k \coloneqq \mathcal{E}[|m_k|^2]$ for all k. Note that the channel coefficient and the noise on the same propagation path are also jointly independent.

3.1.3 Sensor nodes

We model each SN by an amplify-and-forward unit, where the ratio of the output to the input signal is described by the non-negative real-valued amplification factor u_k which is assumed to be constant over the whole bandwidth and power-range. Thus, the output signal and the expected value of its instantaneous power are described by

$$x_k \coloneqq (r g_k + m_k) u_k \,, \;\; k \in \mathbb{F}_K \tag{3.1}$$

and

$$X_k \coloneqq \mathcal{E}[|x_k|^2] = (R|g_k|^2 + M_k) u_k^2 \,, \;\; k \in \mathbb{F}_K \,, \tag{3.2}$$

respectively. The amplification factor is an adjustable parameter and will be determined later by the power allocation procedure. The average power consumption of each node is approximately equal to its average output power X_k, if the input signal is negligible in comparison to the output signal and if the nodes have smart power components with low-power dissipation loss. Hereon based, we assume that equality between X_k and the average power consumption of each node is ensured. In the present chapter, we also assume that the output power-range of each SN is individually limited by P_k and that the average power consumption of all SNs together is limited by the sum-power

constraint P_{tot}. This entails the constraints

$$X_k \leq P_k \;\Leftrightarrow\; (R|g_k|^2 + M_k)u_k^2 \leq P_k\,,\; k \in \mathbb{F}_K \tag{3.3}$$

and

$$\sum_{k=1}^{K} X_k \leq P_{\text{tot}} \;\Leftrightarrow\; \sum_{k=1}^{K}(R|g_k|^2 + M_k)u_k^2 \leq P_{\text{tot}}\;. \tag{3.4}$$

Note that the sum-power constraint P_{tot} is a reasonable approach to compare energy-efficient radar systems.

3.1.4 Communication channel

Analogous to the sensing channel, each propagation path of the communication channel is described by a corresponding random channel coefficient h_k. But in contrast to the sensing channel, the concrete realization of the communication channel coefficients is measurable by using pilot sequences at each SN. Accordingly, the channel coefficients can be used for postprocessing of received signals at the fusion center. We assume that the channel coefficients are complex-valued and static during each target observation step. Furthermore, the coherence time of communication channels is also assumed to be much longer than the whole length of the classification process. Thus, the expected value and the quadratic mean of each channel coefficient can be assumed to be equal to their instantaneous values, i.e., $\mathcal{E}[h_k] = h_k$ and $\mathcal{E}[|h_k|^2] = |h_k|^2$. Furthermore, the channel coefficients are assumed to be jointly independent. Note that the channel coefficients include the influence of the antenna, the impact of the filters, as well as all additional attenuation of the corresponding sensor signal.

At the input of the fusion center, the disturbance on each communication path is modeled by the complex-valued AWGN n_k with zero mean and finite variance $N_k \coloneqq \mathcal{E}[|n_k|^2]$ for all k. Note that the channel coefficient and the noise on the same propagation path are also jointly independent.

3.1.5 Fusion center

The fusion center combines the different local observations into a single reliable one by applying a linear combiner. Thus, the received signals are weighted with the complex-valued factors v_k and summed up to yield an estimate $\tilde{r}$ of the actual target signal r. In this way, we obtain

$$y_k \coloneqq \big((rg_k + m_k)u_k h_k + n_k\big)v_k\,,\; k \in \mathbb{F}_K\,, \tag{3.5}$$

and hence,

$$\tilde{r} \coloneqq \sum_{k=1}^{K} y_k = r\sum_{k=1}^{K} g_k u_k h_k v_k + \sum_{k=1}^{K}(m_k u_k h_k + n_k)v_k\,. \tag{3.6}$$

Note that each weight can be written as $v_k = |v_k|\exp(\mathrm{j}\,\vartheta_k)$, $k \in \mathbb{F}_K$, where ϑ_k is a real-valued number which represents the phase of the corresponding weight.

Note that the fusion center can separate the input streams because the communication channel is either wired or the data communication is performed by distinct waveforms for each SN. Consequently, if the communication channel is wireless then a matched-filter bank is essential at the input of the fusion center to separate the data streams of different SNs. In addition, we do not consider inter-user (inter-node) interferences at the fusion center because of the distinct waveform choices.

In order to obtain a single reliable observation at the fusion center, the value $\tilde{r}$ should be a good estimate for the present target signal r. Thus, we optimize the amplification factors u_k and the weights v_k in order to minimize the average absolute deviation between $\tilde{r}$ and the true target signal r. This optimization procedure is elaborated in the next section.

3.1.6 Remarks to the system model

All described assumptions are necessary to obtain a framework suitable for analyzing the power allocation problem, without studying detection, classification and estimation problems in specific systems and their settings.

The accurate estimation of all channel coefficients is necessary for both the radar process and the power allocation. Sometimes it is not possible to estimate the transmission channels; consequently the channel coefficients g_k and h_k remain unknown. In such cases, the radar usually fails to perform its task.

Since the channel coefficients g_k are in practice difficult to estimate or to determine, our approach rather shows theoretical aspects of the power allocation than the practical realization and implementation. Hence, the presented results act as theoretical bounds and references for comparing real radar systems.

Moreover, since the coherence time of communication channels as well as sensing channels is assumed to be much longer than the whole length of the classification process, the proposed power allocation method is applicable only for scenarios with slow-fading channels.

Note that only the linear fusion rule together with the proposed objective function enable an optimization of power allocation in closed-form. The optimization of power allocation is extremely hard for general fusion rules and objective functions.

The introduced system model describes a baseband communication system without considering time, phase and frequency synchronization problems.

In order to distinguish the current operating mode of each SN in what follows, we say a SN is *inactive* or *idle* if the allocated power is zero. We say the SN is *active* if the allocated power is positive. Finally, we say a SN is *saturated* if the limitation of its output power-range is equal to the allocated power, i.e., $P_k = X_k$.

An overview of all notations, that are needed for the description of each observation process, may be found in the glossary.

3.2 Power Optimization

In this section, we introduce the power optimization problem and consecutively present its analytical solutions for different power constraints. First, we investigate the case where the average transmission power of each SN is limited by the output power-range limitation $P_k \in \mathbb{R}_+,\ k \in \mathbb{F}_K$. Afterwards, we present the analytical solution of the power allocation problem for the case where only a sum-power constraint $P_{\text{tot}} \in \mathbb{R}_+$ for the cumulative sum of the expected power consumption of each SN is given. Finally, we extend the power allocation problem to the case where both constraints simultaneously hold and present the corresponding optimal solution.

3.2.1 Optimization problem

As mentioned in the last section, the value $\tilde{r}$ should be a good estimate for the present target signal r. In particular, we aim at finding estimators $\tilde{r}$ of minimum mean squared error in the class of unbiased estimators for each r.

The estimate $\tilde{r}$ is unbiased simultaneously for each r, if $\mathcal{E}[\tilde{r} - r] = 0$ holds, i.e., from equation (3.6) we obtain the identity

$$\sum_{k=1}^{K} g_k u_k h_k v_k = 1\,. \tag{3.7}$$

This identity is our first constraint in what follows. Note that the mean of the second sum in (3.6) vanishes since the noise is zero-mean. Recall that both random variables g_k and h_k are assumed to be known constants, because the coherence time of both channels is assumed to be much longer than the target observation time. Note that equation (3.7) is complex-valued and may be separated as

$$\sum_{k=1}^{K} u_k \,|v_k g_k h_k| \cos(\vartheta_k + \phi_k) = 1 \tag{3.8}$$

and

$$\sum_{k=1}^{K} u_k \,|v_k g_k h_k| \sin(\vartheta_k + \phi_k) = 0\,, \tag{3.9}$$

where ϑ_k and ϕ_k are phases of v_k and $g_k h_k$, respectively.

The objective is to minimize the mean squared error $\mathcal{E}[|\tilde{r} - r|^2]$. By using equation (3.6) and the identity (3.7) we may write the objective function as

$$V \coloneqq \mathcal{E}\big[|\tilde{r} - r|^2\big] = \sum_{k=1}^{K} \big(M_k u_k^2 |h_k|^2 + N_k\big)|v_k|^2\,. \tag{3.10}$$

Note that (3.10) is only valid if m_k and n_k are white and jointly independent.

As mentioned in the last section, each SN has an output power-range limitation and the expected overall power consumption is also limited. Hence, the objective function is also subject to (3.3) and (3.4), which are our second and last constraints, respectively.

In summary, the optimization problem is to minimize the mean squared error in (3.10) with respect to u_k and v_k, subject to constraints (3.3), (3.4), (3.8) and (3.9), i.e.:

$$
\begin{aligned}
\underset{\mathbf{u},\mathbf{v},\boldsymbol{\vartheta}}{\text{minimize}} \quad & \sum_{k=1}^{K} \big(M_k u_k^2 |h_k|^2 + N_k\big)|v_k|^2 \\
\text{subject to} \quad & \sum_{k=1}^{K} u_k \,|v_k g_k h_k| \cos(\vartheta_k + \phi_k) = 1\,, \\
& \sum_{k=1}^{K} u_k \,|v_k g_k h_k| \sin(\vartheta_k + \phi_k) = 0\,, \\
& \sum_{k=1}^{K} (R|g_k|^2 + M_k) u_k^2 \leq P_{\text{tot}}\,, \\
& (R|g_k|^2 + M_k) u_k^2 \leq P_k\,,\ k \in \mathbb{F}_K\,, \\
& \mathbf{u} \in \mathbb{R}_+^K,\ \mathbf{v} \in \mathbb{C}^K,\ \boldsymbol{\vartheta} \in [0, 2\pi]^K\,.
\end{aligned}
$$

Note that this optimization problem is a signomial program, which is a generalization of geometric programming, and is thus non-convex in general, see Definition 2.3.3.

3.2.2 Power allocation subject to individual power constraints

In this subsection, we consider the power allocation problem only subject to individual power constraints (3.3). In order to solve the optimization problem, we use the method of Lagrangian multipliers and obtain the corresponding constrained Lagrange function (relaxation with respect to the range of u_k and $|v_k|$) as

$$
\begin{aligned}
L_1(u_k, |v_k|, \vartheta_k; \eta_1, \eta_2, \lambda_k; \varrho_k) \coloneqq & \sum_{k=1}^{K} \big(M_k u_k^2 |h_k|^2 + N_k\big)|v_k|^2 \\
& + \left(1 - \sum_{k=1}^{K} u_k \,|v_k g_k h_k| \cos(\vartheta_k + \phi_k)\right)\eta_1 \\
& - \sum_{k=1}^{K} u_k \,|v_k g_k h_k| \sin(\vartheta_k + \phi_k)\eta_2 \\
& + \sum_{k=1}^{K} \big(P_k - \varrho_k - (R|g_k|^2 + M_k) u_k^2\big)\lambda_k\,,
\end{aligned}
\tag{3.11}
$$

where η_1, η_2 and λ_k are Lagrange multipliers while ϱ_k are slack variables.

Equation (3.9) is only then satisfied, if all phases $\vartheta_k + \phi_k$ are equal to $q_k\pi$, $q_k \in \mathbb{Z}$, for all $k \in \mathbb{F}_K$. If there were a better solution for $\vartheta_k + \phi_k$, then the first partial derivatives of L_1 with respect to ϑ_k would vanish for that solution, due to the continuity of trigonometric functions. But the first derivatives would lead to equations $\eta_1 \sin(\vartheta_k + \phi_k) = \eta_2 \cos(\vartheta_k + \phi_k)$ which cannot simultaneously satisfy both equations (3.8) and (3.9) for all η_1 and η_2. Thus, $q_k\pi$ is the unique solution. Hence, we may consequently write a modified Lagrange function as

$$\begin{aligned}\tilde{L}_1(u_k, |v_k|, q_k; \eta_1, \lambda_k; \varrho_k) \coloneqq &\sum_{k=1}^{K} \big(M_k u_k^2 |h_k|^2 + N_k\big)|v_k|^2 \\ &+ \left(1 - \sum_{k=1}^{K} u_k \, |v_k g_k h_k| \cos(q_k\pi)\right)\eta_1 \\ &+ \sum_{k=1}^{K} \big(P_k - \varrho_k - (R|g_k|^2 + M_k)u_k^2\big)\lambda_k \,.\end{aligned} \tag{3.12}$$

At any stationary point of $\tilde{L}_1$, all first partial derivatives must vanish, if they exist. This leads to

$$\frac{\partial \tilde{L}_1}{\partial |v_l|} = 2\big(M_l u_l^2 |h_l|^2 + N_l\big)|v_l| - \eta_1 u_l \, |g_l h_l| \cos(q_l\pi) = 0 \,, \;\; l \in \mathbb{F}_K \,, \tag{3.13}$$

$$\frac{\partial \tilde{L}_1}{\partial \eta_1} = 1 - \sum_{k=1}^{K} u_k \, |v_k g_k h_k| \cos(q_k\pi) = 0 \tag{3.14}$$

and

$$\frac{\partial \tilde{L}_1}{\partial \lambda_l} = P_l - \varrho_l - (R|g_l|^2 + M_l)u_l^2 = 0 \,, \;\; l \in \mathbb{F}_K \,. \tag{3.15}$$

Note that the first partial derivative with respect to u_l, $l \in \mathbb{F}_K$, is not needed because the optimal point lies on the boundary of the feasible set, as we will see later.

By multiplying (3.13) with $|v_l|$, summing up the outcome over all l, and using the identities (3.8) and (3.10), we obtain

$$\eta_1 = 2V \tag{3.16}$$

which is a positive real number due to definition of V. Because of the last relationship and according to (3.13), the value of $\cos(q_k\pi)$ must be a positive number and hence each q_k must be an even integer number. Thus, we can choose $q_k^\star = 0$ for all $k \in \mathbb{F}_K$ without loss of generality and conclude

$$\vartheta_k^\star = -\phi_k \,, \;\; k \in \mathbb{F}_K \,. \tag{3.17}$$

This solution gives the identity $\cos(q_k^\star\pi) = 1$ which can be incorporated into (3.13) and (3.14).

From (3.13), we deduce the equation

$$|v_l| = \frac{\eta_1}{2} \frac{u_l |g_l h_l|}{M_l u_l^2 |h_l|^2 + N_l} \,. \tag{3.18}$$

Incorporating (3.18) into (3.14) yields the relationship

$$\frac{\eta_1}{2} = \left(\sum_{k=1}^{K} \frac{u_k^2 |g_k h_k|^2}{M_k u_k^2 |h_k|^2 + N_k} \right)^{-1} . \tag{3.19}$$

In turn, we replace $\frac{\eta_1}{2}$ in (3.18) with (3.19) and obtain

$$|v_l| = \frac{u_l |g_l h_l|}{M_l u_l^2 |h_l|^2 + N_l} \left(\sum_{k=1}^{K} \frac{u_k^2 |g_k h_k|^2}{M_k u_k^2 |h_k|^2 + N_k} \right)^{-1} . \tag{3.20}$$

Note that for each feasible u_k, $k \in \mathbb{F}_K$, equation (3.20) describes a feasible value for each $|v_k|$. Since for each $u_k > 0$ the relation $|v_k| > 0$ consequently follows, the feasible optimal values of each $|v_k| > 0$ are not on the boundary $|v_k| = 0$. Thus, finding optimal values for each u_k, $k \in \mathbb{F}_K$, leads to optimum values for each $|v_k|$, $k \in \mathbb{F}_K$, due to the convexity of (3.11) with respect to each $|v_k|$. Hence, finding a unique global optimum for u_k, $k \in \mathbb{F}_K$, yields the sufficient condition for the globally optimal solution of the minimization problem (3.11).

By considering (3.16) and (3.19), we deduce the identity

$$V = \frac{\eta_1}{2} = \left(\sum_{k=1}^{K} \frac{u_k^2 |g_k h_k|^2}{M_k u_k^2 |h_k|^2 + N_k} \right)^{-1} , \tag{3.21}$$

where the objective and η_1 consequently are in terms of u_k. For the sake of simplicity and in order to compare the results later on, we define two new quantities as[1]

$$\alpha_k \coloneqq \sqrt{\frac{|g_k|^2}{M_k}} \;\Rightarrow\; \alpha_k \in \mathbb{R}_+ \,, \tag{3.22}$$

and

$$\beta_k \coloneqq \sqrt{\frac{N_k (R|g_k|^2 + M_k)}{M_k |h_k|^2}} \;\Rightarrow\; \beta_k \in \mathbb{R}_+ \,. \tag{3.23}$$

By using the new quantities as well as (3.2), the equation (3.21) is equivalent to

$$V = \frac{\eta_1}{2} = \left(\sum_{k=1}^{K} \frac{\alpha_k^2 X_k}{X_k + \beta_k^2} \right)^{-1} . \tag{3.24}$$

[1] We will discuss the physical interpretation of all important parameters and quantities in Subsection 3.3.1.

According to (3.2) and (3.15), we calculate the factors

$$u_l^2 = \frac{P_l - \varrho_l}{R|g_l|^2 + M_l} \quad \Leftrightarrow \quad X_l = P_l - \varrho_l \,,\ l \in \mathbb{F}_K \,, \tag{3.25}$$

where ϱ_l is in the range $0 \leq \varrho_l \leq P_l$. After replacing u_k^2 in (3.21), or X_k in (3.24), with (3.25), we obtain

$$V = \left(\sum_{l=1}^{K} \frac{\alpha_l^2}{1 + \frac{\beta_l^2}{P_l - \varrho_l}} \right)^{-1} , \tag{3.26}$$

which is strictly increasing with respect to ϱ_l and strictly decreasing with respect to K. Thus, minimizing it leads to

$$\varrho_k^\star = 0 \quad \Leftrightarrow \quad X_k^\star = P_k \,,\ k \in \mathbb{F}_K \,, \tag{3.27}$$

$$u_k^\star = \sqrt{\frac{P_k}{R|g_k|^2 + M_k}} \,,\ k \in \mathbb{F}_K \,, \tag{3.28}$$

and hence,

$$V^\star = \left(\sum_{k=1}^{K} \frac{\alpha_k^2 P_k}{P_k + \beta_k^2} \right)^{-1} . \tag{3.29}$$

By incorporating (3.28) into (3.20), we infer

$$|v_k^\star| = \frac{V^\star |g_k h_k| \sqrt{P_k} \sqrt{R|g_k|^2 + M_k}}{M_k |h_k|^2 P_k + N_k (R|g_k|^2 + M_k)} \,,\ k \in \mathbb{F}_K \,. \tag{3.30}$$

Since $\varrho_k^\star = 0$ for all $k \in \mathbb{F}_K$, it follows that the optimal point lies on the boundary of each u_k, $k \in \mathbb{F}_K$, especially on a corner, where the first derivatives of the objective with respect to u_k do not vanish in general.

The equations (3.17) and (3.27)–(3.30) describe the optimal solution of the power allocation problem only subject to the output power-range limitation per SN and hence are the main contribution of the present subsection.

Note that the global optimality of the obtained results is trivially reasoned, first because of the optimization of the relaxed Lagrange function (3.11) with extended range of all variables, and second since the global optimum point of the relaxed problem coincides with the original range of all variables.

3.2.3 Interpretation of the solution

The solution of the power allocation problem has the following interpretation: All K SNs are active and their output power is equal to their output power-range limitation P_k.

By using the amplification factors from (3.28) and the weights from (3.17) and (3.30), the single observation $\tilde{r}$ is an estimator of minimum mean squared error in the class of unbiased estimators for the target signal r. Hence, we obtain the estimate

$$\tilde{r} = r + \sum_{k=1}^{K} (m_k u_k^\star h_k + n_k) v_k^\star \tag{3.31}$$

from (3.6). The above equation shows that $\tilde{r}$ is equal to r with some additional noise. Hence, $\tilde{r} - r$ is a zero-mean Gaussian random variable with an absolute variance of $V^\star$, see (3.10) and (3.29).

Note that $\tilde{r}$ is an unbiased estimator for r due to constraint (3.7). The same methodology seems to be applicable to minimize the mean squared error without restricting ourself to unbiased estimators. Obviously, the optimal value of V will then be smaller than that in (3.29).

3.2.4 Power allocation subject to the sum-power constraint

In this subsection, we consider the power allocation problem only subject to the sum-power constraint from (3.4), which yields the constrained Lagrange function (relaxation with respect to the range of u_k and $|v_k|$)

$$\begin{aligned} L_2(u_k, |v_k|, \vartheta_k; \eta_1, \eta_2, \tau; \xi) \coloneqq & \sum_{k=1}^{K} \big(M_k u_k^2 |h_k|^2 + N_k\big) |v_k|^2 \\ & + \left(1 - \sum_{k=1}^{K} u_k \, |v_k g_k h_k| \cos(\vartheta_k + \phi_k)\right) \eta_1 \\ & - \sum_{k=1}^{K} u_k \, |v_k g_k h_k| \sin(\vartheta_k + \phi_k) \eta_2 \\ & + \left(P_{\text{tot}} - \xi - \sum_{k=1}^{K} (R|g_k|^2 + M_k) u_k^2\right) \tau \end{aligned} \tag{3.32}$$

with additional Lagrange multiplier τ and slack variable ξ.

The first partial derivatives of (3.32) with respect to $|v_l|$ and η_1 are identical to those which are given in (3.13) and (3.14), respectively. Thus, we also obtain the same results for ϑ_l, $|v_l|$ and V as given in (3.17), (3.20) and (3.24), respectively. Consequently, only the sum-power constraint remains unused, thus far.

Note that because of the same statement as mentioned in Subsection 3.2.2, finding a unique global optimum for u_k, $k \in \mathbb{F}_K$, yields the sufficient condition for the globally optimal solution of the minimization problem (3.32).

Since the minimization of the objective V in (3.24) is equivalent to the minimization of $\tilde{V} \coloneqq -V^{-1}$, we only consider the objective $\tilde{V}$ in the following. Initially, we highlight

three important properties of $\tilde{V}$. First, the new objective function is strictly decreasing with respect to each X_k, $k \in \mathbb{F}_K$, which can easily be seen from the representation

$$\tilde{V} = -\sum_{k=1}^{K} \frac{\alpha_k^2}{1+\beta_k^2/X_k}\,. \tag{3.33}$$

Second, the objective function is twice differentiable with respect to each X_k, $k \in \mathbb{F}_K$, because its first and second derivatives exist. Third, the objective function is a jointly convex function with respect to $(X_k)_{k\in\mathbb{F}_K}$ which can be shown by calculating the corresponding Hessian $\mathbf{H} \coloneqq (\frac{\partial^2 \tilde{V}}{\partial X_k \partial X_l})_{k,l\in\mathbb{F}_K}$. The Hessian is positive-definite because of

$$\mathbf{z}'\mathbf{H}\mathbf{z} = \sum_{k=1}^{K} \frac{2\alpha_k^2\beta_k^2 z_k^2}{(X_k+\beta_k^2)^3} > 0\,, \quad \forall\ \mathbf{z} \coloneqq (z_1, z_2, \ldots, z_K)' \in \mathbb{R}^K \setminus \{\mathbf{0}\}\,. \tag{3.34}$$

By considering (3.2), we obtain that the remaining sum-power constraint in (3.32) is linear and thus also jointly convex with respect to $(X_k)_{k\in\mathbb{F}_K}$. Hence, we are able to define a modified convex minimization problem by the unconstrained Lagrangian

$$\tilde{L}_2(X_k;\varphi_k,\tau) \coloneqq -\sum_{k=1}^{K} \frac{\alpha_k^2 X_k}{X_k+\beta_k^2} - \sum_{k=1}^{K} X_k\varphi_k + \left(-P_{\text{tot}} + \sum_{k=1}^{K} X_k\right)\tau\,, \tag{3.35}$$

where φ_k and τ are Lagrange multipliers. Note that the Lagrange multiplier η_1 is positive because of (3.16), and the equality $\sin(\vartheta_k^\star + \phi_k) = 0$ holds due to (3.17). Hence, both constraints (3.8) and (3.9) are discarded in (3.35). Furthermore, the sum-power constraint can be considered as an equality constraint instead of an inequality constraint due to monotonicity of the objective, see also complementary slackness theorem [19].

In order to solve the new convex optimization problem in (3.35), we apply the *Karush-Kuhn-Tucker* (KKT) conditions which are sufficient for optimality in convex problems, see Definition 2.3.2. These conditions are as follows for any optimal point $(X_k^\star, \varphi_k^\star, \tau^\star)$:

$$X_l^\star \geq 0\,, \qquad l \in \mathbb{F}_K\,, \tag{3.36a}$$
$$\varphi_l^\star \geq 0\,, \qquad l \in \mathbb{F}_K\,, \tag{3.36b}$$
$$X_l^\star\varphi_l^\star = 0\,, \qquad l \in \mathbb{F}_K\,, \tag{3.36c}$$
$$\sum_{k=1}^{K} X_k^\star = P_{\text{tot}}\,, \tag{3.36d}$$

and

$$\frac{\partial \tilde{L}_2}{\partial X_l} = -\frac{\alpha_l^2\beta_l^2}{(X_l^\star+\beta_l^2)^2} - \varphi_l^\star + \tau^\star = 0\,, \qquad l \in \mathbb{F}_K\,. \tag{3.36e}$$

If $X_l^\star = 0$ for some $l \in \mathbb{F}_K$, then from (3.36b) and (3.36e) the inequality $\frac{1}{\sqrt{\tau^\star}} \leq \frac{\beta_l}{\alpha_l}$ follows. If $X_l^\star > 0$, then from (3.36c) and (3.36e) both the equality $X_l^\star = \alpha_l \beta_l \big(\frac{1}{\sqrt{\tau^\star}} - \frac{\beta_l}{\alpha_l}\big)$ and the inequality $\frac{1}{\sqrt{\tau^\star}} > \frac{\beta_l}{\alpha_l}$ follow. In summary, we may write

$$X_k^\star = \max\Big\{0, \alpha_k \beta_k \Big(\chi^\star - \frac{\beta_k}{\alpha_k}\Big)\Big\}\,,\ k \in \mathbb{F}_K\,, \tag{3.37}$$

where χ is a replacement for $\frac{1}{\sqrt{\tau}}$ and is called *water-level*. The water-level is implicitly determined by equation (3.36d) and gives the subset $\mathbb{K}$ of active SNs. By considering (3.37), we achieve the necessary and sufficient condition to select the right subset $\mathbb{K}$ of SNs for which the inequality $X_k^\star > 0$ with $k \in \mathbb{K}$ holds. Hence, all SNs for which the inequality $\chi^\star > \frac{\beta_k}{\alpha_k}$ holds are active. In order to determine their corresponding number $\tilde{K}$ as well as the water-level, we re-index all SNs such that the inequality chain

$$c_k \coloneqq \frac{\beta_k}{\alpha_k} = \sqrt{\frac{N_k(R|g_k|^2 + M_k)}{|g_k h_k|^2}} \leq c_{k+1}\,,\ k \in \mathbb{F}_{K-1}\,, \tag{3.38}$$

holds. Then, we can assume that the first $\tilde{K}$ SNs are members of $\mathbb{K} = \mathbb{F}_{\tilde{K}} \subseteq \mathbb{F}_K$. By inserting (3.37) into (3.36d), we obtain

$$\chi^\star = \frac{P_{\text{tot}} + \sum\limits_{k=1}^{\tilde{K}} \beta_k^2}{\sum\limits_{k=1}^{\tilde{K}} \alpha_k \beta_k}\,. \tag{3.39}$$

Due to the increasing order of the sequence $\frac{\beta_k}{\alpha_k}$ for all $k \in \mathbb{F}_K$, the inequality $\frac{\beta_{\tilde{K}}}{\alpha_{\tilde{K}}} < \chi^\star$ must hold for the last active SN. Thus, the number $\tilde{K}$ of active SNs is the largest integer number for which the inequality

$$P_{\text{tot}} > \sum_{k=1}^{\tilde{K}} \alpha_k \beta_k \Big(\frac{\beta_{\tilde{K}}}{\alpha_{\tilde{K}}} - \frac{\beta_k}{\alpha_k}\Big) \tag{3.40}$$

holds.

After incorporating $X_k^\star$ and $\chi^\star$ into (3.2), (3.24) and (3.20), we obtain

$$u_k^\star = \sqrt{\frac{1}{M_k|h_k|^2}\left(\chi^\star \sqrt{\frac{|g_k h_k|^2 N_k}{R|g_k|^2 + M_k}} - N_k\right)}\,,\ k \in \mathbb{K}\,, \tag{3.41}$$

$$V^\star = \left(\sum_{k=1}^{\tilde{K}} \alpha_k^2 - \frac{1}{\chi^\star} \sum_{k=1}^{\tilde{K}} \alpha_k \beta_k\right)^{-1}\,, \tag{3.42}$$

$$|v_k^\star| = \frac{V^\star u_k^\star |g_k h_k|}{M_k (u_k^\star)^2 |h_k|^2 + N_k}\,,\ k \in \mathbb{K}\,, \tag{3.43}$$

and

$$u_k^\star = v_k^\star = 0\,,\ k \in \mathbb{F}_K \setminus \mathbb{K}\,. \tag{3.44}$$

Note that by using the above results, the corresponding fusion rule is simplified by discarding the influence of inactive SNs from the fusion rule. The fusion rule (3.6) becomes

$$\tilde{r} = \sum_{k=1}^{\tilde{K}} y_k\,. \tag{3.45}$$

The equations (3.17), (3.37) and (3.41)–(3.44) together with (3.38)–(3.40) describe the optimal solution of the power allocation problem only subject to the sum-power constraint and hence are the main contribution of the present subsection.

As mentioned in Subsection 3.2.2, the global optimality of the obtained results is also trivially reasoned, first because of the optimization of the relaxed Lagrange function (3.32) with extended range of all variables, and second since the global optimum point of the relaxed problem coincides with the original range of all variables.

3.2.5 Comparison of the solutions

In contrast to the case, where each SN has its individual output power-range limitation, only some of the SNs are active. In this case, the amount of the available sum-power is inadequate to supply all SNs at their output power-range limitation. Hence, the available sum-power can only be allocated to those SNs, which are members of the subset $\mathbb{K}$, while all other SNs remain inactive, since their information reliability is too poor to be considered for data fusion. The best SNs are those which have the smallest ratio of $c_k = \frac{\beta_k}{\alpha_k}$ that can be interpreted as *disturbance-intensity*[2]. This means that for the identification of the most reliable SNs in a certain network, that can be modeled as depicted in Figure 3.2, only the quantities c_k are important. As one can see from (3.38), the best SNs have the largest absolute values of channel coefficients as well as the smallest noise powers. Consequently, SNs which are placed closely to the target source and fusion center are more reliable than other SNs[3].

Note that the obtained results are quite similar but not identical to the well-known *water-filling* solution, see [44]. The distinction arises from our definition of the water-level χ which differs from the general description.

3.2.6 Power allocation subject to both types of power constraints

In the current subsection, we consider the optimization problem from Subsection 3.2.1 subject to all constraints, i.e., sum-power constraint as well as output power-range

[2]We give the name *disturbance-intensity* to c_k because it behaves intrinsically like noise. In Section 3.3 we will introduce a normalized version of c_k and call it *reliability-function*.

[3]We will discuss the relationship between the geometrical position of SNs and their disturbance-intensity in Subsection 4.3 exemplary for an active radar system.

limitation per SN. Two of three different cases can be singled out and reduced to preceding instances.

First, if $\sum_{k\in\mathbb{F}_K} P_k \leq P_{\text{tot}}$, then the sum-power constraint is irrelevant, because the feasible set is only limited by the individual output power-range constraints. Hence, the power allocation problem reduces to the one described in Subsection 3.2.2 with results given in (3.17) and (3.27)–(3.30). The only difference is that possibly a part of the available sum-power remains unallocated and cannot be used.

Secondly, if $P_{\text{tot}} \leq \min\limits_{k\in\mathbb{F}_K}\{P_k\}$, then the individual output power-range constraints are irrelevant, because the feasible set is only limited by the sum-power constraint. Hence, the power allocation problem is equal to the one described in Subsection 3.2.4 with results given in (3.17), (3.37) and (3.41)–(3.44) with (3.38)–(3.40).

The case of $\min\limits_{k\in\mathbb{F}_K}\{P_k\} < P_{\text{tot}} < \sum_{k\in\mathbb{F}_K} P_k$ is the most challenging one. The amount of available sum-power is on the one hand inadequate to supply all SNs at their output power-range limitation. Hence, the available sum-power can only be allocated to some of the SNs while all others remain inactive, as we will see later. On the other hand, some of the SNs can attain the limit of their individual output power-range and are thus saturated. Therefore, we have to separate all active SNs into two groups. The first group contains all active SNs, which are saturated, and is denoted by the subset $\mathbb{K}_{\text{sat}}$. The second group contains all other active SNs, which operate within their output power-range, and is denoted by the subset $\mathbb{K}_{\text{lin}}$. Note that both subsets are disjoint and their union is the subset of all active SNs, i.e., $\mathbb{K} = \mathbb{K}_{\text{sat}} \cup \mathbb{K}_{\text{lin}}$ and $\mathbb{K}_{\text{sat}} \cap \mathbb{K}_{\text{lin}} = \emptyset$ with $\mathbb{K} \subseteq \mathbb{F}_K$.

Since the optimization problem under investigation is the same as in Subsection 3.2.4 with additional constraints, $X_k \leq P_k$ for all $k \in \mathbb{K}$, the first few problem-solving steps are equal to those described in Subsection 3.2.4. Thus, we can start to formulate an extended convex minimization problem by the unconstrained Lagrangian

$$\begin{aligned}\tilde{L}_3(X_k;\varphi_k,\lambda_k,\tau) \coloneqq &-\sum_{k\in\mathbb{F}_K}\frac{\alpha_k^2 X_k}{X_k+\beta_k^2} - \sum_{k\in\mathbb{F}_K} X_k\varphi_k \\ &+\sum_{k\in\mathbb{F}_K}(-P_k+X_k)\lambda_k + \left(-P_{\text{tot}}+\sum_{k\in\mathbb{F}_K} X_k\right)\tau\,.\end{aligned} \tag{3.46}$$

In order to solve the problem in (3.46), we again apply the KKT conditions which

are as follows, for any optimal point $(X_k^\star, \varphi_k^\star, \lambda_k^\star, \tau^\star)$:

$$X_l^\star \geq 0\,, \qquad l \in \mathbb{F}_K\,, \tag{3.47a}$$
$$X_l^\star \leq P_l\,, \qquad l \in \mathbb{F}_K\,, \tag{3.47b}$$
$$\varphi_l^\star \geq 0\,, \qquad l \in \mathbb{F}_K\,, \tag{3.47c}$$
$$\lambda_l^\star \geq 0\,, \qquad l \in \mathbb{F}_K\,, \tag{3.47d}$$
$$X_l^\star \varphi_l^\star = 0\,, \qquad l \in \mathbb{F}_K\,, \tag{3.47e}$$
$$(X_l^\star - P_l)\lambda_l^\star = 0\,, \qquad l \in \mathbb{F}_K\,, \tag{3.47f}$$
$$\sum_{k \in \mathbb{F}_K} X_k^\star = P_{\text{tot}}\,, \tag{3.47g}$$

and

$$\frac{\partial \tilde{L}_3}{\partial X_l} = -\frac{\alpha_l^2 \beta_l^2}{(X_l^\star + \beta_l^2)^2} - \varphi_l^\star + \lambda_l^\star + \tau^\star = 0\,, \qquad l \in \mathbb{F}_K. \tag{3.47h}$$

If $X_l^\star = 0$ for some $l \in \mathbb{F}_K$, then from (3.47c), (3.47f) and (3.47h) the inequality $\frac{1}{\sqrt{\tau^\star}} \leq \frac{\beta_l}{\alpha_l}$ follows. If $X_l^\star = P_l$ for some $l \in \mathbb{F}_K$, then from (3.47d), (3.47e) and (3.47h) the inequality $\frac{1}{\sqrt{\tau^\star}} \geq \frac{P_l + \beta_l^2}{\alpha_l \beta_l}$ follows. If $0 < X_l^\star < P_l$, then from (3.47e), (3.47f) and (3.47h) both the equality $X_l^\star = \alpha_l \beta_l \big(\frac{1}{\sqrt{\tau^\star}} - \frac{\beta_l}{\alpha_l}\big)$ and the inequality $\frac{1}{\sqrt{\tau^\star}} > \frac{\beta_l}{\alpha_l}$ follow. In summary, we may write

$$X_k^\star = \max\Big\{0, \min\Big\{P_k, \alpha_k \beta_k \Big(\chi_{\mathbb{K}}^\star - \frac{\beta_k}{\alpha_k}\Big)\Big\}\Big\},\ k \in \mathbb{F}_K, \tag{3.48}$$

where $\chi_{\mathbb{K}}$ is again a replacement for $\frac{1}{\sqrt{\tau}}$. The water-level $\chi_{\mathbb{K}}$ depends on the subset $\mathbb{K}$ of active SNs and can iteratively be determined by equation (3.47g), as we will show later on. By considering (3.48), we achieve the necessary and sufficient condition to select the right subset $\mathbb{K}$ of SNs for which the inequality $X_k^\star > 0$ with $k \in \mathbb{K}$ holds. Hence, all SNs for which the inequality $\chi_{\mathbb{K}}^\star > \frac{\beta_k}{\alpha_k}$ holds are active. In order to determine the corresponding water-level, we insert (3.48) into (3.47g) and infer

$$\chi_{\mathbb{K}}^\star = \frac{P_{\text{tot}} - \sum\limits_{k \in \mathbb{K}_{\text{sat}}} P_k + \sum\limits_{k \in \mathbb{K}_{\text{lin}}} \beta_k^2}{\sum\limits_{k \in \mathbb{K}_{\text{lin}}} \alpha_k \beta_k}\,. \tag{3.49}$$

As one can see, for calculation of the water-level both subsets $\mathbb{K}_{\text{sat}}$ and $\mathbb{K}_{\text{lin}}$ are needed, and vice versa, we need the water-level to determine the subset of all active SNs. Thus, if we are able to determine which SNs are active, and in turn, which of them are saturated, then we can continue solving the optimization problem in (3.46). Again, it is possible to sort the SNs by $\frac{\beta_k}{\alpha_k}$ in ascending order and extend the approach from Subsection 3.2.4 by particular consideration on saturated SNs, as in (3.48). However, we want to present an efficient algorithm which avoids the sorting of SNs. Note that the proposed algorithm

can be implemented more efficiently, but for sake of comprehensibility, we have chosen the given representation. For developing fast and more efficient algorithms we refer readers to the discussion in Subsection 3.2.8. In the following, we will describe and show that Algorithm 1 optimally determines both subsets $\mathbb{K}_{\text{sat}}$ and $\mathbb{K}_{\text{lin}}$ of active SNs.

Algorithm 1 Separation of active sensor nodes

$\mathbb{K}_{\text{sat}} \leftarrow \emptyset$
$P_{\text{remain}} \leftarrow P_{\text{tot}}$
repeat
  $\mathbb{K}_{\text{lin}} \leftarrow \mathbb{F}_K \setminus \mathbb{K}_{\text{sat}}$
  repeat
    $\chi_{\mathbb{K}} \leftarrow \frac{P_{\text{remain}}+\sum_{k\in\mathbb{K}_{\text{lin}}}\beta_k^2}{\sum_{k\in\mathbb{K}_{\text{lin}}}\alpha_k\beta_k}$ ▷ see (3.49)
    $X_k \leftarrow \alpha_k\beta_k\big(\chi_{\mathbb{K}} - \frac{\beta_k}{\alpha_k}\big)\,,\ k \in \mathbb{K}_{\text{lin}}$ ▷ see (3.48)
    $\mathbb{K}_{-} \leftarrow \{k \in \mathbb{K}_{\text{lin}} \mid X_k \leq 0\}$
    $\mathbb{K}_{\text{lin}} \leftarrow \mathbb{K}_{\text{lin}} \setminus \mathbb{K}_{-}$
  until $\mathbb{K}_{-} = \emptyset$ **or** $\mathbb{K}_{\text{lin}} = \emptyset$
  $\mathbb{K}_{+} \leftarrow \{k \in \mathbb{K}_{\text{lin}} \mid X_k \geq P_k\}$
  $\mathbb{K}_{\text{sat}} \leftarrow \mathbb{K}_{\text{sat}} \cup \mathbb{K}_{+}$
  $P_{\text{remain}} \leftarrow P_{\text{remain}} - \sum_{k\in\mathbb{K}_{+}} P_k$
until $\mathbb{K}_{+} = \emptyset$ **or** $\mathbb{K}_{\text{sat}} = \mathbb{F}_K$
$\mathbb{K}_{\text{lin}} \leftarrow \mathbb{K}_{\text{lin}} \setminus \mathbb{K}_{+}$
return $(\mathbb{K}_{\text{lin}}, \mathbb{K}_{\text{sat}})$

First, the results from Subsection 3.2.4 are applied in the inner loop to achieve an optimal solution neglecting the individual output power-range constraints. In the first repetition, this is performed on all SNs and in each further repetition on all SNs included in the subset $\mathbb{K}_{\text{lin}}$ in order to determine all active SNs of the current repetition. At the end of the inner loop, $\mathbb{K}_{+}$ contains all SNs which operate at their individual output power-range limitation. They are added to the subset of all saturated SNs $\mathbb{K}_{\text{sat}}$. At last, the power used by those SNs is subtracted from the available sum-power which gives the remaining sum-power P_{remain}. With these updated settings, the procedure is repeated until, for a new set of active SNs, the subset $\mathbb{K}_{+}$ of saturated SNs is empty. Note that $\mathbb{K}_{\text{sat}}$ might be empty. We will show later on, that the water-level, and thereby, the power for each non-saturated SN is increasing in each repetition of the outer loop. Thus, it is possible that SNs may become active, and hence, all non-saturated SNs are potential active candidates. Finally, we get the (optimal) subsets of active SNs to continue solving the optimization problem in (3.46).

After determination of $\mathbb{K}_{\text{sat}}$ and $\mathbb{K}_{\text{lin}}$, we use (3.49) to calculate $\chi_{\mathbb{K}}^{\star}$, and subsequently, by inserting $\chi_{\mathbb{K}}^{\star}$ into (3.48) we obtain $X_k^{\star}$. In turn, from (3.2), (3.24) and (3.20), we infer

$$u_k^{\star} = \sqrt{\frac{P_k}{R|g_k|^2 + M_k}}\,,\ k \in \mathbb{K}_{\text{sat}}\,, \tag{3.50}$$

$$u_k^\star = \sqrt{\frac{1}{M_k|h_k|^2}\left(\chi_{\mathbb{K}}^\star\sqrt{\frac{|g_k h_k|^2 N_k}{R|g_k|^2+M_k}}-N_k\right)}\,,\ k\in\mathbb{K}_{\text{lin}}\,, \tag{3.51}$$

$$V^\star = \left(\sum_{k\in\mathbb{K}_{\text{sat}}}\frac{\alpha_k^2 P_k}{P_k+\beta_k^2}+\sum_{k\in\mathbb{K}_{\text{lin}}}\alpha_k^2-\frac{1}{\chi_{\mathbb{K}}^\star}\sum_{k\in\mathbb{K}_{\text{lin}}}\alpha_k\beta_k\right)^{-1}, \tag{3.52}$$

$$|v_k^\star| = \frac{V^\star u_k^\star |g_k h_k|}{M_k (u_k^\star)^2|h_k|^2+N_k}\,,\ k\in\mathbb{K}\,, \tag{3.53}$$

and

$$u_k^\star = v_k^\star = 0\,,\ k\in\mathbb{F}_K\setminus\mathbb{K}\,. \tag{3.54}$$

The equations (3.17), (3.48) and (3.50)–(3.54) together with (3.49) and Algorithm 1 describe the optimal solution of the power allocation problem and hence are the main contribution of the present subsection. Note that the obtained results are obviously mixtures of both solutions from Subsection 3.2.2 and 3.2.4.

An example for the described power allocation is depicted in Figure 3.3. Obviously, Algorithm 1 terminates and gives a feasible solution. Moreover, the final water-level is as in (3.49) if $\mathbb{K}_{\text{sat}}$ is optimally determined. However, $\mathbb{K}_{\text{sat}}$ is easily given for all SNs, because the condition $\chi_{\mathbb{K}}^\star \geq \frac{P_l+\beta_l^2}{\alpha_l\beta_l}$ is satisfied for all saturated SNs if the water-level is increasing in each step of the outer loop. Hence, for optimality of Algorithm 1, it only remains to show that in each repetition the water-level is increasing in the outer loop. Note that in contrast the water-level is decreasing in the inner loop in each repetition. These statements are discussed in the following.

Whenever $X_l \geq P_l$ holds for a specific $l\in\mathbb{K}_{\text{lin}}$, from (3.48) the inequality

$$X_l = \alpha_l\beta_l\Big(\chi_{\mathbb{K}}-\frac{\beta_l}{\alpha_l}\Big)\geq P_l \ \Rightarrow\ -P_l-\beta_l^2\geq-\alpha_l\beta_l\chi_{\mathbb{K}} \tag{3.55}$$

follows. Using $\tilde{\mathbb{K}} \coloneqq \tilde{\mathbb{K}}_{\text{lin}}\cup\tilde{\mathbb{K}}_{\text{sat}}$ with $\tilde{\mathbb{K}}_{\text{lin}} \coloneqq \mathbb{K}_{\text{lin}}\setminus\{l\}$ and $\tilde{\mathbb{K}}_{\text{sat}} \coloneqq \mathbb{K}_{\text{sat}}\cup\{l\}$, definition (3.49), and the inequality (3.55), easily leads to

$$\begin{aligned}\chi_{\tilde{\mathbb{K}}} &= \frac{P_{\text{tot}}-\sum\limits_{k\in\tilde{\mathbb{K}}_{\text{sat}}}P_k+\sum\limits_{k\in\tilde{\mathbb{K}}_{\text{lin}}}\beta_k^2}{\sum\limits_{k\in\tilde{\mathbb{K}}_{\text{lin}}}\alpha_k\beta_k} = \frac{-P_l-\beta_l^2+P_{\text{tot}}-\sum\limits_{k\in\mathbb{K}_{\text{sat}}}P_k+\sum\limits_{k\in\mathbb{K}_{\text{lin}}}\beta_k^2}{-\alpha_l\beta_l+\sum\limits_{k\in\mathbb{K}_{\text{lin}}}\alpha_k\beta_k}\\ &\geq \frac{P_{\text{tot}}-\sum\limits_{k\in\mathbb{K}_{\text{sat}}}P_k+\sum\limits_{k\in\mathbb{K}_{\text{lin}}}\beta_k^2}{\sum\limits_{k\in\mathbb{K}_{\text{lin}}}\alpha_k\beta_k} = \chi_{\mathbb{K}}\,.\end{aligned} \tag{3.56}$$

This means that omitting the power exceeding SN l and recalculating the water-level leads to an increased water-level and in turn to more transmission power for all remaining SNs. It might even turn out that new SNs may be included in the subset $\mathbb{K}_{\text{lin}}$ of active candidates. However, this will just slow down, but not stop the increase of the water-level. In summary, the individual transmission power of each SN, which is

a member of $\mathbb{K}_{\text{lin}}$, will be higher than in the previous loop. The same argumentation can now be used to show that omitting the SN l with non-positive allocated power and recalculating the water-level leads to a decreased water-level.

Whenever $X_l \leq 0$ holds for a specific $l \in \mathbb{K}_{\text{lin}}$, from (3.48) the inequality

$$X_l = \alpha_l \beta_l \Big(\chi_{\mathbb{K}} - \frac{\beta_l}{\alpha_l} \Big) \leq 0 \;\Rightarrow\; -\beta_l^2 \leq -\alpha_l \beta_l \chi_{\mathbb{K}} \tag{3.57}$$

follows. Using the above set definitions, the definition (3.49), and the inequality (3.57), easily leads to

$$\begin{aligned} \chi_{\mathbb{K}\setminus\{l\}} &= \frac{P_{\text{tot}} - \sum\limits_{k\in\mathbb{K}_{\text{sat}}} P_k + \sum\limits_{k\in\tilde{\mathbb{K}}_{\text{lin}}} \beta_k^2}{\sum\limits_{k\in\tilde{\mathbb{K}}_{\text{lin}}} \alpha_k\beta_k} = \frac{-\beta_l^2 + P_{\text{tot}} - \sum\limits_{k\in\mathbb{K}_{\text{sat}}} P_k + \sum\limits_{k\in\mathbb{K}_{\text{lin}}} \beta_k^2}{-\alpha_l\beta_l + \sum\limits_{k\in\mathbb{K}_{\text{lin}}} \alpha_k\beta_k} \\ &\leq \frac{P_{\text{tot}} - \sum\limits_{k\in\mathbb{K}_{\text{sat}}} P_k + \sum\limits_{k\in\mathbb{K}_{\text{lin}}} \beta_k^2}{\sum\limits_{k\in\mathbb{K}_{\text{lin}}} \alpha_k\beta_k} = \chi_{\mathbb{K}} \,. \end{aligned} \tag{3.58}$$

Note that increasing the power of inactive SNs cannot lead to an improvement of our solution, because this would contradict the results from Subsection 3.2.4.

3.2.7 Discussion of the solutions

The main difficulty and difference between both solutions from Subsection 3.2.4 and 3.2.6 arises from the individual output power-range limitation per SN. In both cases, the operating mode of each SN mainly depends on its corresponding disturbance-intensity $\frac{\beta_k}{\alpha_k}$ which is easily visible from (3.37) and (3.48). In Subsection 3.2.6, we have given an efficient algorithm which avoids the sorting of SNs by their disturbance-intensity. Moreover, the same algorithm might be applied to the problem in Subsection 3.2.4, as well. In practice, it is hence more complicated to calculate the optimal solution of the power allocation problem from Subsection 3.2.6 than that from Subsection 3.2.4. Eventually, the complexity of obtained results is not surprising, because all discussed optimization problems are signomial programs, as mentioned in Subsection 3.2.1. Nevertheless, they lead to convex optimization problems which are analytically solvable in closed-form.

3.2.8 Another access for identifying reliable sensor nodes

In order to develop fast algorithms for separating all SNs into one of the subsets $\mathbb{K}_{\text{lin}}$, $\mathbb{K}_{\text{sat}}$ or $\mathbb{F}_K \setminus \mathbb{K}$, we again consider all equations in (3.47) in the following. Furthermore, if the negative value of the first derivative of the equivalent objective (3.33) is denoted by

$$\tilde{J}_k(X_k) \coloneqq \frac{\alpha_k^2\beta_k^2}{(X_k+\beta_k^2)^2} \,,\; k \in \mathbb{F}_K \,, \tag{3.59}$$

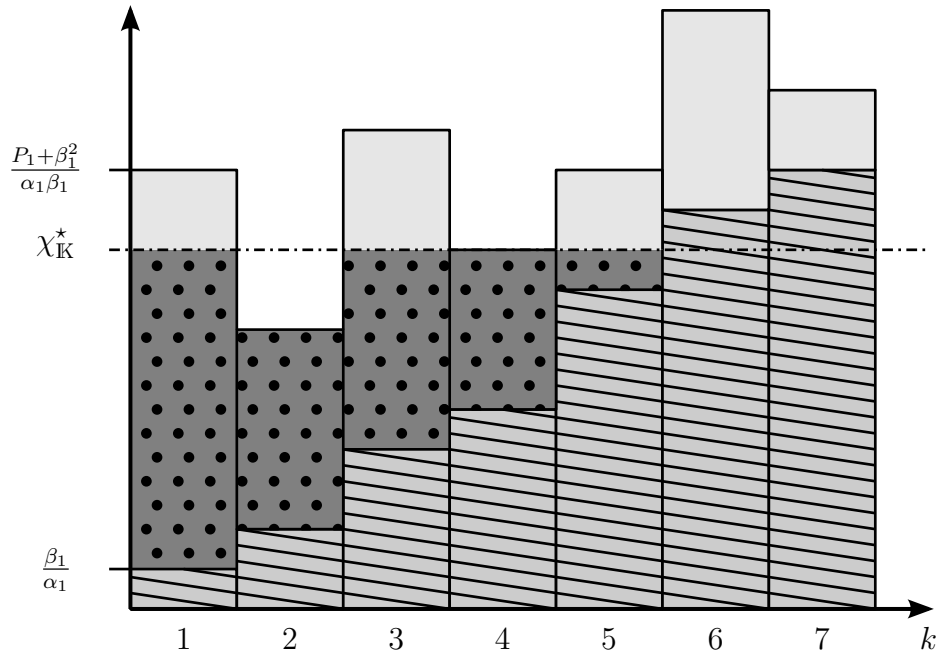

Figure 3.3: An example of the power allocation for $K = 7$ sensor nodes is shown. The dotted dark area is the allocated power. The sensor nodes are ascendingly ordered with respect to disturbance-intensities β_k/α_k. The striped area represents the individual disturbance-intensities. The bright shaded area is the remaining part of the available output power-range for each sensor node. The water-level $\chi^\star_{\mathbb{K}}$ is indicated by the dashed line, where the number of active sensor nodes is equal to $\tilde{K} = 5$. Sensor 2 and 4 are saturated, while 6 and 7 are inactive.

then the double inequality

$$\tilde{J}_k(P_k) < \tilde{J}_k(X_k) < \tilde{J}_k(0)\,,\ k \in \mathbb{F}_K\,, \tag{3.60}$$

follows trivially for all $0 < X_k < P_k$. Now, we can highlight three important cases, which yield new conditions for the current operating mode of each SN:

1. For $0 < X_k^\star < P_k$ both equations $\varphi_k^\star = 0$ and $\lambda_k^\star = 0$ result from KKT conditions (3.47e) and (3.47f), respectively. By considering (3.47h), this implies $\tilde{J}_k(X_k^\star) = \tau^\star$ for all $k \in \mathbb{K}_{\text{lin}}$, which means that the slope of the objective (3.33) with respect to each X_k is equal to $\tau^\star$ for all SNs included in $\mathbb{K}_{\text{lin}}$. We infer

$$\tilde{J}_k(P_k) < \tilde{J}_k(X_k^\star) = \tau^\star < \tilde{J}_k(0)\,,\ k \in \mathbb{K}_{\text{lin}}\,. \tag{3.61}$$

2. For $X_k^\star = P_k$ both relationships $\varphi_k^\star = 0$ and $\lambda_k^\star \geq 0$ result from KKT conditions (3.47e) and (3.47d), respectively. Again by considering (3.47h), it follows that $\tilde{J}_k(P_k) \geq \tilde{J}_k(P_k) - \lambda_k^\star = \tau^\star$ for all $k \in \mathbb{K}_{\text{sat}}$. This means that if a SN is saturated, then its corresponding slope $\tilde{J}_k(X_k^\star)$ at $X_k^\star = P_k$ is greater than or equal to $\tau^\star$. We obtain

$$\tau^\star \leq \tilde{J}_k(P_k) = \tilde{J}_k(X_k^\star) < \tilde{J}_k(0)\,,\ k \in \mathbb{K}_{\text{sat}}\,. \tag{3.62}$$

3. For $X_k^\star = 0$ both relationships $\varphi_k^\star \geq 0$ and $\lambda_k^\star = 0$ result from KKT conditions (3.47c) and (3.47f), respectively. Again by considering (3.47h), it follows that $\tilde{J}_k(0) \leq \tilde{J}_k(0) + \varphi_k^\star = \tau^\star$ for all $k \in \mathbb{F}_K \setminus \mathbb{K}$. This means that if a SN is inactive, then its corresponding slope $\tilde{J}_k(X_k^\star)$ at $X_k^\star = 0$ is less than or equal to $\tau^\star$. It follows that

$$\tilde{J}_k(P_k) < \tilde{J}_k(X_k^\star) = \tilde{J}_k(0) \leq \tau^\star\,,\ k \in \mathbb{F}_K \setminus \mathbb{K}\,. \tag{3.63}$$

From the new conditions (3.61), (3.62) and (3.63), we derive a main region for the value of $\tau^\star$ as

$$\max_{\substack{k\in\mathbb{K}_{\text{lin}}\\ l\in\mathbb{F}_K\setminus\mathbb{K}}} \left\{\tilde{J}_k(P_k), \tilde{J}_l(0)\right\} \leq \tau^\star \leq \min_{\substack{k\in\mathbb{K}_{\text{lin}}\\ l\in\mathbb{K}_{\text{sat}}}} \left\{\tilde{J}_k(0), \tilde{J}_l(P_l)\right\}. \tag{3.64}$$

By the aid of condition (3.64), we see that sorting the sequence $\left(\tilde{J}_k(P_k), \tilde{J}_k(0)\right)_{k\in\mathbb{F}_K}$ monotonically yields a new searching sequence in which each element represents a boundary for the unknown value $\tau^\star$. By applying successively a bisection method, the new sequence of boundaries can rapidly be searched for a proper region. If $\tau^\star$ is a member of the current region, then its value can be verified by the evaluation of (3.49) and the relationship $\chi_{\mathbb{K}}^\star = \frac{1}{\sqrt{\tau^\star}}$. If the evaluated value of $\tau^\star$ overlaps with the current region, the search is successful and no more iteration (searching) steps are needed. Otherwise, the next region is to be tested. The choice of next regions may either be performed by *divide and conquer* methods or by stochastic algorithms, which use the previous evaluated value of $\tau^\star$ to estimate the next position of a proper region within the searching sequence. A detailed description and discussion of the divide and conquer method can be found in [11].

3.3 Technical Interpretation and Visualization of Results

As derived in Subsection 3.2.6, the power allocation problem in its general form is analytically solved in closed-form. For achieving these results, we only have focused on the mathematical analysis, synthesis and methods. However, it is difficult to gain insight into the technical analysis, synthesis and description, due to the presented form. In this section, we introduce physical parameters in order to highlight important aspects of the underlying system and technically interpret the optimal solution of the power allocation problem. Following this, selected results are visualized by corresponding curves.

3.3.1 Measurable parameters and technical interpretation of results

In practice, a common measurable quantity is the signal-to-noise ratio, which is in principle determinable by simple physical methods and experiments. We denote the

signal-to-noise ratio at the receiver of each SN and the signal-to-noise ratio at the receiver of the fusion center respectively by

$$\mathrm{SNR}_k^{\mathrm{S}} \coloneqq \frac{R|g_k|^2}{M_k} \quad \text{and} \quad \mathrm{SNR}_k^{\mathrm{C}}(X) \coloneqq \frac{X|h_k|^2}{N_k}\,, \quad 0 < X \leq \min\{P_k, P_{\mathrm{tot}}\}\,,\ k \in \mathbb{F}_K\,. \tag{3.65}$$

Since the output power at each SN is adjustable and is determined by the optimal method of power allocation, the specific value of $\mathrm{SNR}_k^{\mathrm{C}}(X)$ depends on the setting of X. Alternatively, the signal-to-noise ratio at the receiver of the fusion center can be described by both $\mathrm{SNR}_k^{\mathrm{S}}$ and $\mathrm{SNR}_k^{\mathrm{C}}(X)$ as

$$\mathrm{SNR}_k(X) \coloneqq \frac{\mathcal{E}[|rg_ku_kh_k|^2]}{\mathcal{E}[|m_ku_kh_k + n_k|^2]} = \frac{\mathrm{SNR}_k^{\mathrm{S}} \cdot \mathrm{SNR}_k^{\mathrm{C}}(X)}{1 + \mathrm{SNR}_k^{\mathrm{S}} + \mathrm{SNR}_k^{\mathrm{C}}(X)}\,,\ k \in \mathbb{F}_K\,. \tag{3.66}$$

The ratio $\mathrm{SNR}_k(X)$ is the signal-to-noise ratio of the k^{th} path from the target to the fusion center. By substitution of α_k and β_k by

$$\alpha_k = \sqrt{\frac{\mathrm{SNR}_k^{\mathrm{S}}}{R}} \quad \text{and} \quad \beta_k = \sqrt{P \cdot \frac{1 + \mathrm{SNR}_k^{\mathrm{S}}}{\mathrm{SNR}_k^{\mathrm{C}}(P)}}\,, \quad k \in \mathbb{F}_K, \tag{3.67}$$

and incorporating all these into equation (3.24), we obtain a signal-to-noise ratio at the output of the fusion center as given by

$$\mathrm{SNR}_{\mathrm{tot}} \coloneqq \frac{R}{V} = \sum_{k \in \mathbb{F}_K} \frac{\mathrm{SNR}_k^{\mathrm{S}} \cdot \mathrm{SNR}_k^{\mathrm{C}}(X_k)}{1 + \mathrm{SNR}_k^{\mathrm{S}} + \mathrm{SNR}_k^{\mathrm{C}}(X_k)} = \sum_{k \in \mathbb{F}_K} \mathrm{SNR}_k(X_k)\,. \tag{3.68}$$

This means that after optimization of the variables v_k, only the path signal-to-noise ratios SNR_k are important at the fusion center. In this way, the minimization of the mean square deviation in (3.10) leads to the maximization of the total signal-to-noise ratio at the output of the fusion center. This is equivalent with

$$\begin{aligned} \underset{\mathbf{X}}{\text{maximize}} \quad & \sum_{k \in \mathbb{F}_K} \frac{\mathrm{SNR}_k^{\mathrm{S}} \cdot \mathrm{SNR}_k^{\mathrm{C}}(X_k)}{1 + \mathrm{SNR}_k^{\mathrm{S}} + \mathrm{SNR}_k^{\mathrm{C}}(X_k)} \\ \text{subject to} \quad & \sum_{k \in \mathbb{F}_K} X_k \leq P_{\mathrm{tot}}\,,\ X_k \leq P_k\,,\ k \in \mathbb{F}_K\,,\ \mathbf{X} \in \mathbb{R}_+^K\,. \end{aligned} \tag{3.69}$$

The role of u_k, which is connected with X_k by (3.2), is to optimize the cumulative sum of all path signal-to-noise ratios SNR_k. Since the signal-to-noise ratio of each path is concave with respect to its $\mathrm{SNR}_k^{\mathrm{C}}(X_k)$ due to the discussion in Subsection 3.2.6, and in turn the above maximization problem is a concave problem, we obtain the results

$$\mathrm{SNR}_{\mathrm{tot}}^{\star} \coloneqq \frac{R}{V^{\star}} = \sum_{k \in \mathbb{K}_{\mathrm{sat}}} \frac{\mathrm{SNR}_k^{\mathrm{S}} \cdot \mathrm{SNR}_k^{\mathrm{C}}(P_k)}{1 + \mathrm{SNR}_k^{\mathrm{S}} + \mathrm{SNR}_k^{\mathrm{C}}(P_k)} + \sum_{k \in \mathbb{K}_{\mathrm{lin}}} \mathrm{SNR}_k^{\mathrm{S}} \cdot \left(1 - \frac{\tilde{c}_k(X)}{\tilde{\chi}_{\mathbb{K}}^{\star}(X)}\right) \tag{3.70}$$

and

$$X_k^\star = \max\Big\{0, \min\Big\{P_k, X \cdot \tilde{c}_k(X) \cdot \mathrm{SNR}_k^{\mathrm{S}} \cdot \big(\tilde{\chi}_{\mathbb{K}}^\star(X) - \tilde{c}_k(X)\big)\Big\}\Big\},\ k \in \mathbb{F}_K, \tag{3.71}$$

where two new definitions

$$\tilde{c}_k(X) \coloneqq \frac{c_k}{\sqrt{RX}} = \sqrt{\frac{1+\mathrm{SNR}_k^{\mathrm{S}}}{\mathrm{SNR}_k^{\mathrm{S}} \cdot \mathrm{SNR}_k^{\mathrm{C}}(X)}}\,, \quad k \in \mathbb{F}_K, \tag{3.72}$$

and

$$\tilde{\chi}_{\mathbb{K}}^\star(X) \coloneqq \frac{\chi_{\mathbb{K}}^\star}{\sqrt{RX}} = \frac{P_{\mathrm{tot}} - \sum\limits_{k\in\mathbb{K}_{\mathrm{sat}}} P_k + X \cdot \sum\limits_{k\in\mathbb{K}_{\mathrm{lin}}} \frac{1+\mathrm{SNR}_k^{\mathrm{S}}}{\mathrm{SNR}_k^{\mathrm{C}}(X)}}{X \cdot \sum\limits_{k\in\mathbb{K}_{\mathrm{lin}}} \sqrt{\frac{\mathrm{SNR}_k^{\mathrm{S}} \cdot (1+\mathrm{SNR}_k^{\mathrm{S}})}{\mathrm{SNR}_k^{\mathrm{C}}(X)}}}\,, \tag{3.73}$$

are used. In contrast to previous definitions, both the new *reliability-function* $\tilde{c}_k(X)$ and the new normalized water-level $\tilde{\chi}_{\mathbb{K}}^\star(X)$ are unitless. In fact, both $\tilde{c}_k(X)$ and $\tilde{\chi}_{\mathbb{K}}^\star(X)$ depend on the particular value of X, however, for any choice of X within the range $0 < X \leq \min\{P_k, P_{\mathrm{tot}}\}$, $k \in \mathbb{F}_K$, the values in (3.70) and (3.71) will not change. The best choice for X is to be equal to $\min_k\{P_k, P_{\mathrm{tot}}\}$, because in this case no SN will exceed its power limitation P_k.

The interpretation behind the optimal power allocation is that at the globally optimum the passive sensor network combines independently all signal-to-noise ratios $\mathrm{SNR}_k^{\mathrm{S}}$, $\mathrm{SNR}_k^{\mathrm{C}}(P_k)$ and $\mathrm{SNR}_k^{\mathrm{C}}(X)$ of all active SNs, with fixed powers R, P_k and X, as demonstrated in (3.70). In turn, at the globally optimum only the signal-to-noise ratios $\mathrm{SNR}_k^{\mathrm{S}}$, $\mathrm{SNR}_k^{\mathrm{C}}(P_k)$ and $\mathrm{SNR}_k^{\mathrm{C}}(X)$ are needed to determine the total signal-to-noise ratio $\mathrm{SNR}_{\mathrm{tot}}^\star$ at the fusion center. Hence, one only needs the equation (3.70) with (3.72) and (3.73) in order to investigate or to discuss the entire sensor network in a simple manner. In a practical application, the consecutive steps in Table 3.1 are to perform for an optimal allocation of power.

Since $\mathrm{SNR}_{\mathrm{tot}}^\star$ is the sum of the $\tilde{K}$ largest observations in the sample of K independent observations SNR_k, the distribution of $\mathrm{SNR}_{\mathrm{tot}}^\star$ is amenable by the theory of *order statistics*. For example, if the samples SNR_k are gamma distributed, the density of $\mathrm{SNR}_{\mathrm{tot}}^\star$ is given as a sum of gamma densities [45]. It is possible to show that the distribution of $\mathrm{SNR}_{\mathrm{tot}}^\star$ asymptotically tends towards the *generalized extreme value* distribution. Hence, for a wide range of continuous distributions of the samples SNR_k, the distribution of $\mathrm{SNR}_{\mathrm{tot}}^\star$ can accurately be fitted by the *Fréchet distribution*, see [46].

3.3.2 Visualization of results

In order to visualize selected results, we assume that all channel coefficients are complex normal distributed. The envelope of a complex normal distributed random variable, with equal variance σ^2 for both real and imaginary part, is Rayleigh distributed with the parameter $\sigma^2 \in \mathbb{R}_+$. The Rayleigh density of a random variable $Z \sim \mathfrak{R}(\sigma^2)$ is given by

$$\max\Big\{0, \frac{z}{\sigma^2}\exp\Big(-\frac{z^2}{2\sigma^2}\Big)\Big\}\,. \tag{3.74}$$

Table 3.1: Consecutive steps for an optimal allocation of power in passive sensor networks.

Step Number	Step Description
1.	Choose $X = \min_{k \in \mathbb{F}_K} \{P_k, P_{\text{tot}}\}$ for the communication power of each SN,
2.	measure each signal-to-noise ratio SNR_k^{S} at the input of the corresponding SN,
3.	measure each signal-to-noise ratio $\text{SNR}_k^{\text{C}}(X)$ at the input of the fusion center,
4.	determine α_k and β_k by relationships in (3.67),
5.	use Algorithm 1 to determine both subsets $\mathbb{K}_{\text{sat}}$ and $\mathbb{K}_{\text{lin}}$,
6.	determine $\tilde{c}_k(X)$ and $\tilde{\chi}_{\mathbb{K}}^{\star}(X)$ by (3.72) and (3.73), respectively,
7.	evaluate equation (3.71) to obtain the optimal powers $X_k^{\star}$,
8.	in order to estimate the current quality of data fusion the signal-to-noise ratio in (3.70) can in addition be calculated.

In turn, the square $Z_2 \coloneqq Z_1^2$ of a Rayleigh distributed random variable $Z_1 \sim \mathfrak{R}(\sigma^2)$ is gamma distributed, i.e., $Z_2 \sim \mathfrak{G}(1, 2\sigma^2)$. The gamma density of a random variable $Z \sim \mathfrak{G}(\kappa, \sigma)$ with parameters $\kappa \in \mathbb{R}_+$ and $\sigma \in \mathbb{R}_+$ is given by

$$\max\Big\{0, \frac{z^{\kappa-1}}{\sigma^{\kappa}\,\Gamma(\kappa)} \exp\Big(-\frac{z}{\sigma}\Big)\Big\}, \tag{3.75}$$

where its expected value is equal to $\mathcal{E}[Z] = \kappa\sigma$. Hence, the signal-to-noise ratio over a complex normal distributed channel coefficient is gamma distributed. In this way, to visualize the total signal-to-noise ratio (3.70), we perform a Monte-Carlo simulation [47] with 100000 iterations per simulation point. All signal-to-noise ratios SNR_k^{S} and $\text{SNR}_k^{\text{C}}(X)$ are randomly generated for each simulation step with densities $\mathfrak{G}(1, \sigma_s^2)$ and $\mathfrak{G}(1, \sigma_c^2)$, respectively. Note that σ_s^2 and σ_c^2 are equal to $R \cdot \mathcal{E}\big[\frac{|g_k|^2}{M_k}\big]$ and $X \cdot \mathcal{E}\big[\frac{|h_k|^2}{N_k}\big]$, respectively, in which the expectation is performed over all k. By the aid of these signal-to-noise ratios, we apply consecutively the steps 4. to 8. from Table 3.1 to obtain the corresponding value of $\text{SNR}_{\text{tot}}^{\star}$ in each simulation step. In Figures 3.4 and 3.5 the expected value of $\frac{\text{SNR}_{\text{tot}}^{\star}}{K}$, with expectation over all simulation steps, is depicted. In particular, for different choices of $\frac{P_{\text{tot}}}{X} = \frac{P_k}{X} \in \{\frac{1}{10}, 1, 10, 100\}\,\forall\, k$ and $K \in \{10, 100, 1000\}$ the behavior of $\frac{\text{SNR}_{\text{tot}}^{\star}}{K}$ with respect to σ_s^2 and σ_c^2 is shown. As can be seen, the deviation of $\frac{\text{SNR}_{\text{tot}}^{\star}}{K}$ with respect to σ_c^2 is in general smaller than the deviation with respect to σ_s^2. This behavior results from the unsymmetric property of $\text{SNR}_{\text{tot}}^{\star}$ with respect to SNR_k^{S}

and $\mathrm{SNR}_k^{\mathrm{C}}(X)$. All figures show that an increment of sensing powers results in a better performance compared to the same increment in communication powers.

In order to visualize the density of $\frac{\mathrm{SNR}_{\mathrm{tot}}^{\star}}{K}$, we perform the above described Monte-Carlo simulation with the same parameter setup. At the end of the simulation, all 100000 observations of $\frac{\mathrm{SNR}_{\mathrm{tot}}^{\star}}{K}$ are used to generate a corresponding histogram with 30 bins. Note that the last bin contains all tail observations. In addition, all 100000 observations are applied to fit the histogram by both the Fréchet and the gamma density, where all density parameters are calculated with the maximum likelihood method. Furthermore, the sample mean of the 100000 observations is calculated for reasons of comparison. For selected values of involved parameters, some curves are shown in Figures 3.6 and 3.7. It is in evidence that in some cases the Fréchet density and in other cases the gamma density is an accurate fit for the density of $\frac{\mathrm{SNR}_{\mathrm{tot}}^{\star}}{K}$.

3.4 Summary

The main contribution of the present chapter is the optimal solution of the power allocation problem in distributed passive multiple-radar systems. We have introduced a system model, a linear fusion rule and a simple objective function, which enable us to solve the power allocation problem analytically. Three different cases of power constraints have been investigated. For limited transmission power of single sensor nodes as well as for a sum-power limitation, we have analytically obtained optimal solutions in closed-form. We have seen that the power allocation problem is harder to solve if both constraints shall simultaneously be satisfied. Hence, we have developed an efficient algorithm to solve the last problem optimally. By applying the obtained solutions, the overall system performance of the sensor network is increased while the power consumption of the whole network is kept constant. The achieved results enable us to calculate the optimal power allocation fast and accurately which is essential for distributed passive multiple-radar systems with a large number of sensor nodes.

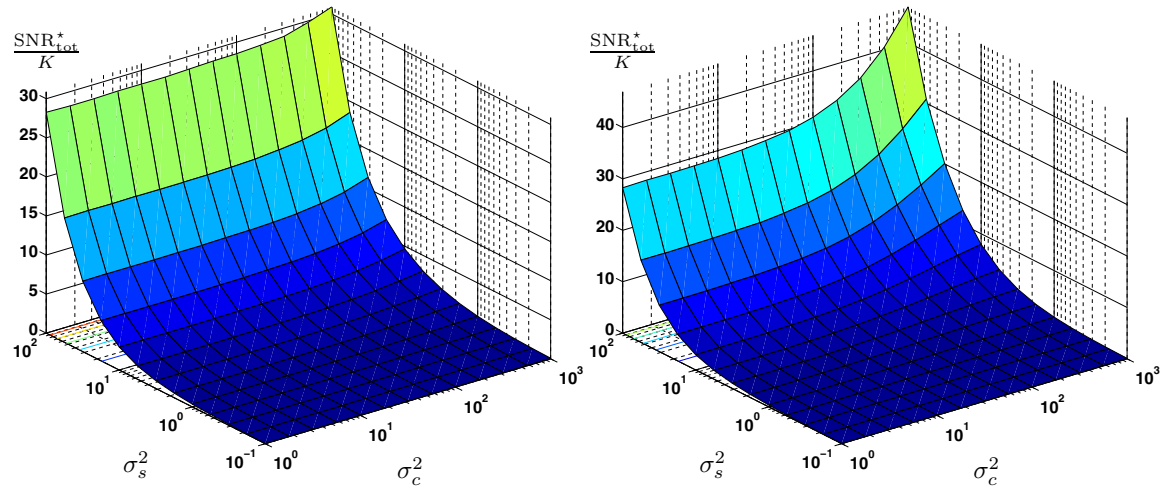

(a) $\frac{P_{\mathrm{tot}}}{X} = \frac{1}{10}$, $K = 10$

(b) $\frac{P_{\mathrm{tot}}}{X} = 1$, $K = 10$

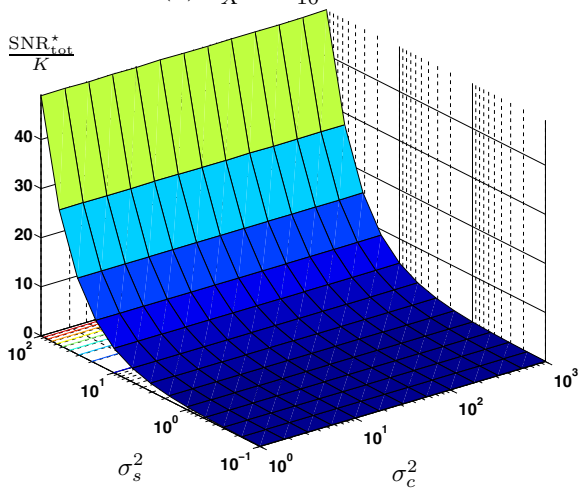

(c) $\frac{P_{\mathrm{tot}}}{X} = \frac{1}{10}$, $K = 100$

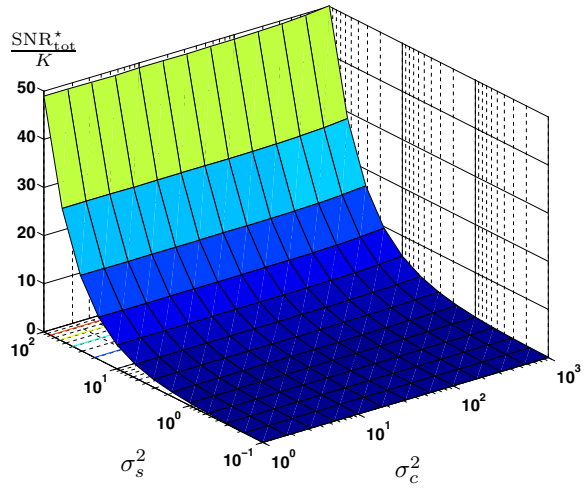

(d) $\frac{P_{\mathrm{tot}}}{X} = 1$, $K = 100$

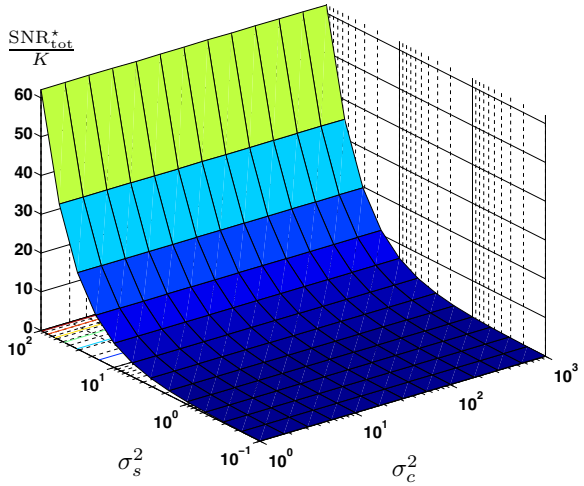

(e) $\frac{P_{\mathrm{tot}}}{X} = \frac{1}{10}$, $K = 1000$

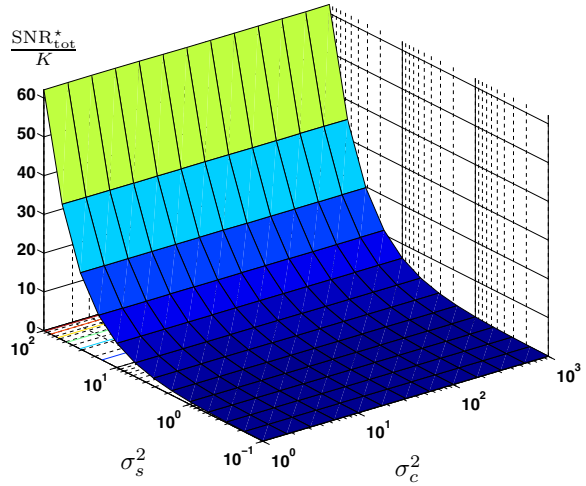

(f) $\frac{P_{\mathrm{tot}}}{X} = 1$, $K = 1000$

Figure 3.4: Visualization of $\frac{\mathrm{SNR}^{\star}_{\mathrm{tot}}}{K}$ for $\frac{P_{\mathrm{tot}}}{X} \in \{\frac{1}{10}, 1\}$ and $K \in \{10, 100, 1000\}$ with $\frac{P_k}{X} = \frac{P_{\mathrm{tot}}}{X} \, \forall \, k$ over the range $\frac{1}{10} \leq \sigma_s^2 \leq 100$ and $1 \leq \sigma_c^2 \leq 1000$.

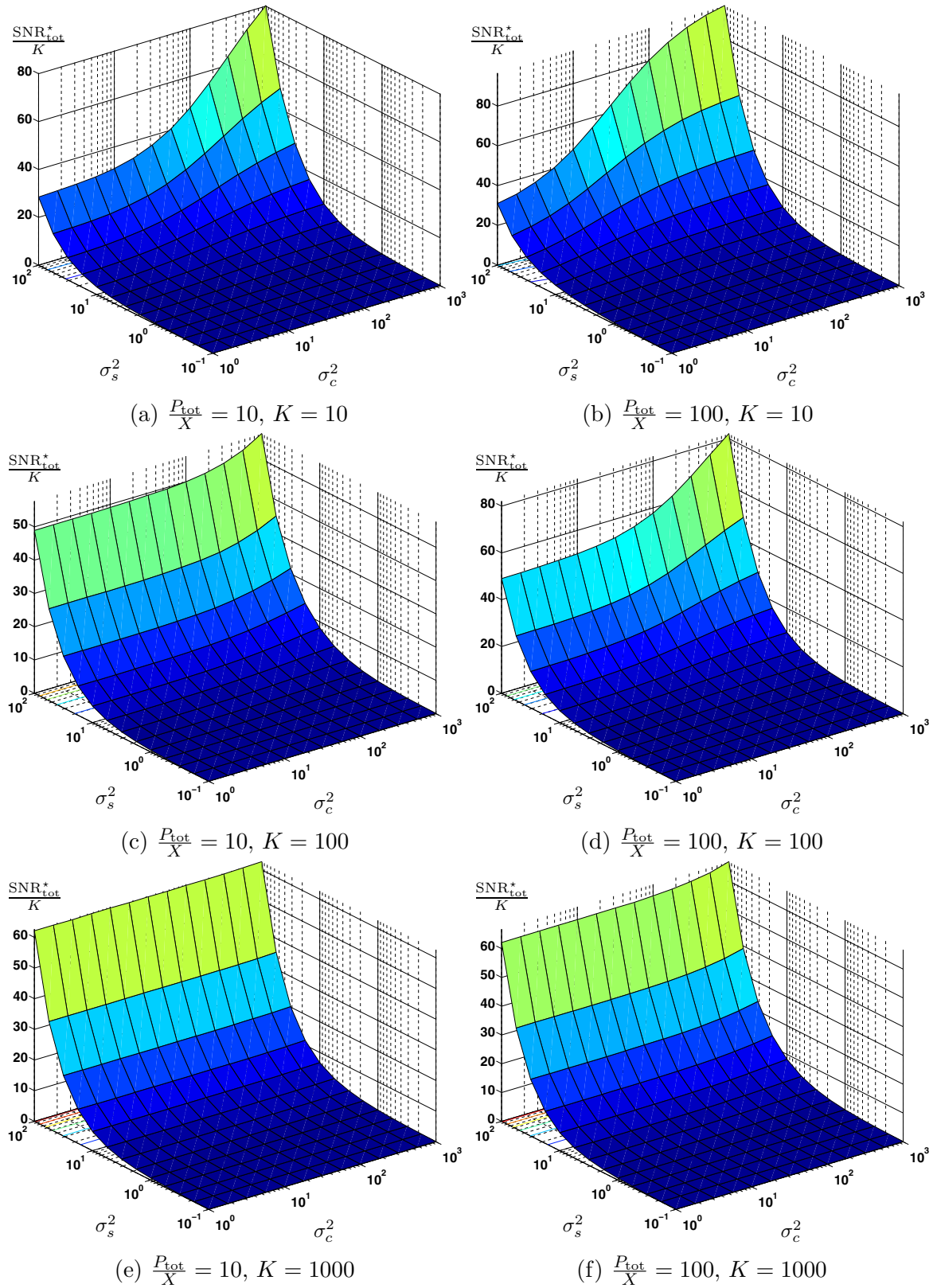

(a) $\frac{P_{\mathrm{tot}}}{X} = 10$, $K = 10$

(b) $\frac{P_{\mathrm{tot}}}{X} = 100$, $K = 10$

(c) $\frac{P_{\mathrm{tot}}}{X} = 10$, $K = 100$

(d) $\frac{P_{\mathrm{tot}}}{X} = 100$, $K = 100$

(e) $\frac{P_{\mathrm{tot}}}{X} = 10$, $K = 1000$

(f) $\frac{P_{\mathrm{tot}}}{X} = 100$, $K = 1000$

Figure 3.5: Visualization of $\frac{\mathrm{SNR}^\star_{\mathrm{tot}}}{K}$ for $\frac{P_{\mathrm{tot}}}{X} \in \{10, 100\}$ and $K \in \{10, 100, 1000\}$ with $\frac{P_k}{X} = \frac{P_{\mathrm{tot}}}{X} \, \forall \, k$ over the range $\frac{1}{10} \leq \sigma_s^2 \leq 100$ and $1 \leq \sigma_c^2 \leq 1000$.

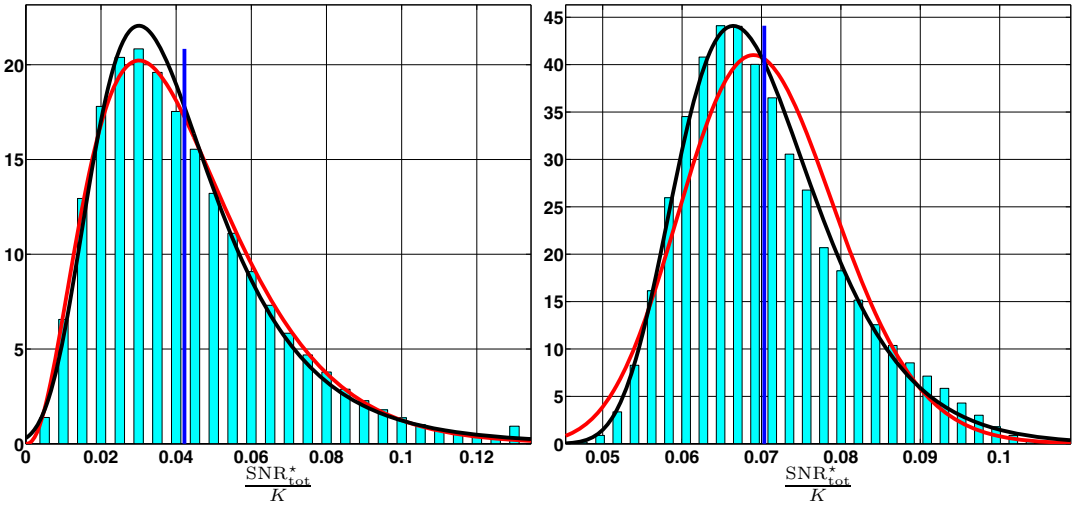

(a) $K = 10$, $10\sigma_s^2 = \sigma_c^2 = 1$ (b) $K = 1000$, $10\sigma_s^2 = \sigma_c^2 = 1$

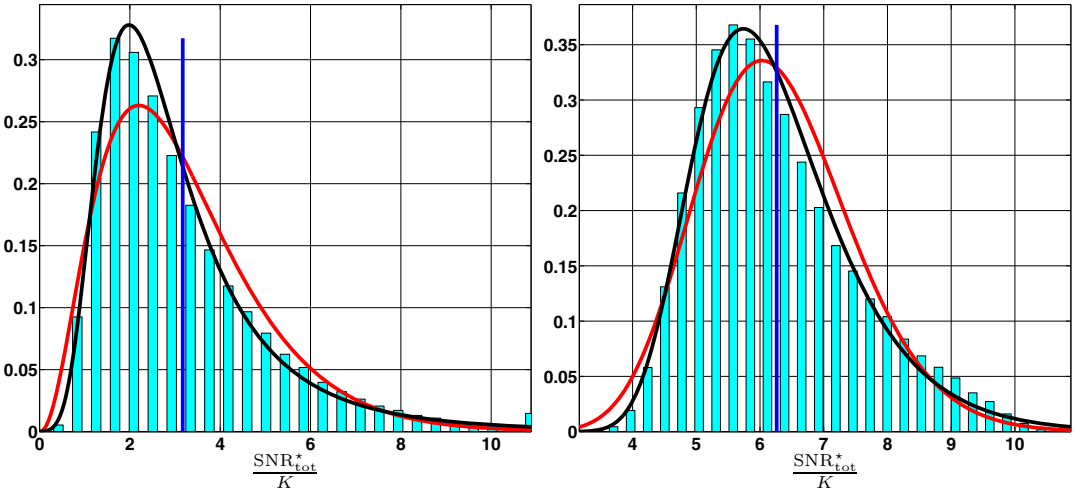

(c) $K = 10$, $10\sigma_s^2 = \sigma_c^2 = 100$ (d) $K = 1000$, $10\sigma_s^2 = \sigma_c^2 = 100$

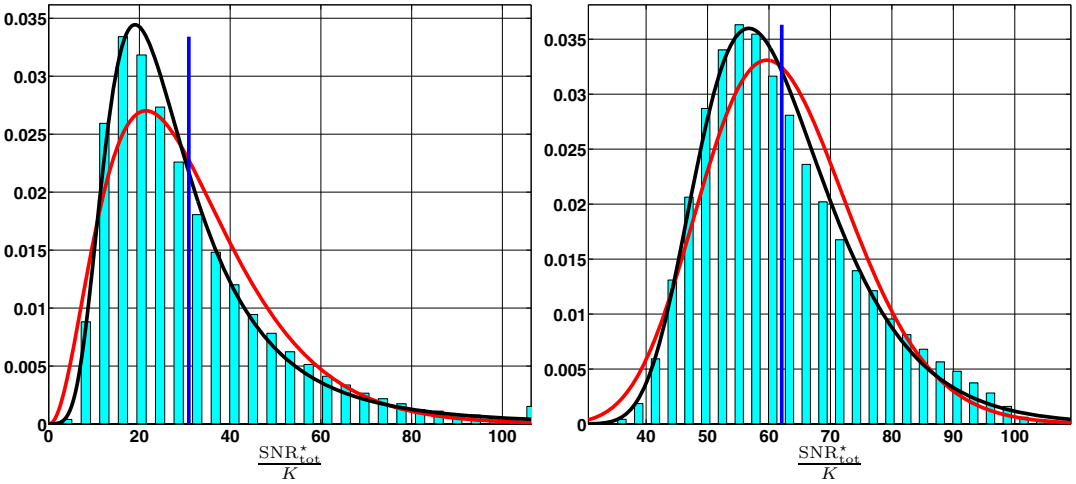

(e) $K = 10$, $10\sigma_s^2 = \sigma_c^2 = 1000$ (f) $K = 1000$, $10\sigma_s^2 = \sigma_c^2 = 1000$

Figure 3.6: Visualization of the density of $\frac{\mathrm{SNR}^\star_{\mathrm{tot}}}{K}$ for $\frac{P_{\mathrm{tot}}}{X} = \frac{1}{10}$, $K \in \{10, 1000\}$ and $10\sigma_s^2 = \sigma_c^2 \in \{1, 100, 1000\}$. The histogram of $\frac{\mathrm{SNR}^\star_{\mathrm{tot}}}{K}$, its maximum likelihood fit by the gamma density, and its maximum likelihood fit by the Fréchet density are shown in cyan, red and black color, respectively. The sample mean is indicated by the blue line to be compared with the corresponding values in Figures 3.4 and 3.5.

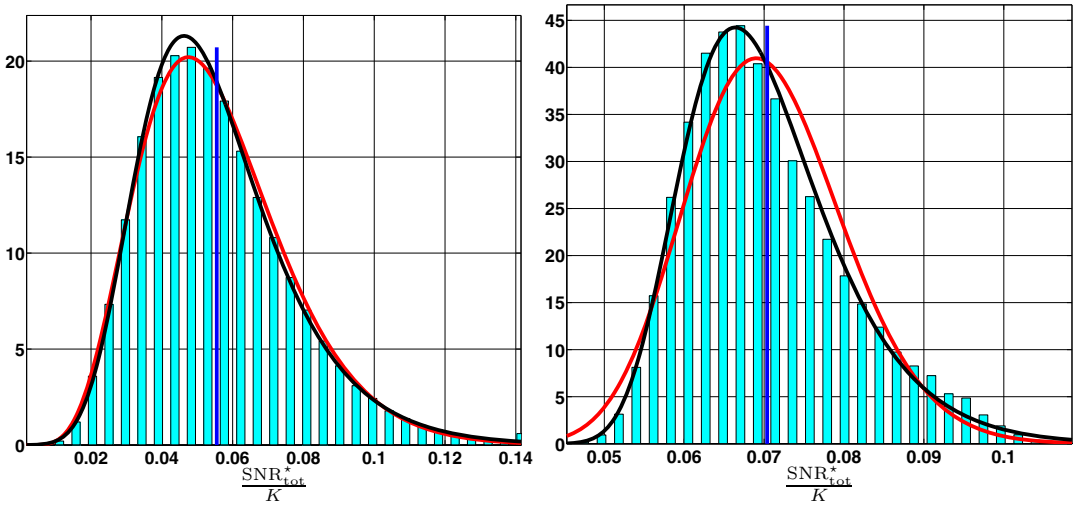

(a) $K = 10$, $10\sigma_s^2 = \sigma_c^2 = 1$ (b) $K = 1000$, $10\sigma_s^2 = \sigma_c^2 = 1$

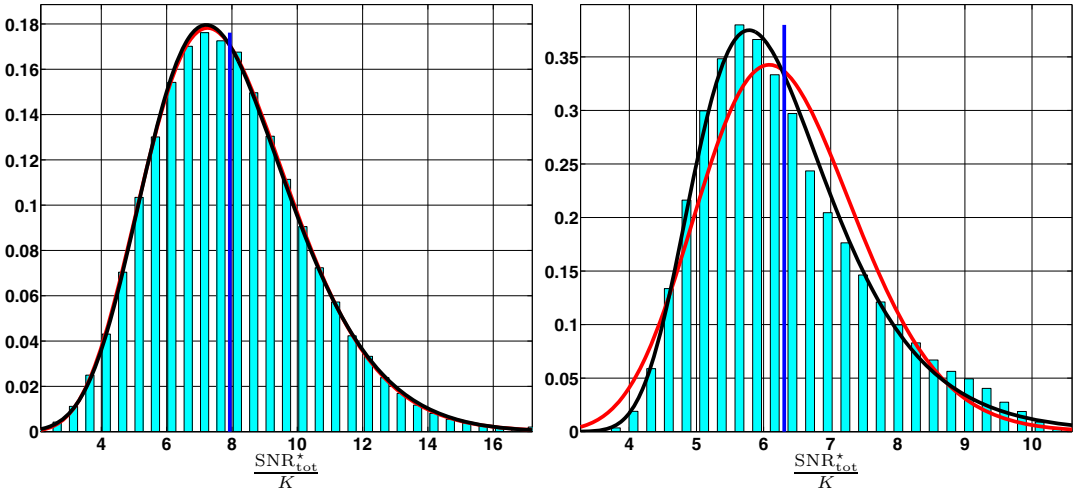

(c) $K = 10$, $10\sigma_s^2 = \sigma_c^2 = 100$ (d) $K = 1000$, $10\sigma_s^2 = \sigma_c^2 = 100$

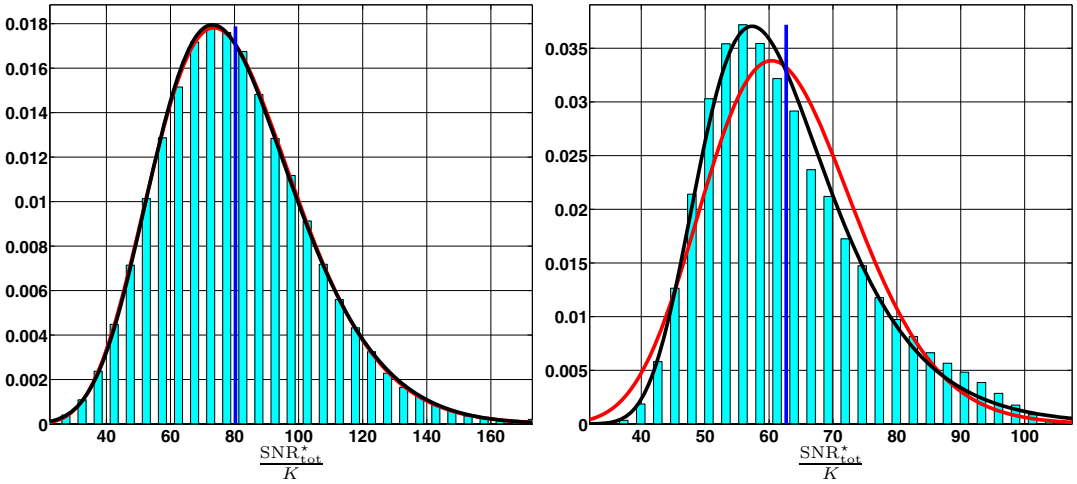

(e) $K = 10$, $10\sigma_s^2 = \sigma_c^2 = 1000$ (f) $K = 1000$, $10\sigma_s^2 = \sigma_c^2 = 1000$

Figure 3.7: Visualization of the density of $\frac{\mathrm{SNR}^\star_{\mathrm{tot}}}{K}$ for $\frac{P_{\mathrm{tot}}}{X} = 10$, $K \in \{10, 1000\}$ and $10\sigma_s^2 = \sigma_c^2 \in \{1, 100, 1000\}$. The histogram of $\frac{\mathrm{SNR}^\star_{\mathrm{tot}}}{K}$, its maximum likelihood fit by the gamma density, and its maximum likelihood fit by the Fréchet density are shown in cyan, red and black color, respectively. The sample mean is indicated by the blue line to be compared with the corresponding values in Figures 3.4 and 3.5.

4 Optimum Power Allocation for Active Sensor Networks

As we have seen in the previous chapter, the power allocation problem in sensor networks, that commonly are used as distributed passive multiple-radar systems, can be determined analytically in closed-form under certain power constraints and system requirements. In the current chapter, we extend our previous optimization method and apply it to the power allocation problem in sensor networks for active radar applications. In contrast to passive radar systems, active radar nodes consume electrical power for emitting radio waves in order to observe target objects. Thus, quite naturally the problem arises how to allocate an available amount of power for first emitting the radar signal for sensing and secondly communicating the received message to a remotely located fusion center. This fundamental distinction leads to power allocation problems which are in general more challenging than the allocation problems in the previous chapter.

In active sensor networks, each SN individually and independently emits a radar signal and receives the reflected echo from a jointly observed target object. These observations are used to classify the type of the present target object. Since the local observations at each SN are noisy and thus unreliable, they are combined into a single reliable observation at a remotely located fusion center to increase the overall system performance. In the classification process, the absence, the presence, and the type of the present target object are distinguished. The fusion center uses the best linear unbiased estimator in order to accurately estimate the reflection coefficient of a presence target object, where each object is assumed to be uniquely characterized by its reflection coefficient. This setup is illustrated in Figure 4.1, whose technical components will be specified in detail later. We demonstrate that the corresponding optimization of the power allocation leads to a signomial program which is in general quite hard to solve. Nonetheless, by using the proposed system architecture, fusion rule and objective function, again a closed-form solution of the power allocation problem for a network of amplify-and-forward SNs will analytically be achieved. The key idea is to utilize the average deviation between the estimated and the actual reflection coefficient as the objective function. Since the power consumption of the entire network may be limited in various aspects, three different cases of power constraints are discussed and compared with each other. Explicit policies for the optimal power allocation are given. These are the main contributions of the current chapter.

The research on distributed detection was originated from the attempt to combine signals of different radar devices [48]. Currently, distributed detection is discussed in the context of wireless sensor networks, where the sensor units may also be radar

nodes [32, 49, 50]. In [2], the power allocation problem for distributed wireless sensor networks, which perform object detection and classification, is only treated for ultra-wide bandwidth (UWB) technology. Other applications, which require or benefit from detection and classification capabilities, are localization and tracking [38] or through-wall surveillance [51]. In [3], an approximate solution of the power allocation problem is proposed, which provides an analytical treatment of output power-range limitation per sensor node. However, a closed-form optimal solution to the power allocation problem has not yet been investigated in the context of object classification. The main difficulty is associated with finding a closed-form equation for the overall classification probability. As an example, for the Bayesian hypothesis test criterion the overall classification probability cannot be analytically evaluated [52]. This limits the usability of this criterion for solving the power allocation problem. Bounds, such as the Bhattacharyya bound [53], are also difficult to use for optimizing multidimensional problems. Hence, the best power allocation scheme is still an open problem in order to improve the overall classification probability.

The present chapter is organized as follows. We start with a description of the underlying technical system in the next section. Subsequently, the power allocation problem is specified and analytically solved. The achieved results are then discussed and carefully compared with each other.

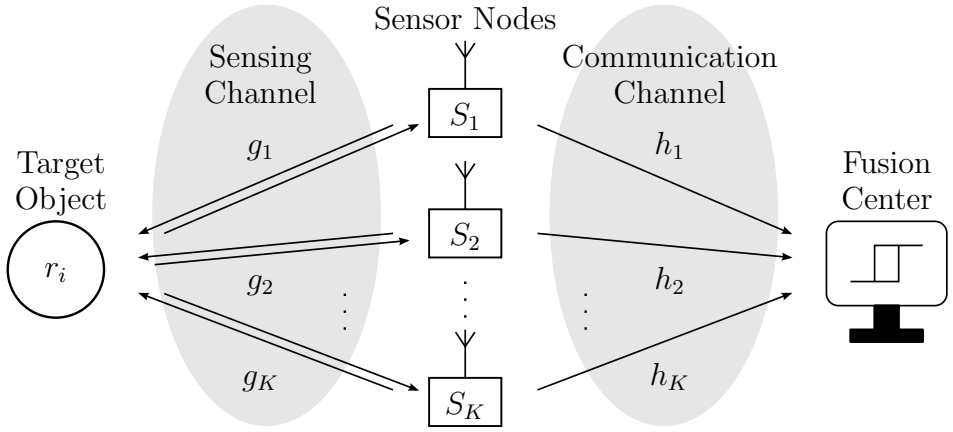

Figure 4.1: Abstract representation of the distributed sensor network.

4.1 Overview and Technical System Description

At any instance of time, a network of $K \in \mathbb{N}$ independent and spatially distributed SNs receives random observations. If a target object is present, then the received power at the SN S_k is a part of its own emitted power which is back-reflected from the jointly observed target object and is weighted by its reflection coefficient r_i. The object may be of I different types. It should be noted that sheer detection may be treated as the special case of $I = 2$ which corresponds to the decision '*some object is present*' versus '*there is no object*'. We assume that all different object types and their

corresponding reflection coefficients are known by the network. Moreover, the received signal at each SN is weighted by the corresponding channel coefficient and disturbed by additive noise. It is obvious that the sensing channel is wireless. The sensing task and its corresponding communication task for a single classification process are performed in consecutive time slots. All SNs take samples from the disturbed received signal and amplify them without any additional data processing in each time slot. The amplified samples remain buffered in the SNs during the current time slot. Simultaneously in the same time slot, new radio waves are emitted by all SNs for the next observation and classification process. In addition, the buffered samples of the former classification process are communicated to the fusion center which is placed in a remote location. We assume that SNs have only limited sum-power available for sensing the object and communicating to the fusion center. Furthermore, each SN may be limited in its transmission power-range due to transmission-power regulation standards or due to the functional range of its circuit elements. The sensing task as well as the communication to the fusion center are performed by using distinct waveforms (pulse shapes) for each SN so as to distinguish sensing and communication of different SNs. Each waveform has to be suitably chosen in order to suppress inter-user (inter-node) interference at all SNs and also at the fusion center. Practical examples for waveforms are Gold-code and Kasami-code sequences [54] for both sensing and communication task. Furthermore, we assume that in the frequency domain each waveform is orthogonal to all other waveforms in order to calculate the sensing power of each SN independent from its communication power. Hence, the K received signals at the fusion center are uncorrelated and assumed to be conditionally independent. Each received signal at the fusion center is influenced by the corresponding channel coefficient and additive noise, as well. The communication channel between the SNs and the fusion center can either be wireless or wired. The disturbed received signals at the fusion center are weighted and combined together in order to obtain a single reliable observation $\tilde{r}$ of the actual reflection coefficient r_i. Note that we disregard time delays within all transmissions and assume synchronized data communication.

In the following subsections, we mathematically describe the underlying system model that is depicted in Figure 4.2. The continuous-time system is modeled by its discrete-time equivalent, where the sampling rate of the corresponding signals is equal to the target observation rate, for the sake of simplicity.

Note that the present system model, and hence its description, coincides in parts with the system model of the previous chapter. Thus, the commonly shared assumptions and conditions are recited and the system description is further extended in the following subsections. As will be shown later on, the extensions lead to significantly different results.

4.1.1 Target object

We assume that all objects have the same size, shape and alignment, but different material and, hence, complex-valued reflection coefficients $r_i \in \mathbb{C}$, $i \in \mathbb{F}_I$. Thus, the reflection coefficients are the only recognition features in this chapter. The a-priori

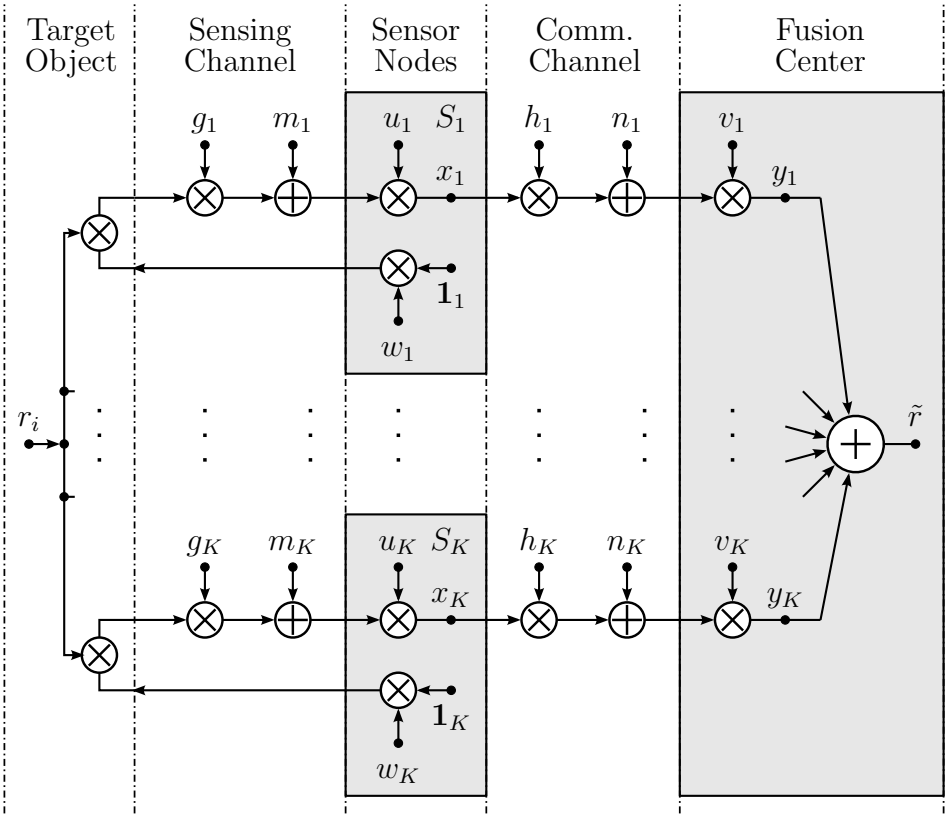

Figure 4.2: System model of the distributed active sensor network.

probability of occurrence for each object type is denoted by $\pi_i \in \mathbb{R}_+$, $i \in \mathbb{F}_I$, with $\sum_{i=1}^{I} \pi_i = 1$. The root mean squared value of the reflection coefficients is given as

$$r_{\mathrm{rms}} \coloneqq \sqrt{\sum_{i \in \mathbb{F}_I} \pi_i \left| r_i \right|^2} \,. \tag{4.1}$$

Furthermore, the actual target object is assumed to be static during consecutive observation steps.

4.1.2 Sensing channel

Each propagation path of the sensing channel, from SN to the object and again back to the SN, is described by a corresponding random channel coefficient g_k. For the investigation of the power allocation problem, the concrete realization of the channel coefficients is needed and hence can be used for postprocessing of the received signals at the SNs. We assume that the channel coefficients are complex-valued and static during each target observation step. Furthermore, the coherence time of sensing channels is assumed to be much longer than the whole length of the classification process. Thus, the expected value and the quadratic mean of each coefficient during each observation step can be assumed to be equal to their instantaneous values, i.e., $\mathcal{E}[g_k] = g_k$ and

$\mathcal{E}[|g_k|^2] = |g_k|^2$. In practice, it is often difficult to measure or estimate these coefficients. Thus, the results of the present chapter are applicable for scenarios where the channel coefficients can somehow be accurately estimated during each observation process or they are nearly deterministic and thus can be measured before starting the radar task.

Furthermore, the channel coefficients are assumed to be jointly independent. Note that the channel coefficients include the radar cross section, the influence of the antenna, the impact of the filters, as well as all additional attenuation of the target signal.

At the input of each SN, the disturbance is modeled by the complex-valued AWGN m_k with zero mean and finite variance $M_0 \coloneqq \mathcal{E}[|m_k|^2]$ for all k. Note that the channel coefficient and the noise on the same propagation path are also jointly independent.

4.1.3 Sensor nodes

We model each SN by an amplify-and-forward unit with extended capabilities, where both sensing and communication signal are transmitted simultaneously. Without loss of generality, we suppose that each sensing signal $\mathbf{1}_k$ has unit-energy, a matched-filter for the sensing signal $\mathbf{1}_k$ exists at the input of the k^{th} SN, and each sample is taken at the maximum of the corresponding autocorrelation function of $\mathbf{1}_k$. In this way, we can omit this signal in the description of all other equations from now on, for the sake of conciseness. The deterministic sensing signal is amplified by a real-valued and non-negative factor w_k to adjust the sensing power. The expected value of the instantaneous output power is then described by

$$W_k \coloneqq \mathcal{E}[|w_k|^2] = |w_k|^2\,,\ k \in \mathbb{F}_K\,. \tag{4.2}$$

Note that the specific value of w_k will be determined later by the power allocation procedure.

The ratio of the communication signal to the received signal is described by the non-negative and real-valued amplification factor u_k. Thus, the communication signal and the expected value of its instantaneous power are described by

$$x_k \coloneqq (r_i g_k w_k + m_k)u_k\,,\ k \in \mathbb{F}_K \tag{4.3}$$

and

$$X_k \coloneqq \mathcal{E}[|x_k|^2] = (r_{\text{rms}}^2 |g_k|^2 W_k + M_0)u_k^2\,,\ k \in \mathbb{F}_K\,, \tag{4.4}$$

respectively. The amplification factor is an adjustable parameter and will be determined later by the power allocation procedure, as well. Note that the instantaneous power fluctuates from observation to observation depending on the present target object.

If the received signal is negligible in comparison to the output signal and if the nodes have smart power components with low-power dissipation loss, then the average power consumption of each node is approximately equal to its average output power $W_k + X_k$. The addition of both transmission powers is justified because the corresponding signals are assumed to be separated by distinct waveforms. We also assume that the output

power-range of each SN is limited by $P_{\max}$ and that the average power consumption of all SNs together is limited by the sum-power constraint P_{tot}. Hence, the constraints

$$W_k + X_k \leq P_{\max} \quad \Leftrightarrow \quad \big(1 + r_{\text{rms}}^2 |g_k|^2 u_k^2\big) W_k + M_0 u_k^2 \leq P_{\max}\,,\ k \in \mathbb{F}_K \tag{4.5}$$

and

$$\sum_{k \in \mathbb{F}_K} \underbrace{\underbrace{W_k}_{\text{Radar task}} + \underbrace{X_k}_{\text{Data communication}}}_{\text{Average transmission power of one sensor for a single observation}} \leq P_{\text{tot}}$$

$$\Leftrightarrow \sum_{k \in \mathbb{F}_K} \big(1 + r_{\text{rms}}^2 |g_k|^2 u_k^2\big) W_k + M_0 u_k^2 \leq P_{\text{tot}} \tag{4.6}$$

have to be considered. We remark that the described method can also be extended to individual output power-range constraints per SN.

Note that the sum-power constraint P_{tot} is a reasonable approach to compare energy-efficient radar systems.

4.1.4 Communication channel

Analogous to the sensing channel, each propagation path of the communication channel is described by a corresponding random channel coefficient h_k. But in contrast to the sensing channel, the concrete realization of the communication channel coefficients is measurable by using pilot sequences at each SN. Accordingly, the channel coefficients can be used for postprocessing of received signals at the fusion center. We assume that the channel coefficients are complex-valued and static during each target observation step. Furthermore, the coherence time of communication channels is also assumed to be much longer than the whole length of the classification process. Thus, the expected value and the quadratic mean of each channel coefficient can be assumed to be equal to their instantaneous values, i.e., $\mathcal{E}[h_k] = h_k$ and $\mathcal{E}[|h_k|^2] = |h_k|^2$. Furthermore, the channel coefficients are assumed to be jointly independent. Note that the channel coefficients include the influence of the antenna, the impact of the filters, as well as all additional attenuation of the corresponding sensor signal.

At the input of the fusion center, the disturbance on each communication path is modeled by the complex-valued AWGN n_k with zero mean and finite variance $N_0 \coloneqq \mathcal{E}[|n_k|^2]$ for all k. Note that the channel coefficient and the noise on the same propagation path are also jointly independent.

4.1.5 Fusion center

The fusion center combines the different local observations into a single reliable one by applying a linear combiner. Thus, the received signals are weighted with the complex-valued factors v_k and summed up to yield an estimate $\tilde{r}$ of the actual target signal r_i. In this way, we obtain

$$y_k \coloneqq (x_k h_k + n_k) v_k\,,\ k \in \mathbb{F}_K\,, \tag{4.7}$$

and hence,

$$\tilde{r} \coloneqq \sum_{k \in \mathbb{F}_K} y_k = r_i \sum_{k \in \mathbb{F}_K} w_k g_k u_k h_k v_k + \sum_{k \in \mathbb{F}_K} (m_k u_k h_k + n_k) v_k \,. \tag{4.8}$$

Note that each weight can be written as $v_k = |v_k| \exp(\mathrm{j}\,\vartheta_k)$, $k \in \mathbb{F}_K$, where ϑ_k is a real-valued number which represents the phase of the corresponding weight.

Note that the fusion center can separate the input streams because the communication channel is either wired or the data communication is performed by distinct waveforms for each SN. Consequently, if the communication channel is wireless then a matched-filter bank is essential at the input of the fusion center to separate the data streams of different SNs. In addition, we do not consider inter-user (inter-node) interferences at the fusion center because of the distinct waveform choices.

In order to obtain a single reliable observation at the fusion center, the value $\tilde{r}$ should be a good estimate for the present reflection coefficient r_i. Thus, we optimize the sensing power W_k, the amplification factors u_k, and the weights v_k in order to minimize the average absolute deviation between $\tilde{r}$ and the true reflection coefficient r_i. This optimization procedure is elaborately explained in the next section. After determining W_k, u_k and v_k, the fusion center observes a disturbed version of the true reflection coefficient r_i at the input of its decision unit. Hence, by using the present system model, we are able to separate the power allocation problem from the classification problem and optimize both independently.

4.1.6 Remarks to the system model

Because of the similarity of the present system model to that of the previous chapter, we list only the additional remarks in the following.

In general, SNs have only one power amplifier and a single antenna. The antenna is usually connected to a circulator in order to separate the signal of the transmitter to the antenna from the signal of the antenna to the receiver, which is not depicted in Figure 4.2. The power amplifier is also shared for sensing and communication tasks, but not considered in this work.

In order to increase the available power-range at each SN, time-division multiple-access (TDMA) can be used to separate the sensing task from the communication task and perform each task in a different time slot.

The amplification factors u_k and w_k are in practice frequency and voltage dependent. This dependency is neglected in this work.

To distinguish the current operating mode of each SN in what follows, we say a SN is *inactive* or *idle* if the allocated power is zero. We say the SN is *active* if the allocated power is positive. Finally, we say a SN is *saturated* if the limitation of its output power-range is equal to the allocated power, i.e., $P_{\max} = W_k + X_k$.

An overview of all notations that we will use hereinafter and are needed for the description of each observation process is summarized in the glossary.

4.2 Power Optimization

In this section, we introduce the power optimization problem and consecutively present its analytical solutions for different power constraints. First, we investigate the case where only a sum-power constraint $P_{\text{tot}} \in \mathbb{R}_+$ for the cumulative sum of the expected power consumption of each SN is given. Afterwards, we present the analytical solution of the power allocation problem for the case where the average transmission power of each SN is limited by the output power-range limitation $P_{\max} \in \mathbb{R}_+$. Finally, we extend the power allocation problem to the case where both constraints hold simultaneously and present the corresponding optimal solution.

In general, the objective is to maximize the overall classification probability, however, a direct solution to the allocation problem does not exist, since no analytical expression for the overall classification probability is available. Instead, we minimize the average deviation between $\tilde{r}$ and r_i, in order to determine the power allocation. The motivation for this method is the separation of the power allocation problem from the object classification procedure, as described in the last section. The corresponding optimization problem is elaborately described in the next subsection.

4.2.1 Optimization problem

As mentioned in the last section, the value $\tilde{r}$ should be a good estimate for the actual reflection coefficient r_k of the present target object. In particular, we aim at finding estimators $\tilde{r}$ of minimum mean squared error in the class of unbiased estimators for each i.

The estimate $\tilde{r}$ is unbiased simultaneously for each i, if $\mathcal{E}[\tilde{r} - r_i] = 0$ holds, i.e., from equation (4.8) with (4.2) we obtain the identity

$$\sum_{k \in \mathbb{F}_K} \sqrt{W_k}\, g_k u_k h_k v_k = 1\,. \tag{4.9}$$

This identity is our first constraint in what follows. Note that the mean of the second sum in (4.8) vanishes since the noise is zero-mean. Recall that both random variables g_k and h_k are assumed to be known constants, because the coherence time of both channels is assumed to be much longer than the target observation time. Note that equation (4.9) is complex-valued and may be separated as

$$\sum_{k \in \mathbb{F}_K} \sqrt{W_k}\, u_k\, |v_k g_k h_k| \cos(\vartheta_k + \phi_k) = 1 \tag{4.10}$$

and

$$\sum_{k \in \mathbb{F}_K} \sqrt{W_k}\, u_k\, |v_k g_k h_k| \sin(\vartheta_k + \phi_k) = 0\,, \tag{4.11}$$

where ϑ_k and ϕ_k are phases of v_k and $g_k h_k$, respectively.

The objective is to minimize the mean squared error $\mathcal{E}[|\tilde{r} - r_i|^2]$. By using equation (4.8) and the identity (4.9) we may write the objective function as

$$V \coloneqq \mathcal{E}\left[|\tilde{r} - r_i|^2\right] = \sum_{k \in \mathbb{F}_K} |v_k|^2 \left(u_k^2 |h_k|^2 M_0 + N_0\right). \tag{4.12}$$

Note that (4.12) is only valid if m_k and n_k are white and jointly independent.

As mentioned in the last section, each SN has an output power-range limitation and the expected overall power consumption is also limited. Hence, the objective function is also subject to (4.5) and (4.6), which are our second and last constraints, respectively.

In summary, the optimization problem is to minimize the mean squared error in (4.12) with respect to u_k, v_k, and W_k, subject to constraints (4.5), (4.6), (4.10) and (4.11), i.e.:

$$\begin{aligned}
\underset{\mathbf{u},\mathbf{v},\mathbf{W},\boldsymbol{\vartheta}}{\text{minimize}} \quad & \sum_{k=1}^{K} |v_k|^2 \left(u_k^2 |h_k|^2 M_0 + N_0\right) \\
\text{subject to} \quad & \sum_{k=1}^{K} \sqrt{W_k}\, u_k\, |v_k g_k h_k| \cos(\vartheta_k + \phi_k) = 1\,, \\
& \sum_{k=1}^{K} \sqrt{W_k}\, u_k\, |v_k g_k h_k| \sin(\vartheta_k + \phi_k) = 0\,, \\
& \sum_{k=1}^{K} \left(1 + r_{\text{rms}}^2 |g_k|^2 u_k^2\right) W_k + M_0 u_k^2 \leq P_{\text{tot}}\,, \\
& \left(1 + r_{\text{rms}}^2 |g_k|^2 u_k^2\right) W_k + M_0 u_k^2 \leq P_{\max}\,,\ k \in \mathbb{F}_K\,, \\
& \mathbf{u} \in \mathbb{R}_+^K,\ \mathbf{v} \in \mathbb{C}^K,\ \mathbf{W} \in \mathbb{R}_+^K,\ \boldsymbol{\vartheta} \in [0, 2\pi]^K\,.
\end{aligned}$$

Note that this optimization problem is again a *signomial program*, see Definition 2.3.3. Thus, we apply the general method of Lagrangian multiplier with equality constraints to solve all optimization problems in the present work. In order to ensure the global optimality of our results, we consecutively show the following four steps during each solving procedure. First, we relax each problem to an optimization problem with an extended subspace of all involved variables to ensure an optimization within the *interior-set*. Second, all stationary points of the associated Lagrangian are localized by considering the corresponding derivatives to obtain *necessary* conditions. Third, we show that the number of stationary points is equal to one, which indirectly implies that the considered stationary point is also a *regular* point for all (active) constraints. Finally, to obtain a *sufficient* condition, we then show that the stationary point has a convex neighborhood which corresponds with a minimum. In summary, the applied method is based on the regularity of all active constraints as well as first and second order optimality conditions which together guarantee for global optimality. At this point, we emphasize that obtaining global optimality is similarly achievable by applying vector space methods [55], using interval analysis [56], or utilizing a proper constraint qualification (CQ) together with Karush-Kuhn-Tucker conditions [57].

4.2.2 Power allocation subject to the sum-power constraint

In this case, the output power-range constraint per SN is assumed to be greater than the sum-power constraint and thus does not have any effect on the optimization problem, because the feasible set of the optimization problem is only limited by the sum-power constraint. This leads to the corresponding constrained Lagrange function (relaxation with respect to the range of W_k, u_k and $|v_k|$)

$$\begin{aligned} L_1(W_k, u_k, v_k; \eta_1, \eta_2, \tau; \xi) \coloneqq & \sum_{k\in\mathbb{F}_K} |v_k|^2 \left(u_k^2 |h_k|^2 M_0 + N_0\right) \\ & + \left(1 - \sum_{k\in\mathbb{F}_K} \sqrt{W_k} u_k \, |v_k g_k h_k| \cos(\vartheta_k + \phi_k)\right)\eta_1 \\ & - \left(\sum_{k\in\mathbb{F}_K} \sqrt{W_k} u_k \, |v_k g_k h_k| \sin(\vartheta_k + \phi_k)\right)\eta_2 \\ & + \left(P_{\text{tot}} - \xi - \sum_{k\in\mathbb{F}_K} \left(1 + r_{\text{rms}}^2 |g_k|^2 u_k^2\right) W_k + M_0 u_k^2\right)\tau \,, \end{aligned} \tag{4.13}$$

where η_1, η_2 and τ are Lagrange multipliers while ξ is a slack variable.

In order to satisfy (4.11), all phases $\vartheta_k + \phi_k$ have to be equal to $q_k\pi$, $q_k \in \mathbb{Z}$, for all $k \in \mathbb{F}_K$. If there were a better solution for $\vartheta_k + \phi_k$, then the first partial derivatives of L_1 with respect to ϑ_k would vanish at that solution, due to the continuity of trigonometric functions. But the first derivatives would lead to the equations $\eta_1 \sin(\vartheta_k + \phi_k) = \eta_2 \cos(\vartheta_k + \phi_k)$, $k \in \mathbb{F}_K$, which cannot simultaneously satisfy both equations (4.10) and (4.11) for all η_1 and η_2. Thus, $q_k\pi$ is the unique solution. Hence, we may consequently write a modified Lagrange function as

$$\begin{aligned} \tilde{L}_1(W_k, u_k, |v_k|, q_k; \eta_1, \tau; \xi) \coloneqq & \sum_{k\in\mathbb{F}_K} |v_k|^2 \left(u_k^2 |h_k|^2 M_0 + N_0\right) \\ & + \left(1 - \sum_{k\in\mathbb{F}_K} \sqrt{W_k} u_k \, |v_k g_k h_k| \cos(q_k\pi)\right)\eta_1 \\ & + \left(P_{\text{tot}} - \xi - \sum_{k\in\mathbb{F}_K} \left(1 + r_{\text{rms}}^2 |g_k|^2 u_k^2\right) W_k + M_0 u_k^2\right)\tau \,. \end{aligned} \tag{4.14}$$

At any stationary point of $\tilde{L}_1$ the first partial derivatives of $\tilde{L}_1$ with respect to W_k, u_k, $|v_k|$, η_1 and τ must vanish, if they exist. This leads to

$$\frac{\partial \tilde{L}_1}{\partial W_l} = -\frac{u_l \, |v_l h_l g_l| \cos(q_l\pi)}{2\sqrt{W_l}}\eta_1 - \left(1 + r_{\text{rms}}^2 |g_l|^2 u_l^2\right)\tau = 0 \,, \; l \in \mathbb{F}_K \,, \tag{4.15}$$

$$\frac{\partial \tilde{L}_1}{\partial |v_l|} = 2|v_l|\left(u_l^2 |h_l|^2 M_0 + N_0\right) - \sqrt{W_l} u_l \, |h_l g_l| \cos(q_l\pi)\eta_1 = 0 \,, \; l \in \mathbb{F}_K \,, \tag{4.16}$$

$$\frac{\partial \tilde{L}_1}{\partial u_l} = 2|v_l|^2 u_l |h_l|^2 M_0 - \sqrt{W_l}\,|v_l h_l g_l| \cos(q_l \pi)\eta_1 - 2u_l(W_l r_{\mathrm{rms}}^2 |g_l|^2 + M_0)\tau = 0\,,\ l \in \mathbb{F}_K\,, \tag{4.17}$$

$$\frac{\partial \tilde{L}_1}{\partial \eta_1} = 1 - \sum_{k \in \mathbb{F}_K} \sqrt{W_k} u_k |v_k g_k h_k| \cos(q_k \pi) = 0 \tag{4.18}$$

and

$$\frac{\partial \tilde{L}_1}{\partial \tau} = P_{\mathrm{tot}} - \xi - \sum_{k \in \mathbb{F}_K} \big(1 + r_{\mathrm{rms}}^2 |g_k|^2 u_k^2\big) W_k + M_0 u_k^2 = 0\,. \tag{4.19}$$

By multiplying (4.16) with $|v_l|$, summing up the outcome over all l, and using the identities (4.10) and (4.12), we obtain

$$\eta_1 = 2V \tag{4.20}$$

which is a positive real number due to definition of V. Because of the last relationship and according to (4.16), the value of $\cos(q_l \pi)$ must be a positive number and hence each q_l must be an even integer number. Thus, we can choose $q_l^\star = 0$ for all $l \in \mathbb{F}_K$ and conclude

$$\vartheta_l^\star = -\phi_l\,,\ l \in \mathbb{F}_K\,. \tag{4.21}$$

This solution gives the identity $\cos(q_l^\star \pi) = 1$ which can be incorporated into (4.15), (4.16), (4.17) and (4.18).

Again by multiplying (4.16) with

$$\frac{1}{2}\,\frac{u_l |h_l g_l| \sqrt{W_l}}{u_l |h_l|^2 M_0 + N_0}\,, \tag{4.22}$$

summing up the outcome over all l, and using (4.10), (4.12) and (4.20), we obtain

$$V = \frac{\eta_1}{2} = \left[\sum_{k \in \mathbb{F}_K} \frac{u_k^2 |h_k g_k|^2 W_k}{u_k^2 |h_k|^2 M_0 + N_0} \right]^{-1}. \tag{4.23}$$

In turn, by incorporating (4.23) into (4.16), it yields

$$|v_l| = \frac{V u_l |h_l g_l| \sqrt{W_l}}{u_l^2 |h_l|^2 M_0 + N_0} \tag{4.24}$$

for all $l \in \mathbb{F}_K$.

Note that for each feasible u_l and W_l, $l \in \mathbb{F}_K$, equation (4.24) describes a feasible value for each $|v_l|$. Since for each $u_l W_l > 0$ the relation $|v_l| > 0$ consequently follows, the feasible optimal values of each $|v_l| > 0$ are not on the boundary $|v_l| = 0$. Thus, finding optimal values for each u_l and W_l, $l \in \mathbb{F}_K$, leads to optimum values for each $|v_l|$, $l \in \mathbb{F}_K$, due to the convexity of (4.14) with respect to each $|v_l|$. Hence, finding a unique global optimum for u_l and W_l, $l \in \mathbb{F}_K$, yields the sufficient condition for the globally optimal solution of the minimization problem (4.14).

We replace each $|v_l|$ in (4.15) and (4.17) with (4.24) and thus we obtain two equations for τ as

$$\tau = \frac{-V^2 u_l^2 |g_l h_l|^2}{\left(1 + u_l^2 r_{\mathrm{rms}}^2 |g_l|^2\right)\left(u_l^2 |h_l|^2 M_0 + N_0\right)} \tag{4.25}$$

and

$$\tau = \frac{-V^2 W_l |g_l h_l|^2 N_0}{\left(W_l r_{\mathrm{rms}}^2 |g_l|^2 + M_0\right)\left(u_l^2 |h_l|^2 M_0 + N_0\right)^2} \,. \tag{4.26}$$

Note that because of the negativity of τ, due to (4.25) or (4.26), and positivity of η_1 there exists a feasible subspace in which the optimization problem (4.14) is convex in both u_l and W_l, $l \in \mathbb{F}_K$, as well. Hence, the Lagrange function (4.14) is convex near the optimum/stationary point in each u_l, $|v_l|$ and W_l, but it seems not to be a jointly convex function, at all. Since the Lagrangian is separately convex in each direction, the stationary point cannot be a maximum. To be a saddle point is also not possible, because then there would at least exist one additional stationary point which is not the case here. Thus, the Lagrangian (4.14) must actually be a jointly convex function in the neighborhood of its stationary point. Furthermore, since the number of stationary points is equal to one, all equality (active) constraints are regular. Hence, the separate convexity together with the regularity condition is even a sufficient condition for global optimality in the present case.

For the sake of simplicity and in order to compare the results later on, we define new quantities as[1]

$$\alpha_k \coloneqq \frac{M_0}{r_{\mathrm{rms}}^2 |g_k|^2} \;\Rightarrow\; \alpha_k \in \mathbb{R}_+ \,, \tag{4.27}$$

$$\beta_k \coloneqq \frac{N_0}{|h_k|^2} \;\Rightarrow\; \beta_k \in \mathbb{R}_+ \,, \tag{4.28}$$

and

$$\tilde{u}_k \coloneqq M_0 u_k^2 \;\Leftrightarrow\; u_k = +\sqrt{\frac{\tilde{u}_k}{M_0}} \,. \tag{4.29}$$

By direct algebra from (4.25) and (4.26), we infer

$$W_l = \frac{\tilde{u}_l \alpha_l (\tilde{u}_l + \beta_l)}{\alpha_l \beta_l - \tilde{u}_l^2} \,,\; l \in \mathbb{F}_K \,. \tag{4.30}$$

To satisfy the positivity of each W_l, the inequality

$$\alpha_l \beta_l > \tilde{u}_l^2 \,,\; l \in \mathbb{F}_K \,, \tag{4.31}$$

must hold, which will be used later. By using (4.27)–(4.30), we may rewrite (4.19) and (4.23) as

$$1 = (P_{\mathrm{tot}} - \xi) \Bigg[\sum_{k \in \mathbb{F}_K} \underbrace{\frac{\tilde{u}_k^2 (\alpha_k + \beta_k) + 2\tilde{u}_k \alpha_k \beta_k}{\alpha_k \beta_k - \tilde{u}_k^2}}_{=:\gamma_k} \Bigg]^{-1} \tag{4.32}$$

[1] We will discuss the physical interpretation of all important parameters and quantities in Subsection 4.4.1.

and

$$V^{-1} = \frac{1}{r_{\text{rms}}^2} \sum_{k \in \mathbb{F}_K} \frac{\tilde{u}_k^2}{\alpha_k \beta_k - \tilde{u}_k^2} \tag{4.33}$$

respectively. In turn, we incorporate (4.32) into (4.33) and infer

$$V^{-1} = \frac{P_{\text{tot}} - \xi}{r_{\text{rms}}^2 \sum_{k \in \mathbb{F}_K} \gamma_k} \sum_{k \in \mathbb{F}_K} \frac{\gamma_k \tilde{u}_k}{\tilde{u}_k(\alpha_k + \beta_k) + 2\alpha_k \beta_k} \,. \tag{4.34}$$

As is well-known, the arithmetic mean in (4.34) is less than its greatest element such that the inequality

$$V^{-1} \leq \frac{P_{\text{tot}} - \xi}{r_{\text{rms}}^2} \max_{k \in \mathbb{F}_K} \Big\{ \frac{\tilde{u}_k}{\tilde{u}_k(\alpha_k + \beta_k) + 2\alpha_k \beta_k} \Big\} \tag{4.35}$$

arises consequently. It is obvious that (4.35) is strictly decreasing with respect to ξ. Thus, the optimal value for the slack variable is zero, i.e., $\xi^\star = 0$. In (4.35), equality holds, if and only if, some elements are zero and all other ones are equal. In addition, it is obvious that (4.35) is strictly increasing in each $\tilde{u}_k$ and in turn the maximum value of a certain $\tilde{u}_k$ is achieved if for all $l \neq k$, $l \in \mathbb{F}_K$, the identity $\tilde{u}_l = 0$ holds, since the sum-power is kept constant. This means that only one SN is active and all other ones are idle. Hence, we can calculate the value of the corresponding $\tilde{u}_k$ from (4.32) as

$$\tilde{u}_k = \sqrt{\Big(\frac{\alpha_k \beta_k}{\alpha_k + \beta_k + P_{\text{tot}}} \Big)^2 + \frac{\alpha_k \beta_k P_{\text{tot}}}{\alpha_k + \beta_k + P_{\text{tot}}}} - \frac{\alpha_k \beta_k}{\alpha_k + \beta_k + P_{\text{tot}}} \,. \tag{4.36}$$

This value can be incorporated into (4.35) to obtain

$$V^{-1} = \frac{P_{\text{tot}}^2}{r_{\text{rms}}^2} \max_{k \in \mathbb{F}_K} \Big\{ \frac{1}{c_k^2(P_{\text{tot}}) - P_{\text{tot}}^2} \Big\} \tag{4.37}$$

with the *disturbance-intensity*[2]

$$c_k(P) \coloneqq \sqrt{\alpha_k \beta_k} + \sqrt{(\alpha_k + P)(\beta_k + P)} \,, \; k \in \mathbb{F}_K, P \in \mathbb{R}_+ \,. \tag{4.38}$$

The value of V^{-1} is maximal if the disturbance-intensity $c_k(P_{\text{tot}})$ is minimal. Hence, we re-index all SNs such that the inequality chain

$$c_k(P_{\text{tot}}) \leq c_{k+1}(P_{\text{tot}}) \;, \; k \in \mathbb{F}_{K-1} \,, \tag{4.39}$$

holds and with that only the first SN is active, even if the first few disturbance-intensities are equal. From (4.24), (4.29), (4.30),(4.36) and (4.37) we thus conclude

$$V^\star = \frac{r_{\text{rms}}^2}{P_{\text{tot}}^2} \big(c_1^2(P_{\text{tot}}) - P_{\text{tot}}^2 \big) \,, \tag{4.40}$$

[2]We give the name *disturbance-intensity* to c_k because it behaves intrinsically like noise. In Section 4.4 we will introduce a normalized version of c_k and call it *reliability-function*

$$\tilde{u}_1^\star = \sqrt{\Big(\frac{\alpha_1\beta_1}{\alpha_1+\beta_1+P_{\text{tot}}}\Big)^2 + \frac{\alpha_1\beta_1 P_{\text{tot}}}{\alpha_1+\beta_1+P_{\text{tot}}}} - \frac{\alpha_1\beta_1}{\alpha_1+\beta_1+P_{\text{tot}}}\,, \tag{4.41}$$

$$u_1^\star = \sqrt{\frac{\tilde{u}_1^\star}{M_0}}\,, \tag{4.42}$$

$$X_1^\star = \frac{\tilde{u}_1^\star(P_{\text{tot}}+\alpha_1)}{\alpha_1+\tilde{u}_1^\star}\,, \quad W_1^\star = \frac{\alpha_1(P_{\text{tot}}-\tilde{u}_1^\star)}{\alpha_1+\tilde{u}_1^\star}\,, \tag{4.43}$$

$$|v_1^\star| = \frac{V^\star \tilde{u}_1^\star}{r_{\text{rms}}|h_1|\sqrt{\tilde{u}_1^\star+\beta_1}\sqrt{\alpha_1\beta_1-(\tilde{u}_1^\star)^2}}\,, \tag{4.44}$$

and

$$|v_k^\star| = X_k^\star = W_k^\star = u_k^\star = 0\,,\ k \in \mathbb{F}_K,\, k \neq 1\ . \tag{4.45}$$

Note that by using the above results, the corresponding fusion rule is simplified by discarding the influence of inactive SNs from the fusion rule. The fusion rule (4.8) becomes

$$\tilde{r} = y_1 = r_i + (m_1 h_1 u_1^\star + n_1)v_1^\star\,,\ i \in \mathbb{F}_I\ . \tag{4.46}$$

The equations (4.40)–(4.45) and (4.21) are the optimal solutions of the power allocation problem only subject to the sum-power constraint. They are hence the main contribution of the present subsection.

Note that the global optimality of the obtained results is trivially reasoned, first because of the optimization of the relaxed Lagrange function (4.13) with extended range of all variables, and second since the global optimum point of the relaxed problem coincides with the original range of all variables.

4.2.3 Power allocation subject to individual power constraints

In the current case, the sum-power constraint is assumed to be much greater than the output power-range constraint and thus does not have any effect on the optimization problem, because the feasible set of the optimization problem is only limited by the output power-range constraints. This leads to the corresponding constrained Lagrange function (relaxation with respect to the range of W_k, u_k and $|v_k|$)

$$\begin{aligned} L_2(W_k,u_k,v_k;\eta_1,\eta_2,\lambda_k;\varrho_k) \coloneqq & \sum_{k\in\mathbb{F}_K} |v_k|^2\left(u_k^2|h_k|^2M_0+N_0\right) \\ & + \Big(1-\sum_{k\in\mathbb{F}_K}\sqrt{W_k}u_k\,|v_k g_k h_k|\cos(\vartheta_k+\phi_k)\Big)\eta_1 \\ & - \Big(\sum_{k\in\mathbb{F}_K}\sqrt{W_k}u_k\,|v_k g_k h_k|\sin(\vartheta_k+\phi_k)\Big)\eta_2 \\ & + \sum_{k\in\mathbb{F}_K}\Big(P_{\max}-\varrho_k-\big(1+r_{\text{rms}}^2|g_k|^2u_k^2\big)W_k-M_0u_k^2\Big)\lambda_k\,, \end{aligned} \tag{4.47}$$

where λ_k are new Lagrange multipliers while ϱ_k are new slack variables.

Since the behavior of L_2 is identical to that of L_1 with respect to $|v_k|$ and ϑ_k, we obtain the same results for the phases as given in (4.21). Hence, we may modify L_2 as

$$\begin{aligned}\tilde{L}_2(W_k, u_k, |v_k|\,; \eta_1, \lambda_k; \varrho_k) \coloneqq & \sum_{k\in\mathbb{F}_K} |v_k|^2 \left(u_k^2 |h_k|^2 M_0 + N_0\right) \\ & + \left(1 - \sum_{k\in\mathbb{F}_K} \sqrt{W_k} u_k \, |v_k g_k h_k|\right)\eta_1 \\ & + \sum_{k\in\mathbb{F}_K} \Big(P_{\max} - \varrho_k - \big(1 + r_{\mathrm{rms}}^2 |g_k|^2 u_k^2\big) W_k - M_0 u_k^2\Big)\lambda_k \,.\end{aligned} \tag{4.48}$$

Note that since the equality $\sin(\vartheta_k^\star + \phi_k) = 0$ holds due to (4.21), the constraint (4.11) is discarded in (4.48).

At any stationary point of $\tilde{L}_2$ the first partial derivatives of $\tilde{L}_2$ with respect to W_k, u_k, $|v_k|$, η_1 and λ_k must vanish, if they exist. This leads to

$$\frac{\partial \tilde{L}_2}{\partial W_l} = -\frac{u_l |v_l h_l g_l|}{2\sqrt{W_l}}\eta_1 - \big(1 + u_l^2 r_{\mathrm{rms}}^2 |g_l|^2\big)\lambda_l = 0\,,\ l \in \mathbb{F}_K\,, \tag{4.49}$$

$$\frac{\partial \tilde{L}_2}{\partial\, |v_l|} = 2\,|v_l|\left(u_l^2 |h_l|^2 M_0 + N_0\right) - \sqrt{W_l} u_l |h_l g_l| \eta_1 = 0\,,\ l \in \mathbb{F}_K\,, \tag{4.50}$$

$$\frac{\partial \tilde{L}_2}{\partial u_l} = 2|v_l|^2 u_l |h_l|^2 M_0 - \sqrt{W_l}|v_l h_l g_l|\eta_1 - 2u_l\big(W_l r_{\mathrm{rms}}^2 |g_l|^2 + M_0\big)\lambda_l = 0\,,\ l \in \mathbb{F}_K\,, \tag{4.51}$$

$$\frac{\partial \tilde{L}_2}{\partial \eta_1} = 1 - \sum_{k\in\mathbb{F}_K} \sqrt{W_k} u_k \, |v_k g_k h_k| = 0 \tag{4.52}$$

and

$$\frac{\partial \tilde{L}_2}{\partial \lambda_l} = P_{\max} - \varrho_l - \big(1 + r_{\mathrm{rms}}^2 |g_l|^2 u_l^2\big) W_l - M_0 u_l^2 = 0\,,\ l \in \mathbb{F}_K\,. \tag{4.53}$$

By similar procedure as described in Subsection 4.2.2, we obtain the same results as given in (4.23), (4.24) and (4.30), because the equations (4.49)–(4.52) and (4.15)–(4.18) are pairwise the same except of the difference between τ and λ_l. On the one hand, incorporating W_l from (4.53) into (4.23), and using the same definition as in (4.27)–(4.29), lead to

$$V^{-1} = \frac{1}{r_{\mathrm{rms}}^2} \sum_{k\in\mathbb{F}_K} \frac{\tilde{u}_k (P_{\max} - \varrho_k - \tilde{u}_k)}{(\tilde{u}_k + \alpha_k)(\tilde{u}_k + \beta_k)}\,, \tag{4.54}$$

which is obviously strictly decreasing with respect to each ϱ_k. Thus, the optimal value for each slack variable is zero, i.e., $\varrho_k^\star = 0$ for all $k \in \mathbb{F}_K$. On the other hand, comparing W_l from (4.53) with (4.30), leads to

$$\tilde{u}_k^\star = \sqrt{\Big(\frac{\alpha_k \beta_k}{\alpha_k + \beta_k + P_{\max}}\Big)^2 + \frac{\alpha_k \beta_k P_{\max}}{\alpha_k + \beta_k + P_{\max}}} - \frac{\alpha_k \beta_k}{\alpha_k + \beta_k + P_{\max}}\,,\ k \in \mathbb{F}_K\,. \tag{4.55}$$

Since equation (4.54) is strictly increasing in the number K of SNs and (4.55) holds for all SNs, we infer that all SNs are active. From (4.24), (4.29), (4.30), (4.38), (4.54) and (4.55) we thus conclude

$$V^\star = \left[\frac{P_{\max}^2}{r_{\text{rms}}^2} \sum_{k \in \mathbb{F}_K} \frac{1}{c_k^2(P_{\max}) - P_{\max}^2} \right]^{-1}, \tag{4.56}$$

$$u_k^\star = \sqrt{\frac{\tilde{u}_k^\star}{M_0}}\,,\ k \in \mathbb{F}_K\,, \tag{4.57}$$

$$X_k^\star = \frac{\tilde{u}_k^\star(P_{\max} + \alpha_k)}{\alpha_k + \tilde{u}_k^\star}\,, \quad W_k^\star = \frac{\alpha_k(P_{\max} - \tilde{u}_k^\star)}{\alpha_k + \tilde{u}_k^\star}\,,\ k \in \mathbb{F}_K\,, \tag{4.58}$$

$$|v_k^\star| = \frac{V^\star \tilde{u}_k^\star}{r_{\text{rms}}|h_k|\sqrt{\tilde{u}_k^\star + \beta_k}\sqrt{\alpha_k\beta_k - (\tilde{u}_k^\star)^2}}\,,\ k \in \mathbb{F}_K\,. \tag{4.59}$$

Note that by using the above results, the corresponding fusion rule cannot be simplified, since all SNs are active and they cannot thus be discarded from the fusion rule.

The equations (4.55)–(4.59) and (4.21) are the optimal solution of the power allocation problem only subject to the output power-range constraint per SN. They are hence the main contribution of the present subsection.

As mentioned in Subsection 4.2.2, the global optimality of the obtained results is also trivially reasoned, first because of the optimization of the relaxed Lagrange function (4.47) with extended range of all variables, and second since the global optimum point of the relaxed problem coincides with the original range of all variables.

4.2.4 Comparison of the solutions

As we have shown in Subsection 4.2.2, the SN with the smallest $c_k(P_{\text{tot}})$ consumes the whole available sum-power P_{tot}, because the combination of its sensing and communication channel is the best compared to other SNs. All other SNs do not get any transmission power, since their information reliability is too poor to be considered for data fusion. They can be discarded from the fusion rule such that the observation of the target object is less interfered by noise and consequently results in a better data communication. Note that the information reliability of each SN is only determined by the value of its corresponding $c_k(P_{\text{tot}})$.

In contrast, if the transmission power of each SN is individually limited and no sum-power constraint is given, then all SNs are active and their transmission power is equal to the output power-range constraint $P_{\max}$, according to (4.53). In order to compare both methods from Subsection 4.2.2 and 4.2.3, the values in (4.40) and (4.56) are needed. Note that for a fair comparison of both allocation methods in a certain scenario, an equal overall power is necessary, i.e., $P_{\text{tot}} = KP_{\max}$.

Note that $\tilde{r}$ is an unbiased estimator for each r_i due to constraint (4.9). By similar methods we can also minimize the mean squared error in both cases without restricting

ourself to unbiased estimators. Obviously, the optimal value of V will then be smaller than that in (4.40) or (4.56).

4.2.5 Power allocation subject to both types of power constraints

In the current subsection, we consider the optimization problem from Subsection 4.2.1 subject to both types of power constraints, i.e., sum-power constraint as well as output power-range constraint per SN. Two of three different cases can be singled out and reduced to preceding instances.

First, if $KP_{\max} < P_{\text{tot}}$, then the sum-power constraint is irrelevant, because the feasible set is only limited by the output power-range constraints. Hence, the power allocation problem reduces to the one described in Subsection 4.2.3 with results given in (4.55)–(4.59) and (4.21). The only difference is that a part of the available sum-power remains unallocated and cannot be used.

Secondly, if $P_{\text{tot}} \leq P_{\max}$, then the output power-range constraints are irrelevant, because the feasible set is only limited by the sum-power constraint. Hence, the power allocation problem is equal to the one described in Subsection 4.2.2. The corresponding results are described by (4.40)–(4.45) and (4.21).

The case of $P_{\max} < P_{\text{tot}} \leq KP_{\max}$ is most challenging. The amount of the available sum-power is possibly inadequate to supply all SNs with power $P_{\max}$. Besides, it is not possible to allocate the available sum-power only to a single SN since $P_{\max} < P_{\text{tot}}$. Hence, it will be shown that for the optimal solution only a subset of $\tilde{K} \leq K$, $\tilde{K} > 1$, SNs are active. Similar to the procedures in the previous subsections, we consider the corresponding constrained Lagrange function (relaxation with respect to the range of W_k, u_k and $|v_k|$)

$$\begin{aligned} L_3(W_k, u_k, v_k; \eta_1, \eta_2, \tau, \lambda_k; \xi, \varrho_k) \coloneqq & \sum_{k\in\mathbb{F}_K} |v_k|^2 \left(u_k^2 |h_k|^2 M_0 + N_0\right) \\ & + \left(1 - \sum_{k\in\mathbb{F}_K} \sqrt{W_k} u_k \, |v_k g_k h_k| \cos(\vartheta_k + \phi_k)\right)\eta_1 \\ & - \left(\sum_{k\in\mathbb{F}_K} \sqrt{W_k} u_k \, |v_k g_k h_k| \sin(\vartheta_k + \phi_k)\right)\eta_2 \\ & + \left(P_{\text{tot}} - \xi - \sum_{k\in\mathbb{F}_K} \left(1 + r_{\text{rms}}^2 |g_k|^2 u_k^2\right) W_k + M_0 u_k^2\right)\tau \\ & + \sum_{k\in\mathbb{F}_K} \left(P_{\max} - \varrho_k - \left(1 + r_{\text{rms}}^2 |g_k|^2 u_k^2\right) W_k - M_0 u_k^2\right)\lambda_k \,. \end{aligned} \tag{4.60}$$

Since the behavior of L_3 is identical to that of L_1 and L_2 with respect to $|v_k|$ and ϑ_k, we obtain the same results for the phases as given in (4.21). Hence, we may modify L_3

as

$$\begin{aligned}\tilde{L}_3(W_k, u_k, |v_k|\,; \eta_1, \tau, \lambda_k; \xi, \varrho_k) \coloneqq & \sum_{k\in\mathbb{F}_K} |v_k|^2 \left(u_k^2 |h_k|^2 M_0 + N_0\right) \\ & + \left(1 - \sum_{k\in\mathbb{F}_K} \sqrt{W_k} u_k \, |v_k g_k h_k|\right)\eta_1 \\ & + \left(P_{\mathrm{tot}} - \xi - \sum_{k\in\mathbb{F}_K} \left(1 + r_{\mathrm{rms}}^2 |g_k|^2 u_k^2\right) W_k + M_0 u_k^2\right)\tau \\ & + \sum_{k\in\mathbb{F}_K} \left(P_{\max} - \varrho_k - \left(1 + r_{\mathrm{rms}}^2 |g_k|^2 u_k^2\right) W_k - M_0 u_k^2\right)\lambda_k \,. \end{aligned} \tag{4.61}$$

Note that since the equality $\sin(\vartheta_k^\star + \phi_k) = 0$ holds due to (4.21), the constraint (4.11) is discarded in (4.61).

At any stationary point of $\tilde{L}_3$ the first partial derivatives of $\tilde{L}_3$ with respect to W_k, u_k, $|v_k|$, η_1, τ and λ_k must vanish, if they exist. This leads to

$$\frac{\partial \tilde{L}_3}{\partial W_l} = -\frac{u_l |v_l h_l g_l|}{2\sqrt{W_l}}\eta_1 - \left(1 + u_l^2 r_{\mathrm{rms}}^2 |g_l|^2\right)(\tau + \lambda_l) = 0 \,, \; l \in \mathbb{F}_K \,, \tag{4.62}$$

$$\frac{\partial \tilde{L}_3}{\partial\, |v_l|} = 2\,|v_l| \left(u_l^2 |h_l|^2 M_0 + N_0\right) - \sqrt{W_l} u_l |h_l g_l| \eta_1 = 0 \,, \; l \in \mathbb{F}_K \,, \tag{4.63}$$

$$\frac{\partial \tilde{L}_3}{\partial u_l} = 2|v_l|^2 u_l |h_l|^2 M_0 - \sqrt{W_l} |v_l h_l g_l| \eta_1 - 2u_l \left(W_l r_{\mathrm{rms}}^2 |g_l|^2 + M_0\right)(\tau + \lambda_l) = 0 \,, \; l \in \mathbb{F}_K \,, \tag{4.64}$$

$$\frac{\partial \tilde{L}_3}{\partial \eta_1} = 1 - \sum_{k\in\mathbb{F}_K} \sqrt{W_k} u_k \, |v_k g_k h_k| = 0 \,, \tag{4.65}$$

$$\frac{\partial \tilde{L}_3}{\partial \tau} = P_{\mathrm{tot}} - \xi - \sum_{k\in\mathbb{F}_K} \left(1 + r_{\mathrm{rms}}^2 |g_k|^2 u_k^2\right) W_k + M_0 u_k^2 = 0 \tag{4.66}$$

and

$$\frac{\partial \tilde{L}_3}{\partial \lambda_l} = P_{\max} - \varrho_l - \left(1 + r_{\mathrm{rms}}^2 |g_l|^2 u_l^2\right) W_l - M_0 u_l^2 = 0 \,, \; l \in \mathbb{F}_K \,. \tag{4.67}$$

By the same method as described in Subsection 4.2.2, we obtain the same results as given in (4.23), (4.24) and (4.30), because the equations (4.62)–(4.66) and (4.15)–(4.19) are pairwise the same except of the difference between τ and $\tau + \lambda_l$. According to (4.67), we are able to calculate the powers W_l in terms of ϱ_l and u_l. By using the same definition as in (4.27)–(4.29) and incorporating (4.30), (4.38) and (4.67) into (4.23) and (4.66), we derive

$$V^{-1} = \frac{1}{r_{\mathrm{rms}}^2} \sum_{k\in\mathbb{F}_K} \frac{1}{\left(\frac{c_k (P_{\max} - \varrho_k)}{P_{\max} - \varrho_k}\right)^2 - 1} \tag{4.68}$$

and

$$P_{\text{tot}} - \xi = \sum_{k \in \mathbb{F}_K} (P_{\max} - \varrho_k) \,. \tag{4.69}$$

As one can see, the minimization of the signomial program in (4.60) is reduced to the maximization of (4.68) subject to (4.69) and $0 \leq \varrho_k \leq P_{\max} < P_{\text{tot}}$ for all $k \in \mathbb{F}_K$ with respect to each ϱ_k. Since the new maximization problem is of special structure, it is amenable to an optimal solution via monotonicity and convexity of the objective (4.68) with respect to each $P_{\max} - \varrho_k$. The first derivative of $\frac{c_k(P)}{P}$ with respect to P leads to

$$\frac{\mathrm{d}}{\mathrm{d}P} \frac{c_k(P)}{P} = -\frac{P(\alpha_k + \beta_k) + 2\alpha_k\beta_k}{2P^2\sqrt{(\alpha_k + P)(\beta_k + P)}} - \frac{\sqrt{\alpha_k\beta_k}}{P^2} \,, \tag{4.70}$$

which is obviously negative for all positive P. Thus, $\frac{c_k(P)}{P}$ is strictly decreasing in P, and in turn, the objective in (4.68) is strictly decreasing in each ϱ_k. To show the convexity more effort is needed. Since each element of the series (4.68) is equal to

$$\frac{1}{\left(\frac{c_k(P)}{P}\right)^2 - 1} = \frac{\left(\sqrt{\alpha_k\beta_k} - \sqrt{(\alpha_k + P)(\beta_k + P)}\,\right)^2 - P^2}{(\alpha_k - \beta_k)^2}, \tag{4.71}$$

the second derivative of each element is given by

$$\frac{\sqrt{\alpha_k\beta_k}}{2\sqrt{(\alpha_k + P)^3(\beta_k + P)^3}} > 0 \,, \;\; P \in \mathbb{R}_+ \,. \tag{4.72}$$

From this result, the objective in (4.68) is convex, and even jointly convex, with respect to each ϱ_k. Since the objective is convex and strictly decreasing with respect to each ϱ_k, a stationary point on the range $0 < \varrho_k < P_{\max}$ cannot exist. If there were a stationary point defined by $(\tilde{\varrho}_1, \tilde{\varrho}_2, \tilde{\varrho}_3, \ldots, \tilde{\varrho}_K)$, then the addition of an $\varepsilon > 0$ to the slack variable $\tilde{\varrho}_{k_1}$, which has the smallest slope among all considered slack variables, and subtraction of the same amount ε from the slack variable $\tilde{\varrho}_{k_2}$, which has the greatest slope among all considered slack variables, would lead to a greater value of the objective, because of its monotonicity and convexity. However, this would contradict the existence of a stationary point on the range $0 < \varrho_k < P_{\max}$. Hence, the optimization of the maximization problem yields a unique optimal value for each slack variable on the boundary of its feasible set. Furthermore, the optimal solution for the slack variable ξ is zero, i.e., $\xi^\star = 0$, due to monotonicity of the objective (4.68) with respect to the number of SNs. This means that the first $\tilde{K} - 1$ SNs operate on $P_{\max}$, the $\tilde{K}^{\text{th}}$ SN operates on the remaining power $P_{\text{remain}} \coloneqq P_{\text{tot}} - (\tilde{K} - 1)P_{\max}$ with $0 < P_{\text{remain}} \leq P_{\max}$, while all other SNs stay idle. Consequently, the optimal power allocation method is simply described as follows.

First, all SNs are re-indexed to satisfy the inequality chain

$$c_k(P_{\max}) \leq c_{k+1}(P_{\max}) \;, \;\; k \in \mathbb{F}_{K-1} \,. \tag{4.73}$$

In turn, the first $\tilde{K}-1$ SNs are kept fix while the remaining SNs are re-indexed again to satisfy the inequality chain

$$c_k(P_{\text{remain}}) \leq c_{k+1}(P_{\text{remain}}) \;,\; k \in \mathbb{F}_{K-1} \setminus \mathbb{F}_{\tilde{K}-1} \,. \tag{4.74}$$

Then, we can conclude

$$(\varrho_1^\star, \ldots, \varrho_{\tilde{K}-1}^\star, \varrho_{\tilde{K}}^\star, \varrho_{\tilde{K}+1}^\star, \ldots, \varrho_K^\star) = (0, \ldots, 0, P_{\max} - P_{\text{remain}}, P_{\max}, \ldots, P_{\max}) \,. \tag{4.75}$$

From (4.24), (4.29), (4.30), (4.38), (4.67) and (4.68), we infer

$$V^\star = \left[\frac{1}{r_{\text{rms}}^2} \left(\frac{1}{\left(\frac{c_{\tilde{K}}(P_{\text{remain}})}{P_{\text{remain}}} \right)^2 - 1} + \sum_{k=1}^{\tilde{K}-1} \frac{1}{\left(\frac{c_k(P_{\max})}{P_{\max}} \right)^2 - 1} \right) \right]^{-1} , \tag{4.76}$$

$$\tilde{u}_k^\star = \sqrt{\left(\frac{\alpha_k \beta_k}{\alpha_k + \beta_k + P_{\max}} \right)^2 + \frac{\alpha_k \beta_k P_{\max}}{\alpha_k + \beta_k + P_{\max}}} - \frac{\alpha_k \beta_k}{\alpha_k + \beta_k + P_{\max}} \;,\; k \in \mathbb{F}_{\tilde{K}-1} \,, \tag{4.77}$$

$$\tilde{u}_{\tilde{K}}^\star = \sqrt{\left(\frac{\alpha_{\tilde{K}} \beta_{\tilde{K}}}{\alpha_{\tilde{K}} + \beta_{\tilde{K}} + P_{\text{remain}}} \right)^2 + \frac{\alpha_{\tilde{K}} \beta_{\tilde{K}} P_{\text{remain}}}{\alpha_{\tilde{K}} + \beta_{\tilde{K}} + P_{\text{remain}}}} - \frac{\alpha_{\tilde{K}} \beta_{\tilde{K}}}{\alpha_{\tilde{K}} + \beta_{\tilde{K}} + P_{\text{remain}}} \,, \tag{4.78}$$

$$u_k^\star = \sqrt{\frac{\tilde{u}_k^\star}{M_0}} \;,\; k \in \mathbb{F}_{\tilde{K}} \,, \tag{4.79}$$

$$X_k^\star = \frac{\tilde{u}_k^\star (P_{\max} + \alpha_k)}{\alpha_k + \tilde{u}_k^\star} \,, \quad W_k^\star = \frac{\alpha_k (P_{\max} - \tilde{u}_k^\star)}{\alpha_k + \tilde{u}_k^\star} \;,\; k \in \mathbb{F}_{\tilde{K}-1} \,, \tag{4.80}$$

$$X_{\tilde{K}}^\star = \frac{\tilde{u}_{\tilde{K}}^\star (P_{\text{remain}} + \alpha_{\tilde{K}})}{\alpha_{\tilde{K}} + \tilde{u}_{\tilde{K}}^\star} \,, \quad W_{\tilde{K}}^\star = \frac{\alpha_{\tilde{K}} (P_{\text{remain}} - \tilde{u}_{\tilde{K}}^\star)}{\alpha_{\tilde{K}} + \tilde{u}_{\tilde{K}}^\star} \,, \tag{4.81}$$

$$|v_k^\star| = \frac{V^\star \tilde{u}_k^\star}{r_{\text{rms}} |h_k| \sqrt{\tilde{u}_k^\star + \beta_k} \sqrt{\alpha_k \beta_k - (\tilde{u}_k^\star)^2}} \;,\; k \in \mathbb{F}_{\tilde{K}} \,, \tag{4.82}$$

and

$$|v_k^\star| = X_k^\star = W_k^\star = u_k^\star = 0 \,,\; k \in \mathbb{F}_K \setminus \mathbb{F}_{\tilde{K}} \;. \tag{4.83}$$

The number $\tilde{K}$ of active SNs results from the inequality $0 < P_{\text{remain}} \leq P_{\max}$, that must be fulfilled for the last SN, and is given by the smallest integer number for which the inequality

$$\tilde{K} \geq \frac{P_{\text{tot}}}{P_{\max}} \tag{4.84}$$

holds.

Note that in the considered case, the fusion rule may be more complicated than in (4.46), since more SNs are active in general. On the other hand, the fusion rule may be less complicated than that from Subsection 4.2.3, because not all SNs are possibly active.

In summary, equations (4.75)–(4.84) and (4.21) are the optimal solution to the power allocation problem subject to both types of constraints. They are hence the main contribution of the present subsection.

Note that because of the same argumentation as in Subsection 4.2.2 and 4.2.3, the global optimality of the obtained results is ensured.

4.2.6 A numerical access

As mentioned before, the optimization problem in Subsection 4.2.1 is a signomial program and as we have demonstrated in Subsection 4.2.5 its general optimal solution is quite hard to work out. The main difficulty of dealing with optimization problems like (4.13), (4.47) and (4.60) is the absence of a specific mathematical structure, e.g., monotonicity, convexity and higher order properties. The absence of a specific mathematical structure exacerbates also a numerical access to the optimal solution and a considerable effort is thus needed for solving all aforementioned optimization problems, see [58]. In the current subsection, we provide a proper numerical method to obtain iteratively the optimum of the general optimization problem, discussed in Subsection 4.2.5.

In particular, the optimization problem considered in (4.60) is rewritten such that to obtain a sequential convex program (SCP), which in turn can easily be solved by standard numerical tools like MATLAB® [59] with the aid of CVX [60]. Our approach is based on the substitution of all variables by

$$u_k = \mathrm{e}^{u'_k}\,,\ |v_k| = \mathrm{e}^{v'_k}\,,\ |w_k| = \mathrm{e}^{w'_k}\,,\ k \in \mathbb{F}_K\,, \tag{4.85}$$

where all new variables are real valued. Then an equivalent optimization problem of (4.61) is given by

$$\begin{aligned}
\underset{\mathbf{u}',\ \mathbf{v}',\ \mathbf{w}'}{\text{minimize}} \quad & \sum_{k\in\mathbb{F}_K} \mathrm{e}^{2v'_k}\big(\mathrm{e}^{2u'_k}|h_k|^2 M_0 + N_0\big)\,, \\
\text{subject to} \quad & \sum_{k\in\mathbb{F}_K} \mathrm{e}^{u'_k+v'_k+w'_k}\,|g_k h_k| = 1\,, \\
& \sum_{k\in\mathbb{F}_K} \big(1 + r_{\mathrm{rms}}^2|g_k|^2\mathrm{e}^{2u'_k}\big)\mathrm{e}^{2w'_k} + M_0\mathrm{e}^{2u'_k} \le P_{\mathrm{tot}}\,, \\
& \big(1 + r_{\mathrm{rms}}^2|g_k|^2\mathrm{e}^{2u'_k}\big)\mathrm{e}^{2w'_k} + M_0\mathrm{e}^{2u'_k} \le P_{\max}\,,\ k \in \mathbb{F}_K\,, \\
& \mathbf{u}',\ \mathbf{v}',\ \mathbf{w}' \in \mathbb{R}^K\,,
\end{aligned} \tag{4.86}$$

where the equality constraint is not an affine function. To convexify the above problem, we linearize the equality constraint and obtain the SCP

$$\begin{aligned}
\underset{\mathbf{u}'_n,\,\mathbf{v}'_n,\,\mathbf{w}'_n}{\text{minimize}} \quad & \sum_{k\in\mathbb{F}_K} \mathrm{e}^{2v'_{k,n}}\big(\mathrm{e}^{2u'_{k,n}}|h_k|^2 M_0 + N_0\big)\,, \\
\text{subject to} \quad & \sum_{k\in\mathbb{F}_K} \mathrm{e}^{\delta_{k,n-1}}\big(1 + \delta_{k,n} - \delta_{k,n-1}\big)\,|g_k h_k| = 1\,, \\
& \sum_{k\in\mathbb{F}_K} \big(1 + r_{\mathrm{rms}}^2|g_k|^2\mathrm{e}^{2u'_{k,n}}\big)\mathrm{e}^{2w'_{k,n}} + M_0\mathrm{e}^{2u'_{k,n}} \le P_{\mathrm{tot}}\,, \\
& \big(1 + r_{\mathrm{rms}}^2|g_k|^2\mathrm{e}^{2u'_{k,n}}\big)\mathrm{e}^{2w'_{k,n}} + M_0\mathrm{e}^{2u'_{k,n}} \le P_{\max}\,,\ k \in \mathbb{F}_K\,, \\
& \mathbf{u}'_n,\ \mathbf{v}'_n,\ \mathbf{w}'_n \in \mathbb{R}^K\,,
\end{aligned} \tag{4.87}$$

where the auxiliary variable $\boldsymbol{\delta}_n \coloneqq \mathbf{u}'_n + \mathbf{v}'_n + \mathbf{w}'_n$ is used. The counting index $n \in \mathbb{N}$ thereby represents the n^{th} solution of the SCP (4.87) with arbitrary feasible initial-values $\mathbf{u}'_0$, $\mathbf{v}'_0$ and $\mathbf{w}'_0$. The value of the objective after the n^{th} iteration is denoted by V_n. For sufficiently large n and an accurate choice of initial-values, we expect that the solution of (4.87) converges to the solutions derived in Subsection 4.2.5 which means $V_n \underset{n\mapsto\infty}{\longrightarrow} V^\star$.

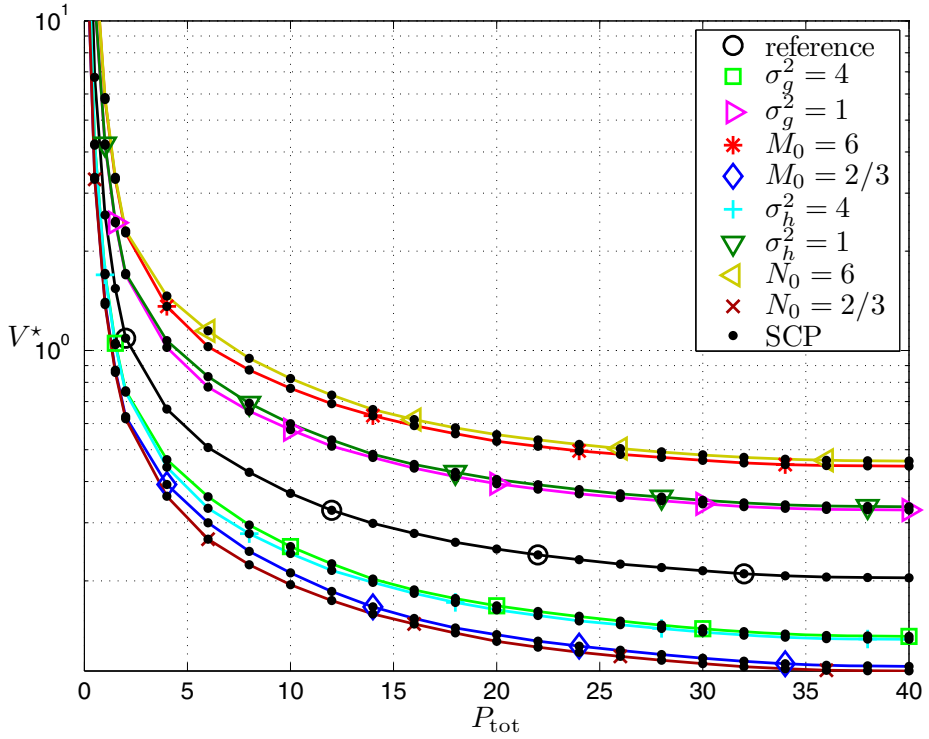

Figure 4.3: The behavior of $V^\star$ from equation (4.76) with respect to P_{tot} is visualized together with the numerical results obtained by the computation of the SCP (4.87). All curves show a decreasing property in P_{tot}. The results of the SCP for sufficiently large number of iterations are equivalent to the closed-form solutions. In order to show a wide range of different cases, we simulate a *reference* curve with the default parameters $K = 20$, $P_{\max} = 2$, $r^2_{\text{rms}} = 1$, $\mathcal{E}[|g_k|^2] = 2\,\forall k$, $\mathcal{E}[|h_k|^2] = 2\,\forall k$, $M_0 = 2$ and $N_0 = 2$. We usually create a new curve by changing only the value of a single parameter which is given in the legend.

In Figure 4.3, both analytical and numerical results for the optimal objective respectively obtained by (4.76) and (4.87) are presented. The SCP is calculated with three criteria of termination. The first one is a minimum number of iterations which is achieved for $n \geq 8$. The second criterion is a feasibility check and is fulfilled by $|1 - \sum_{k\in\mathbb{F}_K} \mathrm{e}^{\delta_{k,n-1}}\big(1 + \delta_{k,n} - \delta_{k,n-1}\big)\,|g_k h_k|\,| \leq 10^{-4}$. The last one is a check of convergency and is determined by the relative value condition $|V_n - V_{n-5}| \leq V_n \cdot 10^{-3}$. All above criteria are based on experiences in this field. Furthermore, each SCP point is calculated with three randomly and independently generated initial-values, where at

the end of each three runs the best achieved result is depicted. Since the precision of the numerical solutions are very high, due to the strict termination criteria from above, all SCP points fall onto the analytical curves. This coincidence reinforces the statement for global optimality of the analytical results on the one hand, and the convergence of the numerical method on the other hand.

4.2.7 Discussion of the solutions

In the case $P_{\max} < P_{\text{tot}} \leq KP_{\max}$ from Subsection 4.2.5 the overall system performance is reduced because of two reasons. First, the SNR of each SN is reduced compared to the results from Subsection 4.2.2, due to the output power-range limitation by $P_{\max} < P_{\text{tot}}$. Second, not all SNs can in general be active, due to the sum-power limitation by $P_{\text{tot}} \leq KP_{\max}$, such that the system performance is weaker compared to the results of Subsection 4.2.3. Hence, the value in (4.76) is in general greater than the ones in (4.40) and (4.56). This behavior is not surprising and the performance reduction was predictable, since we have included more restrictions into the optimization problem. Note that all optimal solutions from Subsections 4.2.2, 4.2.3 and 4.2.5 are different to the well-known *water-filling* solution, see [44]. The difference to the water-filling solution emerges from the fact that the information flow over each effective path, consisting of a single SN, its sensing channel, the modest signal processing of the same SN, and its communication channel followed by the associated weight in the fusion center, is adjustable due to the power optimization. Thus, on the one hand, the diversity of each effective path is not predetermined such that the water-filling solution cannot hold in its general form. On the other hand, the diversity of best effective paths is amplified in comparison to the diversity of poorest effective paths because of the optimal solution to the power allocation.

In practice, the value of each $c_k(P_{\max})$ is in general unique such that the inequality chain $c_k(P_{\max}) < c_{k+1}(P_{\max})$ for all $k \in \mathbb{F}_{K-1}$ holds. In this case, the optimal value of the objective (4.76) is decreasing with respect to both P_{tot} and $P_{\max}$. If $P_{\max}$ is fixed and P_{tot} varies in the range $P_{\max} \leq P_{\text{tot}} \leq KP_{\max}$, then the optimal value of the objective (4.76) is decreasing with respect to P_{tot} because the SNR of the whole sensor network is increasing with P_{tot}. The best situation is achieved only when all SNs are active, i.e., $P_{\text{tot}} = KP_{\max}$. In contrast, if P_{tot} is fixed and $P_{\max}$ varies in the range $\frac{1}{K}P_{\text{tot}} \leq P_{\max} \leq P_{\text{tot}}$, then the optimal value of the objective (4.76) is decreasing with respect to $P_{\max}$ because the capability of each SN is increasing with $P_{\max}$. The best situation is achieved only when a single SN is active, i.e., $P_{\max} = P_{\text{tot}}$.

In a practical application, the value of $P_{\max}$ is fixed and P_{tot} can suitably be adjusted within the extended range $0 < P_{\text{tot}} \leq KP_{\max}$. In order to save energy, the value of P_{tot} should be as less as possible, which means that a single SN or only a few SNs are active. On the other hand, to accurately estimate additional quantities such as position, velocity, acceleration, angle of movement, and other important properties and parameters of the target object, more than few SNs are needed to be active. Hence, if the number $\tilde{K}$ of active SNs is satisfactory to accurately estimate all important parameters of the target, then the best energy-aware value of P_{tot} is equal to $\tilde{K}P_{\max}$.

In turn, the value of $P_{\max}$ should be large enough to achieve a desired classification or detection probability. With this setup, all three system parameters $\tilde{K}$, $P_{\max}$ and P_{tot} are optimally determined for an energy-aware system design.

4.3 Geometric Position of Most Reliable Sensor Nodes

In this section, we are aiming for an analytic-geometric solution to determine regions containing only the subset of most reliable and therefore active SNs. In general, as depicted in Figure 4.4, only a single region, not necessary a connected space, exists such that all containing SNs are active and correspond with the optimum power allocation. The Figure 4.4 shows a cut through the disturbance-intensity (4.38) yielding the optimum selection area of SNs in a 2-dimensional case, where all SNs, the fusion center and the target object are placed on a single plane. By assuming a uniform distribution of SNs and a simple channel model without multipath and fading effects, we are able to determine a 3-dimensional region for identifying the most reliable SNs. Although the mathematical integration for determining the number of active SNs within the corresponding geometrical subspace is challenging, we analytically derive novel relationships in closed-form between the number of active SNs, their reliability and geometrical positions. Since these results are cumbersome in practice, we propose in addition an accurate and simple approximation for the mentioned relationship. Our insights might be used for replacing the selection procedure or for pre-selection of most reliable SNs to limit the complexity of subsequent algorithms.

4.3.1 Identifying the best sensor nodes

In the current subsection, we again consider the optimization problem from Subsection 4.2.5 and recapitulate selected results first. Without loss of generality, we set the useful range of $P_{\max}$ and P_{tot} equal to $0 < P_{\max} \leq P_{\text{tot}} \leq KP_{\max}$ and assume a quantized sum-power constraint, which is described by $\frac{P_{\text{tot}}}{P_{\max}} \in \mathbb{N}$ or equivalently $P_{\text{remain}} = P_{\max}$, for reasons of simplicity. If all SNs are such re-indexed that the inequality chain in (4.73) holds, then the reliability of the best and the worst SN is described by $c_1(P_{\max})$ and $c_K(P_{\max})$, respectively. Since the reliability of the first $\tilde{K}$ SNs, with $\tilde{K} \in \mathbb{F}_K$, is better than that of the remaining ones, only these $\tilde{K}$ SNs are active and participate in sensing and data communication. Each of $\tilde{K}$ SNs receives $P_{\max}$ for the sum of its sensing and communication powers.

Based on this, the main problem of sensor selection is to sort all SNs such that the inequality chain in (4.73) holds. Since each quantity $c_k(P_{\max})$ is dependent on its $|g_k|$ and $|h_k|$, the geometric position of fusion center, target object and the k^{th}-SN predescribe the expected value of $c_k(P_{\max})$. Thus, for selecting the most reliable SNs, an investigation of the interaction of all positions is essential. In the following, we consider a scenario described by Figure 4.5, where the fusion center is located at the origin of the Cartesian coordinates, the target object at the position $(\sigma_0, 0, 0)$, $\sigma_0 \in \mathbb{R}_+$, and the

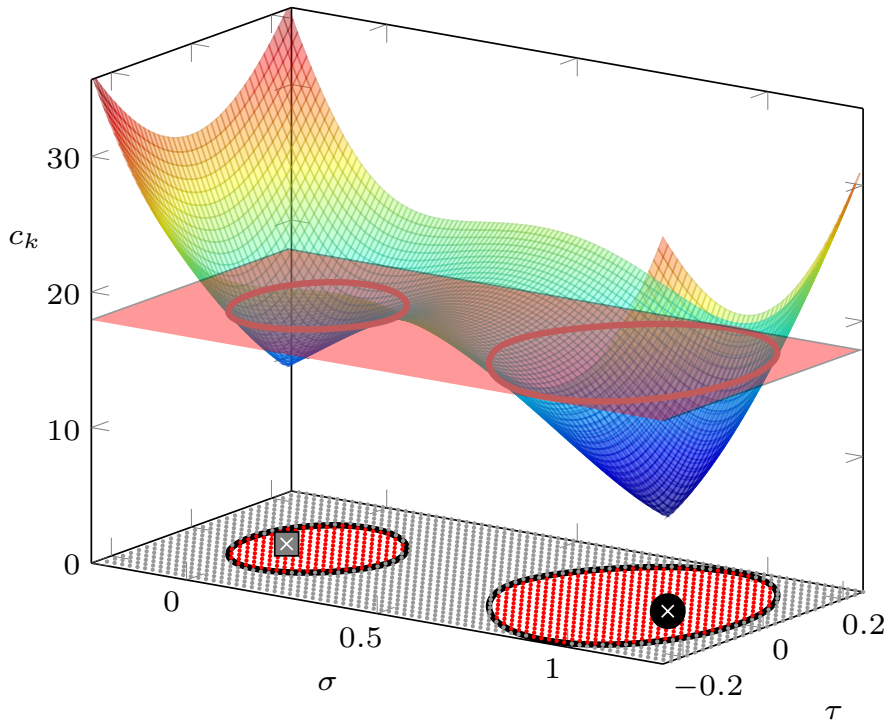

Figure 4.4: A visualization of the 2-d disturbance-intensity containing the slice plane and its projection. Active and idle sensor nodes are marked in red and gray, respectively. The fusion center and the target object are marked by a square and a circle, respectively.

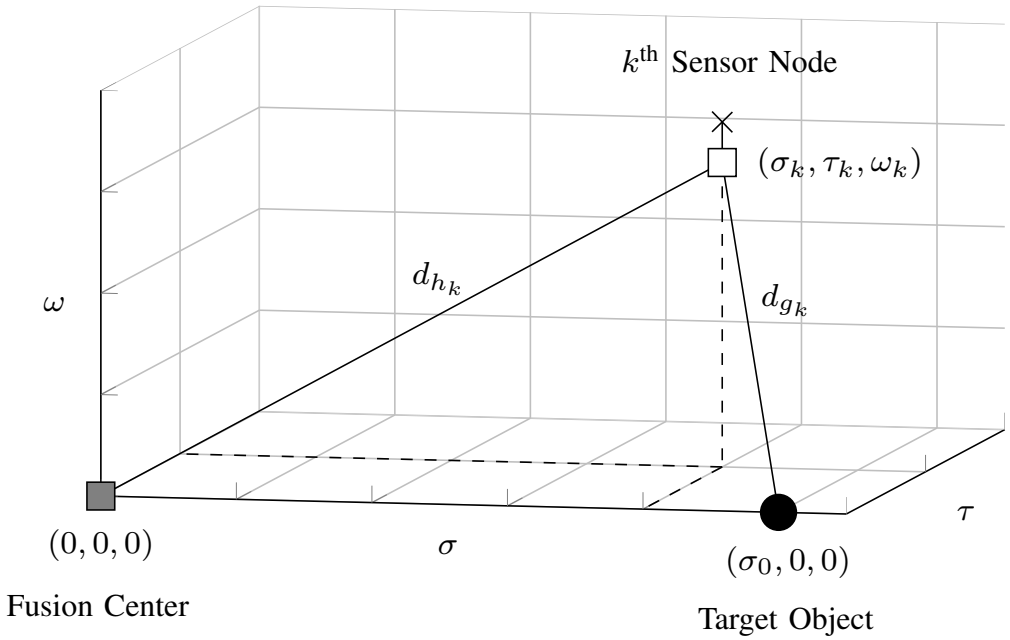

Figure 4.5: The placement of fusion center, target object and all sensor nodes in Cartesian coordinates.

k^{th}-SN at the position $(\sigma_k, \tau_k, \omega_k) \in \mathbb{R}^3$. If we only consider the free-space path loss without fading, then both channel coefficients of the k^{th}-SN are described by

$$|g_k| = \frac{\lambda}{4\,\pi\,2\,d_{g_k}} \quad \text{and} \quad |h_k| = \frac{\lambda}{4\,\pi\,d_{h_k}}\ ,\ k \in \mathbb{F}_K\,, \tag{4.88}$$

where the distance between the k^{th}-SN to the fusion center is described by $d_{h_k} \in \mathbb{R}_+$ while the distance from the k^{th}-SN to the target object and back to the same SN is described by $2d_{g_k} \in \mathbb{R}_+$. The value λ is the signal wavelength. Both Euclidean distances d_{g_k} and d_{h_k} are described by

$$d_{g_k} \coloneqq \sqrt{(\sigma_k - \sigma_0)^2 + \tau_k^2 + \omega_k^2} \quad \text{and} \quad d_{h_k} \coloneqq \sqrt{\sigma_k^2 + \tau_k^2 + \omega_k^2}\ ,\ k \in \mathbb{F}_K\,. \tag{4.89}$$

By incorporating all above equations into (4.38), we obtain

$$\begin{aligned} c_k(P) = &\sqrt{a^2\,[(\sigma_k - \sigma_0)^2 + \tau_k^2 + \omega_k^2]} \cdot \sqrt{b^2\,[\sigma_k^2 + \tau_k^2 + \omega_k^2]} \\ &+ \sqrt{P + a^2[(\sigma_k - \sigma_0)^2 + \tau_k^2 + \omega_k^2]} \cdot \sqrt{P + b^2[\sigma_k^2 + \tau_k^2 + \omega_k^2]}\,, \end{aligned} \tag{4.90}$$

where both parameters a and b are independent from index k and are given as

$$a^2 \coloneqq \frac{M_0\,4^3\,\pi^2}{\lambda^2\,r_{\text{rms}}^2} > 0 \quad \text{and} \quad b^2 \coloneqq \frac{N_0\,4^2\,\pi^2}{\lambda^2} > 0\,. \tag{4.91}$$

For a given c and $P_{\max}$, with $c_{\tilde{K}}(P_{\max}) < c \leq c_K(P_{\max})$, the associated subspace $\mathbb{S}(c)$, in which the most reliable SNs are included, is described with the aid of (4.38) by

$$\begin{aligned} \mathbb{S}(c) \coloneqq \big\{(\sigma, \tau, \omega) \in \mathbb{R}^3 \mid &\sqrt{a^2\,[(\sigma - \sigma_0)^2 + \tau^2 + \omega^2]} \cdot \sqrt{b^2\,[\sigma^2 + \tau^2 + \omega^2]} \\ &+ \sqrt{P_{\max} + b^2[\sigma^2 + \tau^2 + \omega^2]} \cdot \sqrt{P_{\max} + a^2[(\sigma - \sigma_0)^2 + \tau^2 + \omega^2]} \leq c\big\}\,. \end{aligned} \tag{4.92}$$

The surface of the subspace (4.92) describes a 2-dimensional submanifold, or equivalently a 3-dimensional subspace of $\mathbb{R}^3$, which in turn is described by a multivariate polynomial with a degree equal to four, in three variables, and five parameters. Thus, it is analytically challenging to calculate its volume in closed-form, since for this calculation the evaluation of all polynomial roots is needed to obtain the integration boundaries. Nevertheless, in the following, we set out to obtain a relationship between the number $\tilde{K}$ of active SNs and corresponding values of the disturbance-intensity $c_k(P_{\max})$ by calculating the volume of (4.92).

At first, we reduce the number of parameters by the substitutions $P_a \coloneqq P_{\max}/a^2$, $P_b \coloneqq P_{\max}/b^2$ and $c_{ab} \coloneqq c/(a \cdot b)$. Second, we reduce the number of variables for integration by transforming the coordinate system with the aid of $\xi^2 \coloneqq \tau^2 + \omega^2$, since $\mathbb{S}$ is symmetric with respect to rotations in the τ-ω-plane. Hence, we obtain equivalent forms

$$\begin{aligned} \mathbb{S}(c_{ab}) &= \big\{(\sigma, \xi, \varphi) \in \mathbb{R} \times \mathbb{R}_+ \times [0, 2\pi] \mid \sqrt{(\sigma - \sigma_0)^2 + \xi^2} \cdot \sqrt{\sigma^2 + \xi^2} \\ &\quad + \sqrt{P_b + \sigma^2 + \xi^2} \cdot \sqrt{P_a + (\sigma - \sigma_0)^2 + \xi^2} \leq c_{ab}\big\} \\ &= [0, 2\pi] \times \big\{(\sigma, \xi) \in \mathbb{R} \times \mathbb{R}_+ \mid \sqrt{(\sigma - \sigma_0)^2 + \xi^2} \cdot \sqrt{\sigma^2 + \xi^2} \\ &\quad + \sqrt{P_b + \sigma^2 + \xi^2} \cdot \sqrt{P_a + (\sigma - \sigma_0)^2 + \xi^2} \leq c_{ab}\big\} =: [0, 2\pi] \times \tilde{\mathbb{S}}(c_{ab})\,. \end{aligned} \tag{4.93}$$

In order to calculate the corresponding number $\tilde{K}$ of SNs, which are members of the subspace $\mathbb{S}(c_{ab})$, an integration over the sensor distribution in this subspace is needed. If we assume that all SNs are uniformly distributed, with a density of ρ SNs per volume-unit, then we are analytically able to calculate the corresponding integrals

$$\tilde{K}(c_{ab}) \coloneqq \int\limits_{\mathbb{S}(c_{ab})} \rho \,\mathrm{d}\sigma \,\mathrm{d}\tau \,\mathrm{d}\omega = 2\pi \int\limits_{\tilde{\mathbb{S}}(c_{ab})} \rho \,\xi \,\mathrm{d}\sigma \,\mathrm{d}\xi \tag{4.94}$$

in closed form. However, for the integration all proper boundaries are needed. These boundaries are equivalent with some real roots of the equation

$$\sqrt{(\sigma-\sigma_0)^2+\xi^2}\cdot\sqrt{\sigma^2+\xi^2}+\sqrt{P_b+\sigma^2+\xi^2}\cdot\sqrt{P_a+(\sigma-\sigma_0)^2+\xi^2}-c_{ab}=0\,. \tag{4.95}$$

By some algebra, we infer four real roots for ξ while only one of them can be satisfied by the range of σ and is in addition always positive. The corresponding root is given by

$$\begin{aligned}\xi_0^2(\sigma) \coloneqq{}& \frac{(P_a+P_b)\cdot[2c_{ab}^2-2P_aP_b-\sigma_0(P_a-P_b)\cdot(2\sigma-\sigma_0)]}{2(P_a+P_b)^2-8c_{ab}^2}\\ &+\frac{(2\sigma^2+\sigma_0^2-2\sigma\sigma_0)\cdot[4c_{ab}^2-(P_a+P_b)^2]}{2(P_a+P_b)^2-8c_{ab}^2}\\ &-\frac{4c_{ab}\sqrt{c_{ab}^2-(P_a-2\sigma\sigma_0+\sigma_0^2)\cdot(P_b+2\sigma\sigma_0-\sigma_0^2)}\cdot\sqrt{c_{ab}^2-P_aP_b}}{2(P_a+P_b)^2-8c_{ab}^2}\,.\end{aligned} \tag{4.96}$$

Furthermore, we infer four roots for σ which define possible integration boundaries over σ and in turn yield real positive values for $\xi_0^2(\sigma)$. The first two roots of σ are always real while the domain of the other two is real or complex depending on certain choices of parameters. These roots are given as

$$\sigma_1 \coloneqq \frac{2\sigma_0(P_b+c_{ab})-\sqrt{c_{ab}^2-P_aP_b}\cdot\sqrt{P_a+P_b+2c_{ab}+\sigma_0^2}}{2(P_a+P_b+2c_{ab})}\,, \tag{4.97a}$$

$$\sigma_2 \coloneqq \frac{2\sigma_0(P_b+c_{ab})+\sqrt{c_{ab}^2-P_aP_b}\cdot\sqrt{P_a+P_b+2c_{ab}+\sigma_0^2}}{2(P_a+P_b+2c_{ab})}\,, \tag{4.97b}$$

$$\sigma_3 \coloneqq \frac{2\sigma_0(P_b-c_{ab})-\sqrt{c_{ab}^2-P_aP_b}\cdot\sqrt{P_a+P_b-2c_{ab}+\sigma_0^2}}{2(P_a+P_b-2c_{ab})} \tag{4.97c}$$

and

$$\sigma_4 \coloneqq \frac{2\sigma_0(P_b-c_{ab})+\sqrt{c_{ab}^2-P_aP_b}\cdot\sqrt{P_a+P_b-2c_{ab}+\sigma_0^2}}{2(P_a+P_b-2c_{ab})}\,. \tag{4.97d}$$

Since the subspace $\mathbb{S}(c_{ab})$ is for some certain choices of parameters a connected space and for other choices a disconnected space, different cases for the evaluation of the integral (4.94) are to distinguish. In summary, we obtain the following five cases.

1. If $c_{ab} \leq \min\{\sqrt{(P_b+\sigma_0^2)P_a}, \sqrt{(P_a+\sigma_0^2)P_b}\}$, the value of c_{ab} is too small to obtain any positive volume:
$$\Rightarrow \quad \tilde{K}(c_{ab}) = 0 \tag{4.98a}$$

2. If $\min\{\sqrt{(P_b+\sigma_0^2)P_a}, \sqrt{(P_a+\sigma_0^2)P_b}\} < c_{ab} \leq \max\{\sqrt{(P_b+\sigma_0^2)P_a}, \sqrt{(P_a+\sigma_0^2)P_b}\}$ and $P_a > P_b$, the subspace $\mathbb{S}$ is a disconnected space and separated in two regions, where only one of both regions has a positive real volume:
$$\Rightarrow \quad \tilde{K}(c_{ab}) = \pi\rho \int_{\sigma_1}^{\sigma_4} \xi_0^2(\sigma)\,\mathrm{d}\sigma \tag{4.98b}$$

3. If $\min\{\sqrt{(P_b+\sigma_0^2)P_a}, \sqrt{(P_a+\sigma_0^2)P_b}\} < c_{ab} \leq \max\{\sqrt{(P_b+\sigma_0^2)P_a}, \sqrt{(P_a+\sigma_0^2)P_b}\}$ and $P_a < P_b$, the structure of the subspace $\mathbb{S}$ is analogous to the previous case:
$$\Rightarrow \quad \tilde{K}(c_{ab}) = \pi\rho \int_{\sigma_3}^{\sigma_2} \xi_0^2(\sigma)\,\mathrm{d}\sigma \tag{4.98c}$$

4. If $\max\{\sqrt{(P_b+\sigma_0^2)P_a}, \sqrt{(P_a+\sigma_0^2)P_b}\} < c_{ab} \leq \frac{P_a+P_b+\sigma_0^2}{2}$ and $\sigma_0^2 > |P_b - P_a|$, the disconnected subspace $\mathbb{S}$ consists of two regions and has two positive real volumes:
$$\Rightarrow \quad \tilde{K}(c_{ab}) = \pi\rho \int_{\sigma_1}^{\sigma_4} \xi_0^2(\sigma)\,\mathrm{d}\sigma + \pi\rho \int_{\sigma_3}^{\sigma_2} \xi_0^2(\sigma)\,\mathrm{d}\sigma \tag{4.98d}$$

5. If otherwise, the subspace $\mathbb{S}$ is a connected space with a single positive volume:
$$\Rightarrow \quad \tilde{K}(c_{ab}) = \pi\rho \int_{\sigma_1}^{\sigma_2} \xi_0^2(\sigma)\,\mathrm{d}\sigma\,. \tag{4.98e}$$

Note that for the above cases the unbounded integral $\int \xi_0^2(\sigma)\,\mathrm{d}\sigma$ is given in closed-form with the aid of [29, p. 95, eq. 2.262.1] and [29, p. 94, eq. 2.261]. Unfortunately, after incorporating both integration boundaries, this solution becomes too long such that we omit the presentation of this integration result in this thesis, for the sake of compactness.

Since the obtained results in (4.98) are lengthy, we present in addition the approximation
$$\tilde{K}(c_{ab}) \approx \frac{\pi\rho\sqrt{2}\left(c_{ab} - \min\{\sqrt{(P_b+\sigma_0^2)P_a}, \sqrt{(P_a+\sigma_0^2)P_b}\}\right)^{3/2}}{3}\,, \tag{4.99}$$
which has a simple structure and is very accurate for all $c_{ab} \gg \frac{P_a+P_b+\sigma_0^2}{2}$, without proof. A detailed investigation of similar approximations is discussed in [12].

All equations in (4.98) analytically determine the number $\tilde{K}$ of active SNs as a function of any maximum reliability value c_{ab} in closed-form. These are the main contributions of the present subsection.

4.3.2 Visualization and numerical evaluation

In Figure 4.6, the relationship between the number $\tilde{K}$ of active SNs and the maximum reliability c_{ab} is shown for two different sets of parameters. All markers represent numerical evaluations while all continuous curves represent analytical results. Furthermore, the approximation in (4.99) is depicted which converges very fast for large values of c_{ab}.

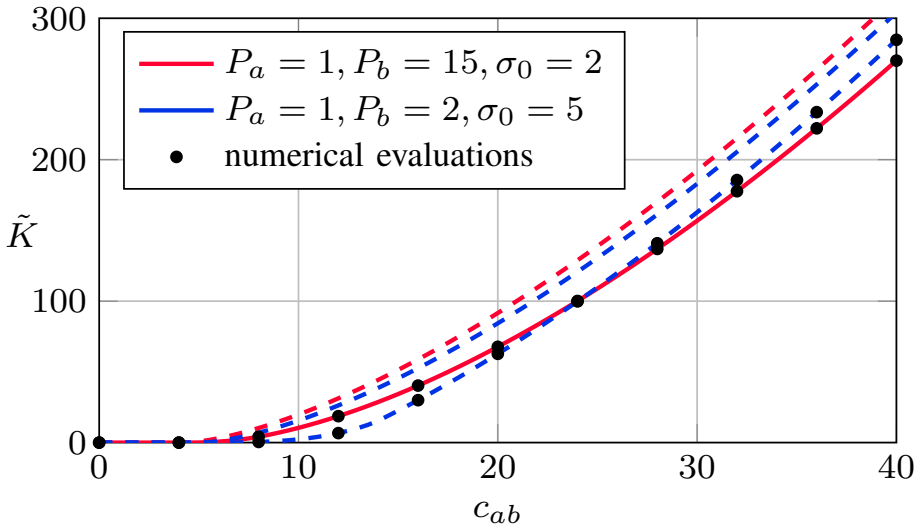

Figure 4.6: Number $\tilde{K}$ of active sensor nodes, which are included in the subspace $\mathbb{S}(c_{ab})$, as a function of the maximum reliability c_{ab} for $\rho = 1$. Two different sets of parameters are chosen to visualize all five cases described analytically by equations in (4.98). Markers show numerical evaluations of (4.94) for comparison. Equation (4.99) is also visualized by two dashed curves for the same two sets of parameters.

In order to develop an imagination for the subspace $\mathbb{S}$, its surface is exemplary depicted in Figure 4.7a. As can be seen, this subspace has a complicated surface compared to an ellipsoid. Hence, the geometric region of most reliable SNs is highly dependent on the specific values for the parameters a, b, $P_{\max}$ and σ_0.

In Figure 4.7b the ω-ordinate is fixed to $\omega = 0$ in order to show the effect of the parameter c over the main slice plane of $\mathbb{S}$. Because of a certain choice of the parameters a, b, $P_{\max}$ and σ_0, it is obvious that the regions become asymmetric and hence for small values of c each single subspace is divided into two parts. This behavior is very clearly shown in Figure 4.4, as well.

4.4 Technical Interpretation and Visualization of Results

As derived in Subsection 4.2.5, the power allocation problem in its general form is analytically solved in closed-form. For achieving these results, we only have focused

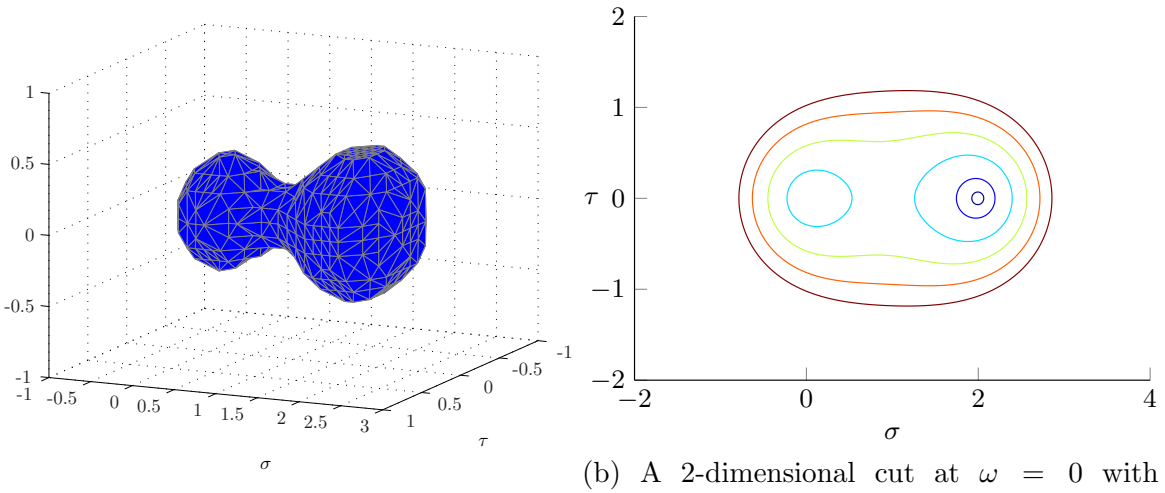

(a) A 3-dimensional view for $c = 0.023$

(b) A 2-dimensional cut at $\omega = 0$ with $c \in \{0.005, 0.01, 0.02, 0.03, 0.04, 0.05\}$

Figure 4.7: Visualization of the subspace $\mathbb{S}$ for the specific choice of $a = 0.2$, $b = 0.05$, $P_{\max} = 0.001$ and $\sigma_0 = 2$.

on the mathematical analysis, synthesis and methods. However, it is difficult to gain insight into the technical analysis, synthesis and description, due to the presented form. In this section, we introduce physical parameters in order to highlight important aspects of the underlying system and technically interpret the optimal solution of the power allocation problem. Following this, selected results are visualized by corresponding curves.

4.4.1 Measurable parameters and technical interpretation of results

Analogous to Subsection 3.3.1, we denote the signal-to-noise ratio at the receiver of each SN and the signal-to-noise ratio at the receiver of the fusion center respectively by

$$\mathrm{SNR}_k^{\mathrm{S}}(W) \coloneqq \frac{W r_{\mathrm{rms}}^2 |g_k|^2}{M_0} \quad \text{and} \quad \mathrm{SNR}_k^{\mathrm{C}}(X) \coloneqq \frac{X |h_k|^2}{N_0}, \quad k \in \mathbb{F}_K, \tag{4.100}$$

for all $0 < W \leq \min\{P_{\max}, P_{\mathrm{tot}}\}$ and $0 < X \leq \min\{P_{\max}, P_{\mathrm{tot}}\}$. Alternatively, the signal-to-noise ratio at the receiver of the fusion center can be described by both $\mathrm{SNR}_k^{\mathrm{S}}(W)$ and $\mathrm{SNR}_k^{\mathrm{C}}(X)$ as

$$\mathrm{SNR}_k(W, X) \coloneqq \frac{\mathcal{E}[|w_k r_i g_k u_k h_k|^2]}{\mathcal{E}[|m_k u_k h_k + n_k|^2]} = \frac{\mathrm{SNR}_k^{\mathrm{S}}(W) \cdot \mathrm{SNR}_k^{\mathrm{C}}(X)}{1 + \mathrm{SNR}_k^{\mathrm{S}}(W) + \mathrm{SNR}_k^{\mathrm{C}}(X)}, \quad k \in \mathbb{F}_K. \tag{4.101}$$

The ratio $\mathrm{SNR}_k(W, X)$ is the signal-to-noise ratio of the k^{th} path from the k^{th} SN to the target, back to the same SN, and from there to the fusion center. Note that all

above definitions depend on the specific values of W and X. By substitution of α_k and β_k by

$$\alpha_k = \frac{P}{\mathrm{SNR}_k^{\mathrm{S}}(P)} \quad \text{and} \quad \beta_k = \frac{P}{\mathrm{SNR}_k^{\mathrm{C}}(P)}\,, \quad P > 0\,,\ k \in \mathbb{F}_K, \tag{4.102}$$

and incorporating all these into equation (4.23), we obtain a signal-to-noise ratio at the output of the fusion center as given by

$$\mathrm{SNR}_{\mathrm{tot}} \coloneqq \frac{r_{\mathrm{rms}}^2}{V} = \sum_{k\in\mathbb{F}_K} \frac{\mathrm{SNR}_k^{\mathrm{S}}(W_k)\cdot\mathrm{SNR}_k^{\mathrm{C}}(X_k)}{1+\mathrm{SNR}_k^{\mathrm{S}}(W_k)+\mathrm{SNR}_k^{\mathrm{C}}(X_k)} = \sum_{k\in\mathbb{F}_K} \mathrm{SNR}_k(W_k,X_k)\,. \tag{4.103}$$

This means that after optimization of the variables v_k, only the path signal-to-noise ratios SNR_k are important at the fusion center. In this way, the minimization of the mean square deviation in (4.12) leads to the maximization of the total signal-to-noise ratio at the output of the fusion center. This is equivalent with

$$\begin{aligned} &\underset{\mathbf{X},\mathbf{W}}{\text{maximize}} \quad \sum_{k\in\mathbb{F}_K} \frac{\mathrm{SNR}_k^{\mathrm{S}}(W_k)\cdot\mathrm{SNR}_k^{\mathrm{C}}(X_k)}{1+\mathrm{SNR}_k^{\mathrm{S}}(W_k)+\mathrm{SNR}_k^{\mathrm{C}}(X_k)} \\ &\text{subject to} \quad \sum_{k\in\mathbb{F}_K} X_k + W_k \le P_{\mathrm{tot}}\,,\ X_k + W_k \le P_{\max}\,,\ k\in\mathbb{F}_K\,,\ \mathbf{X}\in\mathbb{R}_+^K\,,\ \mathbf{W}\in\mathbb{R}_+^K\,. \end{aligned} \tag{4.104}$$

In contrast to the case described in Subsection 3.3.1, the above maximization problem is neither a convex nor a concave optimization problem such that more effort is needed to solve it as shown in Subsection 4.2.5. It is to mention, that the above maximization problem is symmetric in $\mathrm{SNR}_k^{\mathrm{S}}(W_k)$ and $\mathrm{SNR}_k^{\mathrm{C}}(X_k)$ and thus it can be expected that all results behave also symmetric in $\mathrm{SNR}_k^{\mathrm{S}}(W_k)$ and $\mathrm{SNR}_k^{\mathrm{C}}(X_k)$. After maximization we obtain the results

$$\tilde{u}_k^\star = \frac{P_{\max}}{1+\sqrt{1+\mathrm{SNR}_k^{\mathrm{S}}(P_{\max})+\mathrm{SNR}_k^{\mathrm{C}}(P_{\max})+\mathrm{SNR}_k^{\mathrm{S}}(P_{\max})\cdot\mathrm{SNR}_k^{\mathrm{C}}(P_{\max})}}\,,\ k\in\mathbb{F}_{\tilde{K}-1}\,, \tag{4.105}$$

$$\tilde{u}_{\tilde{K}}^\star = \frac{P_{\mathrm{remain}}}{1+\sqrt{1+\mathrm{SNR}_{\tilde{K}}^{\mathrm{S}}(P_{\mathrm{remain}})+\mathrm{SNR}_{\tilde{K}}^{\mathrm{C}}(P_{\mathrm{remain}})+\mathrm{SNR}_{\tilde{K}}^{\mathrm{S}}(P_{\mathrm{remain}})\cdot\mathrm{SNR}_{\tilde{K}}^{\mathrm{C}}(P_{\mathrm{remain}})}}\,, \tag{4.106}$$

$$\begin{aligned} \mathrm{SNR}_{\mathrm{tot}}^\star \coloneqq \frac{r_{\mathrm{rms}}^2}{V^\star} &= \frac{\mathrm{SNR}_{\tilde{K}}^{\mathrm{S}}(P_{\mathrm{remain}})\cdot\mathrm{SNR}_{\tilde{K}}^{\mathrm{C}}(P_{\mathrm{remain}})}{\left(\sqrt{1+\mathrm{SNR}_{\tilde{K}}^{\mathrm{S}}(P_{\mathrm{remain}})}+\sqrt{1+\mathrm{SNR}_{\tilde{K}}^{\mathrm{C}}(P_{\mathrm{remain}})}\right)^2} \\ &\quad + \sum_{k=1}^{\tilde{K}-1} \frac{\mathrm{SNR}_k^{\mathrm{S}}(P_{\max})\cdot\mathrm{SNR}_k^{\mathrm{C}}(P_{\max})}{\left(\sqrt{1+\mathrm{SNR}_k^{\mathrm{S}}(P_{\max})}+\sqrt{1+\mathrm{SNR}_k^{\mathrm{C}}(P_{\max})}\right)^2}\,, \end{aligned} \tag{4.107}$$

$$X_k^\star = P_{\max} \cdot \frac{\frac{\tilde{u}_k^\star}{P_{\max}} \left(1 + \mathrm{SNR}_k^{\mathrm{S}}(P_{\max})\right)}{1 + \frac{\tilde{u}_k^\star}{P_{\max}} \mathrm{SNR}_k^{\mathrm{S}}(P_{\max})}, \quad W_k^\star = P_{\max} \cdot \frac{1 - \frac{\tilde{u}_k^\star}{P_{\max}}}{1 + \frac{\tilde{u}_k^\star}{P_{\max}} \mathrm{SNR}_k^{\mathrm{S}}(P_{\max})}, \; k \in \mathbb{F}_{\tilde{K}-1}, \tag{4.108}$$

and

$$X_{\tilde{K}}^\star = P_{\mathrm{remain}} \cdot \frac{\frac{\tilde{u}_{\tilde{K}}^\star}{P_{\mathrm{remain}}} \left(1 + \mathrm{SNR}_{\tilde{K}}^{\mathrm{S}}(P_{\mathrm{remain}})\right)}{1 + \frac{\tilde{u}_{\tilde{K}}^\star}{P_{\mathrm{remain}}} \mathrm{SNR}_{\tilde{K}}^{\mathrm{S}}(P_{\mathrm{remain}})}, \quad W_{\tilde{K}}^\star = P_{\mathrm{remain}} \cdot \frac{1 - \frac{\tilde{u}_{\tilde{K}}^\star}{P_{\mathrm{remain}}}}{1 + \frac{\tilde{u}_{\tilde{K}}^\star}{P_{\mathrm{remain}}} \mathrm{SNR}_{\tilde{K}}^{\mathrm{S}}(P_{\mathrm{remain}})}, \tag{4.109}$$

where an equivalent definition for the disturbance-intensity c_k, the so called *reliability-function*, given as

$$\tilde{c}_k(P) \coloneqq \sqrt{\frac{c_k^2(P)}{P^2} - 1} = \sqrt{\frac{1 + \mathrm{SNR}_k^{\mathrm{S}}(P)}{\mathrm{SNR}_k^{\mathrm{S}}(P) \cdot \mathrm{SNR}_k^{\mathrm{C}}(P)}} + \sqrt{\frac{1 + \mathrm{SNR}_k^{\mathrm{C}}(P)}{\mathrm{SNR}_k^{\mathrm{S}}(P) \cdot \mathrm{SNR}_k^{\mathrm{C}}(P)}}, \quad k \in \mathbb{F}_K, \tag{4.110}$$

for all $0 < P \leq \min\{P_{\max}, P_{\mathrm{tot}}\}$, is used. The best choice for P is to be equal to $\min\{P_{\max}, P_{\mathrm{tot}}\}$ or equal to P_{remain} depending on k, because in this case no SN will exceed its power limitation $P_{\max}$. The advantage of the new definition (4.110) is that this equivalent definition is easily comparable with the reliability-function in (3.72). In contrast to (3.72) the reliability in (4.110) is symmetric in both $\mathrm{SNR}_k^{\mathrm{S}}(P)$ and $\mathrm{SNR}_k^{\mathrm{C}}(P)$. Because of this distinction, the optimal method for power allocation is in case of passive networks similar to water-filling while in case of active networks is not water-filling. The interpretation behind the optimal power allocation is that at the globally optimum the active sensor network combines independently all signal-to-noise ratios $\mathrm{SNR}_k^{\mathrm{S}}(P_{\max})$, $\mathrm{SNR}_k^{\mathrm{C}}(P_{\max})$, $\mathrm{SNR}_k^{\mathrm{S}}(P_{\mathrm{remain}})$ and $\mathrm{SNR}_k^{\mathrm{C}}(P_{\mathrm{remain}})$ of all active SNs, with fixed powers $P_{\max}$ and P_{remain}, as demonstrated in (4.107). In turn, at the globally optimum only the signal-to-noise ratios $\mathrm{SNR}_k^{\mathrm{S}}(P_{\max})$, $\mathrm{SNR}_k^{\mathrm{C}}(P_{\max})$, $\mathrm{SNR}_k^{\mathrm{S}}(P_{\mathrm{remain}})$ and $\mathrm{SNR}_k^{\mathrm{C}}(P_{\mathrm{remain}})$ are needed to determine the total signal-to-noise ratio $\mathrm{SNR}_{\mathrm{tot}}^\star$ at the fusion center. Hence, one only needs the equation (4.107) with (4.110) in order to investigate or to discuss the entire sensor network in a simple manner. In a practical application, the consecutive steps in Table 4.1 are to perform for an optimal allocation of power.

Since $\mathrm{SNR}_{\mathrm{tot}}^\star$ is again the sum of the $\tilde{K}$ largest observations in the sample of K independent observations SNR_k, the distribution of $\mathrm{SNR}_{\mathrm{tot}}^\star$ is amenable by the theory of order statistics. As already mentioned in Subsection 3.3, for a wide range of continuous distributions of the samples SNR_k, the distribution of $\mathrm{SNR}_{\mathrm{tot}}^\star$ can accurately be fitted by the Fréchet distribution.

4.4.2 Visualization of results

Analogous to Subsection 3.3.2, we assume that all channel coefficients are complex normal distributed such that resulting signal-to-noise ratios are gamma distributed. Furthermore, we assume $\frac{P_{\mathrm{tot}}}{P_{\max}} \in \mathbb{N}$ such that $P_{\mathrm{remain}} = P_{\max}$. To visualize the total signal-to-noise ratio (4.107), we perform a Monte-Carlo simulation with 100000 iterations per simulation point. All signal-to-noise ratios $\mathrm{SNR}_k^{\mathrm{S}}(P_{\max})$ and $\mathrm{SNR}_k^{\mathrm{C}}(P_{\max})$ are

Table 4.1: Consecutive steps for an optimal allocation of power in active sensor networks.

Step Number	Step Description
1.	Choose $W = \min\{P_{\max}, P_{\text{tot}}\}$ for the sensing power of each SN,
2.	choose $X = W$ for the communication power of each SN,
3.	measure each signal-to-noise ratio $\text{SNR}_k^{\text{S}}(W)$ at the input of the corresponding SN,
4.	measure each signal-to-noise ratio $\text{SNR}_k^{\text{C}}(X)$ at the input of the fusion center,
5.	determine α_k and β_k by relationships in (4.102),
6.	determine $\tilde{c}_k(P_{\max})$ by (4.110) and sort all SNs such that the corresponding values of $\tilde{c}_k(P_{\max})$ are in an ascending manner,
7.	calculate the smallest number $\tilde{K}$ of active SNs for which the inequality $\tilde{K} \geq \frac{P_{\text{tot}}}{P_{\max}}$ holds,
8.	calculate the remaining power by $P_{\text{remain}} = P_{\text{tot}} - (\tilde{K} - 1)P_{\max}$,
9.	use (4.105) and (4.108) to obtain the optimal powers $X_k^\star$ and $W_k^\star$ for the first $\tilde{K} - 1$ SNs,
10.	exclude the first $\tilde{K} - 1$ SNs from further considerations,
11.	choose $W = X = P_{\text{remain}}$ for the sensing and communication power of the remaining SNs,
12.	measure each signal-to-noise ratio $\text{SNR}_k^{\text{S}}(P_{\text{remain}})$ and $\text{SNR}_k^{\text{C}}(P_{\text{remain}})$ at the input of the remaining SNs and at the fusion center, respectively,
13.	determine α_k and β_k by relationships in (4.102) for all $k > \tilde{K} - 1$,
14.	determine $\tilde{c}_k(P_{\text{remain}})$ by (4.110) and sort again all remaining SNs such that the corresponding values of $\tilde{c}_k(P_{\text{remain}})$ are in an ascending manner,
15.	use (4.106) and (4.109) to obtain the optimal powers $X_{\tilde{K}}^\star$ and $W_{\tilde{K}}^\star$ for the last active SN,
16.	in order to estimate the current quality of data fusion the signal-to-noise ratio in (4.107) can in addition be calculated.

randomly generated for each simulation step with the densities $\mathfrak{G}(1,\sigma_s^2)$ and $\mathfrak{G}(1,\sigma_c^2)$, respectively. Note that σ_s^2 and σ_c^2 are equal to $P_{\max}\cdot\mathcal{E}\left[\frac{r_{\text{rms}}^2|g_k|^2}{M_0}\right]$ and $P_{\max}\cdot\mathcal{E}\left[\frac{|h_k|^2}{N_0}\right]$, respectively, in which the expectation is performed over all k. By the aid of these signal-to-noise ratios, we apply consecutively the steps 5. to 16. from Table 4.1 to obtain the corresponding value of $\text{SNR}_{\text{tot}}^{\star}$ in each simulation step. In Figures 4.8 and 4.9 the expected value of $\frac{\text{SNR}_{\text{tot}}^{\star}}{K}$, with expectation over all simulation steps, is depicted. In particular, for different choices of $\frac{\tilde{K}}{K}\in\{\frac{1}{10},\frac{2}{10},\frac{4}{10},\frac{6}{10},\frac{8}{10},\frac{10}{10}\}$ and $K\in\{10,1000\}$ the behavior of $\frac{\text{SNR}_{\text{tot}}^{\star}}{K}$ with respect to σ_s^2 and σ_c^2 is shown. As can be seen, the deviation of $\frac{\text{SNR}_{\text{tot}}^{\star}}{K}$ with respect to σ_c^2 is equal to the deviation with respect to σ_s^2. This behavior results from the symmetric property of $\text{SNR}_{\text{tot}}^{\star}$ with respect to $\text{SNR}_k^{\text{S}}(P_{\max})$ and $\text{SNR}_k^{\text{C}}(P_{\max})$. Although the behavior of $\text{SNR}_{\text{tot}}^{\star}$ is dependent on both K and $\tilde{K}$, the behavior of $\frac{\text{SNR}_{\text{tot}}^{\star}}{K}$ is virtually dependent on the ratio $\frac{\tilde{K}}{K}$.

In order to highlight an important insight, we consider the following example and look at both Figures in 4.9a and 4.9b. Note that all curves in 4.8 and 4.9 behave apparently convex in both σ_s^2 and σ_c^2. Furthermore, all curves behave apparently increasing with respect to $\tilde{K}$ while K is kept constant. Now, we consider the transition from $\tilde{K}=100$ to $\tilde{K}=200$ while $K=1000$ is kept constant. This transition, which doubles the number of active SNs, is performed by one of the following ways. The first way is to double the total power P_{tot} in which the values of σ_s^2 and σ_c^2 will remain unchanged while the value of $\frac{\text{SNR}_{\text{tot}}^{\star}}{K}$ will be improved, due to its monotonicity in $\tilde{K}$. The second way is to halve the power constraint P_{tot} in which both σ_s^2 and σ_c^2 will be reduced to one half and the value of $\frac{\text{SNR}_{\text{tot}}^{\star}}{K}$ will be worsen, due to its convexity in σ_s^2 and σ_c^2. As can be seen, this example is valid for any transition in which $\tilde{K}$ is increased while K is kept constant. This fact reinforces the discussion in Subsection 4.2.7.

In order to visualize the density of $\frac{\text{SNR}_{\text{tot}}^{\star}}{K}$, we perform the above described Monte-Carlo simulation with the same parameter setup. At the end of the simulation, all 100000 observations of $\frac{\text{SNR}_{\text{tot}}^{\star}}{K}$ are used to generate a corresponding histogram with 30 bins. Note that the last bin contains all tail observations. In addition, all 100000 observations are applied to fit the histogram by both the Fréchet and the gamma density, where all density parameters are calculated with the maximum likelihood method. Furthermore, the sample mean of the 100000 observations is calculated for reasons of comparison. For selected values of involved parameters, some curves are shown in Figures 4.10 and 4.11. It is in evidence that in some cases the Fréchet density and in other cases the gamma density is an accurate fit for the density of $\frac{\text{SNR}_{\text{tot}}^{\star}}{K}$.

4.5 Summary

The main contribution of the present chapter is to present an optimal solution to the power allocation problem in distributed active multiple-radar systems subject to different power constraints. Analogously to the previous chapter, we have introduced a system model, a linear fusion rule and a simple objective function, which enable us to solve the power allocation problem analytically. Three different cases of power constraints have been investigated. For a limitation of transmission power per sensor node and a sum-power limitation as well as their combination, we have analytically obtained optimal solutions in closed-form. Furthermore, all proposed solutions are valid for AWGN channels as well as for frequency-flat slow-fading channels, provided that channel state information is available at each receiver. The obtained results have rather theoretical aspects and can be used for comparing the system performance of sensor networks while the power consumption of the whole network is kept constant. In addition, we analytically have derived novel relationships in closed-form between the number of active sensor nodes, their reliability and geometrical positions. These relationships might be used for replacing a complicated procedure for sensor selections or for pre-selection of most reliable SNs to limit the complexity of subsequent algorithms.

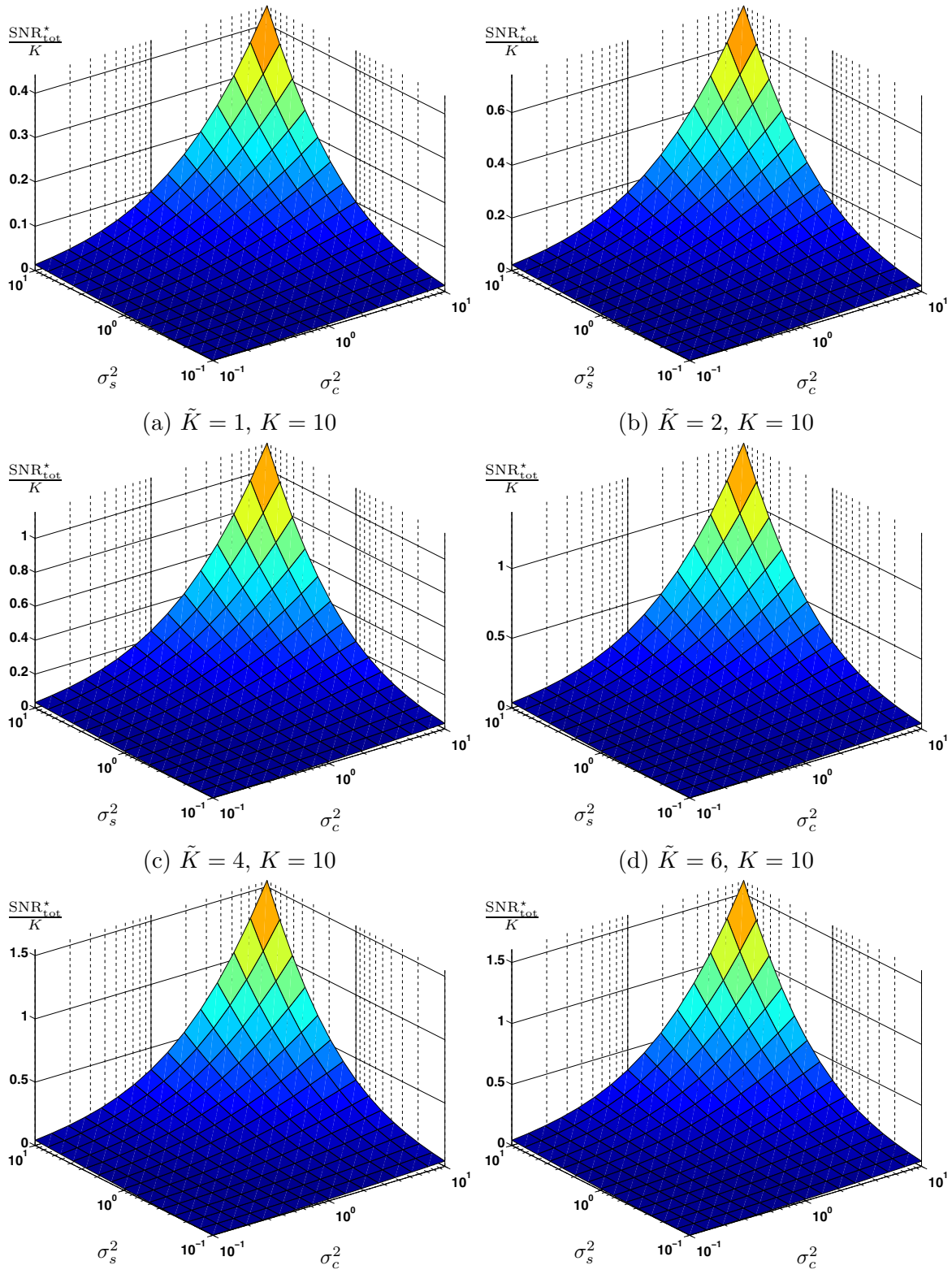

(a) $\tilde{K} = 1$, $K = 10$

(b) $\tilde{K} = 2$, $K = 10$

(c) $\tilde{K} = 4$, $K = 10$

(d) $\tilde{K} = 6$, $K = 10$

(e) $\tilde{K} = 8$, $K = 10$

(f) $\tilde{K} = 10$, $K = 10$

Figure 4.8: Visualization of $\frac{\mathrm{SNR}^{\star}_{\mathrm{tot}}}{K}$ for $\tilde{K} \in \{1, 2, 4, 6, 8, 10\}$ and $K = 10$ over the range $\frac{1}{10} \leq \sigma_s^2 \leq 10$ and $\frac{1}{10} \leq \sigma_c^2 \leq 10$.

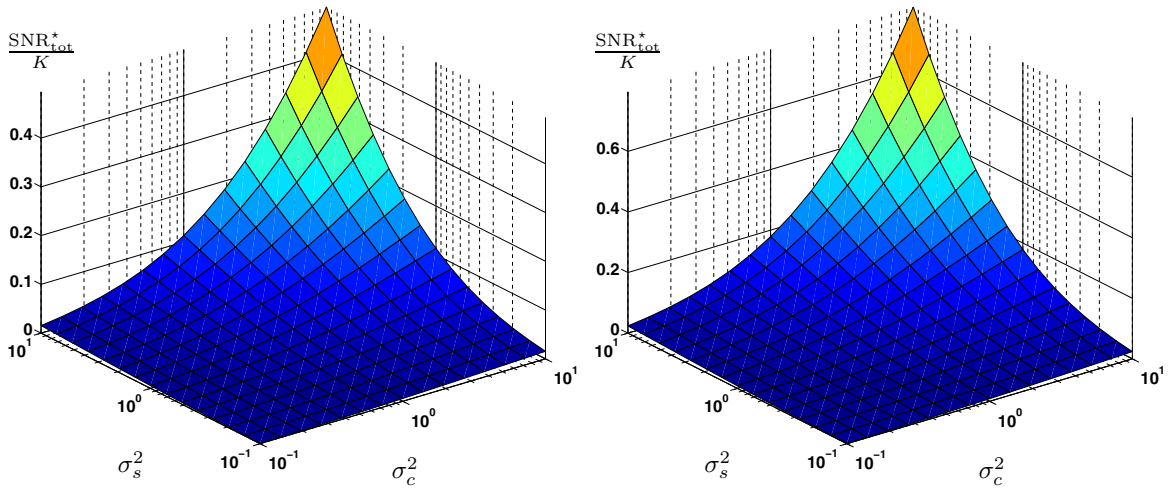

(a) $\tilde{K} = 100$, $K = 1000$

(b) $\tilde{K} = 200$, $K = 1000$

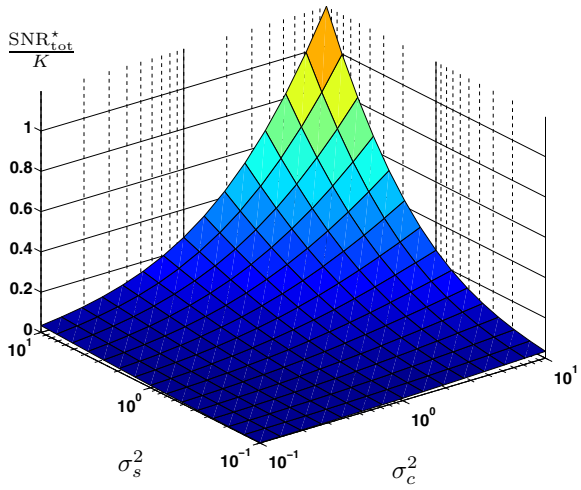

(c) $\tilde{K} = 400$, $K = 1000$

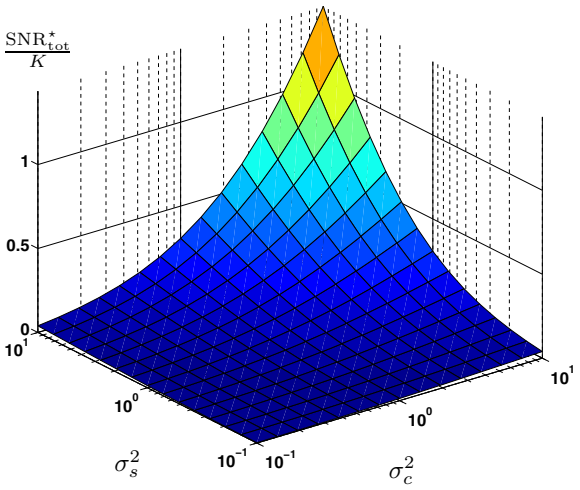

(d) $\tilde{K} = 600$, $K = 1000$

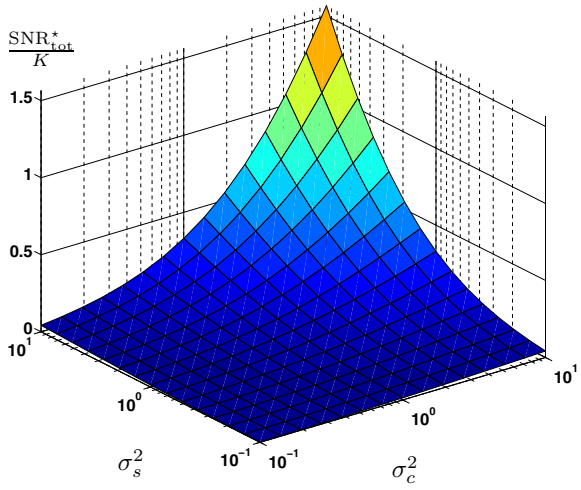

(e) $\tilde{K} = 800$, $K = 1000$

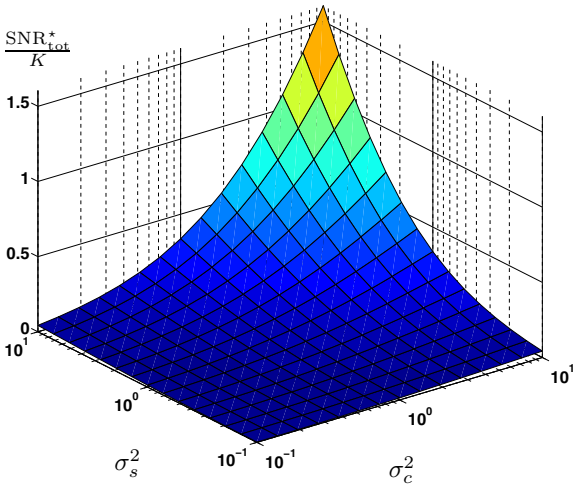

(f) $\tilde{K} = 1000$, $K = 1000$

Figure 4.9: Visualization of $\frac{\mathrm{SNR}^{\star}_{\mathrm{tot}}}{K}$ for $\tilde{K} \in \{100, 200, 400, 600, 800, 1000\}$ and $K = 1000$ over the range $\frac{1}{10} \leq \sigma_s^2 \leq 10$ and $\frac{1}{10} \leq \sigma_c^2 \leq 10$.

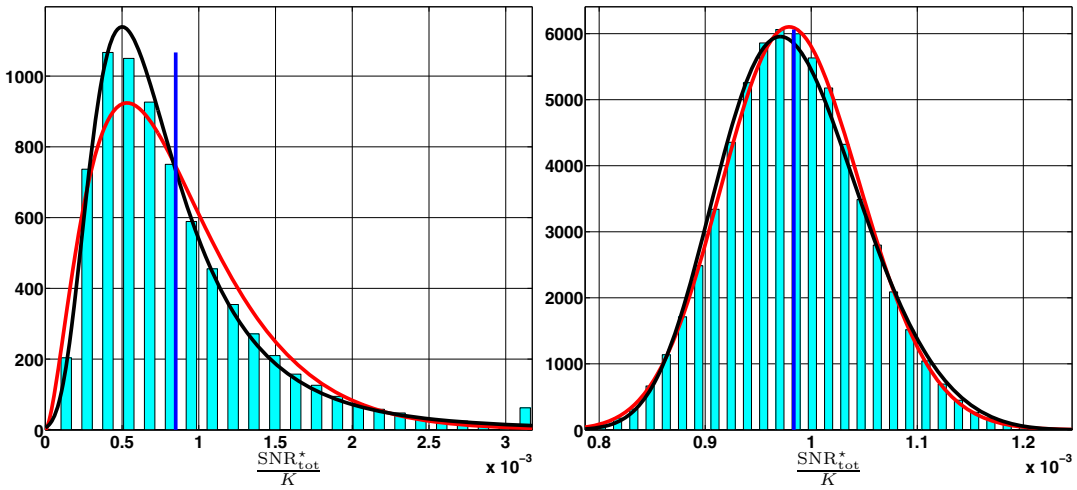

(a) $\tilde{K} = 1$, $K = 10$, $\sigma_s^2 = \sigma_c^2 = \frac{1}{10}$ (b) $\tilde{K} = 100$, $K = 1000$, $\sigma_s^2 = \sigma_c^2 = \frac{1}{10}$

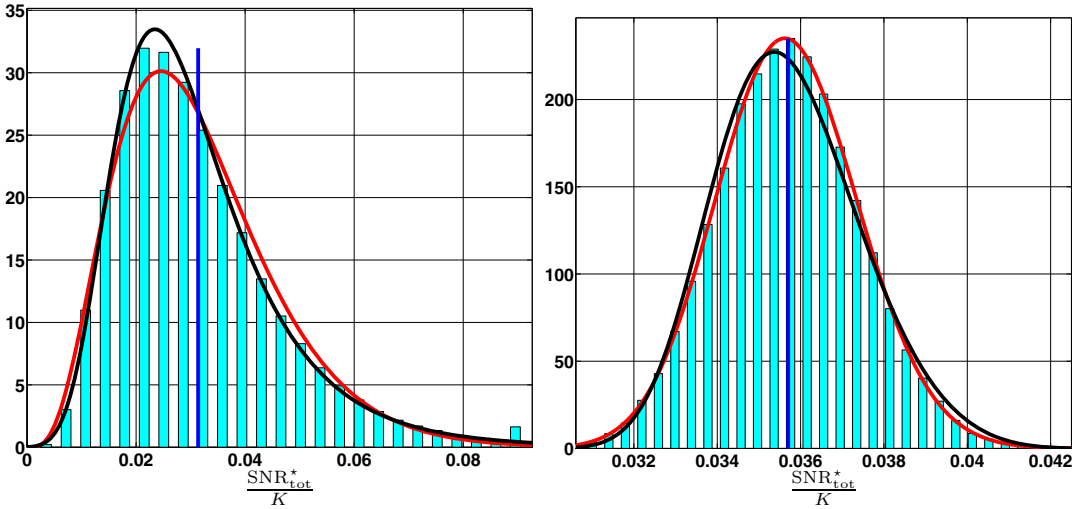

(c) $\tilde{K} = 1$, $K = 10$, $\sigma_s^2 = \sigma_c^2 = 1$ (d) $\tilde{K} = 100$, $K = 1000$, $\sigma_s^2 = \sigma_c^2 = 1$

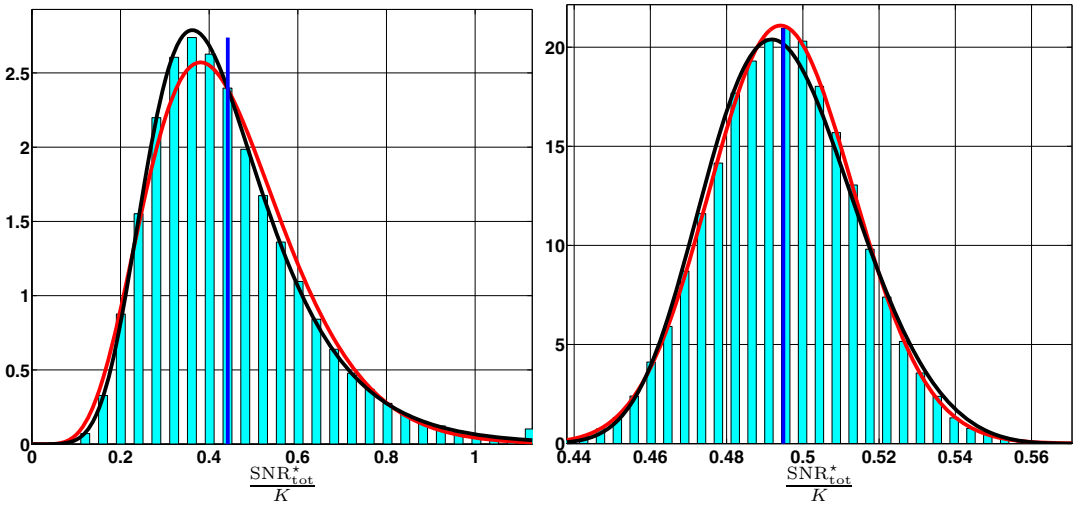

(e) $\tilde{K} = 1$, $K = 10$, $\sigma_s^2 = \sigma_c^2 = 10$ (f) $\tilde{K} = 100$, $K = 1000$, $\sigma_s^2 = \sigma_c^2 = 10$

Figure 4.10: Visualization of the density of $\frac{\mathrm{SNR}^\star_{\mathrm{tot}}}{K}$ for $\tilde{K} \in \{1, 100\}$, $K \in \{10, 1000\}$ and $\sigma_s^2 = \sigma_c^2 \in \{\frac{1}{10}, 1, 10\}$. The histogram of $\frac{\mathrm{SNR}^\star_{\mathrm{tot}}}{K}$, its maximum likelihood fit by the gamma density, and its maximum likelihood fit by the Fréchet density are shown in cyan, red and black color, respectively. The sample mean is indicated by the blue line to be compared with the corresponding values in Figures 4.8 and 4.9.

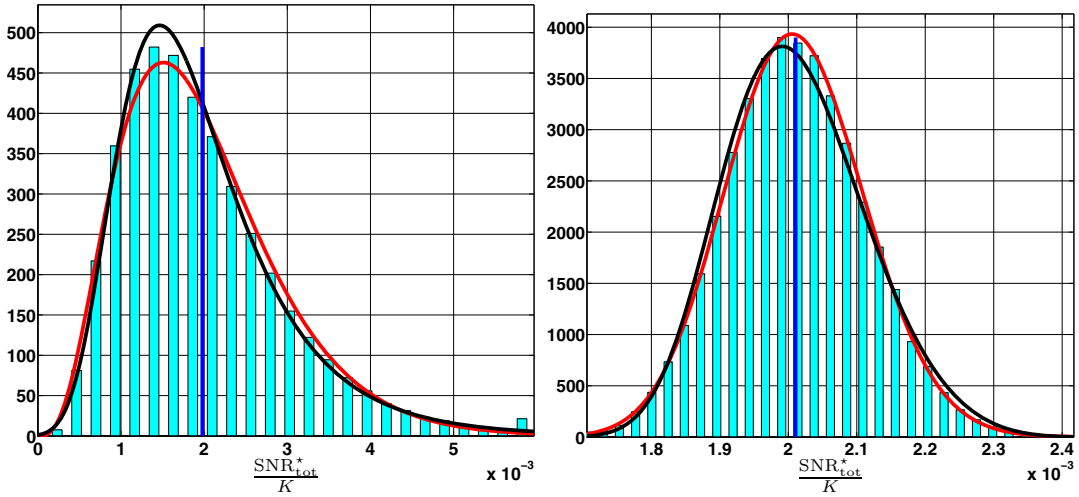

(a) $\tilde{K} = 6$, $K = 10$, $\sigma_s^2 = \sigma_c^2 = \frac{1}{10}$ (b) $\tilde{K} = 600$, $K = 1000$, $\sigma_s^2 = \sigma_c^2 = \frac{1}{10}$

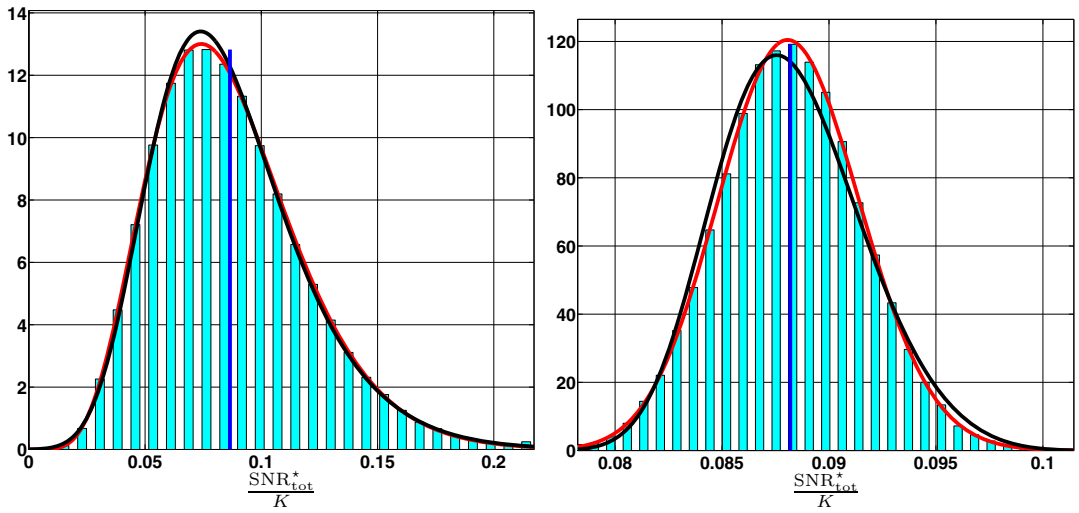

(c) $\tilde{K} = 6$, $K = 10$, $\sigma_s^2 = \sigma_c^2 = 1$ (d) $\tilde{K} = 600$, $K = 1000$, $\sigma_s^2 = \sigma_c^2 = 1$

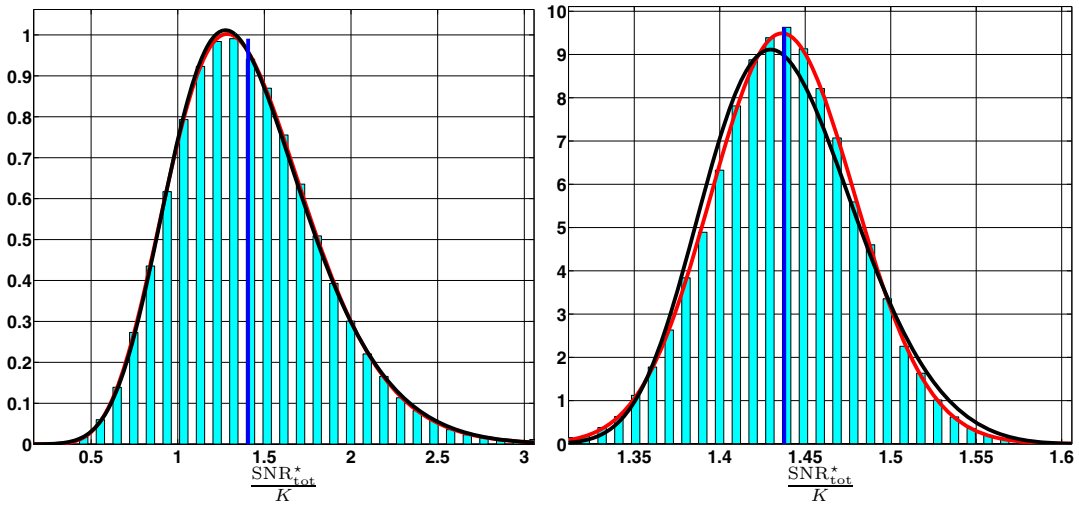

(e) $\tilde{K} = 6$, $K = 10$, $\sigma_s^2 = \sigma_c^2 = 10$ (f) $\tilde{K} = 600$, $K = 1000$, $\sigma_s^2 = \sigma_c^2 = 10$

Figure 4.11: Visualization of the density of $\frac{\mathrm{SNR}^\star_{\mathrm{tot}}}{K}$ for $\tilde{K} \in \{6, 600\}$, $K \in \{10, 1000\}$ and $\sigma_s^2 = \sigma_c^2 \in \{\frac{1}{10}, 1, 10\}$. The histogram of $\frac{\mathrm{SNR}^\star_{\mathrm{tot}}}{K}$, its maximum likelihood fit by the gamma density, and its maximum likelihood fit by the Fréchet density are shown in cyan, red and black color, respectively. The sample mean is indicated by the blue line to be compared with the corresponding values in Figures 4.8 and 4.9.

5 Classification

As demonstrated in Chapters 3 and 4, we are able to separate the power allocation problem from the classification process and optimize the power allocation independently. We have also seen that the proposed power optimization leads to an unbiased estimate for the actual recognition feature of the target at the output of the combiner in the fusion center. Hence, for the classification process a decision unit is necessary to classify the target by its estimate. This setup is illustrated in Figure 5.1. Since classification algorithms are comprehensively investigated in the literature, we discuss only an elementary version and show that the explicit evaluation of the classification probability is extremely hard. The evaluation is even harder under influence of channel fading, as we will see later.

In the following, we exemplarily consider the classification problem of target objects. Based on the system model in Chapter 4, we utilize a distance classifier and present the corresponding instantaneous classification probability in its integral form for the general case, as well as closed-form equations for some particular cases. Afterwards, we discuss the average classification probability under influence of channel fading. Finally, we show an important relationship between the evaluation of average classification probabilities and the evaluation of average symbol-error probabilities.

5.1 Distribution of the Estimates

In order to optimize the classification process, we need more information about statistical properties of the estimates, which are observed at the input of the decision unit. By considering (4.8) together with the identity (4.9), we obtain the equation

$$\tilde{r} = r_i + \underbrace{\sum_{k=1}^{K} (m_k h_k u_k^\star + n_k) v_k^\star}_{\text{white Gaussian noise}}, \; i \in \mathbb{F}_I \,. \tag{5.1}$$

This equation shows that first the input signal $\tilde{r}$ is unbiased for each i, because all noise signals m_k and n_k are assumed to be zero mean, and second it has a Gaussian distribution, due to Gaussian distribution of all noise signals. Note that the coherence time of all channels is assumed to be much longer than the duration of each classification process, i.e., all channel coefficients h_k are assumed to be static during the whole classification process and thus cannot influence the signal distribution. The input of the decision unit is hence a noisy version of the actual reflection coefficient r_i, where the associated additive noise is complex-valued and Gaussian distributed with zero-mean.

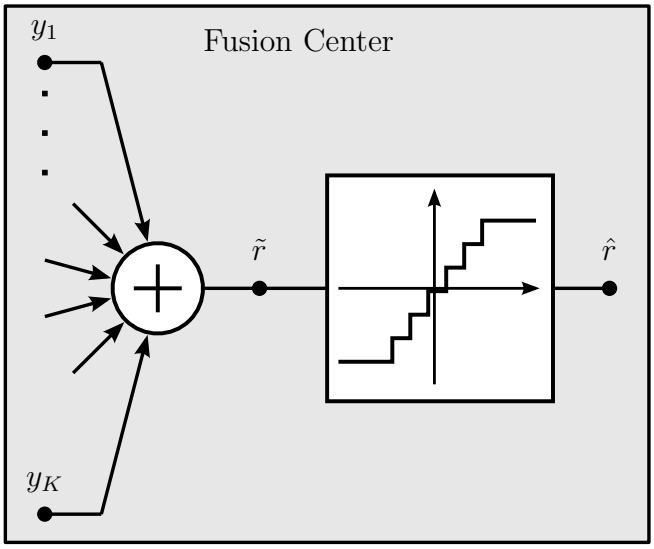

Figure 5.1: System model of combiner and decision unit.

In addition, if we consider definition (4.12) and use one of the results (4.40), (4.56) or (4.76), then the corresponding covariance matrix of $\tilde{r}$ for each i is given as

$$\frac{V^\star}{2}\begin{pmatrix}1 & 0\\ 0 & 1\end{pmatrix}. \tag{5.2}$$

Note that both diagonal values are identical because both in-phase and quadrature component of each noise signal are assumed to have the same variance. Finally, the conditional probability density of $\tilde{r}$, given object i, is obtained as

$$f_i(r) = \frac{1}{\pi V^\star}\exp\left(-\frac{|r-r_i|^2}{V^\star}\right),\ r\in\mathbb{C}, i\in\mathbb{F}_I. \tag{5.3}$$

5.2 Classification Rule and Probability

Due to the simple form of the conditional densities and identical covariance matrices for all i, we may use a distance classifier (nearest-neighbor algorithm) for the global classification rule. On the one hand, distance classifiers are easily implementable because in the present case we deal with linear discriminant functions. On the other hand, distance classifiers are optimal and yield high classification performance [52] because they coincide with the Bayes classifier. The corresponding classification rule is described by the selection

$$\hat{i} = \underset{i\in\mathbb{F}_I}{\operatorname{argmin}}\ |\tilde{r}-r_i| \tag{5.4}$$

and in turn it follows

$$\hat{r} = r_{\hat{i}}\,, \tag{5.5}$$

where $\hat{r}$ denotes the output of the decision unit. By applying the above decision rule, the corresponding instantaneous probability of correct classification is well-known [52]. It is given by

$$\sum_{i=1}^{I} \mathcal{P}[r_i]\, \mathcal{P}[\hat{r} = r_i \mid r_i] = \sum_{i=1}^{I} \pi_i\, \mathcal{P}[\hat{r} = r_i \mid r_i] \tag{5.6}$$

and can be calculated by

$$\int_{r\in\mathbb{C}} \max_{i\in\mathbb{F}_I}\big(\pi_i f_i(r)\big)\,\mathrm{d}r \tag{5.7}$$

for a single observation. Integral (5.7) is in general extremely hard to evaluate analytically, if at all possible. However, accurate numerical solutions are attainable. Nevertheless, the integral (5.7) can be evaluated for some special cases in terms of the complementary error function. These cases are considered in the next section.

If the reflection coefficients are placed very close to each other in the complex plane, then the outcome of (5.7) can sometimes be unsatisfactory. In such cases, the performance of the target classification can be enhanced by increasing the number of observations, provided that the whole network with its parameters and the target object are static during all observations. If we use M independent observations for each classification process, then the corresponding instantaneous probability of correct classification is given by

$$\int_{\mathbf{r}\in\mathbb{C}^M} \max_{i\in\mathbb{F}_I}\left(\pi_i \prod_{m=1}^{M} f_i(r_m)\right)\mathrm{d}\mathbf{r}\,, \tag{5.8}$$

where $\mathbf{r} = (r_1, r_2, \ldots, r_M)$.

Note that the outcome of both integrals must finally be averaged over the position of the target object as well as the realization of each channel coefficient. As we will see in the next chapter, the evaluation of this average is difficult in general and hence we will propose some useful bounds to replace the averaging.

5.3 Instantaneous Classification Probability for Particular Cases

In this section, we show that in some particular cases the evaluation of (5.7) leads to probabilities which are described by the complementary error function. Considering the case of equal a-priori probability of occurrences, i.e., $\pi_i = \frac{1}{I}$ for all $i \in \mathbb{F}_I$, we can use the densities in (5.3) and rewrite the integral (5.7) as

$$\frac{1}{I}\int_{r\in\mathbb{C}} \max_{i\in\mathbb{F}_I}\big(f_i(r)\big)\,\mathrm{d}r = \frac{1}{I\pi V^\star}\int_{r\in\mathbb{C}} \exp\left(-\frac{1}{V^\star}\min_{i\in\mathbb{F}_I}\big(|r-r_i|^2\big)\right)\mathrm{d}r\,. \tag{5.9}$$

As can be easily seen, the above integration is complicated because of the integrand which contains the function $\min(\cdot)$ combined with the Gaussian density. In order to

simplify the integrand and thus also the integration, we determine the boundaries of subsets in which the integrand is free from the difficulties of the function $\min(\cdot)$. For each pair of adjacent integration areas $\mathbb{D}_i \subseteq \mathbb{C}$ and $\mathbb{D}_j \subseteq \mathbb{C}$, the boundary between both areas is given implicitly by the equation

$$|r - r_i|^2 = |r - r_j|^2 \quad \Leftrightarrow \quad \Re(r)\Re(r_j - r_i) + \Im(r)\Im(r_j - r_i) = \frac{|r_j|^2 - |r_i|^2}{2}\,, \tag{5.10}$$

which describes a straight line in the complex plain for all $i \neq j$, $i, j \in \mathbb{F}_I$. Hence, each integration area $\mathbb{D}_i \subseteq \mathbb{C}$, $i \in \mathbb{F}_I$, is a polygon (Voronoi cell [61]) in the complex domain and we may rewrite (5.9) as

$$\frac{1}{I\pi V^\star} \int\limits_{r\in\mathbb{C}} \exp\!\left(-\frac{1}{V^\star} \min_{i\in\mathbb{F}_I}\!\left(|r - r_i|^2\right)\right) \mathrm{d}r = \frac{1}{I\pi V^\star} \sum_{i=1}^{I} \int\limits_{r\in\mathbb{D}_i} \exp\!\left(-\frac{|r - r_i|^2}{V^\star}\right) \mathrm{d}r\,. \tag{5.11}$$

Note that the subsets $\mathbb{D}_i$ are pairwise disjoint and their union is the whole complex domain. The last Integral is still challenging to evaluate, see [15, pp. 936–940]. In addition to the aforementioned assumption $\pi_i = \frac{1}{I}$, if the reflection coefficients r_i are placed symmetrically on an equidistant rectangular grid such that each integration area $\mathbb{D}_i$ is also rectangularly shaped, then we are able to define each subset by $\mathbb{D}_i = [\alpha_i, \beta_i] \times [\gamma_i, \delta_i] \subseteq \mathbb{R} \times \mathbb{R}$, $\alpha_i < \beta_i$ and $\gamma_i < \delta_i$. In this case, the outcome of each integration is described by the complementary error function. Hence, the integral in (5.11) may be written as

$$\begin{aligned}\frac{1}{I\pi V^\star} \sum_{i=1}^{I} \int\limits_{r\in\mathbb{D}_i} \exp\!\left(-\frac{|r - r_i|^2}{V^\star}\right) \mathrm{d}r &= \frac{1}{I\pi V^\star} \sum_{i=1}^{I} \int_{\alpha_i}^{\beta_i} \int_{\gamma_i}^{\delta_i} \exp\!\left(-\frac{|\nu + \mathrm{j}\,\omega - r_i|^2}{V^\star}\right) \mathrm{d}\omega \mathrm{d}\nu \\ &= \tfrac{1}{4I} \sum_{i=1}^{I} \left[\operatorname{erfc}\!\left(\tfrac{\beta_i - \Re(r_i)}{\sqrt{V^\star}}\right) - \operatorname{erfc}\!\left(\tfrac{\alpha_i - \Re(r_i)}{\sqrt{V^\star}}\right)\right] \left[\operatorname{erfc}\!\left(\tfrac{\delta_i - \Im(r_i)}{\sqrt{V^\star}}\right) - \operatorname{erfc}\!\left(\tfrac{\gamma_i - \Im(r_i)}{\sqrt{V^\star}}\right)\right], \end{aligned} \tag{5.12}$$

where ν and ω denote the real and imaginary part of r, respectively.

In case of $I = 2$, there exist only one boundary between the reflection coefficients r_1 and r_2 such that the complex domain is divided into two parts. Thus, without loss of generality, we can assume that both reflection coefficients are placed symmetrically on the real line. Hence, the equalities $\Im(r_1) = \Im(r_2) = 0$ and $\Re(r_2) = -\Re(r_1) = -r_1$, $r_1 > 0$ hold. By considering $\delta_i \mapsto \infty$, $\gamma_i \mapsto -\infty$ for $i \in \{1, 2\}$, and $\alpha_1 \mapsto 0$, $\beta_1 \mapsto \infty$, $\alpha_2 \mapsto -\infty$ and $\beta_2 \mapsto 0$, we conclude

$$\frac{1}{2} \operatorname{erfc}\!\left(\frac{-r_1}{\sqrt{V^\star}}\right) \tag{5.13}$$

for the classification probability of correct decision from (5.12). Since for any admissible reflection coefficient r_i the inequality $|r_i| \leq 1$ holds, a basic upper bound for the classification probability (5.13) is obtained as

$$\frac{1}{2} \operatorname{erfc}\!\left(\frac{-r_1}{\sqrt{V^\star}}\right) \leq \frac{1}{2} \operatorname{erfc}\!\left(\frac{-1}{\sqrt{V^\star}}\right)\,. \tag{5.14}$$

Note that in the present case the classification probability is comparable with the converse of the bit-error probability of BPSK-modulated signals over AWGN channels. Inequality (5.14) shows that the maximum classification probability of correct decision is strongly dependent on $V^\star$ and hence is also strongly dependent on the quality of the specific method for the power allocation.

In case of $I = 4$, there exist at least two boundaries between the reflection coefficients r_1, r_2, r_3 and r_4 such that the complex domain is at least divided into four equal parts. If we assume that all reflection coefficients are placed symmetrically on both sides of real and imaginary axes, then the equalities $|\Im(r_i)| = |\Re(r_i)| = \frac{|r_1|}{\sqrt{2}}$, $i \in \{1, 2, 3, 4\}$, hold. Since in the current case the integration problem (5.12) is symmetric, we may write

$$\frac{1}{I\pi V^\star} \sum_{i=1}^{I} \int_{\alpha_i}^{\beta_i} \int_{\gamma_i}^{\delta_i} \exp\left(\frac{-\left|\nu + \mathrm{j}\,\omega - r_i\right|^2}{V^\star}\right) \mathrm{d}\nu \mathrm{d}\omega$$

$$= \frac{1}{\pi V^\star} \int_{0}^{\infty} \int_{0}^{\infty} \exp\left(\frac{-\left|\nu + \mathrm{j}\,\omega - r_1\right|^2}{V^\star}\right) \mathrm{d}\nu \mathrm{d}\omega = \frac{1}{4} \operatorname{erfc}^2\left(\frac{-|r_1|}{\sqrt{2V^\star}}\right) \quad (5.15)$$

for the probability of correct classification. Again, by using the inequality $|r_i| \leq 1$, we obtain the upper bound

$$\frac{1}{4} \operatorname{erfc}^2\left(\frac{-|r_1|}{\sqrt{2V^\star}}\right) \leq \frac{1}{4} \operatorname{erfc}^2\left(\frac{-1}{\sqrt{2V^\star}}\right) . \quad (5.16)$$

Analogously, the classification probability, in case of $I = 4$, is comparable with the converse of the symbol-error probability of QPSK-modulated signals over AWGN channels. Similar to the previous case, the maximum probability of correct classification is strongly dependent on $V^\star$, even more than in the previous case. In general, the optimization of power allocation becomes more important as the number of different types of objects increases.

There are some other cases, e.g., $I = 16$ or $I = 64$ with a symmetric placement of reflection coefficients in the complex domain, in which the classification probability can similarly to (5.14) and (5.16) be upper-bounded in terms of a complementary error function. However, some more interesting cases, e.g., $I = 3$ or $I = 5$, are still challenging to investigate and thus remain as open problems.

5.4 Average Classification Probability

As we have seen, in some particular cases, the instantaneous classification probability is determined by (5.12), especially if both sensing and communication channels are static. In contrast, if at least one of the channels is time-varying, then the average classification probability is of importance. In these cases, the optimal value $V^\star$ is time-varying and each realization depends on the underlying probability distribution of corresponding channels. Assuming that the probability density of $V^\star$ is described

by $f_{V^\star}(v)$, the support of $V^\star$ is denoted by $\mathbb{D} \subseteq \mathbb{R}_+$, and the instantaneous probability of correct classification is given as in (5.12), we may write the average probability of correct classification as

$$\frac{1}{4I} \sum_{i=1}^{I} \int_{v \in \mathbb{D}} \left[\operatorname{erfc}\left(\frac{\beta_i - \Re(r_i)}{\sqrt{v}} \right) - \operatorname{erfc}\left(\frac{\alpha_i - \Re(r_i)}{\sqrt{v}} \right) \right] \left[\operatorname{erfc}\left(\frac{\delta_i - \Im(r_i)}{\sqrt{v}} \right) - \operatorname{erfc}\left(\frac{\gamma_i - \Im(r_i)}{\sqrt{v}} \right) \right] f_{V^\star}(v) \, \mathrm{d}v \,. \tag{5.17}$$

As an example, the average error probability with a uniform power allocation as well as an optimized power allocation is depicted in Figure 5.2.

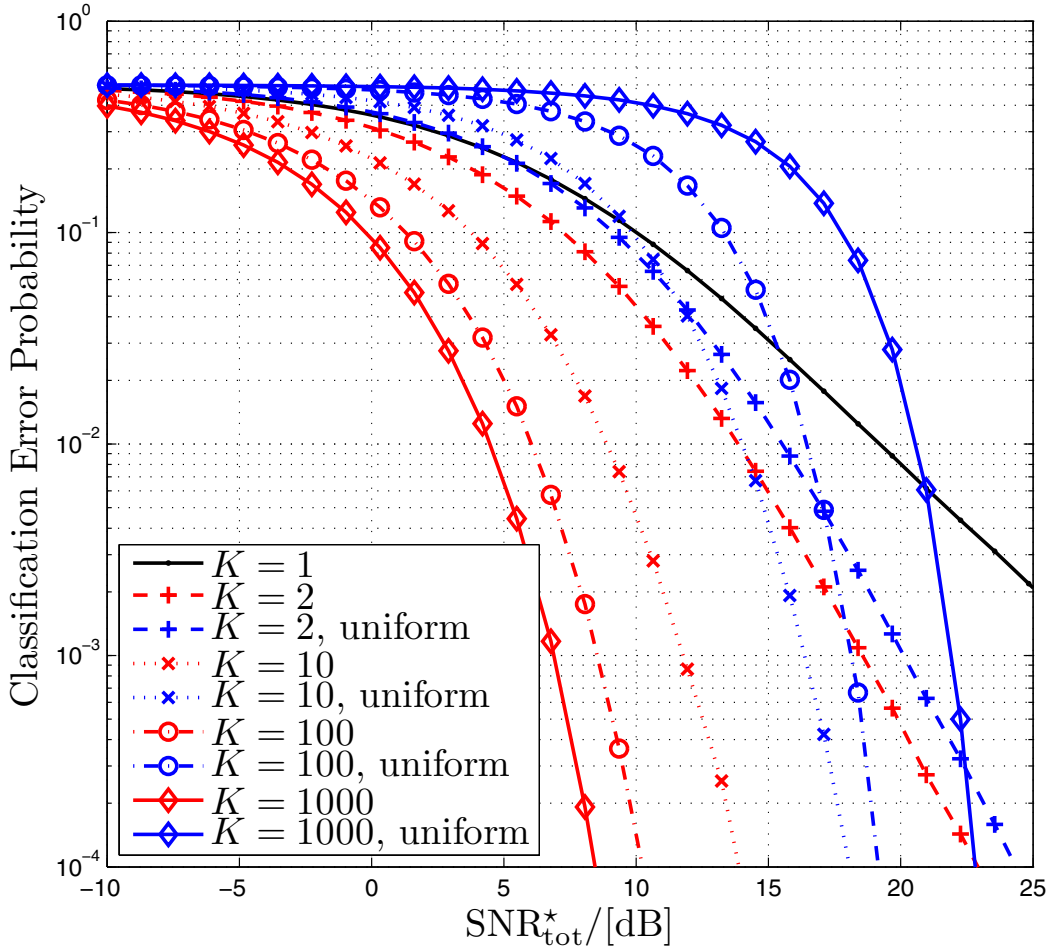

Figure 5.2: Visualization of the average classification probability for $I = 2$ under influence of Rayleigh block-fading. The red curves represent a power optimized active sensor network with solutions given in Subsection 4.4, while the blue curves represent a sensor network with uniformly distributed powers. In case of $K = 1$, the whole total power can only be allocated to one single SN which is represented by the black curve.

As one can easily see, the evaluation of the average classification probability in (5.17) yields the following three types of integration problems. The first one is described by

$$\int_{w\in\mathbb{D}} \operatorname{erfc}\big(c\sqrt{w}\big) f(w)\mathrm{d}w\,,\ c\in\mathbb{R}, \tag{5.18}$$

while the more complicated ones are described by

$$\int_{w\in\mathbb{D}} \operatorname{erfc}^2\big(c\sqrt{w}\big) f(w)\mathrm{d}w\,,\ c\in\mathbb{R}, \tag{5.19}$$

and

$$\int_{w\in\mathbb{D}} \operatorname{erfc}\big(c_1\sqrt{w}\big)\operatorname{erfc}\big(c_2\sqrt{w}\big) f(w)\mathrm{d}w\,,\ c_1,c_2\in\mathbb{R}. \tag{5.20}$$

In general, the particular evaluation of (5.18), (5.19) or (5.20) depends on the specific type of the density $f(w)$. In communication theory, common densities are the Nakagami and Rice distribution [62]. Each of them in combination with the complementary error function cannot be integrated in closed-form. Hence, the average probability of correct classification (5.17) can only be calculated by numerical methods if the underlying densities are Nakagami or Rice distributed. But numerical methods have many disadvantages especially when the number of parameters are high. For example, solutions can be difficult to interpret and often one must vary the parameters to get a full understanding of the numerical result, or in a broader sense, theoretical statements for limiting cases of involved parameters are not always easy to substantiate. In spite of that, or precisely because of that, it is highly interesting to investigate all three integration problems since they appear in different fields of communication theory. For example, similar expressions are known for the symbol-error probability in communication over fading channels. Furthermore, an accurate approximation of the integrals is already sufficient in most applications. Hence, we investigate the approximation of (5.18) in the next chapter in order to simplify the evaluation of the average classification probability as well as some related problems. A more detailed and direct investigation of (5.19) and (5.20) is of interest and will be devoted to future works.

6 Error Probability for Nakagami-Distributed Fading

In the previous chapter, we have shown that the expression of the average classification probability is similar to the expression of the average symbol-error probability in communication over fading channels. Hence, investigations on the average symbol-error probability over fading channels yield insight into the average classification probability. In fact, practically relevant fading channels are much less understood and investigated. The main reason is that analytical expressions become nearly intractable and require the use of complicated functions. Thus, numerical methods are typically applied in simulations to optimize, analyze or verify a communication system, or parts of it. These methods are indeed appropriate for many applications, but inadequate to truly understand and describe the behavior of transceivers and their performance. A prominent example is the explicit evaluation of the average error probability in signal transmission over Nakagami- or Rice-distributed fading channels. It is mathematically challenging to derive a closed-form equation of the average error probability from its integral representation, if at all possible. Closed-form and analytical solutions are only known for some special cases. In this situation, mathematical approximations by simple functions are of great help and fully sufficient for most practical purposes. It is the main purpose of the present chapter to provide such approximations in form of analytical bounds, and at the same time guarantee a minimum deviation from the true values. In particular, we investigate the average symbol-error probability that appears in data communication over Nakagami-distributed fading channels. First, we present some new identities and properties of the integral representation of the average error probability. Second, we propose two novel analytical bounds in closed-form on the average error probability. Our aim is to suggest a lower and an upper bound which have a simple mathematical expression and are accurate over a wide range of parameters. Both bounds achieve a relative error of approximately less than 1.2% over the whole parameter set. Furthermore, users can adapt the proposed bounds to their needs in order to obtain mathematically simpler expressions at the cost of a lower precision. Third, we determine tight analytical upper bounds on the maximum relative error between the proposed bounds and the true average error probability. Finally, we visualize selected results to demonstrate the achieved accuracy.

To the best of our knowledge, the identities and bounds in this chapter are new. They have been examined neither in the original work by Nakagami [63] nor in other publications. The main reason is that approximating the integrand by simpler functions is much easier than the approximation of the integral itself. Thus, in many publications we can find approximations for the Gauss error function or for the Bessel function which

are subsequently used to approximate the average error probability from the Nakagami or Rice distribution, respectively. For instance, in [64–71] and [72] relatively good approximations of the integrands are suggested. In general, there exists a trade-off between improvement of integrand approximation and complication of the subsequent integration. Some examples of sharp integrand approximations, however not including the integration of the conditional error probability, are given in [73–75] and [76]. We also want to mention some pioneering works, like [77–82] and [83], in which the error probability and some corresponding approximations in terms of special functions and finite or infinite series are investigated. These approximations are rather useful for numerical evaluations. The approximation of the whole integral by lower and upper bounds is an open problem, and the main objective of the present chapter.

In the next section, the average error probability is represented in its integral form. Subsequently, we derive particular identities and properties of the integral and, as a main result, sharp analytical upper and lower bounds. Thereafter, the maximum relative deviation between the proposed bounds and the true integral value is also analytically upper-bounded. In between, selected results are visualized by corresponding curves.

Note that our results and proofs are based on the special ratio (2.31) and its corresponding inequality (2.34). Thus, the ratio $\tau(\cdot)$ is essential throughout the entire chapter.

6.1 Problem Description and Associated Identities

In many situations the bit or the symbol error probability is exactly described or can be accurately approximated by the function

$$P(\xi) \coloneqq c_1 \operatorname{erfc}(c_2\sqrt{\xi}) \tag{6.1}$$

with positive real constants c_1 and c_2 depending on the modulation scheme, where the variable ξ denotes the *signal-to-noise ratio* (SNR) at the receiver. Coherently detected M-ary PAM [84, p. 265] and BPSK [84, p. 268] are examples where the corresponding error probability is exactly described by equation (6.1). M-ary PSK, M-ary QAM [85, p. 180], and M-ary FSK [86, p. 230] are other examples where the corresponding error probability can be accurately approximated by (6.1). Now, assuming that the SNR itself is a random variable and the envelope of the channel response is Nakagami-distributed[1]. Then, the average error probability (AEP) is calculated by

$$P_{\text{avg}}(m,\bar{\xi}\,) \coloneqq \int_0^\infty P(s) \left(\frac{m}{\bar{\xi}}\right)^m \frac{s^{m-1}}{\Gamma(m)} \exp\Big(-\frac{ms}{\bar{\xi}}\Big)\,\mathrm{d}s\,, \tag{6.2}$$

where $\bar{\xi}$ is the average value of ξ and parameter m is called *fading-figure*, see [88]. Reparameterizing in (6.2) $m = \frac{p+1}{2}$, $\bar{\xi} = \frac{p+1}{2xc_2^2}$, $s = \frac{t^2}{c_2^2}$, and normalizing with $c_1^{-1}\,\tau(p)x^{-\frac{p+1}{2}}$ yields the following general integral form.

[1] In particular, we consider the so called *Nakagami-m distribution*, see also [87].

Definition 6.1.1. For all $p \in \mathbb{R}$, $-1 < p < \infty$[2] and for all $x \in \mathbb{R}_+$, we define the *Beta-Nakagami Integral* (BeNaI) by

$$g(p,x) \coloneqq \frac{(p+1)\sqrt{\pi}}{\Gamma\left(\frac{p+2}{2}\right)} \int_0^\infty t^p \, \mathrm{e}^{-xt^2} \operatorname{erfc}(t) \mathrm{d}t \; . \tag{6.3}$$

Note that the normalization factor yields $g(p,0) = 1$ which results from the identity[3]

$$\int_0^\infty t^p \operatorname{erfc}(t) \mathrm{d}t = \frac{\Gamma\left(\frac{p+2}{2}\right)}{(p+1)\sqrt{\pi}} \; . \tag{6.4}$$

Hence, the relationship between (6.2) and (6.3) is given by

$$P_{\text{avg}}\Big(\frac{p+1}{2}, \frac{p+1}{2xc_2^2}\Big) = \frac{x^{\frac{p+1}{2}} c_1}{\tau(p)} \, g(p,x) \, . \tag{6.5}$$

The AEP and thus also the BeNaI are usually evaluated numerically. In order to decrease computational effort and to improve numerical accuracy, we deduce new identities in the following.

Lemma 6.1.2. *For all $n \in \mathbb{N}$, the n^{th} partial derivative of $g(p,x)$ with respect to x is given by*

$$g^{(n)}(p,x) \coloneqq \frac{\partial^n g(p,x)}{\partial x^n} = (-1)^n \frac{p+1}{p+1+2n} \, g(p+2n,x) \prod_{m=1}^{n} \frac{p+2m}{2} \; . \tag{6.6}$$

In particular, it leads to

$$g'(p,x) \coloneqq \frac{\partial g(p,x)}{\partial x} = -\frac{p+1}{2} \frac{p+2}{p+3} \, g(p+2,x) \; . \tag{6.7}$$

Proof. Differentiating $g(p,x)$ n-times with respect to x and using the identity in (2.3) gives

$$\begin{aligned} g^{(n)}(p,x) &= (-1)^n \frac{(p+1)\sqrt{\pi}}{\Gamma\left(\frac{p+2}{2}\right)} \int_0^\infty t^{p+2n} \, \mathrm{e}^{-xt^2} \operatorname{erfc}(t) \mathrm{d}t \\ &= (-1)^n \frac{\Gamma\left(\frac{p+2}{2}+n\right)}{\Gamma\left(\frac{p+2}{2}\right)} \frac{p+1}{p+1+2n} \, g(p+2n,x) \\ &= (-1)^n \frac{p+1}{p+1+2n} \, g(p+2n,x) \prod_{m=1}^{n} \frac{p+2m}{2} \; . \end{aligned} \tag{6.8}$$

□

[2]The domain of p may be extended to $\{p \in \mathbb{R} \mid p > -1\} \cup \{\infty\}$, and therewith, all results can be proven by concepts of *uniform integrability*. But this extension is pointless for the purpose of the present work and hence is not considered.

[3]Identity (6.4) is well-known and was first published in [89, p. 56, eq. 12].

Lemma 6.1.3. *The BeNaI satisfies the following ordinary differential equation*

$$g(p,x) + \frac{2x}{p+1}\, g'(p,x) = \frac{1}{(1+x)^{\frac{p+2}{2}}} \ . \tag{6.9}$$

Proof. Considering (6.3) and using integration by parts, where t^p is integrated and $\mathrm{e}^{-xt^2}\operatorname{erfc}(t)$ is differentiated with respect to t, we deduce the identity

$$g(p,x) = \frac{p+2}{p+3}\, x\, g(p+2,x) + \frac{1}{(1+x)^{\frac{p+2}{2}}} \ . \tag{6.10}$$

Incorporating equation (6.7) into (6.10) leads to (6.9). □

Theorem 6.1.4. *For all $-1 < p < \infty$ and for all $x \in \mathbb{R}_+$, the BeNaI has the series representation*[4]

$$g(p,x) = \frac{p+1}{p\,(1+x)^{\frac{p+2}{2}}} \sum_{n=0}^{\infty} \Big(\frac{x}{1+x}\Big)^n \prod_{m=0}^{n} \frac{p+2m}{p+1+2m} \, . \tag{6.11}$$

Proof. By elementary algebra and from (6.11), we obtain the equality

$$\begin{aligned} \frac{p+2}{p+3}\, x\, g(p+2,x) &= \frac{x}{(1+x)^{\frac{p+4}{2}}} \sum_{n=0}^{\infty} \Big(\frac{x}{1+x}\Big)^n \prod_{m=0}^{n} \frac{p+2+2m}{p+3+2m} \\ &= \frac{1}{(1+x)^{\frac{p+2}{2}}} \sum_{i=1}^{\infty} \Big(\frac{x}{1+x}\Big)^i \prod_{m=0}^{i-1} \frac{p+2+2m}{p+3+2m} \\ &= \frac{p+1}{p\,(1+x)^{\frac{p+2}{2}}} \sum_{i=1}^{\infty} \Big(\frac{x}{1+x}\Big)^i \prod_{j=0}^{i} \frac{p+2j}{p+1+2j} \\ &= g(p,x) - \frac{1}{(1+x)^{\frac{p+2}{2}}} \, , \end{aligned} \tag{6.12}$$

which is equivalent to (6.10). □

Theorem 6.1.5. *It holds that*

$$g(p,x) = \frac{p+1}{2\, x^{\frac{p+1}{2}}} \int_0^x \frac{t^{\frac{p-1}{2}}}{(1+t)^{\frac{p+2}{2}}} \mathrm{d}t \tag{6.13a}$$

$$= \frac{p+1}{2} \int_0^1 \frac{t^{\frac{p-1}{2}}}{(1+xt)^{\frac{p+2}{2}}} \mathrm{d}t \tag{6.13b}$$

for all $-1 < p < \infty$ and for all $x \in \mathbb{R}_+$.

[4] Note that $p = 0$ is a removable discontinuity.

Proof. The proof is by inspection. The right hand side of (6.13a) is a solution of differential equation (6.9) as can be seen from

$$\begin{aligned}\frac{\partial}{\partial x}\left[\frac{p+1}{2x^{\frac{p+1}{2}}}\int_0^x \frac{t^{\frac{p-1}{2}}}{(1+t)^{\frac{p+2}{2}}}\mathrm{d}t\right] &= \frac{p+1}{2}\left[-\frac{p+1}{2x^{\frac{p+3}{2}}}\int_0^x \frac{t^{\frac{p-1}{2}}}{(1+t)^{\frac{p+2}{2}}}\mathrm{d}t + \frac{1}{x^{\frac{p+1}{2}}}\frac{x^{\frac{p-1}{2}}}{(1+x)^{\frac{p+2}{2}}}\right] \\ &= \frac{p+1}{2x}\left[-g(p,x) + \frac{1}{(1+x)^{\frac{p+2}{2}}}\right].\end{aligned} \tag{6.14}$$

Since the initial values of (6.3) and (6.13a) are equal, both representations coincide.

By substituting t in equation (6.13a) with tx, we deduce (6.13b). □

We are now in a position to easily prove interesting connections between BeNaI and the special functions ${}_2\mathrm{F}_1$ and B from (2.10) and (2.6), respectively.

Corollary 6.1.6. *It holds that*

$$g(p,x) = {}_2\mathrm{F}_1\Big(\frac{p+1}{2}, \frac{p+2}{2}; \frac{p+3}{2}; -x\Big) \tag{6.15a}$$

$$= \frac{1}{(1+x)^{\frac{p}{2}}}\ {}_2\mathrm{F}_1\Big(\frac{1}{2}, 1; \frac{p+3}{2}; -x\Big) \tag{6.15b}$$

$$= \frac{p+1}{2\,x^{\frac{p+1}{2}}}\,\mathrm{B}\Big(\frac{p+1}{2}, \frac{1}{2}; \frac{x}{1+x}\Big) \tag{6.15c}$$

for all $-1 < p < \infty$ *and for all* $x \in \mathbb{R}_+$.

Proof. By using the integral identity in (2.11), the representation in (6.13b), and the identity in (2.3), we infer (6.15a)[5]. By applying the transformation formula from [15, p. 559, eq. 15.3.3], we obtain identity (6.15b). Identity (6.15c) follows from comparing equation (6.13a) with (2.7). □

***A short verification*:** In order to verify the distribution of the SNR, we start the following discussion from an alternative representation of the BeNaI. Because of identity (6.15c), the BeNaI is related to the cumulative density function (CDF) of a real positive random variable which has a beta-prime distribution or synonymously a beta distribution of the second kind, see [91, p. 50, eq. 4.3] and [92, p. 248, eq. 25.79]. The corresponding CDF of a beta-prime distributed random variable X with parameters a and b is in general described by $\mathcal{P}(X \leq x) = \frac{1}{\mathrm{B}(a,b)}\mathrm{B}\big(a, b; \frac{x}{1+x}\big)$. The random variable $X = \frac{X_1}{X_2}$ is beta-prime distributed with parameters $a = \frac{p+1}{2}$ and $b = \frac{1}{2}$, if both random variables X_1 and X_2 are independent and gamma distributed with parameters $k_1 = p+1$ and $k_2 = 1$, respectively. Note that we only consider a particular case of gamma distributions for which the density is defined as $\frac{x^{k-1}\,\mathrm{e}^{-x/2}}{\Gamma(k)2^k}$ with parameter $k > 0$. In turn, the random variables $X_1 = Y_1^2$ and $X_2 = Y_2^2$ are gamma distributed, if

[5] See also the equation in [90, p. 310, eq. 20]

the random variables Y_1 and Y_2 are Nakagami and standard normal distributed, respectively. For example, the random variable Y_2 could describe the AWGN at the receiver while the variable Y_1 might model the underlying multi-path propagation channel. This short verification confirms the validity of the underlaying communication model and the distribution of the SNR, which is discussed in the introduction of this section[6].

Note that by applying other transformation formulas, such as the ones in [15] and [29], the reader is able to deduce additional important identities. In particular, identities related to the associated Legendre function of the second kind with complex argument or equations related to the Meijer's G-function can be derived.

The new identity (6.13a) or (6.13b) enables us to evaluate the value of $g(p,x)$, for certain p and x, numerically more accurate than the evaluation of $g(p,x)$ by equation (6.3). There are three reasons for this fact. First, the integration domain is finite and includes a singularity at the origin for all $-1 < p < 1$. Second, the integrand does not contain any complicated functions. Third, all operations and functions in the integrand are numerically stable. Both last properties are also fulfilled for the AEP. This can be seen by incorporating (6.13a), (2.3) and (2.33) into (6.5), which gives[7]

$$\begin{aligned} P_{\text{avg}}\Big(\frac{p+1}{2}, \frac{p+1}{2xc_2^2}\Big) &= \frac{c_1}{\pi}\,\tau(p-1)\int\limits_0^x \frac{t^{\frac{p-1}{2}}\mathrm{d}t}{(1+t)^{\frac{p+2}{2}}} \\ &= \frac{pc_1}{2\pi}\int\limits_0^\infty \frac{\mathrm{d}t}{(1+t)^{\frac{p+1}{2}}\sqrt{t}}\int\limits_0^x \frac{t^{\frac{p-1}{2}}\mathrm{d}t}{(1+t)^{\frac{p+2}{2}}}\,. \end{aligned} \tag{6.16}$$

Furthermore, by the new representations, it becomes much easier to calculate the BeNaI explicitly in certain special cases, as is demonstrated by the following examples.

Example 6.1.7. For $p = 1$ and all $x \geq 0$, we derive the known identity[8]

$$g(1,x) = \frac{2}{1+x+\sqrt{1+x}}\,. \tag{6.17}$$

Proof. We deduce the above equality from Theorem 6.1.5 by substitution of $t-1$ for t and a subsequent integration of the outcome. □

Example 6.1.8. For $p = 0$ and all $x \geq 0$, we derive the known identity[9]

$$g(0,x) = \frac{1}{\sqrt{x}}\arctan\big(\sqrt{x}\big)\,. \tag{6.18}$$

[6] As we will show later, the range of $g(px)$ is between zero and one. Hence, $g(p,x)$ can be regarded as a probability. Since it has roots to the beta-prime distribution and arises from the Nakagami distribution, we call it *Beta-Nakagami Integral* (BeNaI), as stated in Definition 6.1.1.

[7] A transformed version of identity (6.16) in terms of *regularized incomplete beta function* is already discussed in [82, eq. A.5], however, its solution is given without a full proof.

[8] Identity (6.17), initially mentioned in [89, p. 49, eq. 14], was derived from (6.3) by a certain relation to the complementary gamma function.

[9] Equation (6.18), initially mentioned in [93, p. 37], was first derived from equation (6.3) by using the method of Laplace transform.

Proof. We deduce the above equality from Theorem 6.1.5 by substitution of t^2 for t and a subsequent integration of the outcome. □

Example 6.1.9. For $p = -1$ and all $x \geq 0$, we derive the new equality

$$\lim_{p \mapsto -1} g(p, x) = 1 \ . \tag{6.19}$$

Proof. The limit of $g(p, x)$ as p tends towards -1 is not obvious when we consider only equation (6.3). However, this limit follows easily from (6.10) by using (6.17). □

More analytical properties of the BeNaI are presented and discussed in the following section.

6.2 Functional Properties of the BeNaI

In this section, we investigate some commonly used properties of the BeNaI from Definition 6.1.1. Moreover, the behavior of the BeNaI for the limits $x \mapsto 0$ and $x \mapsto \infty$ is discussed.

Positivity, continuity and monotonicity are obvious due to representation in (6.3). Hence, the following holds.

Lemma 6.2.1. *For all $-1 < p < \infty$ and for all $x \geq 0$, the function $g(p, x)$ is*

a) non-negative,

b) continuous in both arguments, and

c) strictly decreasing with respect to x.

To prove the convexity more effort is needed. As is well-known and stated in Corollary 2.2.2, logarithmically convex functions are also convex. We hence set out to prove this stronger property.

Lemma 6.2.2. *For all $-1 < p < \infty$ and for all $x \geq 0$, the function $g(p, x)$ is logarithmically convex with respect to x.*

Proof. In order to prove the log-convexity, we show that the inequality

$$g\big(p, \lambda x_1 + (1-\lambda)x_2\big) \leq g^{\lambda}(p, x_1)\, g^{1-\lambda}(p, x_2) \tag{6.20}$$

holds for all $-1 < p < \infty$, $x_1 \geq 0$, $x_2 \geq 0$ and $1 \geq \lambda \geq 0$. By using Hölder's inequality for integrals, see Lemma 2.2.6, we deduce from Definition 6.1.1 the inequality

$$\begin{aligned} \int_0^{\infty} t^p \, \mathrm{e}^{-(\lambda x_1 + (1-\lambda)x_2)t^2} \operatorname{erfc}(t) \mathrm{d}t &= \int_0^{\infty} \Big(t^p \, \mathrm{e}^{-x_1 t^2} \operatorname{erfc}(t) \Big)^{\lambda} \Big(t^p \, \mathrm{e}^{-x_2 t^2} \operatorname{erfc}(t) \Big)^{1-\lambda} \mathrm{d}t \\ &\leq \Big(\int_0^{\infty} t^p \, \mathrm{e}^{-x_1 t^2} \operatorname{erfc}(t) \mathrm{d}t \Big)^{\lambda} \Big(\int_0^{\infty} t^p \, \mathrm{e}^{-x_2 t^2} \operatorname{erfc}(t) \mathrm{d}t \Big)^{1-\lambda} \end{aligned} \tag{6.21}$$

which shows the assertion. □

Lemma 6.2.3. *The Taylor expansion of $g(p,x)$ at $x=0$ is given by*

$$\begin{aligned} g(p,x) &= \frac{p+1}{p}\sum_{n=0}^{\infty}\frac{(-1)^n\,x^n}{(p+1+2n)\,n!\,2^n}\prod_{m=0}^{n}(p+2m) \\ &= 1-\frac{(p+1)(p+2)x}{2(p+3)}+\frac{(p+1)(p+2)(p+4)x^2}{8(p+5)}-\mathcal{O}\big(x^3\big)\ . \end{aligned} \tag{6.22}$$

Proof. Using the derivatives from Lemma 6.1.2 and the fact $g(p,0)=1$, $-1<p<\infty$, see (6.4), lead to the Taylor expansion (6.22). □

Moreover, combining (2.10) and (6.15b) gives the series expansion

$$g(p,x)=\frac{1}{(1+x)^{\frac{p}{2}}}\,\frac{\Gamma\big(\frac{p+3}{2}\big)}{\sqrt{\pi}}\sum_{n=0}^{\infty}\frac{\Gamma\big(n+\frac{1}{2}\big)\,(-1)^n\,x^n}{\Gamma\big(n+\frac{p+3}{2}\big)}\ , \tag{6.23}$$

which is of interest in its own.

We next consider an asymptotic series expansion of $g(p,x)$ as $x\mapsto\infty$, see also Definition 2.4.2.

Lemma 6.2.4. *The asymptotic series expansion of $g(p,x)$ for $x\mapsto\infty$ is given by*

$$\begin{aligned} g(p,x) &= \frac{\tau(p)}{x^{\frac{p+1}{2}}}-\frac{p+1}{p\,x^{\frac{p+2}{2}}}\sum_{n=0}^{\infty}\frac{(-1)^n}{(2n+1)\,n!\,2^n\,x^n}\prod_{m=0}^{n}(p+2m) \\ &= \frac{\tau(p)}{x^{\frac{p+1}{2}}}-\frac{(p+1)}{x^{\frac{p+2}{2}}}+\frac{(p+1)(p+2)}{6x^{\frac{p+4}{2}}}-\mathcal{O}\big(x^{-\frac{p+6}{2}}\big)\ . \end{aligned} \tag{6.24}$$

Proof. Substituting the complementary error function in equation (6.3) with its series (2.9) and by using the identity

$$\frac{\Gamma(\frac{p+1}{2})}{2x^{\frac{p+1}{2}}}=\int_0^{\infty}t^p\,\mathrm{e}^{-xt^2}\,\mathrm{d}t\ ,\ p>-1,x>0, \tag{6.25}$$

which can be derived from equation (2.1), it follows that

$$g(p,x)=\frac{p+1}{2}\,\frac{\Gamma(\frac{p+1}{2})\,\sqrt{\pi}}{\Gamma(\frac{p+2}{2})\,x^{\frac{p+1}{2}}}-\frac{p+1}{\Gamma(\frac{p+2}{2})}\sum_{n=0}^{\infty}\frac{(-1)^n}{(2n+1)\,n!}\,\frac{\Gamma(\frac{p+2}{2}+n)}{x^{\frac{p+2}{2}+n}}\ . \tag{6.26}$$

In the light of equality (2.3) and (2.31), and after some algebra, Lemma 6.2.4 follows. □

It is sometimes necessary to deal with another representation of the asymptotic expansion than that in Lemma 6.2.4. In such cases, we refer the reader to the books [23] and [94].

As it was shown, the BeNaI has some pronounced mathematical properties. Since we are interested in accurately bounding the BeNaI, we need to look for bounds with similar properties. In the next section, we first motivate the proper choice of the bounds. Subsequently, we present the bounds and discuss their properties.

6.3 Choosing the Proper Class of Bounds

In this section, we provide the motivation for selecting the proper class of bounds, which is essential for an accurate approximation of the BeNaI. As shown in (6.13b), the BeNaI is equivalent to

$$g(p,x) = \frac{p+1}{2} \int_0^1 \frac{t^{\frac{p-1}{2}}\,\mathrm{d}t}{(1+xt)^{\frac{p+2}{2}}}\,. \tag{6.27}$$

In order to get a first impression about a proper class, we apply some basic inequalities to the above identity and obtain the double inequality

$$\frac{p+1}{2} \int_0^1 \frac{t^{\frac{p-1}{2}}\,\mathrm{d}t}{(1+xt)^{\frac{p+3}{2}}} \;\le\; g(p,x) \;\le\; \frac{p+1}{2} \int_0^1 \frac{t^{\frac{p-2}{2}}\,\mathrm{d}t}{(1+xt)^{\frac{p+2}{2}}}\,. \tag{6.28}$$

By using the identity[10]

$$\int \frac{t^{\rho-1}\,\mathrm{d}t}{(1+xt)^{\rho+1}} = \frac{t^{\rho}}{\rho\,(1+xt)^{\rho}}\,, \quad \rho > 0\,, \tag{6.29}$$

we can calculate both sides of the double inequality and conclude

$$\frac{1}{(1+x)^{\frac{p}{2}}} \cdot \frac{1}{\sqrt{1+x}} \;\le\; g(p,x) \;\le\; \frac{1}{(1+x)^{\frac{p}{2}}} \cdot \frac{p+1}{p}\,. \tag{6.30}$$

As can be seen, a proper approximation is described by a product of two functions. The first function is the mutual factor on both sides of the above double inequality which may be considered as the main part of a proper approximation. Note that the same factor can be observed in equation (6.15b). The second function is a function which should lie between $\frac{1}{\sqrt{1+x}}$ and $\frac{p+1}{p}$ on the one hand, and on the other hand, the entire product of both functions should have the same discussed properties of the BeNaI. As we will see later, the choice of

$$\frac{e_1}{e_2 + \sqrt{1+x\,e_3}}\,, \quad e_1, e_2, e_3 \in \mathbb{R}_+, \tag{6.31}$$

for the second function is accurate enough for most applications.

6.4 Bounds and Approximations

In this section, we propose two new bounds for the BeNaI from Definition 6.1.1. We will determine bounds in a parametric class of functions given by

$$\frac{1}{(1+x)^{\frac{p}{2}}}\,\frac{e_1}{e_2 + \sqrt{1+x\,e_3}} \tag{6.32}$$

[10] Identity (6.29) is devised in the present thesis. However, we think that this identity is already known.

with positive real coefficients e_1, e_2 and e_3. This specific class of functions has advantageous properties to bound the BeNaI as we will describe later. Since the BeNaI depends on x and p, the coefficients e_1, e_2 and e_3 must also depend on p to achieve accurate bounds. In the following, we first present both bounds with optimal coefficients. The particular choice of the coefficients will be explained later. Second, we introduce an important property of the bounds with respect to their coefficients, which enables the users to choose other coefficients in order to adapt the bounds for their needs.

Theorem 6.4.1. *Let $f(p,x)$ be defined by*

$$f(p,x) \coloneqq \frac{1}{(1+x)^{\frac{p}{2}}} \frac{a_f(p)+1}{a_f(p)+\sqrt{1+x\,b_f(p)}} \tag{6.33}$$

with the coefficients

$$a_f(p) \coloneqq \frac{2}{p+3}\,\tau^2(p) - 1 \tag{6.34}$$

and

$$b_f(p) \coloneqq \frac{4\,\tau^2(p)}{(p+3)^2}\,. \tag{6.35}$$

Then for all $p \in \mathbb{R}$, $1 \leq p < \infty$ and for all $x \in \mathbb{R}_+$, the inequality

$$f(p,x) \leq g(p,x) \tag{6.36}$$

holds. If $p \in \mathbb{R}$ and $-1 < p \leq 1$, then the reverse inequality holds.

Proof. See Appendix 6.6. □

Remark 6.4.2. The coefficients in (6.32) with $e_1 = a_f(p)+1$, $e_2 = a_f(p)$ and $e_3 = b_f(p)$ are the best possible ones for the inequality (6.36) to hold. In other words, no coefficient can be replaced by a better value while keeping the other ones fixed in order to further improve the bound. In this sense, the inequality in Theorem 6.4.1 is sharp.

Please note that by incorporating (6.34) into (6.35) we obtain the relationship

$$b_f(p) = 2\,\frac{a_f(p)+1}{p+3}\,. \tag{6.37}$$

We now collect some important properties of the coefficients $a_f(p)$ and $b_f(p)$.

Lemma 6.4.3. *For all $-1 < p < \infty$,*

a) the coefficient $a_f(p)$ is strictly increasing in p,

b) it holds that $0 < a_f(p) < \pi - 1$, and

c) both coefficients $a_f(p)$ and $b_f(p)$ are non-negative.

Proof. The coefficient $a_f(p)$ is strictly increasing, if its first derivative with respect to p is positive. The first derivative is given by

$$\frac{\mathrm{d}a_f(p)}{\mathrm{d}p} = 2\,\tau(p)\,\frac{2(p+3)\,\tau'(p) - \tau(p)}{(p+3)^2} \tag{6.38}$$

where $\tau'(p)$ denotes the first derivative of $\tau(p)$ with respect to p. Positivity is given, if the inequality

$$\frac{\tau'(p)}{\tau(p)} > \frac{1}{2(p+3)} \quad \Leftrightarrow \quad \psi(\tfrac{p+3}{2}) - \psi(\tfrac{p+2}{2}) > \frac{1}{p+3} \tag{6.39}$$

holds. After replacing p with $2(x-1)$, we can use [27, Theorem 3] to deduce

$$\psi(x+\tfrac{1}{2}) - \psi(x) > \frac{1}{2x+1} \tag{6.40}$$

which proves the statement.

Considering the monotonicity of $a_f(p)$, as shown above, we obtain the lower bound for $p \mapsto -1$ and the upper bound for $p \mapsto \infty$. For $p \mapsto -1$, we obtain $\tau(-1) = 1$ from (2.32) and hence

$$a_f(-1) = \frac{2}{-1+3}\,\tau^2(-1) - 1 = 0\ . \tag{6.41}$$

By using the limit in (2.4) and replacing p with $2(x-1)$, we obtain

$$\lim_{p\mapsto\infty} a_f(p) = -1 + \pi \lim_{x\mapsto\infty} \left(\frac{\Gamma(x+\frac{1}{2})}{\sqrt{x}\,\Gamma(x)}\right)^2 = -1 + \pi\ . \tag{6.42}$$

The coefficient $b_f(p)$ is trivially non-negative by definition. Due to $0 < a_f(p) < \pi - 1$, the coefficient $a_f(p)$ is also non-negative. □

Corollary 6.4.4. *By* (6.37) *the representation*

$$f(p,x) = \frac{1}{(1+x)^{\frac{p}{2}}}\,\frac{a_f(p)+1}{a_f(p) + \sqrt{1 + 2x\,\frac{a_f(p)+1}{p+3}}} \tag{6.43}$$

is obtained, which is a strictly increasing function in $a_f(p)$.

Proof. We show that the first partial derivative of $f(p,x)$ with respect to $a_f(p)$ is strictly positive for all $-1 < p < \infty$. The derivative is given by

$$(1+x)^{\frac{p}{2}}\,\frac{\partial f(p,x)}{\partial a_f(p)} = \frac{1 + x\,\frac{a_f(p)+1}{p+3} - \sqrt{1 + 2x\,\frac{a_f(p)+1}{p+3}}}{\left[a_f(p) + \sqrt{1 + 2x\,\frac{a_f(p)+1}{p+3}}\,\right]^2 \sqrt{1 + 2x\,\frac{a_f(p)+1}{p+3}}}\ . \tag{6.44}$$

Elementary algebra shows that the numerator of (6.44) is strictly positive. □

Theorem 6.4.5. *Let $h(p, x)$ be defined by*

$$h(p,x) \coloneqq \frac{1}{(1+x)^{\frac{p}{2}}} \frac{a_h(p)+1}{a_h(p)+\sqrt{1+x\,b_h(p)}} \tag{6.45}$$

with the coefficients

$$a_h(p) \coloneqq \frac{(p+1)}{\tau^2(p)-(p+1)} \tag{6.46}$$

and

$$b_h(p) \coloneqq \left[\frac{\tau(p)}{\tau^2(p)-(p+1)}\right]^2 . \tag{6.47}$$

Then for all $p \in \mathbb{R}$, $1 \leq p < \infty$ and for all $x \in \mathbb{R}_+$, the inequality

$$g(p,x) \leq h(p,x) \tag{6.48}$$

holds. If $p \in \mathbb{R}$ and $-1 < p \leq 1$, then the reverse inequality holds.

Proof. See Appendix 6.6. □

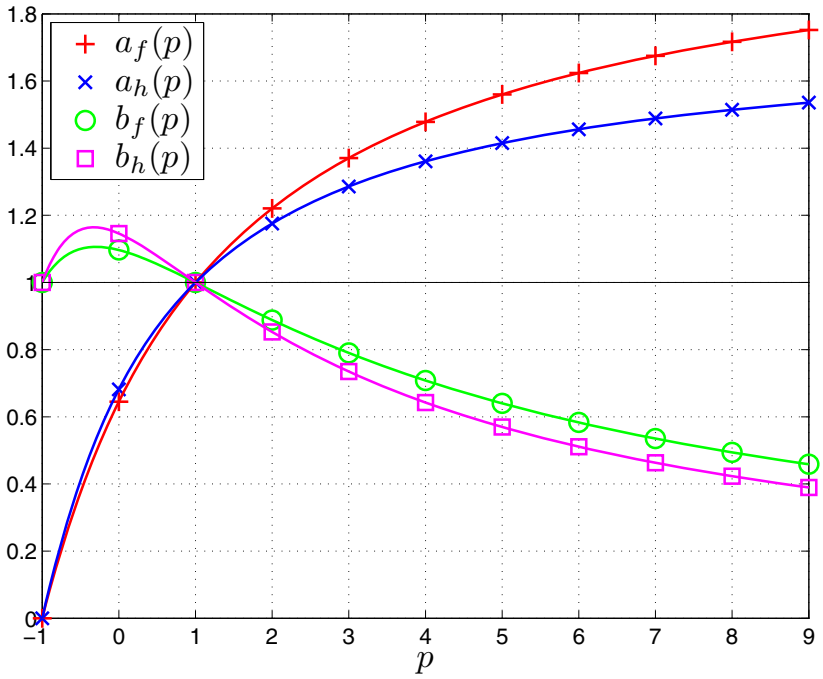

Figure 6.1: The coefficients $a_f(p)$, $b_f(p)$, $a_h(p)$ and $b_h(p)$ are visualized for the range of $-1 < p \leq 9$. $a_f(p)$ and $a_h(p)$ are strictly increasing and they tend towards $\pi - 1$ and $2/(\pi - 2)$ as p approaches infinity, respectively. The coefficients $b_f(p)$ and $b_h(p)$ approach zero as p approaches infinity. Moreover, all coefficients are non-negative for all $-1 < p < \infty$.

Remark 6.4.6. The coefficients in (6.32) with $e_1 = a_h(p) + 1$, $e_2 = a_h(p)$ and $e_3 = b_h(p)$ are the best possible ones for inequality (6.48) to hold. In other words, no coefficient can be replaced by a better value while keeping the other ones fixed in order to further improve the bound. In this sense, the inequality in Theorem 6.4.5 is sharp.

Please note that the bounds in Theorem 6.4.1 and 6.4.5 are converse to each other. For all $1 \leq p < \infty$ the double inequality $f(p,x) \leq g(p,x) \leq h(p,x)$ holds while for all $-1 < p \leq 1$ the converse double inequality $h(p,x) \leq g(p,x) \leq f(p,x)$ holds.

Note that by incorporating (6.46) into (6.47) we obtain the relationship

$$b_h(p) = \frac{a_h(p)+1}{p+1}\, a_h(p) \ . \tag{6.49}$$

Analogously to the properties of $a_f(p)$ and $b_f(p)$ the following holds.

Lemma 6.4.7. *For all $-1 < p < \infty$,*

a) the coefficient $a_h(p)$ is strictly increasing in p,

b) it holds that $0 < a_h(p) < \frac{2}{\pi-2}$, and

c) both coefficients $a_h(p)$ and $b_h(p)$ are non-negative.

Proof. The coefficient $a_h(p)$ is strictly increasing, if its first derivative with respect to p is positive. The first derivative is given by

$$\frac{\mathrm{d}a_h(p)}{\mathrm{d}p} = \tau(p)\, \frac{\tau(p) - 2(p+1)\,\tau'(p)}{[\tau^2(p) - (p+1)]^2} \ . \tag{6.50}$$

Positivity is given, if the inequality

$$\frac{\tau'(p)}{\tau(p)} < \frac{1}{2(p+1)} \quad \Leftrightarrow \quad \psi(\tfrac{p+3}{2}) - \psi(\tfrac{p+2}{2}) < \frac{1}{p+1} \tag{6.51}$$

holds. After replacing p with $2(x-1)$ we can again use [27, Theorem 3] to deduce

$$\psi(x + \tfrac{1}{2}) - \psi(x) < \frac{1}{2x-1} \tag{6.52}$$

which proves the statement.

Considering the monotonicity $a_h(p)$, as shown above, we obtain the lower bound for $p \mapsto -1$ and the upper bound for $p \mapsto \infty$. For $p \mapsto -1$, we obtain $\tau(-1) = 1$ from (2.32) and hence

$$a_h(-1) = \frac{(-1+1)}{\tau^2(-1) - (-1+1)} = 0 \ . \tag{6.53}$$

By using the limit in (2.4) and replacing p with $2(x-1)$, we obtain

$$\lim_{p\mapsto\infty} a_h(p) = \lim_{p\mapsto\infty} \frac{1}{\frac{\tau^2(p)}{p+1} - 1} = \lim_{x\mapsto\infty} \frac{1}{\frac{\pi}{2}\left(\frac{\Gamma(x+\frac{1}{2})}{\sqrt{x}\,\Gamma(x)}\right)^2 - 1} = \frac{1}{\frac{\pi}{2} - 1} \ . \tag{6.54}$$

The coefficient $b_h(p)$ is trivially non-negative by definition. Due to $0 < a_h(p) < \frac{2}{\pi-2}$, the coefficient $a_h(p)$ is also non-negative. □

In Figure 6.1, the coefficients $a_f(p)$, $b_f(p)$, $a_h(p)$ and $b_h(p)$ are depicted. We can observe additional properties of these coefficients which are not important for our purpose and are thus not discussed further.

Corollary 6.4.8. *By* (6.49) *the representation*

$$h(p,x) = \frac{1}{(1+x)^{\frac{p}{2}}} \frac{a_h(p)+1}{a_h(p)+\sqrt{1+x\,\frac{a_h(p)+1}{p+1}\,a_h(p)}} \tag{6.55}$$

is obtained, which is a strictly decreasing function in $a_h(p)$.

Proof. We show that the first partial derivative of $h(p,x)$ with respect to $a_h(p)$ is strictly negative for all $-1 < p < \infty$. The derivative is given by

$$2\,(1+x)^{\frac{p}{2}}\,\frac{\partial h(p,x)}{\partial a_h(p)} = \frac{2 - x\,\frac{a_h(p)+1}{p+1} - 2\sqrt{1+x\,\frac{a_h(p)+1}{p+1}\,a_h(p)}}{\left[a_h(p)+\sqrt{1+x\,\frac{a_h(p)+1}{p+1}\,a_h(p)}\,\right]^2\sqrt{1+x\,\frac{a_h(p)+1}{p+1}\,a_h(p)}}\,. \tag{6.56}$$

By simple rearrangement of the numerator, we derive the assertion from the chain of inequalities

$$x\,\frac{a_h(p)+1}{p+1} + 2\sqrt{1+x\,\frac{a_h(p)+1}{p+1}\,a_h(p)} \geq 0 + 2\sqrt{1+x\,\frac{a_h(p)+1}{p+1}\,a_h(p)} \geq 2\sqrt{1+0}\,. \tag{6.57}$$

□

Remark 6.4.9. Because of Corollary 6.4.4, $f(p,x)$ is monotonically increasing in $a_f(p)$. The coefficient $a_f(p)$, in turn, is increasing in $\tau(p)$ due to the relationship (6.34). By choosing an upper bound of $\tau(p)$, desirably easier to handle than $\tau(p)$ itself, also yields an upper bound for $f(p,x)$. By this, we also obtain a weaker upper bound of $g(p,x)$ for $-1 < p \leq 1$ of potentially simpler form. Analogously, selecting a lower bound of $\tau(p)$ yields a weaker lower bound of $g(p,x)$ for $1 \leq p < \infty$.

Analogously, because of Corollary 6.4.8 and relationship (6.46) any surrogate function, which is greater or less than $\tau(p)$, will provide a weaker lower or a weaker upper bound of $g(p,x)$ in the corresponding domain $-1 < p \leq 1$ or $1 \leq p < \infty$, respectively. This is particularly attractive if the surrogate functions of $\tau(p)$ are of more tractable form. The bounds on $\tau(p)$ from Theorem 2.5.2 may serve as an example for the above approach. Other appropriate bounds on $\tau(p)$ may be found in [25], [26] and [27].

We will later determine the relative error between both bounds, $f(p,x)$ and $h(p,x)$, and the original function $g(p,x)$. The used method does not depend on the concrete form of the bound on $\tau(p)$ and hence is viable also for weaker bounds, cf. (6.94)–(6.97).

In Figure 6.2, the numerical evaluation of the BeNaI lying between the bounds $f(p,x)$ and $h(p,x)$ is depicted for $p = 2$. As we can see, the curves are very similar and closely adjacent to one another. In Figure 6.3, the curves for different values of p are depicted.

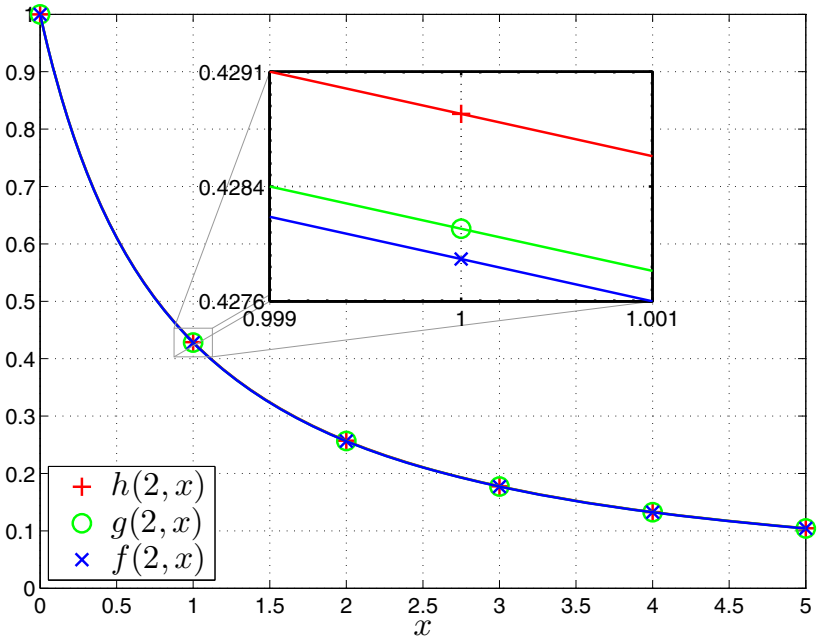

Figure 6.2: The double inequality $f(p,x) \leq g(p,x) \leq h(p,x)$ is visualized for the range of $0 \leq x \leq 5$ and in the case of $p = 2$. The curves are closely adjacent to one another such that without magnification the differences are not really visible. The curves are equal at $x = 0$ and they approach zero as x approaches infinity.

We will mathematically discuss some general properties of the curves in the next section having in mind that this is important for future applications.

In order to determine the quality of the bounds, we have to discuss the achievable accuracy of the bounds and derive some of their properties in the following, as well.

For the sake of brevity, we will write a_f, b_f, a_h and b_h instead of $a_f(p)$, $b_f(p)$, $a_h(p)$ and $b_h(p)$, unless their dependency to p needs to be emphasized.

6.5 Functional Properties of the Bounds

In this section, we investigate some properties of the bounds, that are given in Theorem 6.4.1 and 6.4.5, in order to compare them with the properties of the BeNaI. In particular, positivity, continuity, monotonicity, convexity and series expansions of both bounds are investigated. Furthermore, we show in which cases both bounds are equal to the BeNaI. Two of the properties are given first. As an auxiliary function we use

$$\tilde{g}(p,x) \coloneqq \frac{1}{(1+x)^{\frac{p}{2}}} \frac{a+1}{a+\sqrt{1+x\,b}} \tag{6.58}$$

with non-negative constants a and b, see Lemma 6.4.3 and 6.4.7.

Lemma 6.5.1. *For all $-1 < p < \infty$ and for all $x \geq 0$, both functions $f(p,x)$ and $h(p,x)$ are*

a) non-negative,

b) continuous in both arguments, and

c) strictly decreasing with respect to x.

Proof. The first two properties are obvious, because $a_f(p)$, $b_f(p)$, $a_h(p)$ and $b_h(p)$ are non-negative, due to Lemma 6.4.3 and 6.4.7, and because of continuity of the constituent functions. To prove monotonicity, the function $\tilde{g}(p,x)$ is differentiated, with respect to x, to obtain

$$\frac{\partial \tilde{g}(p,x)}{\partial x} = -\frac{1}{2}\tilde{g}(p,x)\Big(\frac{b}{a+\sqrt{1+x\,b}}\,\frac{1}{\sqrt{1+x\,b}} + \frac{p}{1+x}\Big)\,. \tag{6.59}$$

For all $0 \le p < \infty$, the derivative is always negative because $\tilde{g}(p,x)$ is positive as shown above, and the coefficients a and b are non-negative due to Lemma 6.4.3 and 6.4.7. Hence, $f(p,x)$ and $h(p,x)$ are strictly decreasing. Monotonicity seems to be much harder to prove for the case $-1 < p < 0$. However, we conjecture that $f(p,x)$ and $h(p,x)$ are strictly decreasing functions of x also for $-1 < p < 0$. □

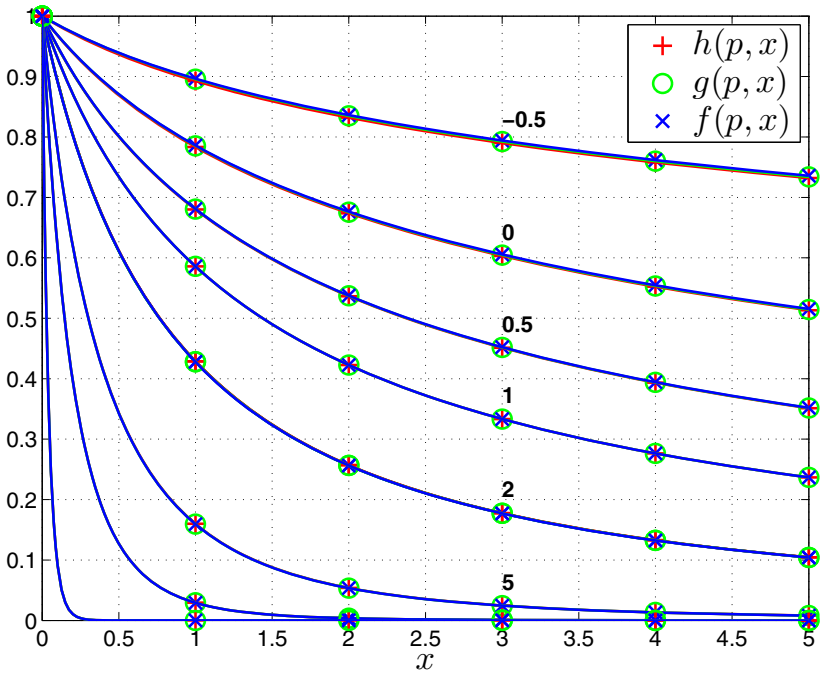

Figure 6.3: For the case of $p \in \{-1/2, 0, 1/2, 1, 2, 5, 10, 50\}$, the behavior of $f(p,x)$, $g(p,x)$ and $h(p,x)$ is visualized for the range of $0 \le x \le 5$. Note, that for all $-1 < p \le 1$ the double inequality $h(p,x) \le g(p,x) \le f(p,x)$ holds, while for all $1 \le p < \infty$ the reverse double inequality holds. All curves are non-negative, continuous, strictly decreasing and logarithmically convex in x. They are equal at $x = 0$ and they approach zero as x approaches infinity. Furthermore, the curves are decreasing in p, as well.

Lemma 6.5.2. *For all $0 \leq p < \infty$, both functions $f(p,x)$ and $h(p,x)$ are logarithmically convex for all arguments $x \geq 0$.*

Proof. In order to prove the above statement, we have to show that the inequality

$$\tilde{g}\big(p, \lambda x_1 + (1-\lambda)x_2\big) \leq \tilde{g}^{\lambda}(p, x_1)\, \tilde{g}^{1-\lambda}(p, x_2) \tag{6.60}$$

holds for all $0 \leq p < \infty$, $x_1 \geq 0$, $x_2 \geq 0$ and $1 \geq \lambda \geq 0$. First, we twice use the arithmetic and geometric means inequality from Corollary 2.2.9 and subsequently the weighted power means inequality from Lemma 2.2.7 which lead to the inequality chain

$$\begin{aligned}
&\big[(1+x_1)^{\lambda}(1+x_2)^{1-\lambda}\big]^{\frac{p}{2}} \Big[\big(a+\sqrt{1+bx_1}\big)^{\lambda}\big(a+\sqrt{1+bx_2}\big)^{1-\lambda}\Big] \\
&\quad \leq \big[\lambda(1+x_1)+(1-\lambda)(1+x_2)\big]^{\frac{p}{2}} \Big[\lambda\big(a+\sqrt{1+bx_1}\big)+(1-\lambda)\big(a+\sqrt{1+bx_2}\big)\Big] \\
&\quad = \big[1+\lambda x_1+(1-\lambda)x_2\big]^{\frac{p}{2}} \Big[a+\lambda\sqrt{1+bx_1}+(1-\lambda)\sqrt{1+bx_2}\Big] \\
&\quad \leq \big[1+\lambda x_1+(1-\lambda)x_2\big]^{\frac{p}{2}} \Big[a+\sqrt{1+b\lambda x_1+b(1-\lambda)x_2}\Big]\,.
\end{aligned} \tag{6.61}$$

By simple rearrangement of the last inequality and multiplying both sides by $a+1$, we conclude

$$\begin{aligned}
&\frac{1}{[1+\lambda x_1+(1-\lambda)x_2]^{\frac{p}{2}}}\,\frac{a+1}{a+\sqrt{1+b[\lambda x_1+(1-\lambda)x_2]}} \\
&\qquad \leq \frac{1}{\big[(1+x_1)^{\lambda}(1+x_2)^{1-\lambda}\big]^{\frac{p}{2}}} \cdot \Big(\frac{a+1}{a+\sqrt{1+bx_1}}\Big)^{\lambda}\Big(\frac{a+1}{a+\sqrt{1+bx_2}}\Big)^{1-\lambda},
\end{aligned} \tag{6.62}$$

which is equivalent to inequality (6.60). Hence, $f(p,x)$ and $h(p,x)$ are logarithmically convex as well. Convexity seems to be much harder to prove for the case $-1 < p < 0$. However, we also conjecture that $f(p,x)$ and $h(p,x)$ are logarithmically convex in x also for $-1 < p < 0$. □

Lemma 6.5.3. *For all $a \geq 0$, $b \geq 0$ and $-1 < p < \infty$, the expansion*

$$\tilde{g}(p,x) = 1 - \frac{b+(a+1)p}{2(a+1)}\,x + \frac{(a+3)b^2+2(a+1)pb+(a+1)^2(p+2)p}{8(a+1)^2}\,x^2 - \mathcal{O}\big(x^3\big) \tag{6.63}$$

holds at $x = 0$.

Proof. The statement is obtained by using the general definition of the Taylor expansion and straightforward calculation of the first three derivatives of the surrogate function. □

Corollary 6.5.4. *The Taylor expansion of $f(p,x)$ at $x = 0$ is given by*

$$f(p,x) = 1 - \frac{(p+1)(p+2)}{2(p+3)}\,x + \frac{4(a_f+3)+4p(p+3)+p(p+2)(p+3)^2}{8(p+3)^2}\,x^2 - \mathcal{O}\big(x^3\big)\,. \tag{6.64}$$

Proof. The assertion follows by incorporating (6.37) into (6.63). □

Corollary 6.5.5. *The Taylor expansion of $h(p,x)$ at $x=0$ is given by*

$$h(p,x) = 1 - \frac{a_h + p(p+1)}{2(p+1)}\,x + \frac{(a_h+3)a_h^2 + 2p(p+1)a_h + p(p+2)(p+1)^2}{8(p+1)^2}\,x^2 - \mathcal{O}\big(x^3\big)\,. \tag{6.65}$$

Proof. The assertion follows by incorporating (6.49) into (6.63). □

Remark 6.5.6. The first two elements in the Taylor expansions of $f(p,x)$ and $g(p,x)$ are identical, while in the Taylor expansions of $h(p,x)$ and $g(p,x)$ only the both first elements are identical. Thus, $f(p,x)$ achieves a better approximation of $g(p,x)$ than $h(p,x)$ for a sufficiently small x.

Lemma 6.5.7. *For all $a \geq 0$, $b \geq 0$ and $-1 < p < \infty$, the expansion*

$$\tilde{g}(p,x) = \frac{(a+1)}{b^{\frac{1}{2}}x^{\frac{p+1}{2}}} - \frac{(a+1)a}{bx^{\frac{p+2}{2}}} + \frac{(a+1)(2a^2-1-pb)}{2b^{\frac{3}{2}}x^{\frac{p+3}{2}}} - \mathcal{O}\big(x^{-\frac{p+4}{2}}\big) \tag{6.66}$$

holds as $x \mapsto \infty$.

Proof. We use the general definition of asymptotic series expansion from Definition 2.4.2 in the form

$$\lim_{x\mapsto\infty} x^{\frac{n}{2}}\Big[\omega(x) - \sum_{k=0}^{n}\alpha_k\,x^{-\frac{k}{2}}\Big] = 0\,,\ n \in \{0,1,2,3\}\,, \tag{6.67}$$

and apply it for the function

$$\omega(x) \coloneqq x^{\frac{p+1}{2}}\tilde{g}(p,x)\,. \tag{6.68}$$

Then we first consider the case of $n=0$ and obtain the first coefficient $\alpha_0 = \frac{(a+1)}{\sqrt{b}}$ by determining the limit. Second, we increment n by one, determine the limit in (6.67) by applying l'Hospital's rule, and obtain the second coefficient $\alpha_1 = -\frac{(a+1)a}{b}$. The same principe is applied to obtain the coefficient α_2 and the order of the series expansion. Note that the last three steps are straightforward, however, require intensive algebra. Finally, the sequence $\sum_{k=0}^{3}\alpha_k\,x^{-\frac{k}{2}}$ is divided by $x^{\frac{p+1}{2}}$ which completes the proof. □

Substituting a and b in (6.66) by the corresponding coefficients $a_f(p)$, $b_f(p)$, $a_h(p)$ and $b_h(p)$ yields the following two propositions.

Corollary 6.5.8. *The asymptotic series expansion of $f(p,x)$ for $x \mapsto \infty$ is given by*

$$f(p,x) = \frac{\tau(p)}{x^{\frac{p+1}{2}}} - \frac{2\,\tau^2(p) - (p+3)}{2x^{\frac{p+2}{2}}} + \frac{8\,\tau^4(p) - 12(p+2)\,\tau^2(p) + (p+3)^2}{8\,\tau(p)x^{\frac{p+3}{2}}} - \mathcal{O}\big(x^{-\frac{p+4}{2}}\big)\,. \tag{6.69}$$

Corollary 6.5.9. *The asymptotic series expansion of $h(p,x)$ for $x \mapsto \infty$ is given by*

$$h(p,x) = \frac{\tau(p)}{x^{\frac{p+1}{2}}} - \frac{(p+1)}{x^{\frac{p+2}{2}}} + \frac{-\tau^4(p) + (p+2)\,\tau^2(p) + (p+1)^2}{2\,\tau(p) x^{\frac{p+3}{2}}} - \mathcal{O}\big(x^{-\frac{p+4}{2}}\big) \ . \quad (6.70)$$

Remark 6.5.10. Only the both first elements in the asymptotic series expansions of $f(p,x)$ and $g(p,x)$ are identical, while in the asymptotic series expansions of $h(p,x)$ and $g(p,x)$ the first two elements are identical. Thus, $h(p,x)$ achieves a better approximation of $g(p,x)$ than $f(p,x)$ for a sufficiently large x.

As mentioned at the beginning of Section 6.4, the coefficients e_1, e_2 and e_3 in (6.32) are such chosen that Remarks 6.5.6 and 6.5.10 are fulfilled. It is near at hand to aim at choosing the coefficients in an optimal way, namely to minimize the difference between the bounds and the BeNaI. However, because of the analytical complexity this seems to be out of reach.

The above statements show the general and asymptotic behavior of the bounds, while the following ones describe the relationship to the BeNaI. In particular, it is shown in which cases the bounds and the BeNaI are equal.

Corollary 6.5.11. *If $x = 0$, it holds for all $-1 < p < \infty$ that*

$$f(p,0) = h(p,0) = g(p,0) = 1 \ . \quad (6.71)$$

Proof. The equality $g(p,0) = 1$ is given by definition, see (6.4). By inserting $x = 0$ into (6.33) and (6.45), we obtain the equalities $f(p,0) = 1$ and $h(p,0) = 1$, respectively. □

Corollary 6.5.12. *For all $-1 < p < \infty$, the functions $f(p,x)$, $h(p,x)$ and $g(p,x)$ approach the asymptote $\tau(p)x^{-\frac{p+1}{2}}$ as x approaches infinity. Thus, it follows that*

$$\lim_{x\mapsto\infty} f(p,x) = \lim_{x\mapsto\infty} h(p,x) = \lim_{x\mapsto\infty} g(p,x) = 0 \ . \quad (6.72)$$

Proof. The asymptote $\tau(p)x^{-\frac{p+1}{2}}$ follows from the asymptotic expansions, which are stated in Lemma 6.2.4, Corollary 6.5.8 and Corollary 6.5.9. From this asymptote we derive the limit which tends towards zero. □

Corollary 6.5.13. *In case of $p \mapsto -1$ and for all $x \geq 0$, we observe the equality*

$$f(-1,x) = h(-1,x) = \lim_{p\mapsto -1} g(p,x) = 1 \ . \quad (6.73)$$

Proof. By using the identity $\tau(-1) = 1$ from (2.32), we obtain the equalities $a_f(-1) = 0$ and $a_h(-1) = 0$ from (6.34) and (6.46), respectively. By inserting $a_f(-1)$ and $a_h(-1)$ into (6.43) and (6.55), respectively, we derive equation (6.73) by considering (6.19). □

Corollary 6.5.14. *If $p = 0$ and $x \geq 0$, the double inequality*

$$\frac{\pi^2 x}{4 + \sqrt{(\pi^2-4)^2 + 4\pi^2 x^2}} \leq \arctan(x) \leq \frac{\pi^2 x}{\pi^2 - 6 + 2\sqrt{9 + \pi^2 x^2}} \quad (6.74)$$

holds. For all $x < 0$, the reverse double inequality holds.

Proof. The double inequality (6.74) follows from equation (6.18), inequalities (6.36) and (6.48), and by replacing x with x^2. □

The double inequality in Corollary 6.5.14 is tight as can be seen from Figure 6.4. The maximum relative errors of the bounds, related to the inverse tangent function, are approximately less than 0.23% and 0.27%. Inequality (6.74) is obtained as a side result of the general approach in this work. A more detailed discussion may be found in [13].

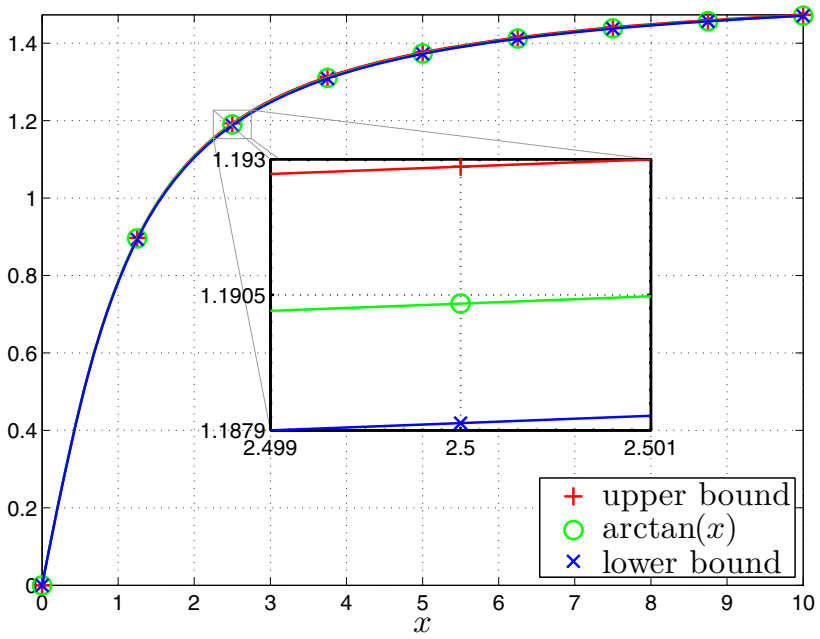

Figure 6.4: The inverse tangent function and its bounds from Corollary 6.5.14 are visualized for the range of $0 \leq x \leq 10$. The curves are closely adjacent to one another such that without magnification the differences are not really visible. The curves are equal at zero and approach the same limit as $|x|$ approaches infinity. Their maximum relative errors are approximately less than 0.23% and 0.27% which shows how sharp both bounds are.

As shown in representation (6.15b), the fractions $\frac{a_f(p)+1}{a_f(p)+\sqrt{1+x\,b_f(p)}}$ and $\frac{a_h(p)+1}{a_h(p)+\sqrt{1+x\,b_h(p)}}$ are approximations of the hypergeometric function ${}_2\mathrm{F}_1\left(\frac{1}{2}, 1; \frac{p+3}{2}; -x\right)$. Thus, they can be used as bounds for other functions that can be described in terms of the hypergeometric function and its transformations.

Corollary 6.5.15. *If $p = 1$, it holds for all $x \geq 0$ that*

$$f(1,x) = h(1,x) = g(1,x) = \frac{2}{1+x+\sqrt{1+x}}\,. \tag{6.75}$$

Proof. By using the identity $\tau(1) = 2$ from (2.32), we obtain the equalities $a_f(1) = 1$ and $a_h(1) = 1$ from (6.34) and (6.46), respectively. By inserting $a_f(1)$ and $a_h(1)$ into (6.43) and (6.55), respectively, we derive equation (6.75) by considering (6.17). □

In the current section, we have shown some mathematical properties of the bounds which are identical to those of the BeNaI. Unfortunately, we could not prove the monotonicity and the convexity of the bounds for the case $-1 < p < 0$ and thus we leave the proof as an open problem. It remains to investigate the accuracy of the bounds which will be the main contribution of the next section.

6.6 Proof of the Bounds

We follow an idea of W. Gautschi [24] in order to prove Theorem 6.4.1 and 6.4.5. Prior to this, we need to consider some definitions and their corresponding statements.

Definition 6.6.1. Let $f(p,x)$ and $g(p,x)$ be defined as in Theorem 6.4.1 and Definition 6.1.1, respectively. Then we define their difference by

$$d_f(p,x) \coloneqq g(p,x) - f(p,x)\ ,\ p \in \mathbb{R},\ -1 < p < \infty,\ x \in \mathbb{R}_+\,, \tag{6.76}$$

and

$$\tilde{d}_f(p,x) \coloneqq x^{\frac{p+1}{2}} d_f(p,x) = \frac{p+1}{2} \int_0^x \frac{t^{\frac{p-1}{2}}\,\mathrm{d}t}{(1+t)^{\frac{p+2}{2}}} - \frac{x^{\frac{p+1}{2}}}{(1+x)^{\frac{p}{2}}} \frac{a_f+1}{a_f+\sqrt{1+x\,b_f}}\ . \tag{6.77}$$

Lemma 6.6.2. *The difference $d_f(p,x)$ has the properties:*

a) $d_f(p,x)$ is continuous without any singularity for all $x \in \mathbb{R}_+$ and $-1 < p < \infty$,

b) the identity

$$\lim_{x\mapsto 0} d_f(p,x) = \lim_{x\mapsto\infty} d_f(p,x) = 0 \tag{6.78}$$

holds, and

c) for suitable large x the inequalities

$$d_f(p,x)|_{x\mapsto\infty} \begin{cases} > 0 & p \in \mathbb{R},\ 1 < p < \infty, \\ < 0 & p \in \mathbb{R},\ -1 < p < 1 \end{cases} \tag{6.79}$$

hold.

Proof. The difference $d_f(p,x)$ has no singularities because a_f and b_f are non-negative, as mentioned in Lemma 6.4.3. Moreover, it is continuous because $g(p,x)$ and $f(p,x)$ are continuous and all operations preserve continuity as stated in Lemma 6.2.1 and Lemma 6.5.1, respectively.

By using the identities in Corollary 6.5.11 and 6.5.12, we simply obtain (6.78).

From the asymptotic expansions in Lemma 6.2.4 and in Corollary 6.5.8, we obtain

$$d_f(p,x) = \Big[\tau^2(p) - \frac{3p+5}{2}\Big] x^{-\frac{p+2}{2}} + \mathcal{O}\big(x^{-\frac{p+3}{2}}\big)\ . \tag{6.80}$$

The first term is positive for all $1 < p < \infty$ and negative for all $-1 < p < 1$ due to Theorem 2.5.2. Thus, the above statement follows for a suitable large x. □

Lemma 6.6.3. *The difference $\tilde{d}_f(p,x)$ has no sign changes.*

Proof. We consider the equation

$$2\,\frac{p+3}{1+a_f}\,b_f\,(1+x)^{\frac{p+2}{2}}\,x^{-\frac{p-1}{2}}\left(a_f+\sqrt{1+xb_f}\right)^2\cdot\sqrt{1+xb_f}\,\frac{\partial\tilde{d}_f(p,x)}{\partial x}\;, \tag{6.81}$$

which is equal to

$$(u-1)^2\big[u\left(2(p+1)-(p+3)a_f\right)+(p+1)-2a_f\big]\;, \tag{6.82}$$

where $u=\sqrt{1+xb_f}\geq 1$, and $b_f=2\,\frac{a_f+1}{p+3}$ is given in equation (6.37). The last equation is a polynomial in u that has exactly three zeros. The difference $\tilde{d}_f(p,x)$ cannot change sign for all $u>1$ or equivalently for all $x>0$, since the first two zeros are at $u=1$, the difference $d_f(p,x)$ has no singularities based on Lemma 6.6.2, and $d_f(p,0)$ is equal to $d_f(p,\infty)$ due to Lemma 6.6.2. In other words, if $\tilde{d}_f(p,x)$ had at least one sign change for some value of $x>0$, then it would have at least two stationary points for $x>0$, but this contradicts the above curve tracing. □

Proof of Theorem 6.4.1. Since $\tilde{d}_f(p,x)$, and hence $d_f(p,x)$ as well, have no sign changes as stated in Lemma 6.6.3, we deduce that $f(p,x)\leq g(p,x)$ for all $1\leq p<\infty$ and $f(p,x)\geq g(p,x)$ for all $-1<p\leq 1$, both due to inequality (6.79). □

Definition 6.6.4. Let $h(p,x)$ and $g(p,x)$ be defined as in Theorem 6.4.5 and Definition 6.1.1, respectively. Then we define their difference by

$$d_h(p,x)\coloneqq h(p,x)-g(p,x)\;,\;\; p\in\mathbb{R},\;\; -1<p<\infty,\;\; x\in\mathbb{R}_+\,, \tag{6.83}$$

and

$$\tilde{d}_h(p,x)\coloneqq x^{\frac{p+1}{2}}d_h(p,x)=\frac{x^{\frac{p+1}{2}}}{(1+x)^{\frac{p}{2}}}\,\frac{a_h+1}{a_h+\sqrt{1+x\,b_h}}\;-\;\frac{p+1}{2}\int_0^x\frac{t^{\frac{p-1}{2}}\,\mathrm{d}t}{(1+t)^{\frac{p+2}{2}}}\;. \tag{6.84}$$

Lemma 6.6.5. *The difference $d_h(p,x)$ has the properties:*

a) $d_h(p,x)$ is continuous without any singularity for all $x\in\mathbb{R}_+$ and $-1<p<\infty$,

b) the identity

$$\lim_{x\mapsto 0}d_h(p,x)=\lim_{x\mapsto\infty}d_h(p,x)=0 \tag{6.85}$$

holds, and

c) for suitable small $x>0$ the inequalities

$$d_h(p,x)|_{x\mapsto 0}\begin{cases}>0 & p\in\mathbb{R},\;1<p<\infty,\\ <0 & p\in\mathbb{R},\;-1<p<1\end{cases} \tag{6.86}$$

hold.

Proof. The difference $d_h(p,x)$ has no singularities because a_h and b_h are non-negative, as mentioned in Lemma 6.4.7. Moreover, it is continuous because $g(p,x)$ and $h(p,x)$ are continuous and all operations preserve continuity as stated in Lemma 6.2.1 and Lemma 6.5.1, respectively.

By using the identities in Corollary 6.5.11 and 6.5.12, we simply obtain (6.85).

From the Taylor expansions in Lemma 6.2.3 and in Corollary 6.5.5, we obtain

$$d_h(p,x) = \left[\frac{2}{p+3} - \frac{1}{\tau^2(p)-(p+1)}\right]\frac{x}{2} + \mathcal{O}\big(x^2\big)\ . \tag{6.87}$$

The first term is positive for all $1 < p < \infty$ and negative for all $-1 < p < 1$ due to Theorem 2.5.2. Thus, the above statement follows for a suitable small x. □

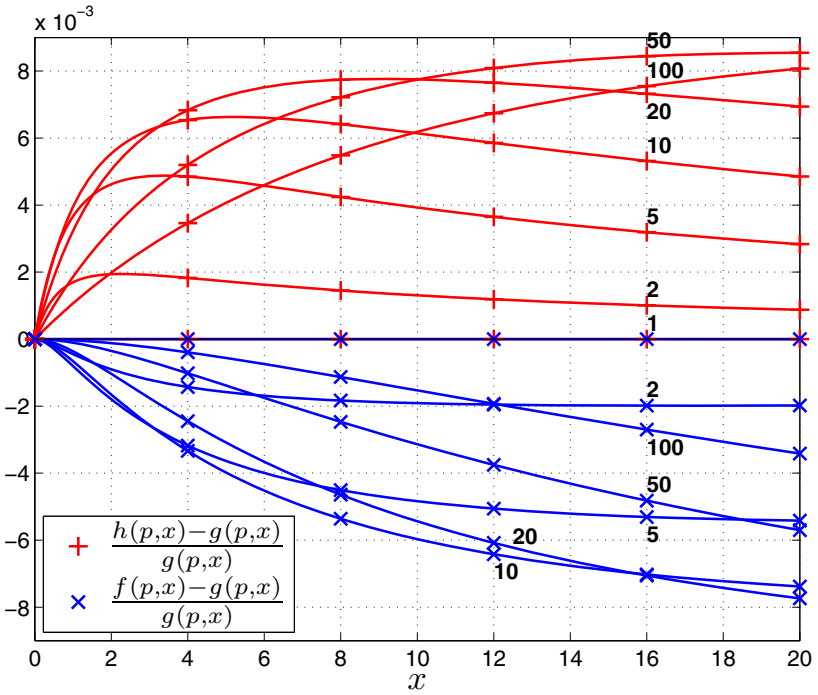

Figure 6.5: Relative errors of both bounds $f(p,x)$ and $h(p,x)$ are depicted for $p \in \{1,2,5,10,20,50,100\}$. Note that for large x, all curves tend towards zero. Due to the range $1 \le p < \infty$, the double inequality $f(p,x) \le g(p,x) \le h(p,x)$ holds. In general, $f(p,x)$ achieves a better approximation of $g(p,x)$ than $h(p,x)$ for sufficiently small x, while for sufficiently large x the opposite is valid. The maximum values of relative errors over all x are about 1.2% and can be observed in Figure 6.7.

Lemma 6.6.6. *The difference $\tilde{d}_h(p,x)$ has no sign changes.*

Proof. We consider the equation

$$2\,\frac{p+1}{1+a_h}\,b_h\,(1+x)^{\frac{p+2}{2}}\,x^{-\frac{p-1}{2}}\,\big(a_h+\sqrt{1+xb_h}\big)^2\cdot\sqrt{1+xb_h}\,\frac{\partial \tilde{d}_h(p,x)}{\partial x}\ , \tag{6.88}$$

which is equal to

$$(u-1)\left[u\left((p+1)+pa_h-(p+2)a_h^2\right)+(p+1)-(1+a_h)a_h\right]\,, \tag{6.89}$$

where $u=\sqrt{1+xb_h}\geq 1$, and $b_h=\frac{a_h+1}{p+1}\,a_h$ is given in equation (6.49). The last equation is a polynomial in u that has exactly two zeros. The difference $\tilde{d}_h(p,x)$ cannot change sign for all $u>1$ or equivalently for all $x>0$, since the first zero is at $u=1$, the difference $d_h(p,x)$ has no singularities based on Lemma 6.6.5, and $d_h(p,0)$ is equal to $d_h(p,\infty)$ due to Lemma 6.6.5. In other words, if $\tilde{d}_h(p,x)$ had at least one sign change for some value of $x>0$, then it would have at least two stationary points for $x>0$, but this contradicts the above curve tracing. □

Proof of Theorem 6.4.5. Since $\tilde{d}_h(p,x)$, and hence $d_h(p,x)$ as well, have no sign changes as stated in Lemma 6.6.6, we deduce that $h(p,x)\geq g(p,x)$ for all $1\leq p<\infty$ and $h(p,x)\leq g(p,x)$ for all $-1<p\leq 1$, both due to inequality (6.86). □

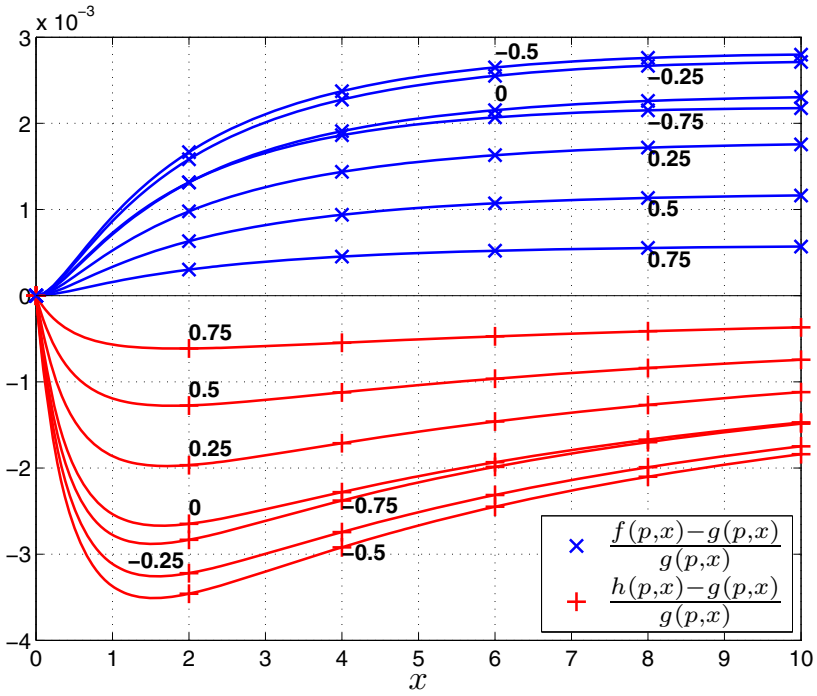

Figure 6.6: Relative errors of both bounds $f(p,x)$ and $h(p,x)$ are depicted for $p\in\{-3/4,-2/4,-1/4,0,1/4,2/4,3/4\}$. Note that for large x, all curves tend towards zero. Due to the range $-1<p\leq 1$, the double inequality $h(p,x)\leq g(p,x)\leq f(p,x)$ holds. In general, $f(p,x)$ achieves a better approximation of $g(p,x)$ than $h(p,x)$ for sufficiently small x, while for sufficiently large x the opposite is valid. The maximum values of relative errors over all x are about 0.36% and can be observed in Figure 6.8.

6.7 Analysis of the Bounds

In this section, we discuss the relative error between the upper and lower bound from Section 6.4 and the value of the BeNaI from Definition 6.1.1. A direct calculation of the relative error seems to be out of reach. We hence derive upper bounds on the maximum relative errors. We start with introducing the relative error.

Definition 6.7.1. The relative errors of the bounds in Theorem 6.4.1 and in Theorem 6.4.5, related to the BeNaI, are defined by

$$r_f(p) \coloneqq \max\left\{ \frac{|g(p,x) - f(p,x)|}{g(p,x)} \mid x \in \mathbb{R}_+ \right\} \tag{6.90}$$

and by

$$r_h(p) \coloneqq \max\left\{ \frac{|h(p,x) - g(p,x)|}{g(p,x)} \mid x \in \mathbb{R}_+ \right\}, \tag{6.91}$$

respectively. The relative error between the bounds is defined by

$$r(p) \coloneqq \max\left\{ \frac{|h(p,x) - f(p,x)|}{g(p,x)} \mid x \in \mathbb{R}_+ \right\} \leq r_f(p) + r_h(p). \tag{6.92}$$

Furthermore, we denote the relative error of the closest bound by

$$\tilde{r}(p) \coloneqq \max\left\{ \frac{\min\{|g(p,x) - f(p,x)|, |h(p,x) - g(p,x)|\}}{g(p,x)} \mid x \in \mathbb{R}_+ \right\}. \tag{6.93}$$

Note that inequality (6.92) follows from triangle inequality.

In Figure 6.5 and 6.6, the relative errors are depicted with respect to x for different values of p. The relative errors are always less than 1.2% for all $1 \leq p < \infty$ or 0.36% for all $-1 < p \leq 1$. Since the relative errors $r_f(p)$ and $r_h(p)$ as well as their maximum values are poorly accessible, we now set out to develop upper bounds on $r_f(p)$ and $r_h(p)$ as well as on their maximum values.

Theorem 6.7.2. *For all $1 \leq p < \infty$, the relative error $r(p)$ is bounded by*

$$r(p) \leq \hat{r}(p) \coloneqq -1 + \frac{a_h + 1}{a_f + 1} \cdot \frac{a_f a_h b_f b_h - \sqrt{b_f b_h (b_h - b_f)[b_f(a_h^2 - 1) - b_h(a_f^2 - 1)]}}{b_h[b_h + b_f(a_h^2 - 1)]}. \tag{6.94}$$

If $-1 < p \leq 1$, then the relative error is bounded by

$$r(p) \leq \check{r}(p) \coloneqq -1 + \frac{a_f + 1}{a_h + 1} \cdot \frac{a_f a_h b_f b_h - \sqrt{b_f b_h (b_f - b_h)[b_h(a_f^2 - 1) - b_f(a_h^2 - 1)]}}{b_f[b_f + b_h(a_f^2 - 1)]}. \tag{6.95}$$

Proof. See Appendix 6.8. □

The bounds in Theorem 6.7.2 have a more direct representation as

$$r(p) \leq \hat{r}(p) = \frac{2\,\tau^2(p) - (3p+5)}{2\,\tau(p)\big[\tau(p) + \sqrt{1-p+2\,\tau^2(p)}\,\big] + (3+p)} \tag{6.96}$$

for all $1 \leq p < \infty$, and

$$r(p) \leq \check{r}(p) = \frac{(3p+5) - 2\,\tau^2(p)}{2\,\tau(p)\big[2\,\tau(p) + \sqrt{1-p+2\,\tau^2(p)}\,\big] - 2(1+p)} \tag{6.97}$$

for all $-1 < p \leq 1$. This may be seen by substituting.

In Figure 6.7 and 6.8, the maximum relative errors are depicted. As we can see, $r(p)$ is a weak upper-bound on the maximum relative errors while $\hat{r}(p)$ and $\check{r}(p)$ are tight upper-bounds on $r(p)$ and thus closely adjacent to $r(p)$.

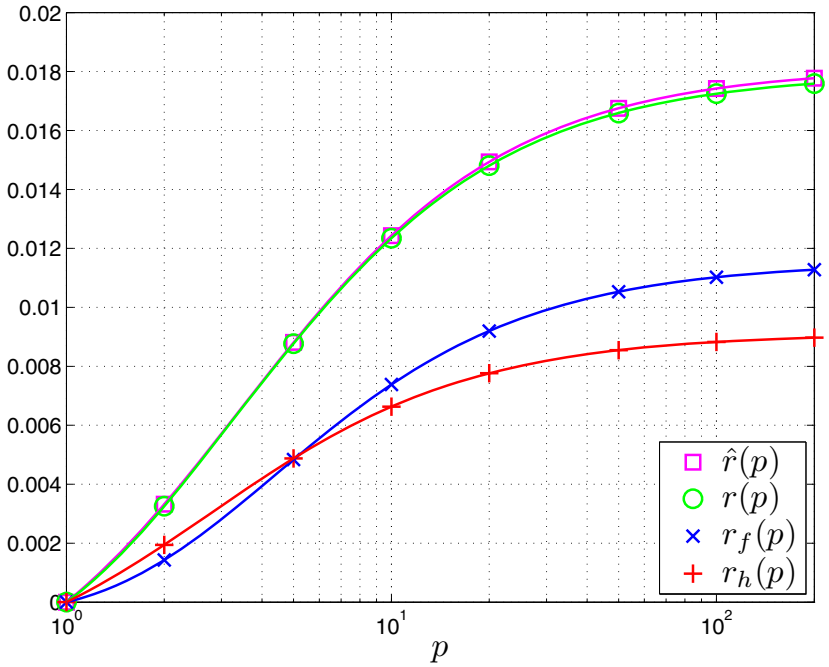

Figure 6.7: Maximum relative errors with respect to x are visualized for $1 \leq p \leq 200$. The value $r_f(p)$ is the maximum relative error between the lower bound $f(p,x)$ and the function $g(p,x)$ while $r_h(p)$ is the maximum relative error between upper bound $h(p,x)$ and $g(p,x)$. The value $r(p)$ is the maximum relative error between the lower and the upper bound while $\hat{r}(p)$ is an upper bound on $r(p)$. We can calculate $r(p)$, $r_f(p)$ and $r_h(p)$ only numerically while the overall upper bound $\hat{r}(p)$ is obtained analytically. $r(p)$ and $\hat{r}(p)$ are limited by 0.0182 for all $1 \leq p < \infty$.

Remark 6.7.3. By numerical analysis we observe

$$r(p) \leq \lim_{p\mapsto\infty} \hat{r}(p) = \frac{\pi - 3}{1 + \pi + \sqrt{2\pi(\pi-1)}} < 0.0182 \tag{6.98}$$

for all $1 \leq p < \infty$, and

$$r(p) \leq \check{r}(p \approx -0.45974) < 0.00535 \tag{6.99}$$

for all $-1 < p \leq 1$.

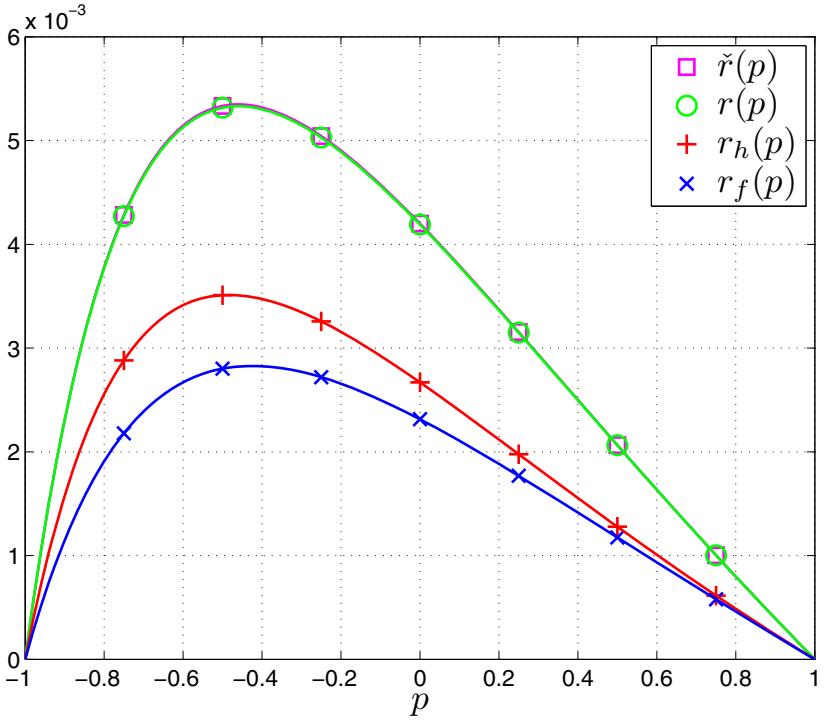

Figure 6.8: Maximum relative errors with respect to x are visualized for $-1 < p \leq 1$. The value $r_h(p)$ is the maximum relative error between the lower bound $h(p, x)$ and the function $g(p, x)$ while $r_f(p)$ is the maximum relative error between upper bound $f(p, x)$ and $g(p, x)$. The value $r(p)$ is the maximum relative error between the lower and the upper bound while $\check{r}(p)$ is an upper bound on $r(p)$. We can calculate $r(p)$, $r_h(p)$ and $r_f(p)$ only numerically while the overall upper bound $\check{r}(p)$ is obtained analytically. $r(p)$ and $\check{r}(p)$ are limited by 0.00535 for all $-1 < p \leq 1$.

Corollary 6.7.4. *The relative error of the closest bound in* (6.93) *is bounded by*

$$\tilde{r}(p) \leq \frac{\hat{r}(p)}{\hat{r}(p) + 2} \leq 0.00899 \tag{6.100}$$

for all $1 \leq p < \infty$, *and*

$$\tilde{r}(p) \leq \frac{\check{r}(p)}{\check{r}(p) + 2} \leq 0.00267 \tag{6.101}$$

for all $-1 < p \leq 1$.

Proof. If we define the functions

$$r_f(p,x) \coloneqq \frac{|g(p,x) - f(p,x)|}{g(p,x)} \,, \tag{6.102}$$

$$r_h(p,x) \coloneqq \frac{|h(p,x) - g(p,x)|}{g(p,x)} \,, \tag{6.103}$$

$$\varrho(p,x) \coloneqq \frac{h(p,x)}{f(p,x)} \tag{6.104}$$

and

$$\varrho(p) \coloneqq \max\left\{ \frac{h(p,x)}{f(p,x)} \mid x \in \mathbb{R}_+ \right\} \tag{6.105}$$

then for all $1 \leq p < \infty$ the relationship

$$g(p,x) = \frac{f(p,x)}{1 - r_f(p,x)} = \frac{h(p,x)}{1 + r_h(p,x)} \quad \Leftrightarrow \quad \frac{1 + r_h(p,x)}{1 - r_f(p,x)} = \varrho(p,x) \leq \varrho(p) \tag{6.106}$$

holds. In the case in which the inequality $r_h(p,x) \leq r_f(p,x)$ is valid for some values of x and fixed p, we can shrink the ratio $\frac{1+r_h(p,x)}{1-r_f(p,x)}$ by replacing $r_f(p,x)$ with $r_h(p,x)$. In the opposite case $r_f(p,x) \leq r_h(p,x)$, we can also shrink the ratio $\frac{1+r_h(p,x)}{1-r_f(p,x)}$ by replacing $r_h(p,x)$ with $r_f(p,x)$. In both cases we derive the inequality

$$\min\bigl\{ r_f(p,x), r_h(p,x) \bigr\} \leq \frac{\varrho(p) - 1}{\varrho(p) + 1} \,, \tag{6.107}$$

which holds for all x. Now, we define $\hat{r}(p)$ by the difference $\varrho(p) - 1$ for all $1 \leq p < \infty$, in order to obtain the first ratio in equation (6.100). Furthermore, the right hand side of (6.107) is increasing in $\varrho(p)$ because its first derivative

$$\frac{\mathrm{d}}{\mathrm{d}\varrho(p)} \frac{\varrho(p) - 1}{\varrho(p) + 1} = \frac{2}{\bigl(\varrho(p) + 1\bigr)^2} = \frac{2}{\bigl(\hat{r}(p) + 2\bigr)^2} \tag{6.108}$$

is always positive. Thus, we can replace $\hat{r}(p)$ with the value in (6.98) to get the upper limit of 0.00899.

The proof of equation (6.101) for $-1 < p \leq 1$ follows analogously by exchanging the roles of $f(p,x)$ with $h(p,x)$, $\hat{r}(p)$ with $\check{r}(p)$, and $\varrho(p)$ with $\frac{1}{\varrho(p)}$. □

In Figure 6.9 and 6.10, the maximum relative errors of the closest bound are depicted. As we can see, one of the bounds has always a smaller relative error than 0.9% for all $1 \leq p < \infty$ or 0.27% for all $-1 < p \leq 1$; see also the results in equation (6.100) and (6.101).

In summary, both maximum relative errors $r_f(p)$ and $r_h(p)$ are upper-bounded by $r(p)$. In turn, $r(p)$ is upper-bounded by $\hat{r}(p)$ or by $\check{r}(p)$ depending on p. Both $\hat{r}(p)$ and $\check{r}(p)$ are sharp bounds on $r(p)$ and have been analytically derived in closed-form. Furthermore, $\tilde{r}(p)$ is bounded by either $\frac{\hat{r}(p)}{\hat{r}(p)+2}$ or by $\frac{\check{r}(p)}{\check{r}(p)+2}$ depending on p, where $\tilde{r}(p)$ describes the relative error of the closest bound.

6.8 Proof of Relative Errors

Definition 6.8.1. Let $f(p,x)$ and $h(p,x)$ be defined as in Theorem 6.4.1 and Theorem 6.4.5, respectively. Then we denote their ratio by

$$\varrho(p,x) := \frac{h(p,x)}{f(p,x)} = \frac{a_h(p)+1}{a_f(p)+1}\,\frac{a_f(p)+\sqrt{1+x\,b_f(p)}}{a_h(p)+\sqrt{1+x\,b_h(p)}}\,, \tag{6.109}$$

for all $p \in \mathbb{R}$, $-1 < p < \infty$ and for all $x \in \mathbb{R}_+$.

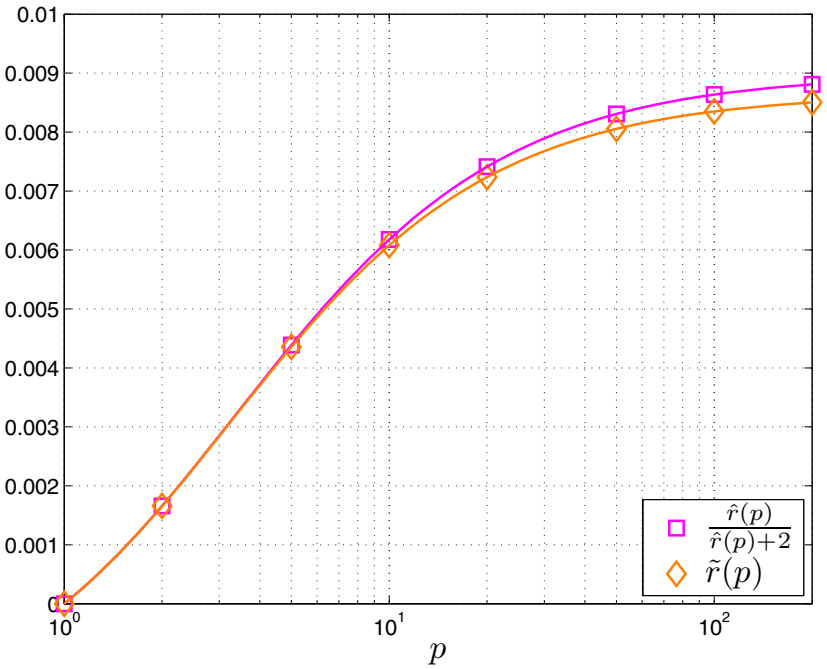

Figure 6.9: Maximum relative errors of the closest bound with respect to x are visualized for $1 \le p \le 200$. The value $\tilde{r}(p)$ is the maximum relative error between $g(p,x)$ and the closest bound, which is either $f(p,x)$ or $h(p,x)$. $\frac{\hat{r}(p)}{\hat{r}(p)+2}$ is an upper bound on $\tilde{r}(p)$ and is obtained analytically, while $\tilde{r}(p)$ can only be calculated numerically. $\tilde{r}(p)$ and $\frac{\hat{r}(p)}{\hat{r}(p)+2}$ are limited by 0.00899 for all $1 \le p < \infty$.

Lemma 6.8.2. *The identity*

$$\lim_{x\mapsto 0} \varrho(p,x) = \lim_{x\mapsto\infty} \varrho(p,x) = 1 \tag{6.110}$$

holds.

Proof. By using Definition 6.8.1, Theorem 6.4.1 and 6.4.5, we obtain

$$\lim_{x\mapsto 0} \varrho(p,x) = \frac{a_h(p)+1}{a_f(p)+1}\,\frac{a_f(p)+1}{a_h(p)+1} = 1 \tag{6.111}$$

and

$$\lim_{x\mapsto\infty} \varrho(p,x) = \frac{a_h(p)+1}{a_f(p)+1}\sqrt{\frac{b_f(p)}{b_h(p)}} = \frac{\tau^2(p)}{\tau^2(p)-(p+1)}\,\frac{p+3}{2\,\tau^2(p)}\,\frac{2\,\tau(p)}{p+3}\,\frac{\tau^2(p)-(p+1)}{\tau(p)} = 1\ . \tag{6.112}$$

□

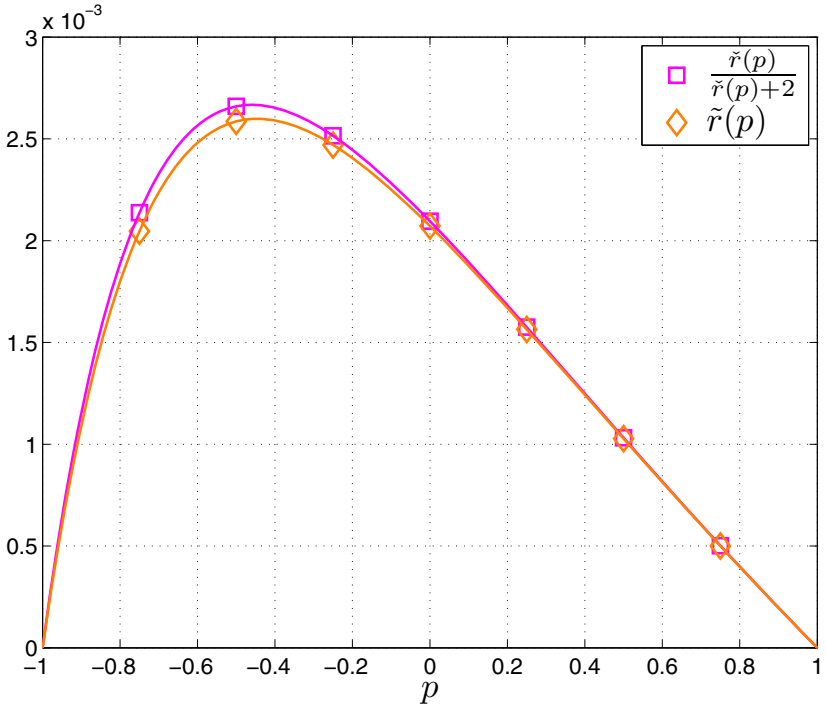

Figure 6.10: Maximum relative errors of the closest bound with respect to x are visualized for $-1 < p \leq 1$. The value $\tilde{r}(p)$ is the maximum relative error between $g(p,x)$ and the closest bound, which is either $f(p,x)$ or $h(p,x)$. $\frac{\check{r}(p)}{\check{r}(p)+2}$ is an upper bound on $\tilde{r}(p)$ and is obtained analytically, while $\tilde{r}(p)$ can only be calculated numerically. $\tilde{r}(p)$ and $\frac{\check{r}(p)}{\check{r}(p)+2}$ are limited by 0.00267 for all $-1 < p \leq 1$.

Proof of Theorem 6.7.2. By using Definition 6.7.1, Theorem 6.4.1 and Theorem 6.4.5, we deduce

$$\begin{aligned} r(p) &= \max\left\{\frac{h(p,x)-f(p,x)}{g(p,x)} \mid x\in\mathbb{R}_+\right\} \\ &\leq \max\left\{\frac{h(p,x)-f(p,x)}{f(p,x)} \mid x\in\mathbb{R}_+\right\}, \quad 1\leq p<\infty\ , \end{aligned} \tag{6.113}$$

and analogously

$$\begin{aligned} r(p) &= \max\left\{ \frac{f(p,x)-h(p,x)}{g(p,x)} \mid x \in \mathbb{R}_+ \right\} \\ &\leq \max\left\{ \frac{f(p,x)-h(p,x)}{h(p,x)} \mid x \in \mathbb{R}_+ \right\}, \quad -1 < p \leq 1 \ . \end{aligned} \tag{6.114}$$

If we use the ratio $\varrho(p,x)$ from Definition 6.8.1 then we obtain the corresponding inequalities

$$r(p) \leq \max\left\{ \varrho(p,x) - 1 \mid x \in \mathbb{R}_+ \right\}, \ 1 \leq p < \infty \ , \tag{6.115}$$

and

$$r(p) \leq \max\left\{ \frac{1}{\varrho(p,x)} - 1 \mid x \in \mathbb{R}_+ \right\}, \ -1 < p \leq 1 \ . \tag{6.116}$$

Thus, we have to maximize $\varrho(p,x)$ with respect to x for all $1 \leq p < \infty$ and minimize $\varrho(p,x)$ with respect to x for all $-1 < p \leq 1$ in order to find an upper bound for $r(p)$. The first derivative of $\varrho(p,x)$ with respect to x is given by

$$\frac{\partial \varrho(p,x)}{\partial x} = \frac{a_h+1}{a_f+1} \cdot \frac{b_f\left[1+a_h\sqrt{1+x\,b_h}\,\right] - b_h\left[1+a_f\sqrt{1+x\,b_f}\,\right]}{2\left[a_h+\sqrt{1+x\,b_h}\,\right]^2\sqrt{1+x\,b_f}\,\sqrt{1+x\,b_h}} \tag{6.117}$$

that must vanish at the extrem points. By simple calculation we conclude that the first derivative can only have two zeros; one at x_1 and one at x_2. They can be calculated by solving the quadratic equation

$$x^2 - 2x\frac{(a_f^2b_h+a_h^2b_f)(b_h-b_f)^2-(a_f^2b_h-a_h^2b_f)(a_f^2b_h^2-a_h^2b_f^2)}{b_fb_h(a_f^2b_h-a_h^2b_f)^2} + \frac{[a_f^2b_h^2+a_h^2b_f^2-(b_h-b_f)^2]^2-4a_f^2a_h^2b_f^2b_h^2}{b_f^2b_h^2(a_f^2b_h-a_h^2b_f)^2} = 0 \ . \tag{6.118}$$

Because of Lemma 6.8.2 the maximum of $\varrho(p,x)$ as well as the maximum of $\frac{1}{\varrho(p,x)}$ must be greater than one, or equivalently $r(p) > 0$ for all $-1 < p < \infty$. We assume, without loss of generality, that $\varrho(p,x)$ attains its maximum at $x = x_1$ for all $1 \leq p < \infty$ or $\frac{1}{\varrho(p,x)}$ attains its maximum at $x = x_1$ for all $-1 < p \leq 1$. Then by incorporating x_1 into $\varrho(p,x)$ the maximum

$$\varrho(p,x_1) = \frac{a_h+1}{a_f+1} \cdot \frac{a_fa_hb_fb_h - \sqrt{b_fb_h(b_h-b_f)[b_f(a_h^2-1)-b_h(a_f^2-1)]}}{b_h[b_h+b_f(a_h^2-1)]} \tag{6.119}$$

follows for all $1 \leq p < \infty$. By changing the roles of $f(p,x)$ and $h(p,x)$ we deduce the corresponding maximum value of $\frac{1}{\varrho(p,x_1)}$ for all $-1 < p \leq 1$ by

$$\frac{1}{\varrho(p,x_1)} = \frac{a_f+1}{a_h+1} \cdot \frac{a_fa_hb_fb_h - \sqrt{b_fb_h(b_f-b_h)[b_h(a_f^2-1)-b_f(a_h^2-1)]}}{b_f[b_f+b_h(a_f^2-1)]} \ . \tag{6.120}$$

Now, we incorporate a_f, b_f, a_h and b_h from Theorem 6.4.1 and 6.4.5 into $\varrho(p,x_1)$ to obtain the bounds in (6.96) and (6.97). In order to show that x_1 is the point at

maximum for all $1 \leq p < \infty$ or the point at minimum for all $-1 < p \leq 1$, which are together equivalent to $r(p) > 0$ for all $-1 < p < \infty$, we minimize the bounds in (6.96) and (6.97) by applying Theorem 2.5.2. By doing so, we see that

$$\frac{2\,\tau^2(p) - (3p+5)}{2\,\tau(p)\big[\tau(p) + \sqrt{1-p+2\,\tau^2(p)}\,\big] + (3+p)} \geq \frac{(3p+5) - (3p+5)}{2\,\tau(p)\big[\tau(p) + \sqrt{1-p+2\,\tau^2(p)}\,\big] + (3+p)} = 0 \quad (6.121)$$

for all $1 \leq p < \infty$, and

$$\frac{(3p+5) - 2\,\tau^2(p)}{2\,\tau(p)\big[2\,\tau(p) + \sqrt{1-p+2\,\tau^2(p)}\,\big] - 2(1+p)} \geq \frac{(3p+5) - 2\,\tau^2(p)}{2\,\tau(p)\big[2\,\tau(p) + \sqrt{1-p+2\,\tau^2(p)}\,\big]} \geq \frac{(3p+5) - (3p+5)}{2\,\tau(p)\big[2\,\tau(p) + \sqrt{1-p+2\,\tau^2(p)}\,\big]} = 0 \quad (6.122)$$

for all $-1 < p \leq 1$. This confirms the statement. □

6.9 Discussion of Results

As shown in Theorem 6.1.5 and subsequent statements, we are able to find new representations for the BeNaI with considerable consequences. On the one hand, equations (6.13a) and (6.13b) do not include any special functions and are thus simpler to handle than (6.3). On the other hand, equations (6.15a), (6.15b) and (6.15c) show general relations to important special functions, which enable further interpretations and discussions of the BeNaI in connection with other special functions.

In addition, we have seen that the BeNaI has some famous mathematical properties. In particular, the BeNaI is non-negative, continuous, strictly decreasing and logarithmically convex with respect to x. The series expansions of the BeNaI are also derived, especially for the limits $x \mapsto 0$ and $x \mapsto \infty$ in order to show its asymptotic behavior for these limits. By studying these properties, we have been able to choose a specific class of functions for bounding the BeNaI.

As stated in Theorem 6.4.1 and 6.4.5, we have presented two new bounds on the BeNaI for the whole range of parameters $-1 < p < \infty$ and $x \geq 0$. Both, the lower bound and the upper bound, are dependent on their coefficients and it is possible to modify the coefficients in order to adapt the bounds for certain applications. This shows that the proposed bounds are scalable and are thus universally useful.

Subsequently, we have established that some of the mathematical properties of the bounds are identical to those of the BeNaI and there exist certain cases where both bounds and the BeNaI are equal to each other. This reinforces the decision about the chosen class of functions from (6.32) for generating the bounds in Theorem 6.4.1 and 6.4.5.

In order to determine the tightness of the bounds, we have investigated the relative error of the bounds in Section 6.7. Numerical results show that both bounds are accurate and they achieve relative errors of approximately less than 1.2% for the whole range of parameters. Since the relative errors and their maximum are hardly analytically accessible, we have upper-bounded the maximum relative errors by some new bounds in closed-form. The new bounds show that the maximum relative errors are approximately less than 1.8%. Hence, the bounds on the maximum relative errors are also accurate.

6.10 Open Problems

We have not found a short proof in order to show the monotonicity and the convexity of the bounds $f(p,x)$ and $h(p,x)$ for the range $-1 < p < 0$. Properties of *completely monotonic* functions, see [95], could be of help to accomplish this task, which we leave for future research. For the time being, both properties are claimed as conjectures.

Conjecture 6.10.1. For all $-1 < p < 0$ and for all $x \geq 0$, both $f(p,x)$ and $h(p,x)$ are strictly decreasing functions of x.

Conjecture 6.10.2. For all $-1 < p < 0$ and for all $x \geq 0$, both $f(p,x)$ and $h(p,x)$ are logarithmically convex functions of x.

6.11 Summary

In the present chapter, we have investigated the general expression of the average symbol-error probability (BeNaI) which appears in data communication over Nakagami-distributed fading channels. We have suggested some useful and novel identities which allow for easy and accurate numerical calculations of the BeNaI. These identities also facilitate the analytical analysis of the BeNaI. We hence have easily derived important mathematical properties and further identities of the BeNaI. In addition, a new lower and upper bound on the BeNaI have been proposed in closed-form. They are sharp and accurate over a wide range of parameters. Their maximum relative errors over the whole range of parameters are approximately less than 1.2%. Furthermore, we have derived closed-form upper bounds on the maximum relative error between the respective bounds and the BeNaI. Finally, the analytical results have been accompanied by graphical representations throughout the chapter.

7 Conclusion

7.1 Summary and Contributions

The content of the presented thesis is motivated at least by two facts. First, finding optimal solutions for balancing the power consumption of the entire network and the overall system performance becomes increasingly complex as the number of deployed sensor nodes becomes large. Second, present numerical methods are too slow to optimize the system performance for realistic network sizes in real-time. Hence, the main goal of the presented work has been to obtain analytical solutions in closed-form instead of numerical results. In particular, we have improved the performance of wireless sensor networks that are used for target detection and classification. Although, closed-form solutions are extremely difficult to obtain and only achievable in special cases, this work has provided first novel results in closed-form. Major contributions concern the optimization of the power allocation in sensor networks and the evaluation of the corresponding classification probability.

Firstly, we have introduced the power allocation problem for distributed multiple-radar systems. Passive and active radar systems have been investigated under sum-power and individual power constraints per sensor node. We have presented explicit policies for the optimal power allocation. The achieved results have shown that the optimal strategy for power allocation in passive radar systems can be different compared to the optimal strategy in active radar systems. In case, where the optimization problem is only subject to individual power constraints, the optimal solution for power allocation is identical in both passive and active radar systems. Each sensor node is active and consumes power equal to its own output power-range limitation. In contrast, if the optimization problem is only subject to the sum-power constraint, then the available sum-power in passive radar systems is shared between several sensor nodes while in active radar systems only a single sensor node consumes the whole sum-power. The only common ground in both radar systems is the selection of active sensor nodes which is based on a rule that includes all system parameters and is specific for each of both radar systems. Based on this specific rule we are able to sort the sensor nodes in order to determine the more reliable nodes and facilitate adaptive resource management in sensor networks. Moreover, the complexity for optimizing the power allocation in very large sensor networks can drastically be decreased, since the obtained results are in closed-form and in addition have simple expressions.

Secondly, since the power allocation problem is optimally solved, an optimal and simple classification rule has been proposed to improve the whole system performance. We have applied the distance classifier and evaluated the corresponding classification

probability in certain cases for active radar systems. As we have shown, the instantaneous classification probability is described by the complementary error function and the evaluation of the average classification probability is closely related to the evaluation of the average symbol-error probability. If the communication channels are random, both the average classification and symbol-error probability lead to a challenging problem of integration, where the integrands are special functions and thus a closed-form solution seems to be out of reach. However, since the integration problem, which is named as Beta-Nakagami Integral (BeNaI), arises from many applications and hence is interesting for investigation, we have examined it carefully.

Finally, we have first improved the Gautschi's double inequality in order to prove our statements for the examination of the BeNaI. Subsequently, the BeNaI has been scrutinized and as main results we have presented equivalent equations and mathematical expressions. In particular, from the obtained ordinary differential equation, relationships to the incomplete beta function and to the Gauss hypergeometric function has been established. Furthermore, an infinite series representation has been developed. By the equivalent representation of the BeNaI, we have pointed out that the BeNaI is also equal to an integral over a broken rational function which does not include any special functions. Moreover, the obtained results lead to more accurate numerical evaluations, due to simple and stable form of the equivalent representation. In order to eliminate numerical methods, we have analytically derived accurate bounds in closed-form for the BeNaI. They yield maximum relative errors of about 1.2% and support the whole range of parameters. A main advantage of the bounds is the simple mathematical form, which can in addition be adapted to the particular need of users. For reinforcing the appropriateness of the bounds and their particular selection, we have shown that important mathematical properties of both bounds coincide with the properties of the BeNaI. Since the evaluation of relative errors is a hard task, we have determined analytical upper-bounds in closed-form on all relative errors. Numerical results have attested the sharpness and the accuracy of the upper-bounds on the relative errors.

7.2 Future Research

As we have seen, the optimization of power allocation in distributed sensor networks subject to well-chosen constraints is amenable in closed-form. Naturally the question arises how to select the constraints to solve the optimization problem in closed-form, or equivalently, is there a specific class of constraints which leads to a closed-form allocation strategy. In order to answer to these questions, more optimization cases with different constraints should be investigated. In particular, we point out the following important extensions of our approach.

- Since an accurate estimation of all channel coefficients in the sensing channel is difficult in practice, robust optimization methods against estimation inaccuracies are of high interest.

- Instead of considering the single constraint $W_k + X_k \leq P_{\max}$ for each sensor node

in active sensor networks, two new constraints $W_k \leq P_{W\max}$ and $X_k \leq P_{X\max}$ should be regarded. These constraints are important in medical applications, since the maximum peak-power values for diagnostic analysis of living tissues are compulsory and should not be exceeded.

- In the considered sensor networks, we have never regarded any constraints for the fusion center. Applying some power constraints for the fusion center can be very interesting since the fusion center itself might be an extended sensor node with enhanced capabilities.

The key motivation of the presented work has been to derive closed-form solutions for the power allocation problem. We have achieved this goal by applying the composition of minimum mean squared error as the objective, a simple system model for the entire network, and a linear fusion rule to combine the local observations. The variation of this composition is highly attractive for examination because by applying non-linear fusion rules the system performance may be further improved. Furthermore, in some applications the objective should be defined by other metrics than the mean squared error. For example, the Kullback-Leibler distance is a crucial candidate for the objective function.

From the viewpoint of information theory, the metric to be minimized in a sensor network is the energy per information bit required to transmit an information bit from source to destination. Since this metric is independent of the architecture of the entire network, its protocols, transmission methods, and the hardware implementation, an optimal solution in the sense of information theory is of high interest. Recently, some relationships between the mutual information and the mean square error estimation have been investigated. Especially, the authors in [96] have shown that minimization of the mean square error leads to a minimized slope of the corresponding mutual information with respect to the signal-to-noise ratio. Since mutual information is increasing and concave with respect to the signal-to-noise ratio, a minimized mean square error results in a maximized mutual information. As we have seen in Subsections 3.3.1 and 4.4.1, we have analytically derived the optimal solution of both power allocation problems in closed-form which in turn are described by signal-to-noise ratios. Integration of these results would lead to expressions describing the maximum achievable mutual information between the source (target) and destination (fusion center). Because of challenging integrals and absence of mathematical concepts in this work area, this investigation is devoted for future.

In the present work, we have investigated the average symbol-error probability for communication over Nakagami-distributed fading channels. In future works, Rice-distributed fading channels could be investigated, due to their diverse applications. Moreover, the evaluation and approximation of both integrals (5.19) and (5.20) are still open problems. Maybe, the approach of approximation in the presented work can be extended and used for approximation of other integrals and difficult functions.

Glossary

List of general Symbols

$\mathbb{D}$	Sets are denoted by double stroked uppercase letters.
$\mathbb{N}$, $\mathbb{N}_0$	Sets of positive integers (natural numbers) and non-negative integers.
$\mathbb{Z}$	Set of integers.
$\mathbb{R}$, $\mathbb{R}_+$	Sets of real and non-negative real numbers.
$\mathbb{C}$	Set of complex numbers.
$\mathbb{F}_N$	A subset of $\mathbb{N}$ defined as $\mathbb{F}_N \coloneqq \{1, \ldots, N\}$ for any given $N \in \mathbb{N}$.
$\mathbb{K}$	The subset $\mathbb{K}_{\text{lin}} \cup \mathbb{K}_{\text{sat}}$ of all sensor nodes which are active and are allocated with transmission power.
$\mathbb{K}_{\text{lin}}$	A subset of $\mathbb{K}$, including all sensor nodes which operate within their power range.
$\mathbb{K}_{\text{sat}}$	A subset of $\mathbb{K}$, including all sensor nodes which operate at their power range limitation.
j	The imaginary unit.
$\Re(z)$, $\Im(z)$	Real and imaginary part of a real or complex-valued number z.
$\mathbf{v}$	Vectors are denoted by boldface lowercase letters.
$\mathbf{M}$	Matrices are denoted by boldface uppercase letters.
$\bar{\mathbf{M}}$	Complex conjugate of a matrix $\mathbf{M}$.
$\mathbf{M}'$	Transpose of a matrix $\mathbf{M}$.
$\bar{\mathbf{M}}'$	Complex-conjugate transpose of a matrix $\mathbf{M}$.
$\mathbf{x} \preceq \mathbf{y}$	Vector $\mathbf{x}$ is majorized by vector $\mathbf{y}$.
$\mathcal{E}[v]$, $\mathcal{E}[\mathbf{v}]$	Expected value of a random variable v and a random vector $\mathbf{v}$.
$\mathcal{P}[A]$	Probability of an event A.
$\mathcal{P}[A \mid B]$	Conditional probability of A given B.
$Z \sim \mathfrak{R}(\sigma^2)$	A Rayleigh distributed random variable with the Rayleigh parameter σ^2.
$\mathfrak{G}(\kappa, \sigma)$	Gamma distribution with the parameters κ and σ.
$\mathcal{O}(\cdot)$	Landau symbol, defining asymptotical behavior of functions.
$V^\star$	Optimal value of an optimization variable V.
$\lvert z \rvert$	Absolute value of some real or complex number z.
$\lVert \mathbf{z} \rVert$	Euclidean norm of some real or complex vector $\mathbf{z}$.
$\lvert \mathbb{D} \rvert$	Cardinality (number of elements) of any finite set $\mathbb{D}$.

List of Symbols Concerning Power Allocation for Passive and Active Networks

K	Number of all sensor nodes.
$\tilde{K}$	Number of active sensor nodes.
g_k, h_k	Complex-valued channel coefficients.
m_k, n_k	Complex-valued zero-mean AWGN.
u_k, v_k	Non-negative amplification factors and complex-valued weights.
ϑ_k	Phase of v_k.
ϕ_k	Phase of the product $g_k h_k$.
y_k	Input signals of the combiner.
X_k	Communication power of k^{th} sensor node.
P_{tot}	Sum-power constraint.
c_k, $\tilde{c}_k$	Disturbance-intensity and reliability-function.
SNR_k^{S}, SNR_k^{C}	Signal-to-noise ratios for the communication over sensing and communication channels.
SNR_k, SNR_{tot}	Signal-to-noise ratios at the input and the output of the fusion center.
σ_s^2, σ_c^2	Expected values of the signal-to-noise ratio for sensing and communication.

List of Symbols Concerning Power Allocation only for Passive Networks

r, R	Target signal and its quadratic absolute mean.
$\tilde{r}$	Estimate of actual r.
M_k, N_k	Variances of m_k and n_k.
P_k	Output power-range constraint of k^{th} sensor node.
χ, $\tilde{\chi}$	Water-level and normalized water-level.
$\tilde{J}_k$	The slope of the objective with respect to the power of k^{th} sensor node.

List of Symbols Concerning Power Allocation only for Active Networks

I	Number of different reflection coefficients.
r_i	Reflection coefficient of i^{th} target object.
r_{rms}	Root mean squared absolute value of reflection coefficients.
$\tilde{r}$	Estimate of the actual reflection coefficient r_i.
M_0, N_0	Variances of each m_k and n_k.
w_k	Non-negative amplification factors.
W_k	Sensing power of k^{th} sensor node.
$P_{\max}$	Output power-range constraint of each sensor node.
(σ, τ, ω), $(\sigma_k, \tau_k, \omega_k)$	A point in the Cartesian coordinates and the position of the k^{th} sensor node.
$(0,0,0)$, $(\sigma_0, 0, 0)$	The position of the fusion center and the target object.
d_{g_k}, d_{h_k}	Euclidean distances between the k^{th} sensor node and the target object as well as between k^{th} sensor node and the fusion center.
$\mathbb{S}$	A 3-d subspace of $\mathbb{R}^3$ in which all active sensor nodes are located.
λ	Wavelength of the signal.
ρ	The density of sensor nodes per volume unit.

List of Symbols Concerning Nakagami-distributed Fading

Γ, ψ	Gamma and digamma (psi) function.
$\mathrm{B}(a,b;x)$, $\mathrm{B}(a,b)$	Incomplete beta and the beta function.
erfc	Complementary error function.
${}_2\mathrm{F}_1$	Hypergeometric function.
arctan	Inverse tangent function.
τ	Ratio of two gamma functions, see (2.31).
P	Symbol-error probability.
P_{avg}	Average symbol-error probability (AEP).
g	Beta-Nakagami Integral (BeNaI).
$\tilde{g}$	Approximation of BeNaI.
f, h	Bounds on the BeNaI.
a_f, b_f	Constants used for the bound f.
a_h, b_h	Constants used for the bound h.
r_f, r_h	Maximum relative errors of the bounds f and h.
r,	Maximum relative error between the bounds f and h.
$\hat{r}$, $\check{r}$	Upper bounds on r.
$\tilde{r}$	Maximum relative error of the closest bound.

List of Abbreviations

AEP	Average symbol-error probability
BER	Bit error rate
SER	Symbol error rate
AWGN	Additive white Gaussian noise
BeNaI	Beta-Nakagami Integral, see Definition 6.1.1
BPSK	Binary phase-shift keying
FSK	Frequency-shift keying
PAM	Pulse amplitude modulation
PSK	Phase-shift keying
QAM	Quadrature amplitude modulation
QPSK	Quadrature phase-shift keying
SN	Sensor node
SNR	Signal-to-noise ratio

Bibliography

[1] G. Alirezaei, "Channel capacity related power allocation for ultra-wide bandwidth sensor networks with application in object detection," in *IEEE International Conference on Ultra-Wideband (ICUWB'12)*, Syracuse, NY, USA, Sep. 2012, pp. 115–119.

[2] G. Alirezaei and R. Mathar, "Channel capacity related power allocation for distributed sensor networks with application in object classification," in *International Conference on Computing, Networking and Communications (ICNC'13)*, San Diego, California, USA, Jan. 2013, pp. 502–507.

[3] ——, "Power allocation for power-limited sensor networks with application in object classification," in *Global Information Infrastructure Symposium (GIIS'12)*, Choroní, Venezuela, Dec. 2012, pp. 1–5.

[4] ——, "Optimum power allocation for sensor networks that perform object classification," in *Australasian Telecommunication Networks and Applications Conference (ATNAC'13)*, Christchurch, New Zealand, Nov. 2013, pp. 1–6, received the Best Paper Award.

[5] G. Alirezaei, R. Mathar, and P. Ghofrani, "Power optimization in sensor networks for passive radar applications," in *The Wireless Sensor Systems Workshop (WSSW'13), co-located with the IEEE International Conference on Wireless for Space and Extreme Environments (WiSEE'13)*, Baltimore, Maryland, USA, Nov. 2013, received the Best Paper Award.

[6] G. Alirezaei, M. Reyer, and R. Mathar, "Optimum power allocation in sensor networks for passive radar applications," *IEEE Transactions on Wireless Communications*, vol. 13, no. 6, pp. 3222–3231, Jun. 2014.

[7] G. Alirezaei and R. Mathar, "Scrutinizing the average error probability for nakagami fading channels," in *The IEEE International Symposium on Information Theory (ISIT'14)*, Honolulu, Hawai'i, USA, Jun. 2014, pp. 2884–2888.

[8] ——, "Optimum power allocation for sensor networks that perform object classification," *IEEE Sensors Journal*, vol. 14, no. 11, pp. 3862–3873, Nov. 2014.

[9] G. Alirezaei, O. Taghizadeh, and R. Mathar, "Optimum power allocation with sensitivity analysis for passive radar applications," *IEEE Sensors Journal*, vol. 14, no. 11, pp. 3800–3809, Nov. 2014.

[10] G. Alirezaei and R. Mathar, "Sensitivity analysis of optimum power allocation in sensor networks that perform object classification," *Australian Journal of Electrical & Electronics Engineer*, vol. 12, no. 3, Sep. 2015, the print as scheduled is subject to changes.

[11] O. Taghizadeh, G. Alirezaei, and R. Mathar, "Complexity-reduced optimal power allocation in passive distributed radar systems," in *The Eleventh International Symposium on Wireless Communication Systems (ISWCS'14)*, Barcelona, Spain, Aug. 2014.

[12] G. Alirezaei and J. Schmitz, "Geometrical sensor selection in large-scale high-density sensor networks," in *The IEEE International Conference on Wireless for Space and Extreme Environments (WiSEE'14)*, Noordwijk, Netherlands, Oct. 2014.

[13] G. Alirezaei, "A sharp double inequality for the inverse tangent function," 2013. [Online]. Available: http://arxiv.org/abs/1307.4983

[14] G. Alirezaei, O. Taghizadeh, and R. Mathar, "Optimum power allocation in sensor networks for active radar applications," *IEEE Transactions on Wireless Communications*, 2014, to be published after November.

[15] M. Abramowitz and I. A. Stegun, *Handbook of Mathematical Functions with Formulas, Graphs, and Mathematical Tables*, 10th ed. Washington D.C.: National Bureau of Standards, Applied Mathematics Series - 55, 1972.

[16] J. E. Pečarić, F. Proschan, and Y. L. Tong, *Convex Functions, Partial Ordering, and Statistical Applications*, 1st ed., ser. Mathematics in science and engineering. USA: Academic Press, 1992, vol. 187.

[17] A. W. Marshall, I. Olkin, and B. C. Arnold, *Inequalities: Theory of Majorization and Its Applications*, 2nd ed. New York: Springer, 2011.

[18] G. H. Hardy, J. E. Littlewood, and G. Pólya, *Inequalities*, ser. Cambridge Mathematical Library. Cambridge University Press, 1952.

[19] S. Boyd and L. Vandenberghe, *Convex Optimization*. California: Cambridge University Press, 2004.

[20] M. Chiang, *Geometric Programming for Communication Systems*. Princeton: now Publishers Inc., 2005.

[21] D. G. Luenberger and Y. Ye, *Linear and Nonlinear Programming*, 3rd ed. Springer Science+Business Media, 2008.

[22] D. P. Bertsekas, *Nonlinear Programming*, 2nd ed. Athena Scientific, 1999.

[23] N. Bleistein and R. A. Handelsman, *Asymptotic Expansions of Integrals*. New York: Dover Publications, 1986.

[24] W. Gautschi, "Some elementary inequalities relating to the gamma and incomplete gamma function," *J. Math. Phys.*, vol. 38, no. 1, pp. 77–81, 1959.

[25] D. Kershaw, "Some extensions of W. Gautschi's inequalities for the gamma function," *Math. Comp.*, vol. 41, no. 164, pp. 607–611, 1983.

[26] M. Merkle, *Inequalities for the gamma function via convexity*, ser. Advances in Inequalities for Special Functions. Hauppauge-NewYork: Nova Science Publishers, 2008, pp. 81–100.

[27] F. Qi and B.-N. Guo, "Wendel's and Gautschi's inequalities: Refinements, extensions, and a class of logarithmically completely monotonic functions," *Applied Mathematics and Computation*, vol. 205, no. 1, pp. 281–290, 2008.

[28] D. N. Shanbhag, "On some inequalities satisfied by the gamma function," *Scandinavian Actuarial Journal*, no. 1-2, pp. 45–49, 1967.

[29] I. S. Gradshteyn and I. M. Ryzhik, *Table of Integrals, Series, and Products*, 6th ed. London: Academic Press, 2000.

[30] (2010, Dec.) Icecube neutrino observatory. University of Wisconsin-Madison and National Science Foundation. Amundsen-Scott South Pole Station, Antarctica. [Online]. Available: http://icecube.wisc.edu/

[31] (2012, Mar.) The very large array. The National Radio Astronomy Observatory. Socorro County, New Mexico, USA. The National Radio Astronomy Observatory is a facility of the National Science Foundation operated under cooperative agreement by Associated Universities, Inc. [Online]. Available: http://www.vla.nrao.edu/

[32] A. L. Hume and C. J. Baker, "Netted radar sensing," in *Proc. IEEE Int. Radar Conf.*, 2001, pp. 23–26.

[33] I. Immoreev and J. Taylor, "Future of radars," in *Ultra Wideband Systems and Technologies, 2002. Digest of Papers. 2002 IEEE Conference on*, 2002, pp. 197–199.

[34] M. I. Skolnik, *Introduction to Radar Systems*, 3rd ed. New York: McGraw-Hill Higher Education, 2002.

[35] P. K. Varshney, *Distributed Detection and Data Fusion*. New York: Springer, 1997.

[36] F. Meshkati, H. Poor, and S. Schwartz, "Energy-efficient resource allocation in wireless networks," *Signal Processing Magazine, IEEE*, vol. 24, no. 3, pp. 58–68, 2007.

[37] H. Godrich, A. Petropulu, and H. Poor, "Power allocation strategies for target localization in distributed multiple-radar architectures," *Signal Processing, IEEE Transactions on*, vol. 59, no. 7, pp. 3226–3240, 2011.

[38] S. Gezici, Z. Tian, G. B. Giannakis, H. Kobayashi, A. F. Molisch, H. V. Poor, and Z. Sahinoglu, "Localization via ultra-wideband radios: A look at positioning aspects for future sensor networks," *IEEE Signal Process. Mag.*, vol. 22, pp. 70–84, Jul. 2005.

[39] Y. Shen, W. Dai, and M. Win, "Optimal power allocation for active and passive localization," in *Global Communications Conference (GLOBECOM), 2012 IEEE*, 2012, pp. 3713–3718.

[40] S. Cui, J.-J. Xiao, A. Goldsmith, Z.-Q. Luo, and H. Poor, "Estimation diversity and energy efficiency in distributed sensing," *Signal Processing, IEEE Transactions on*, vol. 55, no. 9, pp. 4683–4695, 2007.

[41] A. Høst-Madsen and J. Zhang, "Capacity bounds and power allocation for wireless relay channels," *Information Theory, IEEE Transactions on*, vol. 51, no. 6, pp. 2020–2040, 2005.

[42] M. Emadi, A. Davoodi, and M. Aref, "Analytical power allocation for a full-duplex decode-and-forward relay channel," *Communications, IET*, vol. 7, no. 13, pp. 1338–1347, 2013.

[43] M. Chen, S. Serbetli, and A. Yener, "Distributed power allocation strategies for parallel relay networks," *Wireless Communications, IEEE Transactions on*, vol. 7, no. 2, pp. 552–561, 2008.

[44] S. Stańczak, M. Wiczanowski, and H. Boche, *Fundamentals of Resource Allocation in Wireless Networks: Theory and Algorithms*, 2nd ed. Berlin: Springer, 2008.

[45] K. Alam and K. T. Wallenius, "Distribution of a sum of order statistics," *Scandinavian Journal of Statistics*, vol. 6, no. 3, pp. pp. 123–126, 1979. [Online]. Available: http://www.jstor.org/stable/4615746

[46] H. A. David and H. N. Nagaraja, *Order Statistics*, 3rd ed. Wiley-Interscience, 2003.

[47] N. Metropolis, "The beginning of the monte carlo method," *Los Alamos Science*, no. 15, pp. 125–130, 1987.

[48] R. Srinivasan, "Distributed radar detection theory," *IEE Proceedings-F*, vol. 133, no. 1, pp. 55–60, Feb. 1986.

[49] L. Pescosolido, S. Barbarossa, and G. Scutari, "Radar sensor networks with distributed detection capabilities," in *Proc. IEEE Int. Radar Conf.*, May 2008, pp. 1–6.

[50] Y. Yang, R. S. Blum, and B. M. Sadler, "A distributed and energy-efficient framework for Neyman-Pearson detection of fluctuating signals in large-scale sensor networks," *IEEE J. Sel. Areas Commun.*, vol. 28, pp. 1149–1158, Sep. 2010.

[51] C. Debes, J. Riedler, A. M. Zoubir, and M. G. Amin, "Adaptive target detection with application to through-the-wall radar imaging," *IEEE Trans. Signal Process.*, vol. 58, no. 11, pp. 5572–5583, 2010.

[52] R. O. Duda, P. E. Hart, and D. G. Stork, *Pattern Classification*, 2nd ed. John Wiley & Sons, Inc, 2000.

[53] A. Lapidoth, *A Foundation in Digital Communication.* Cambridge University Press, 2009.

[54] H. D. Lüke, *Korrelationssignale*, 1st ed. Berlin: Springer, 1992.

[55] D. G. Luenberger, *Optimization by Vector Space Methods*, 1st ed. John Wiley & Sons, Inc., 1969.

[56] E. Hansen and G. W. Walster, *Global Optimization Using Interval Analysis*, 2nd ed. Marcel Dekker Inc., 2003.

[57] D. W. Peterson, "A review of constraint qualifications in finite-dimensional spaces," *SIAM Review*, vol. Vol. 15, no. No. 3, pp. 639–654, July 1973.

[58] R. Horst and H. Tuy, *Global Optimization: Deterministic Approaches*, 2nd ed. Springer-Verlag, 1992.

[59] MATLAB, *version 7.11.0.584 (R2010b).* Natick, Massachusetts: The MathWorks Inc., 2010.

[60] M. Grant and S. Boyd, "CVX: Matlab software for disciplined convex programming, version 2.1," http://cvxr.com/cvx, Mar. 2014.

[61] M. de Berg, O. Cheong, M. van Kreveld, and M. Overmars, *Computational Geometry: Algorithms and Applications*, 3rd ed. Springer-Verlag, 2008.

[62] J. R. Barry, E. A. Lee, and D. G. Messerschmitt, *Digital Communications*, 3rd ed. Springer-Verlag, 2003.

[63] M. Nakagami, "The m-distribution – A general formula of intensity distribution of rapid fading," in *Statistical Methods in Radio Wave Propagation: Proceedings of a Symposium Held on June 18-20, 1958*, W. Hoffman, Ed. University of California, Los Angeles: Pergamon Press, 1958, pp. 3–36.

[64] M. K. Simon and M.-S. Alouini, "A unified approach to the performance analysis of digital communication over generalized fading channels," *Proceedings of the IEEE*, vol. 86, no. 9, pp. 1860–1877, 1998.

[65] ——, "A unified approach to the probability of error for noncoherent and differentially coherent modulations over generalized fading channels," *Communications, IEEE Transactions on*, vol. 46, no. 12, pp. 1625–1638, 1998.

[66] M. Chiani, D. Dardari, and M. K. Simon, "New exponential bounds and approximations for the computation of error probability in fading channels," *Wireless Communications, IEEE Transactions on*, vol. 2, no. 4, pp. 840–845, 2003.

[67] S. Park, D. Yoon, and K. Cho, "Tight approximation for coherent MPSK symbol error probability," *Electronics Letters*, vol. 39, no. 16, pp. 1220–1222, 2003.

[68] G. Karagiannidis and A. Lioumpas, "An improved approximation for the Gaussian Q-function," *Communications Letters, IEEE*, vol. 11, no. 8, pp. 644–646, 2007.

[69] S. Park and B.-G. Kang, "Upper bounds on the symbol-error probability of MPSK with phase error using Pawula F-function IV," *Communications, IEEE Transactions on*, vol. 57, no. 8, pp. 2198–2203, 2009.

[70] W. M. Jang, "A simple upper bound of the Gaussian Q-function with closed-form error bound," *Communications Letters, IEEE*, vol. 15, no. 2, pp. 157–159, 2011.

[71] ——, "Corrections to 'a simple upper bound of the Gaussian Q-function with closed-form error bound'," *Communications Letters, IEEE*, vol. 15, no. 12, pp. 1274–1274, 2011.

[72] Q. Shi and Y. Karasawa, "An accurate and efficient approximation to the Gaussian Q-function and its applications in performance analysis in Nakagami-m fading," *Communications Letters, IEEE*, vol. 15, no. 5, pp. 479–481, 2011.

[73] A. V. Boyd, "Inequalities for Mills' ratio," *Reports of Statistical Application Research, JUSE*, vol. 6, no. 2, pp. 44–46, 1959.

[74] G. de Abreu, "Supertight algebraic bounds on the Gaussian Q-function," in *Signals, Systems and Computers, 2009 Conference Record of the Forty-Third Asilomar Conference on*, 2009, pp. 948–951.

[75] P. Sofotasios and S. Freear, "Novel expressions for the Marcum and one dimensional Q-functions," in *Wireless Communication Systems (ISWCS), 2010 7th International Symposium on*, 2010, pp. 736–740.

[76] ——, "New analytic results for the incomplete Toronto function and incomplete Lipschitz-Hankel integrals," in *Microwave Optoelectronics Conference (IMOC), 2011 SBMO/IEEE MTT-S International*, 2011, pp. 44–47.

[77] W. Lindsey, "Error probabilities for Rician fading multichannel reception of binary and n-ary signals," *Information Theory, IEEE Transactions on*, vol. 10, no. 4, pp. 339–350, 1964.

[78] R. Esposito, "Error probabilities for the Nakagami channel (corresp.)," *Information Theory, IEEE Transactions on*, vol. 13, no. 1, pp. 145–148, 1967.

[79] Y. Miyagaki, N. Morinaga, and T. Namekawa, "Error probability characteristics for CPSK signal through m-distributed fading channel," *Communications, IEEE Transactions on*, vol. 26, no. 1, pp. 88–100, 1978.

[80] U. Charash, "Reception through Nakagami fading multipath channels with random delays," *Communications, IEEE Transactions on*, vol. 27, no. 4, pp. 657–670, 1979.

[81] E. K. Al-Hussaini and A. Al-Bassiouni, "Performance of MRC diversity systems for the detection of signals with Nakagami fading," *Communications, IEEE Transactions on*, vol. 33, no. 12, pp. 1315–1319, 1985.

[82] A. Wojnar, "Unknown bounds on performance in Nakagami channels," *Communications, IEEE Transactions on*, vol. 34, no. 1, pp. 22–24, 1986.

[83] N. Beaulieu and A. Abu-Dayya, "Analysis of equal gain diversity on Nakagami fading channels," *Communications, IEEE Transactions on*, vol. 39, no. 2, pp. 225–234, 1991.

[84] J. G. Proakis, *Digital Communications*, 4th ed. McGraw-Hill International Edition, 2001.

[85] A. Goldsmith, *Wireless Communications*. Cambridge University Press, 2005.

[86] B. Sklar, *Digital Communications: Fundamentals and Applications*, 2nd ed. Prentice Hall, 2008.

[87] M. Nakagami, "Statistical characters of short-wave fading," *Institutes of Electronics and Communication Engineers of Japan*, vol. 27, pp. 145–, 1943.

[88] M. K. Simon and M.-S. Alouini, *Digital communication over fading channels*, 2nd ed. A Wiley-Interscience publication, 2005.

[89] N. Nielsen, *Theorie des Integrallogarithmus und verwandter Transzendenten*, ser. Cornell University Library historical math monographs. B. G. Teubner, 1906.

[90] A. Erdélyi, W. Magnus, F. Oberhettinger, F. G. Tricomi, and research associates, *Tables of integral transforms: Based, in part, on notes left by Harry Bateman*, ser. California Institute of technology. Bateman Manuscript project. McGraw-Hill, 1954, vol. 1.

[91] W. Feller, *An Introduction to Probability Theory and Its Applications*, 2nd ed. John Wiley & Sons, 1971, vol. 2.

[92] N. L. Johnson, S. Kotz, and N. Balakrishnan, *Continuous Univariate Distributions*, 2nd ed. John Wiley & Sons, 1995, vol. 2.

[93] N. W. Mc Lachlan, P. Humbert, and L. Poli, *Supplément au formulaire pour le calcul symbolique*. Gauthier-Villars, 1950.

[94] A. F. Timan, *Theory of Approximation of Functions of a Real Variable*. USA: Dover Publications, 1994.

[95] K. S. Miller and S. G. Samko, "Completely monotonic functions," *Integr. Transf. and Spec. Funct.*, vol. 12, no. 4, pp. 389–402, 2001.

[96] D. Guo, S. Shamai, and S. Verdu, "Mutual information and minimum mean-square error in gaussian channels," *Information Theory, IEEE Transactions on*, vol. 51, no. 4, pp. 1261–1282, Apr. 2005.

Curriculum Vitae

Gholamreza Alirezaei	Born on the 1st of May 1976 in Esfahan, Iran

Education

1982 - 1987	Elementary school in Esfahan, Iran
1987 - 1996	High school in Aachen, Germany
December 1996	General qualification for university entrance (Abitur)
1996 - 2001	Academic education in electrical engineering at RWTH University, Aachen, Germany
September 2001	Diploma degree in electrical engineering from RWTH University, Aachen, Germany
2010 - 2014	Academic education in mathematics at RWTH University, Aachen, Germany

Professional Experience

2001 - 2002	Applications engineer at Synopsys Inc., Kohlscheid, Aachen, Germany
2002 - 2008	Scientific staff member (research assistant) at the Institute of High Frequency Technology of RWTH University, Aachen, Germany
2008 - 2011	Research and development engineer at ATecoM GmbH, Aachen, Germany
Since 2011	Scientific staff member (research assistant) at the Institute for Theoretical Information Technology of RWTH University, Aachen, Germany